DISSERTATION

submitted to the

Combined Faculties for the Natural Sciences and for Mathematics of the Ruperto-Carola University of Heidelberg, Germany

for the degree of

Doctor of Natural Sciences

presented by

M.Sc. Charlotte Rostock

born in Heidelberg, Germany

Oral examination:

Differentiation and characterization of human stem cell-derived nociceptors and comparison to human and mouse dorsal root ganglia tissue

Referees: Prof. Dr. Ulrike Müller

Prof. Dr. Jan Erik Siemens

Acknowledgements

Scientific Acknowledgements

After an intense time of more than 4 years, it is time for writing these acknowledgements, which also means making final efforts on my dissertation.

The time as a PhD student did not only helped me expanding my knowledge about scientific aspects but also about my personality and in this regard also influenced myself. With this acknowledgement, I would like to address people who accompanied and supported me during the implementation of this thesis.

First of all, I would like to thank Prof. Jan Erik Siemens for giving me the opportunity and confidence to work in his lab and for his scientific advice and supervision during the entire period of my PhD.

I also want to thank my colleagues in the lab with whom I have worked with.

Special thanks go to my first contact person and "stem cell-buddy" Dr. Katrin Schrenk-Siemens, who shared her profound knowledge with me and provided me with great support and advice at any time. Furthermore, thanks to all my other (former) colleagues in the lab for their helpful suggestions and their tremendous (scientific) experience that helped me to improve and develop: Dr. Hong Wang, Dr. Hagen Wende, Dr. Wanessa du Fresne von Hohenesche, Dr. Gretel Kamm, Dr. Jörg Pohle, Dr. Kun Song, Shiying Lu, Moad Abd El Hay, Kristina Zuza, Daniela Petzinger, Annika von Seggern, Christina Steinmeyer-Stannek and Ulrike Baur-Finck.

Furthermore, special thanks to Vincenzo Prato (Institute of Pharmacology Heidelberg) and Dr. Jörg Pohle who did the electrophysiological recordings of differentiated neurons and helped me with statistical analysis.

In addition, I would also like to thank my collaborators from other labs for their technical support and the provision of DNA plasmids: Dr. Alexander Loewer and Gitta Blendinger (MDC Berlin) for the 3rd generation lentiviral helper plasmids, Prof. Thomas Südhof (Stanford University) for the NGN2-lentviral plasmid, Prof. Clifford J. Woolf (Harvard Medical School) for lentiviral plasmids, Dr. Stefan Lechner (Institute of Pharmacology Heidelberg) for the mouse PIEZO1-GFP construct and Dr. Martina Saar (Institute of Pharmacy and Molecular Biotechnology Heidelberg) for the p3xFlag-CMV plasmid.

Finally, I would also like to thank Prof. Ulrike Müller (Institute of Pharmacy and Molecular Biotechnology Heidelberg), my official first supervisor, who initially aroused my interest for stem cells during my master thesis in her lab and she also initiated the first contact to the "Siemens group".

Personal Acknowledgement

My dear Wanessa I am really happy that we got to know each other during your time in Heidelberg and I am very grateful that although you left Germany we are still in regular contact and you really helped and supported me during writing this thesis!

Danken möchte ich außerdem auch dir, Christina. Ich bin froh, dass ich dich nicht nur als eine der besten Bench-Nachbarinnen kennenlernen durfte, sondern auch über die Arbeit hinaus.

Ein ganz lieber Dank gilt auch meinen Freunden (wenn ihr das lest, wisst ihr, dass ihr gemeint seid), für eure Unterstützung, eure Geduld und einfach dafür, dass ihr noch immer für mich da seid ☺.

Der größte Dank geht an meine Familie, und insbesondere an meine Eltern, die mich während des gesamten Studiums und der Doktorandenzeit finanziell, aber vor allem auch persönlich unterstützt haben. Danke, dass ihr immer an mich geglaubt habt.

Summary

The capability to sense and transduce environmental as well as internal sensory stimuli, such as touch, pain or muscle tension, is a fundamental process required for cell survival and the avoidance of tissue damage of the body. Vertebrates can detect these stimuli via specialized cells in the peripheral nervous system - the somatosensory neurons. It is well known that the peripheral nervous system consists of many different types of neurons, but how they are generated and how they establish their functional abilities is at present not fully understood.

Although pain sensation represents an adaptive alarm system detecting signals that are potentially harmful to the body, persistent pain is a maladaptive false alarm and nowadays clinicians have only few, if any, effective means to medicate chronic pain. Therefore, it is indispensable to get a more detailed understanding of how pain signals are transmitted and how human pain-sensitive neurons are established, given that most of the current knowledge about pain or pain sensation is based on animal studies. Although animal models provided a basis for research about causes, onset and course of pain diseases, there is more and more evidence that the translation of these findings to human patients is more challenging than expected.

Therefore, the aim of this Ph.D. thesis was to establish a differentiation protocol for the generation of functional human embryonic stem cell (hESC)-derived nociceptors. I found that a transient overexpression of the bHLH transcription factor neurogenin 1 (NGN1), known to induce neurogenesis and to mediate the differentiation of nociceptive neurons in mice, was sufficient to differentiate progenitor cells of the peripheral nervous system (PNS) into primary sensory neurons with a nociceptive phenotype. Differentiated cells were analyzed and characterized by using Ca^{2+}-imaging, immunohistochemistry, *in situ* hybridization, quantitative RT-PCR and electrophysiological recording techniques, confirming their nociceptor-like properties. To validate whether hESC-derived nociceptors are physiologically relevant and can reflect the *in vivo* equivalent, we compared them to human *post-mortem* DRG tissue where we found a similar marker gene profile. A comparative study that I carried out using human and mouse *post-mortem* DRG tissue highlighted molecular differences of murine and human sensory neurons that need to be considered when using the mouse as a model system for the development of new analgesic drugs.

Furthermore, we were also interested in exploring the role of PIEZO2 in sensory neurons. Recent findings in rodents identified PIEZO2, a large transmembrane protein, as a main transducer of innocuous mechanical stimuli, and we confirmed that PIEZO2 is also required for mechanotransduction in human stem cell-derived touch receptors. However, it is so far uncertain whether PIEZO2 also plays a role in transducing noxious mechanical stimuli to trigger sensation of pain. Rapidly-adapting, mechanically-activated currents (at least those conventionally recorded when using a nanomotor-driven stimulus probe) appeared to be absent in PIEZO2-knockout (KO)

nociceptors, indicating that PIEZO2 is also required for mechanotransduction in stem cell-derived nociceptors. Additionally, I also aimed to identify accessory proteins of PIEZO2 that are involved in human PIEZO2-mediated sensory mechanotransduction, by generating a PIEZO2-tagged hESC line.

The outcome of this study would allow us to identify differences and similarities between human and mouse nociceptors and furthermore, to use this differentiation protocol as a basis for the generation of other distinct human nociceptive subpopulations, to finally provide a model system to study human pain and pain transduction *in vitro*.

Zusammenfassung

Die Fähigkeit sensorische Reize, wie zum Beispiel Berührung, Schmerz oder Muskelanspannung, wahrnehmen und weiterleiten zu können, ist ein grundlegender Vorgang des Körpers, der für das Überleben der Zellen und die Vermeidung von Gewebeschädigungen erforderlich ist. Wirbeltiere können diese Reize durch spezielle Zellen, den somatosensorischen Neuronen, im peripheren Nervensystem erkennen. Es ist allgemein bekannt, dass das periphere Nervensystem aus vielen verschiedenen Arten von Neuronen besteht, jedoch ist nicht vollständig geklärt wie sie entstehen und wie sie ihre funktionalen Fähigkeiten erlangen.

Obwohl die Schmerzwahrnehmung ein anpassungsfähiges Alarmsystem darstellt, welches für den Körper möglicherweise gefährliche Signale erkennt, ist ein andauernder Schmerz ein „Falschalarm“ und es gibt nur wenige, wenn überhaupt, wirksame Medikamente, um chronische Schmerzen zu behandeln. Daher ist es wichtig, eine genauere Erkenntnis zu bekommen, wie humane schmerz-sensitive Neurone entstehen und wie Schmerzsignale übertragen werden, denn fast alles, was bisher über Schmerz oder Schmerzwahrnehmung bekannt ist, basiert auf Studien mit Tieren. Obwohl Tiermodelle als Grundlage zur Erforschung der Ursachen, Entstehung und des Verlaufs von Krankheiten gedient haben, gibt es immer mehr Hinweise darauf, dass das Übertragen der Ergebnisse dieser Tierstudien auf den menschlichen Organismus schwieriger ist als erwartet.

Das Ziel dieser Dissertation war es, ein Differenzierungsprotokoll zu etablieren um humane embryonale Stammzellen in funktionale Nozizeptoren zu differenzieren. Eine transiente Überexpression des Transkriptionsfaktors Neurogenin 1 (NGN1), der bekannt dafür war, Neurogenese zu induzieren und die Differenzierung von Nozizeptoren in der Maus zu vermitteln, war ausreichend um periphere, neuronale Vorläuferzellen in primäre sensorische Neurone mit nozizeptiven Eigenschaften zu differenzieren. Differenzierte Zellen wurden anhand von kalziumbasierten Bildgebungsverfahren, Immunhistochemie, *in situ*-Hybridisierung, quantitativer PCR und elektrophysiologischer Ableitungen charakterisiert, was ihre nozizeptiven Eigenschaften bestätigte. Um zu überprüfen, ob Stammzell-abgeleitete Nozizeptoren physiologisch relevant sind und sie den humanen *in vivo* Nozizeptoren entsprechen, wurden sie mit humanem *post-mortem* Hinterwurzelganglion-Gewebe (DRG-Gewebe) verglichen, wobei ein ähnliches Markergen-Profil zu erkennen war. Eine Vergleichsstudie zwischen Mensch und Maus DRG-Gewebe zeigte, dass bereits auf Ebene der primären sensorischen Neuronen molekulare Unterschiede existieren, die bei der Entwicklung neuer Schmerzmedikamente in Betracht gezogen werden müssen.

Darüber hinaus waren wir daran interessiert, welche Rolle PIEZO2 in sensorischen Neuronen spielt. In Tierstudien konnte gezeigt werden, dass PIEZO2, ein großes Transmembranprotein, als einer der „Haupt-Überträger“ von sanften mechanischen Reizen dient, und wir konnten bestätigen, dass PIEZO2 auch für die Mechanotransduktion in humanen Stammzell-abgeleiteten Tastrezeptoren

erforderlich ist. Bisher war jedoch ungewiss, ob PIEZO2 auch eine Rolle bei der Transduktion von schmerzhaften mechanischen Reizen spielt. PIEZO2-defiziente Nozizeptoren zeigten keine schnell adaptierenden, mechanisch-aktivierbaren Ströme (zumindest keine, die man üblicherweise mit einer motorgetriebenen Sonde misst), was darauf hindeutete, dass PIEZO2 auch für die Mechanotransduktion in differenzierten Nozizeptoren notwendig ist.

Des Weiteren suchten wir mit Hilfe einer humanen Protein-Tag markierten PIEZO2 Stammzelllinie nach Interaktionspartnern von PIEZO2, die an der humanen PIEZO2-vermittelten sensorischen Mechanotransduktion beteiligt sind.

Das Ergebnis dieser Studie ermöglicht es uns, Unterschiede und Gemeinsamkeiten zwischen Mensch und Maus Nozizeptoren zu identifizieren und dieses Differenzierungsprotokoll als Grundlage weiterer Differenzierungsprotokolle zu nutzen, um endlich ein Modellsystem bereitzustellen um Schmerz und humane Schmerz-Transduktion in-vitro untersuchen zu können.

Table of contents

Acknowledgements ..... **I**
Summary ..... **III**
Zusammenfassung ..... **V**
Table of contents ..... **VII**
1 Introduction **1**
1.1 Aspects of pain and pain perception 1
1.1.1 Primary sensory nociceptors and the pain pathway 1
1.1.2 Primary sensory neuron development 3
1.1.3 Primary sensory neuron subtype diversification 5
1.2 Molecular components of the mammalian nociceptor system 9
1.2.1 Voltage-gated sodium channels 9
1.2.2 Transient receptor potential channels 10
1.2.3 PIEZO proteins 13
1.3 Model systems to study signaling of painful stimuli 16
1.3.1 Animal models of pain 16
1.3.2 Human stem cells as a model system to study responses to stimuli that can elicit pain 17
1.3.3 Human DRG tissue as a model system to study molecular components of pain 20
2 Aims of the study **23**
3 Materials **24**
3.1 General Chemicals 24
3.2 Buffers and Solutions 27
3.3 Enzymes and Molecular Weight Markers 32
3.4 Bacteria Strains 32
3.5 Plasmids and Vector Backbones 32
3.6 Cell Lines 33
3.7 Cell Culture Media 33
3.8 Oligonucleotides 34
3.9 Commercial Kits 36
3.10 Antibodies 36
3.11 Equipment 37
4. Methods **39**
4.1 Molecular Biology 39
4.1.1 Preparation of Genomic DNA 39
4.1.2 Polymerase Chain Reaction (PCR) 39
4.1.3 Restriction Digest 40
4.1.4 Gel purification 40

4.1.5 Ligation 40
4.1.6 Phenol/Chloroform/Isoamylalcohol extraction and microdialysis 41
4.1.7 Transformation of Electrocompetent E. coli 41
4.1.8 Minipreparation of Plasmid-DNA 41
4.1.9 Midipreparation of Plasmid DNA 42
4.1.10 Sequencing 42
4.1.11 Riboprobe synthesis (In situ probe synthesis) 42
4.1.12 RNA extraction and cDNA synthesis 43
4.2 Cell Culture 44
4.2.1 Cultivation and Splitting of human embryonic stem cells (hESCs) 44
4.2.2 Genetic modification of human embryonic stem cells by the tag-PIEZO2 targeting vector 44
4.2.3 Picking of Embryonic Stem Cell Clones 45
4.2.4 Southern Blot 45
4.2.5 Differentiation of hESCs into NCLCs 46
4.2.6 Lentivirus production and Lentiviral infection of NCLCs 46
4.2.7 Differentiation of infected NCCs into nociceptive neurons 47
4.2.8 Splitting of differentiating sensory neurons 47
4.2.9 Transient transfection of HEK 293T cells 47
4.2.10 Immunoprecipitation 48
4.3 Animals 49
4.4 Human Donors 49
4.5 Experimental analyses of differentiated neurons or human and mouse tissue 50
4.5.1 Immunohistochemistry 50
4.5.2 In Situ Hybridization 50
4.5.3 Calcium Imaging 51
4.5.4 Real-Time (quantitative) PCR 52
4.5.5 Electrophysiological Recordings done by Dr. Jörg Pohle 54
4.6 Data Analysis 54
4.6.1 Image acquisition and quantification analysis 54
4.6.2 Area distribution analysis 54
4.6.3 Signal intensity analysis 55
4.6.4 Statistical analysis 55
5. Results 56
5.1 Establishing a differentiation protocol for stem cell-derived nociceptors 57
5.1.1 TRKA overexpression 57
5.1.2 RUNX1 overexpression 59
5.1.3 NGN1 overexpression 60
5.1.4 NGN1/RUNX1 overexpression 65

5.1.5 Overexpression of 5 transcription factors (based on Wainger et al., 2015) 66
5.1.6 Simplification I of the Woolf protocol: overexpression of 3 factors 68
5.1.7 Simplification II of the Woolf protocol: overexpression of 1 factor 70
5.1.8 Verification of the TRKA-tomato reporter line 73
5.2 Final differentiation protocol and characterization of stem cell-derived nociceptors 75
5.2.1 Final differentiation protocol 75
5.2.2 Characterization of stem cell-derived nociceptors - Immunostainings 79
5.2.3 Neurotrophin receptor expression in differentiated nociceptors 81
5.2.4 RET expression in differentiated nociceptors 83
5.2.5 Sodium channel expression in differentiated nociceptors 85
5.2.6 Electrophysiological analysis of differentiated nociceptors (done by Dr. Jörg Pohle) 86
5.3 Comparison of human and mouse DRG neurons 88
5.3.1 Optimizing in situ hybridization protocol for human tissue 88
5.3.2 Neurotrophin receptor expression in human and mouse DRG tissue 89
5.3.3 Ret expression in human/mouse DRG tissue 92
5.3.4 NF200 expression in human and mouse DRG tissue 94
5.3.5 Sodium channel expression in human/mouse DRG tissue 95
5.3.6 TRP channel expression in human/mouse DRG tissue 96
5.4 Role of PIEZO2 in stem cell-derived nociceptors 99
5.5 Additional results: Generation and differentiation of a PIEZO2-tagged stem cell line 103
6. Discussion 109
6.1 hESC-derived neurons and comparison to human and mouse DRG 109
6.2 What can differentiated nociceptors be used for? - A translational approach 114
6.3 Why initial protocols did not work 117
6.4 Mechanotransduction of nociceptors and the role of PIEZO2 120
6.5 Accessory proteins of PIEZO2 and targeting strategies 123
7. Conclusion 126
8. References i
I. Abbreviations xviii
II. Units xx
III Nomenclature xxi

1 Introduction

1.1 Aspects of pain and pain perception

1.1.1 Primary sensory nociceptors and the pain pathway

Due to its uncomfortable character, pain or pain sensation is associated with a negative sensory and emotional experience that we want to avoid. However, the capability to perceive potentially harmful stimuli is a fundamental property of the body, which alerts us to tissue damage and provokes protective reflexes. Patients carrying mutations that lead to complete pain insensitivity do not develop adequate protective behaviors and they regularly suffer from bone fractures, burn injuries or other lesions that restrict their quality of life dramatically (Indo, 2001; Indo et al., 2001; Mardy et al., 2001; Verpoorten et al., 2006).

In contrast to this crucial alarm system, hypersensitivity caused by changes in the pain pathway can also lead to persistent and chronic pain, in which sensory inputs are misinterpreted and therefore harmful for the organism. Nevertheless, to a certain extent, hypersensitivity is also present after normal tissue damage such as sunburn, to protect the already injured tissue and to prevent further damage. This phenomenon, where under normal conditions an innocuous stimulus, such as a light brush with a feather, can already trigger pain, is defined as allodynia. The effect where an already noxious stimulus evokes more intensive pain is known as hyperalgesia (Basbaum et al., 2009). The process of pain perception is initiated by the detection of a variety of internal or external sensory stimuli such as temperature, mechanical forces or chemical irritants by a subset of primary sensory neuronal fibers (Basbaum, A.I. and Jessell, T., 2000; Julius and Basbaum, 2001).

More than 100 years ago, Charles Sherrington had already described specific types of cells, today known as nociceptors, activated by noxious stimuli, which could lead to tissue damage, pain sensation, and protective withdrawal reflexes (Sherrington, 1903).

Primary afferent nociceptors innervate the surface of the skin, joints, muscles and inner organs such as bladder, gut or the digestive tract, where they get activated by sensory stimuli. Primary sensory neurons, with their cell bodies in the trigeminal ganglia (TG) or in the dorsal root ganglia (DRG) (innervating respectively the face or the rest of the body) have a pseudo-unipolar morphology. The axon bifurcates and sends the efferent branch to the peripheral tissue and the afferent branch to the spinal cord, where it synapses on second-order neurons. Every pair of DRG is located contiguously to the dorsal nerve root at each level of the spinal column (Woolf and Ma, 2007).

Once primary sensory neurons, also known as first-order neurons, get activated by a certain stimulus, the sensory signal is converted into an electrical stimulus, the membrane potential depolarizes, and an action potential is generated. Axonal processes of the first-order primary afferent neuron, that resides with its cell body in the DRG, enters the spinal cord via the dorsal horn. Nociceptive information is conducted to the superficial laminae I and II as well as to lamina V of the dorsal horn of the spinal cord (Braz et al., 2005). There, nociceptive fibers branch and synapse on second-order neurons that convey the signal through the medulla, pons and midbrain up to the thalamus. From this point on, information is transferred to different areas of the primary somatosensory cortex, the cingulate and insular cortices or the amygdala, where the stimulus is processed and analyzed (Basbaum et al., 2009; Bear et al., Hunt and Mantyh, 2001) (Fig. 1).

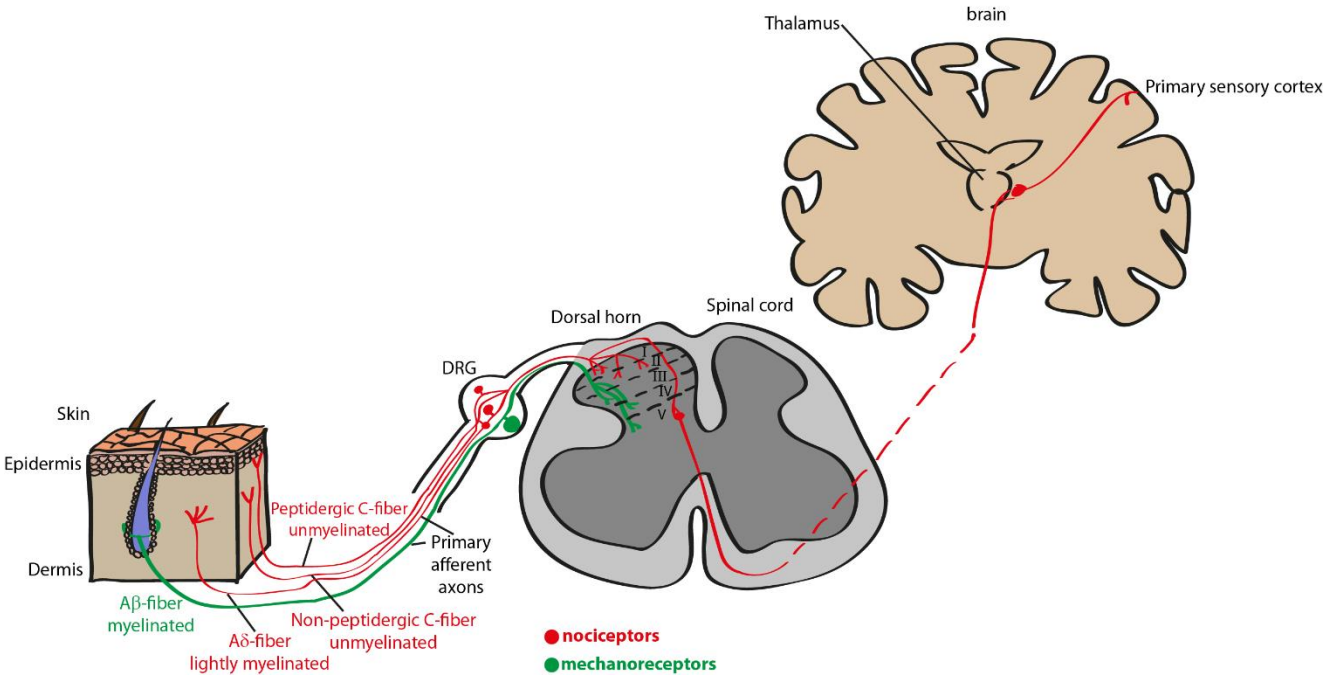

Fig. 1: Scheme of the pain pathway and primary sensory neurons in the skin

Primary sensory afferents, sensing noxious stimuli such as temperature, mechanical forces or chemical irritants innervate the skin. Sensory inputs are transmitted through the axon of the primary sensory neurons to their cell bodies in the DRG, and then further to the dorsal horn of the spinal cord, where information is branched on second-order neurons. Then the signal is conveyed to higher brain centers (Redrawn and modified from Basbaum et al., 2009).

Based on functional and anatomical characteristics, primary sensory neurons can be classified into three groups: Aβ, Aδ and C-fibers. Whereas heavily myelinated, fast-conduction Aβ-fibers are found in large diameter low-threshold mechanoreceptors that detect innocuous mechanical stimuli, lightly myelinated Aδ-fibers and unmyelinated, slowly conducting C-fibers are mainly found in small diameter nociceptors (Julius and Basbaum, 2001). The well-localized “first” pain is thought to be mediated by lightly myelinated Aδ-fibers, while the unmyelinated C-fibers seem to be

responsible for the poor-localized “second” pain impulse (Basbaum et al., 2009; Julius and Basbaum, 2001).

In addition to the anatomical classification, primary sensory neurons can also be neurochemically distinguished, and molecular characterization of small-diameter nociceptive neurons demonstrated their tremendous heterogeneity (Snider and McMahon, 1998; Stucky and Lewin, 1999). Already in the early 1980s, Nagy and Hunt detected two distinct small-diameter sensory neuronal subpopulations: one group of neurons that releases neuropeptides such as substance P (SP) or the calcitonin-gene related neuropeptide (CGRP) and another group that binds the plant glycoprotein isolectin B_4 (IB_4) and lacks peptide expression (Nagy and Hunt, 1982; Silverman and Kruger, 1990).

Today, it is well accepted that developing DRG neurons require neurotrophins for survival and differentiation (Silos-Santiago et al., 1995a; Zylka et al., 2005) and that, at around E15, about 70-80% of all primary sensory neurons express the tyrosine receptor kinase A (TRKA), the receptor for the nerve growth factor (NGF) (Ernsberger, 2009; Molliver and Snider, 1997a; White et al., 1996). Later during development, half of the small diameter neurons downregulate TRKA expression and become sensitive to the glial cell line-derived neurotrophic factor (GDNF) and start to express its receptor RET (Molliver et al., 1997). Remaining TRKA-expressing neurons co-express the already mentioned neuropeptides CGRP and SP and are therefore known as peptidergic nociceptors. This group of neurons projects to the superficial layers of the dorsal spinal cord, to lamina I and outer lamina II. The other group of nociceptors, that downregulates TRKA and upregulates RET, lacks neuropeptide expression and is therefore referred to as non-peptidergic nociceptors. It has been demonstrated that this subpopulation projects to the inner part of lamina II (Molliver et al., 1995; Silverman and Kruger, 1990).

Although electrophysiological analysis of unmyelinated primary sensory neurons (C-fibers) showed that the majority of the DRG neurons are polymodal and about 70% of the nociceptors responded to different painful stimuli such as heat, cold or noxious mechanical forces (Cain et al., 2001; Lawson et al., 2008; Perl, 1996), there is also evidence that primary sensory neuronal subpopulations exist that exclusively convey behavioral responses to specific painful stimuli (Cavanaugh et al., 2009).

1.1.2 Primary sensory neuron development

As already described previously, primary sensory neurons represent a very heterogeneous cell population with the ability to detect and transduce various kinds of internal or external stimuli (Lallemend and Ernfors, 2012). A central question that remains to be answered is how neuronal

progenitor cells are driven to adopt a specific cell fate and how they develop their functional and molecular properties. Due to the fact that primary sensory neurons derive from the neural crest, this group of cells is an attractive model system for studying neuronal diversification during development (Marmigère and Ernfors, 2007).

Neural crest cells (NCCs) derive from the embryonic ectodermal lineage and, after gastrulation, are located at the border of the neural plate and the ectoderm. During neurulation, when the neural tube is formed, neural folds (borders of the neural plate) merge and NCCs are generated at the dorsal part of the neural tube. Under the influence of the signaling molecules WNT and the morphogens BMP, which are required for WNT expression maintenance, dorsal neural tube NCCs start to migrate out and give rise to many different cell populations such as epidermal pigment cells, connective tissue cells, smooth muscle cells and adipose tissue cells, facial cartilage cells as well as cells of the peripheral nervous system (*e.g*. sensory neurons, to which I will refer later), neuroglial cells or Schwann cells (Fig. 2) (García-Castro et al., 2002). At this stage, NCCs undergo an epithelial-to-mesenchymal (ETM) transition, which is influenced by the downregulation of cytoskeleton molecules such as N-cadherin and cadherin 6, changing the cell adhesion characteristics to become versatile and allow NCCs to migrate out (in mice around E8.5-E10) (Bronner-Fraser et al., 1992; Nakagawa and Takeichi, 1998; Newgreen and Gooday, 1985).

In response to specific signaling molecules, trunk neural crest cells start to delaminate from the dorsal neural tube and migrate between the dermamyotome and the neural tube in chain-like structures to generate the dorsal root ganglia (Fig. 2) (Marmigère and Ernfors, 2007; Serbedzija et al., 1990; Teillet et al., 1987).

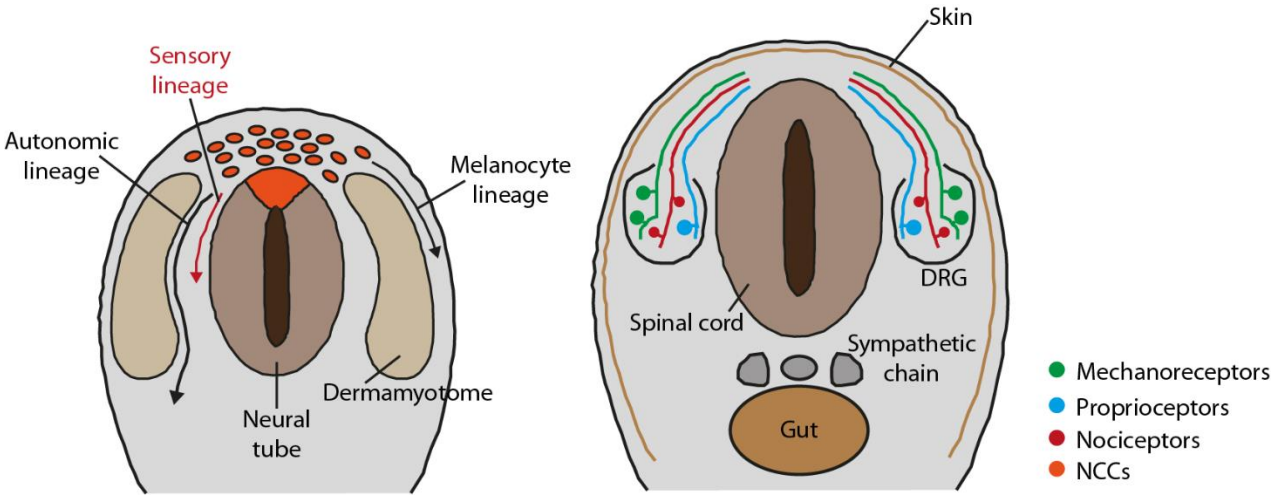

Fig. 2: Neural crest cell migration and sensory neurogenesis

Neural crest cells delaminate from the dorsal neural tube and migrate ventrally to differentiate into various different cell types (sensory lineage, autonomic lineage or melanocyte lineage). After migration, developing sensory neurons coalescent into DRG and differentiate into mature neurons with a nociceptive, mechanoreceptive and proprioceptive phenotype (Redrawn and modified from Marmigère and Ernfors, 2007).

Primary sensory neurogenesis arises in three consecutive waves. The first two waves have been demonstrated by retroviral tracing experiments of NCCs in chicken and mouse while the third wave of migrating cells has been proposed to arise from the so-called boundary cap cells (Frank and Sanes, 1991; Ma et al., 1999a; Maro et al., 2004). The boundary cap is an organized group of cells placed at the border between CNS and PNS that contains multipotent NCCs (Hjerling-Leffler et al., 2005).

Developmental studies in chicken revealed that, during the first wave of neurogenesis, approximately one-third of the NCCs migrate out from the neural tube and differentiate into large diameter proprioceptive and mechanoreceptive neurons, located in the ventrolateral DRG. It is proposed that during this period of neurogenesis in chicken each NCC gives rise to approximately 3 neurons. The other two-thirds of NCCs, generating approximately 36 neurons per NCC, delaminate during the second wave of neurogenesis and differentiate into small diameter TRKA-positive nociceptors, located in the dorsomedial DRG as well as into large diameter neurons of the ventrolateral DRG (Frank and Sanes, 1991; Rifkin et al., 2000).

During the third wave of neurogenesis, where NCC-derived boundary cap cells migrate, mainly small diameter TRKA-positive neurons with nociceptive phenotypes are generated (Maro et al., 2004). These data show that the differentiation of primary sensory neurons already initiates early during development when NCCs start to migrate out.

1.1.3 Primary sensory neuron subtype diversification

Sensory neuronal cell type diversification is thought to be regulated by specific combinatorial gene expression cascades and external cues. During NCC migration, neurogenesis is induced by the expression of the pro-neural basic helix-loop-helix (bHLH) transcription factors neurogenin 1 (NGN1) or neurogenin 2 (NGN2) which are induced by canonical WNT pathway signaling (Burstyn-Cohen et al., 2004; Hari et al., 2002; Ma et al., 1999a) (Fig. 3). While NGN2 is already expressed in early migrating mouse NCCs from E8.75-E9 to E10.5, NGN1 is only detectable after migration, when cells already started to condensate into ganglia, around E9-E9.5 to E13 (Ma et al., 1999a; Sommer et al., 1996). The two waves of neurogenin expression roughly correlate with the two waves of neurogenesis: a first NGN2-expressing wave, of migrating cells, from which mainly large diameter TRKC/TRKB-positive proprioceptive and mechanoreceptive neurons are generated, and a second NGN1-expressing wave, which mainly gives rise to small diameter TRKA-positive neurons with nociceptive properties (see chapter 1.2.2; Fig. 3).

Lineage tracing experiments in chicken and mouse KO-studies demonstrated that neurogenin expression is required at different time-dependent developmental stages to allow the generation of

different primary sensory neuronal subtypes. While NGN2 expression is only essential during the early developmental phase, NGN1 expression is important for early and late phases of sensory neurogenesis. Mouse *Ngn1*-KO studies around E15-E16 revealed a tremendous reduction of cervical DRG sizes due to the complete loss of TRKA-positive neurons and a reduced number of TRKB/TRKC-positive neurons. In contrast, a loss of NGN2 could be compensated by NGN1 and no significant reduction of a specific subpopulation was detectable (Ma et al., 1999a).

Shortly after neurogenesis induction, cells start to express the insulin gene enhancer protein ISLET1 (a LIM-homeodomain transcription factor) and the brain-specific homeobox/POU domain protein 3A (BRN3A), that together terminate the expression of the bHLH transcription factors NGN1 and NGN2 (Eng et al., 2001, 2004, 2007; Sun et al., 2008). Essentially, all primary sensory neurons express BRN3A and ISLET1 at high levels during development and maturity. It was demonstrated that both proteins are important for further sensory specific gene expression patterns, including the expression of neurotrophin receptors such as the tropomyosin related kinases (TRK receptors) or the Runt-related transcription factors RUNX1 and RUNX3 (Dykes et al., 2010, 2011; Huang et al., 1999; Lei et al., 2006; Ma et al., 2003; Sun et al., 2008). A Cre-mediated conditional *Islet1*-KO in sensory neurons decreased the number of TRKA, TRKB and RUNX1-positive neurons, markers for pain and touch-mediating neurons, whereas markers for proprioceptive neurons, TRKC and RUNX3, were not altered. Furthermore, it was also shown that, during early developmental stages, ISLET1 is required for the suppression of hindbrain or spinal cord-specific transcription factors (Sun et al., 2008).

A combined *Islet1/Brn3a* double-KO caused massive defects in target innervation and axon growth. DRG neurons remained in an undifferentiated developmental state and failed to control downstream gene programs (Dykes et al., 2011).

From animal studies, it is known that neurotrophin receptors (TRKA, TRKB and TRKC) are broadly expressed during development. While TRKB and TRKC are expressed in up to 75% of differentiating sensory neurons at around E11-E11.5, TRKA expression is even broader: at around E13, approximately 80% of all developing neurons are TRKA-positive (Ernsberger, 2009; Molliver and Snider, 1997b; White et al., 1996). Later during differentiation, neurotrophin receptor expression gets more defined and TRK receptors can even be used for categorizing different sensory neuronal subpopulations. While during mouse development (if this is also the case in humans is not entirely clear) essentially all nociceptive neurons express TRKA, at later phases cells separate into two subgroups, known as peptidergic nociceptors, that continuously express TRKA and signaling molecules such as SP or CGRP, and the non-peptidergic nociceptor subpopulation, downregulating TRKA expression and upregulating the tyrosine receptor kinase RET (Molliver et al., 1997). KO-studies, in which the NGF/TRKA signaling was disturbed, have shown that about 80% of the DRG neurons are lost and approximately 50% of them are small or medium-sized

neurons, expressing the nociceptive markers TRKA as well as the calcitonin gene-related peptide (CGRP) (Silos-Santiago, 1995; Silos-Santiago et al., 1995b).

Another important gene family known to be involved in primary sensory neuron subtype diversification is the Runt domain transcription factor family. During early sensory neuron development in mouse, RUNX1 is broadly expressed and from E14.5 to P0 more than 80% of the TRKA-positive neurons co-express RUNX1. Later during development RUNX1 expression gets more defined and around P30, RUNX1 is restricted to non-peptidergic TRKA-negative neurons, that start to upregulate RET (Chen et al., 2006). In mice lacking the RUNX1 transcription factor in the PNS, the developmental transition of TRKA-positive neurons into RET-expressing cells (the non-peptidergic nociceptive subpopulation) was disturbed. Furthermore, it was shown that RUNX1 is an essential transcription factor for the expression of many different nociceptive ion channels and sensory membrane receptors such as transient receptor potential channels (TRP channels) or voltage-gated sodium channels (Nav channels) (Chen et al., 2006).

In contrast, RUNX3 is expressed in 85% of TRKC-positive neurons (E12) and regulates the segregation of TRKB and TRKC-positive neurons by repressing TRKB expression in proprioceptive TRKC-expressing neurons (Kramer et al., 2006).

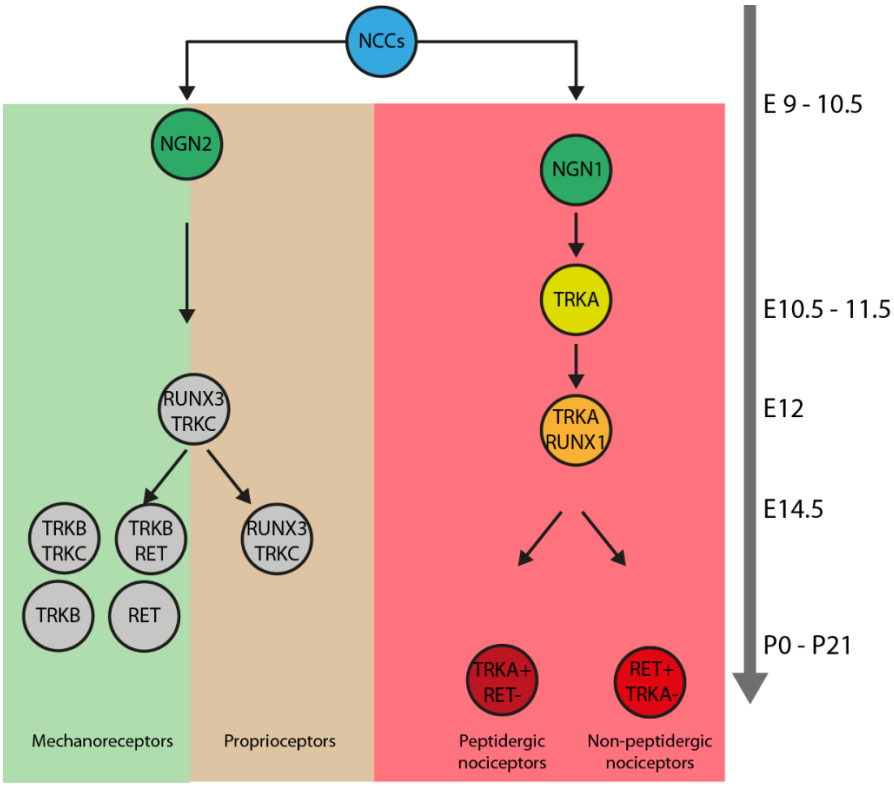

Fig. 3: Primary sensory neuron diversification during development and differentiation into the main lineages

Scheme of mouse DRG neuron diversification during development and the different main lineages that are generated. During NCC migration, neurogenesis is induced by the expression of the transcription factors NGN1 and NGN2. While NGN2 mediates the generation of mostly large TRKB/TRKC-positive mechanoreceptive or proprioceptive neurons, NGN1 mediates the generation of mainly small nociceptive neurons. Shortly after neurogenesis induction, all developing nociceptors start to express TRKA and also the transcription factor RUNX1. Together, they regulate further gene expression programs and sensory neuron diversification (Redrawn and modified from Lallemend and Ernfors, 2012).

Although different key factors important for sensory neuron diversification have been identified and were used for categorizing main neuronal subpopulations (as TRK receptors or RUNX transcription factors), recent transcriptome analysis of single DRG neurons revealed that primary sensory neuronal diversification is even more sophisticated than previously expected, and the three main neuronal subtypes (mechanoreceptors, proprioceptors and nociceptors) can be further subdivided and specified (Li et al., 2016b; Usoskin et al., 2015)

1.2 Molecular components of the mammalian nociceptor system

1.2.1 Voltage-gated sodium channels

Voltage-gated sodium channels (VGSCs) are large integral membrane proteins, crucial for initiating and propagating action potentials in neuronal cells as well as in non-neuronal cells of flies, squid, jellyfish or higher vertebrates (Anderson and Greenberg, 2001; Goldin, 2002). In mammals, the voltage-gated sodium channel family consists of 9 different members, referred to as Nav1.1-Nav1.9. Each functional protein complex includes a large α-subunit (Nav1.1-Nav1.9), of around 220-260 kDa, linked to one or more smaller β-subunits (β1-β4) of around 33-36 kDa (Beneski and Catterall, 1980; Catterall, 2000; Hartshorne and Catterall, 1981; Hartshorne et al., 1982).

Structural analysis of the nine different α-subunits demonstrated a similar organization in four subdomains (I-IV), linked by three intracellular loops (L1-L3). Each subdomain can be further subdivided into six transmembrane α-helices (S1-S6), carrying positively charged amino acids as a voltage sensor in segment S4 of each domain. While the extracellular end of the ion-selective pore is formed by the loop between S5-S6, the intracellular end of the pore is generated by the S6 α-helices (Fig. 4) (Yu and Catterall, 2003). Nuclear magnetic resonance (NMR) analysis proposed a mechanism by which the IFM motif (Ile-Phe-Met motif) in the intracellular loop L3 interacts with the pore-forming sequences and thereupon blocks the ion-selective channel during the inactivation phase (Rohl et al., 1999).

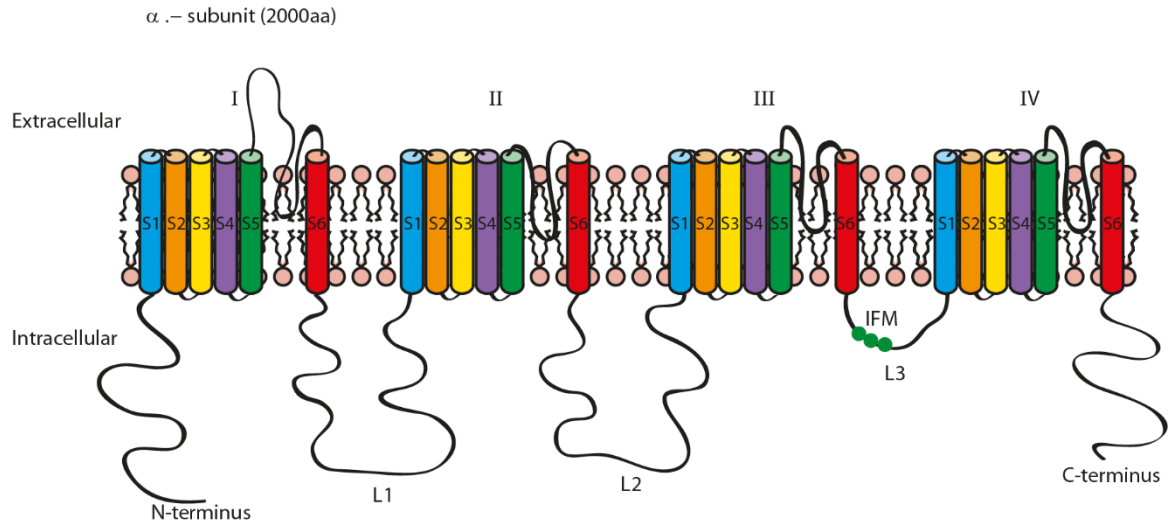

Fig. 4: Schematic representation of Nav α -subunit

Predicted structure of the voltage-gated sodium channel α-subunits with four similar subdomains (I-IV), linked by three intracellular loops (L1-L3). Each subdomain consists of six transmembrane α-helices (S1-S6) The extracellular end of the pore is formed by the loop between S5-S6, the intracellular end of the pore is generated by the S6 α-helices. The IFM motif (Ile-Phe-Met motif) in the intracellular loop L3 interacts with the pore-forming sequences and blocks the channel during the inactivation phase (Redrawn and modified from Dib-Hajj et al., 2002).

Despite structural similarities and more than 50% sequence identity between different human and rodent α-subunits, VGSCs can be classified by their sensitivity to tetrodotoxin (TTX), a puffer fish-derived toxin. While Nav1.1-1.4 and Nav1.6-Nav1.7 are sensitive to TTX and can be blocked by only nanomolar concentrations, Nav1.5 and Nav1.8-Nav1.9 are TTX resistant. Human evolutionary clustering analysis demonstrated that all three TTX-resistant genes are located in one chromosome (3p21-24) and most likely one mutational event, changing one amino acid in domain 1 (loop between S5-S6) from tyrosine to serine (Nav1.8, Nav1.9) or cysteine (Nav1.5), resulted in TTX resistance (Goldin et al., 2000; Satin et al., 1992; Sivilotti et al., 1997).

Three VGSCs, Nav1.7, Nav1.8 and Nav1.9, are most abundantly expressed in primary sensory neurons of the peripheral nervous system and mutations in these channels have been associated with a variety of heritable pain disorders (Cummins et al., 2007; Kanellopoulos and Matsuyama, 2016). While Nav1.7 is broadly expressed in different types of peripheral neurons, Nav1.8 and Nav1.9 are more restricted to small diameter nociceptive neurons (Amaya et al., 2000; Toledo-Aral et al., 1997).

Mutations in the gene encoding Nav1.7 are linked to several syndromes, such as inherited erythromelalgia (an agonizing pain syndrome in the distal limbs in response to non-painful stimuli), paroxysmal extreme pain disorder, and congenital insensitivity to pain (Ahmad et al., 2007; Cummins et al., 2004; Fertleman et al., 2006; Yang et al., 2004). While gain-of-function mutations of Nav1.8 cause predominantly small fiber neuropathies, Zhang and colleagues demonstrated that mutations in the Nav1.9 channel can lead to an heritable form of episodic pain (Faber et al., 2012; Zhang et al., 2013a).

1.2.2 Transient receptor potential channels

Transient receptor potential (TRP) channels are large transmembrane cation channels that have been first described in the fruit fly visual system, where they depolarize photoreceptors in response to a light stimulus. Mutations in the *Drosophila* trp gene caused only transient light responses to persistent light, indicating that the phototransduction cascade was interrupted (Cosens and Manning, 1969; Minke et al., 1975; Montell and Rubin, 1989).

In mammals, the first TRP channel homologs were identified in 1995, followed by the discovery of more than 50 different TRP channel proteins in various species such as insects, fish, worms or mammals. Nowadays, 28 *TRP*-like genes have been described in mice and 27 in humans (Petersen et al., 1995; Voets et al., 2005; Vriens et al., 2004; Wes et al., 1995). TRP channels belong to a large gene family with various physiological functions and differing in their selectivity for certain cations.

Based on sequence similarity, mammalian TRP channels are grouped into seven different subfamilies, designated after their first discovered family member: the closest *Drosophila melanogaster* homolog TRPC (Canonical), the TRPV (Vanilloid), the TRPM (Melastatin), the TRPA (Ankyrin), the TRPP (Polycystin), TRPML (Mucolipin) and the TRPN (No mechanoreceptor potential C) subclasses.

Since the classification of TRP channel proteins depends on sequence similarities (not necessarily reflecting functional similarities between sequence-homologous TRP ion channels), TRP channel members within one subgroup can have distinct functionalities, whereas family members from diverse subgroups can also share functional characteristics, as illustrated by the thermosensitive TRP channels that belong to different subcategories (TRPA, TRPM and TRPV).

Although initially mammalian TRP channels were thought to be the functional counterparts of the *Drosophila melanogaster* trp protein, since the discovery of TRPV1, a calcium-permeable channel activated by capsaicin, the burning component of the chili peppers, and by a noxious heat stimulus above 43°C, this view changed (Caterina et al., 1997). Nowadays it is broadly accepted that TRP channels are biological sensors that can be activated by a variety of different painful as well as non-painful stimuli such as chemicals, mechanical forces or different temperatures and serve as polymodal receptors.

Besides TRPV1 as a thermosensitive channel that is mainly expressed in small diameter DRG neurons, 5 additional temperature-activated TRP channels, also from different subclasses, have been specified so far (Patapoutian et al., 2003; Tominaga, 2007). While TRPA1 and TRPM8 seem to be active at lower temperatures of <17°C and 8-26°C respectively (McKemy et al., 2002; Peier et al., 2002; Story et al., 2003), heat-sensitive channels from the TRPV subgroup (TRPV1, TRPV2, TRPV3 and TRPV4) respond to warm or hot temperatures (Caterina et al., 1997, 1999; Güler et al., 2002; Smith et al., 2002; Xu et al., 2002). As polymodal receptors, thermosensitive TRP channels are activated not only by different temperatures but also by other chemicals or botanical components (Fig. 5).

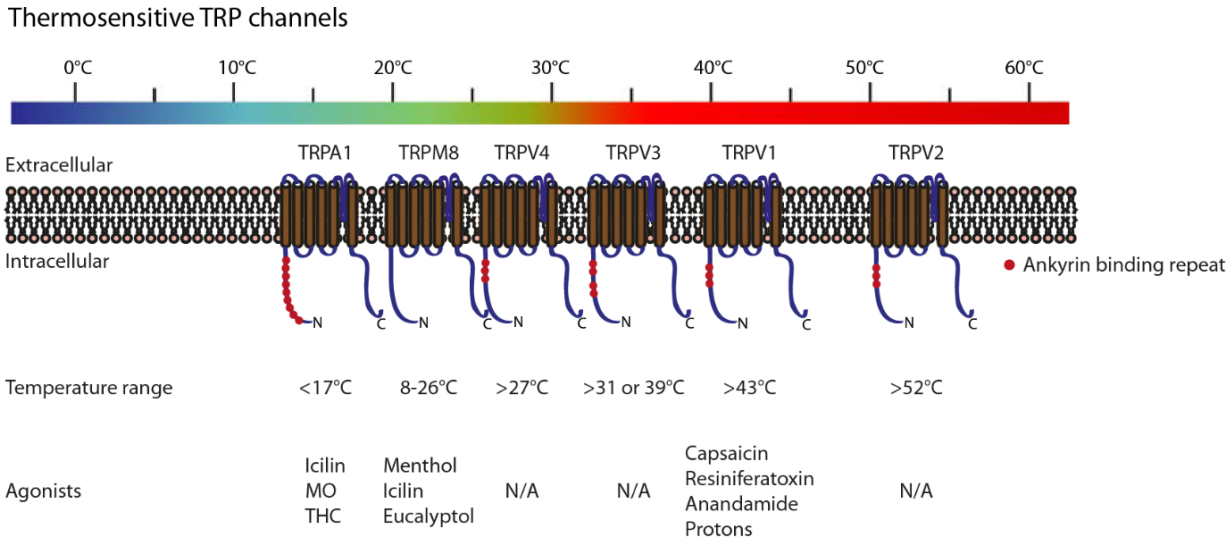

Fig. 5: Schematic representation of different thermosensitive TRP channels

Representation of the different thermosensitive TRP channels, functioning in temperatures from noxious cold to noxious heat. Predicted membrane topology is composed of six transmembrane domains and a pore region between transmembrane domains 5 and 6. Both terminal ends (C-terminus and N-terminus) are cytosolic and contain various interaction domains (ankyrin repeats, or PDZ binding domains) to control channel gating properties and interactions with adjacent proteins (Redrawn and modified from Dhaka et al., 2006).

In addition to their original role in detecting acute thermal stimuli, more recent findings proposed that especially TRPV1 and TRPA1 channels can be sensitized during tissue injury or under inflammatory conditions and therefore serve as crucial components of the sensitization mechanism, leading to inflammatory mediator-induced hypersensitivity (Bautista et al., 2006; Carnevale and Rohacs, 2016). Peripheral sensitization, evoked by signaling molecules such as neurotransmitters, protons, cytokines, or growths factors, is described by increased responsiveness as well as reduced action potential thresholds of sensitized nociceptors, and is known to be mediated by distinct cell membrane transduction proteins that further regulate downstream pain transduction machineries (reviewed by Gangadharan and Kuner, 2013; Gold and Gebhart, 2010; Hucho and Levine, 2007; Julius and Basbaum, 2001).

Structural analysis of mammalian TRP proteins, mainly based on functional studies, proposed a prototypical structure of voltage-gated potassium channels with four similar subdomains consisting of six transmembrane domains. Both terminal ends (C-and N-terminus) are cytosolic and the pore region is formed by transmembrane domain five and six and their connecting loop (Gaudet, 2008; Kedei et al., 2001; Long et al., 2005; Owsianik et al., 2006). Cytosolic regions of different dimensions are thought to contain different regulatory domains such as ankyrin repeats or phosphorylation sites to control for channel gating and protein-protein interactions (Dhaka et al., 2006).

1.2.3 PIEZO proteins

Mechanotransduction and the PIEZO protein family

Mechanotransduction, the ability to convert mechanical stimuli into an electrical signal, is a fundamental process required for various physiological functions such as organ development, regulation of blood pressure, hearing or the perception of touch, pain or muscle movement and orientation (Cahalan et al., 2015; Corey and Hudspeth, 1979; Davis et al., 1992; Florez-Paz et al., 2016; Ranade et al., 2014a, 2014b). Since the discovery of a mechanically-activated ion channel by Corey and Hudspeth in 1979, it is broadly accepted that mechanotransduction is mediated by cation channel activities. Genetic screens in the nematode *C. elegans* or the fruit fly *Drosophila melanogaster* proposed several genes, encoding for DEG/ENaC or TRP proteins, as possible mechanosensitive ion channel candidates (Árnadóttir and Chalfie, 2010; Ernstrom and Chalfie, 2002). Furthermore, mouse studies demonstrated that mechanical stimuli as sound waves or head movements activate transmembrane channel-like proteins (TMC1 and TMC2) in the inner ear hair cells, required for mechanotransduction and vestibular functioning (Kawashima et al., 2011). Although several possible candidates have been described, it is still under debate whether these channels are directly involved in mammalian mechanotransduction.

In 2010, Coste *et al*. described a new gene family, today known as PIEZO channels (from the Greek "πίεση" (piesi), the description for pressure). Knock-down screenings of candidates, highly expressed in the mouse neuroblastoma cell line N2A, revealed that PIEZO1 (Fam38A) and its family member PIEZO2 (Fam38B) are required for mechanical-induced currents (Coste et al., 2010). In vertebrates, the PIEZO protein family consists of two family members. PIEZO proteins have also been identified in lower organisms such as *Drosophila melanogaster*, *C. elegans*, plants (1 ortholog), zebrafish (three orthologs) and protozoa (up to six orthologs) (Faucherre et al., 2013; Kamajaya et al., 2014; Kim et al., 2012; Prole and Taylor, 2013).

In mammals, PIEZO proteins are expressed in a variety of different cell types: while PIEZO1 is mainly expressed in non-neuronal tissue (kidney, lung, bladder and colon), PIEZO2 expression is primarily detectable in sensory cells such as DRG neurons or touch-sensitive Merkel cells (Coste et al., 2010; Woo et al., 2014).

Molecular structure of PIEZO proteins

PIEZO proteins are huge transmembrane proteins of about 2`500-2`800 amino acids with conserved secondary structures among different species. Initial structural analysis by various transmembrane algorithm model programs (such as TMHMM2) proposed PIEZO channels as proteins with the highest number of transmembrane domains, spanning the cell membrane between 30 and 40 times (Fig. 6A) (Coste et al., 2010; Volkers et al., 2015). Based on functional investigations showing that mechanically-activated currents can be blocked by ruthenium red, a sensitive ion-channel blocker, it was hypothesized that PIEZO proteins serve as pore-forming subdomains that assemble to form a functional membrane-bound channel. Total internal reflection microscopy (TIRF) analysis of GFP-mPIEZO1 fusion protein transfected in *Xenopus laevis* oocytes proved this hypothesis, and revealed that PIEZO proteins aggregate as tetramers, forming a functional channel with more than 100 transmembrane domains (Coste et al., 2012).

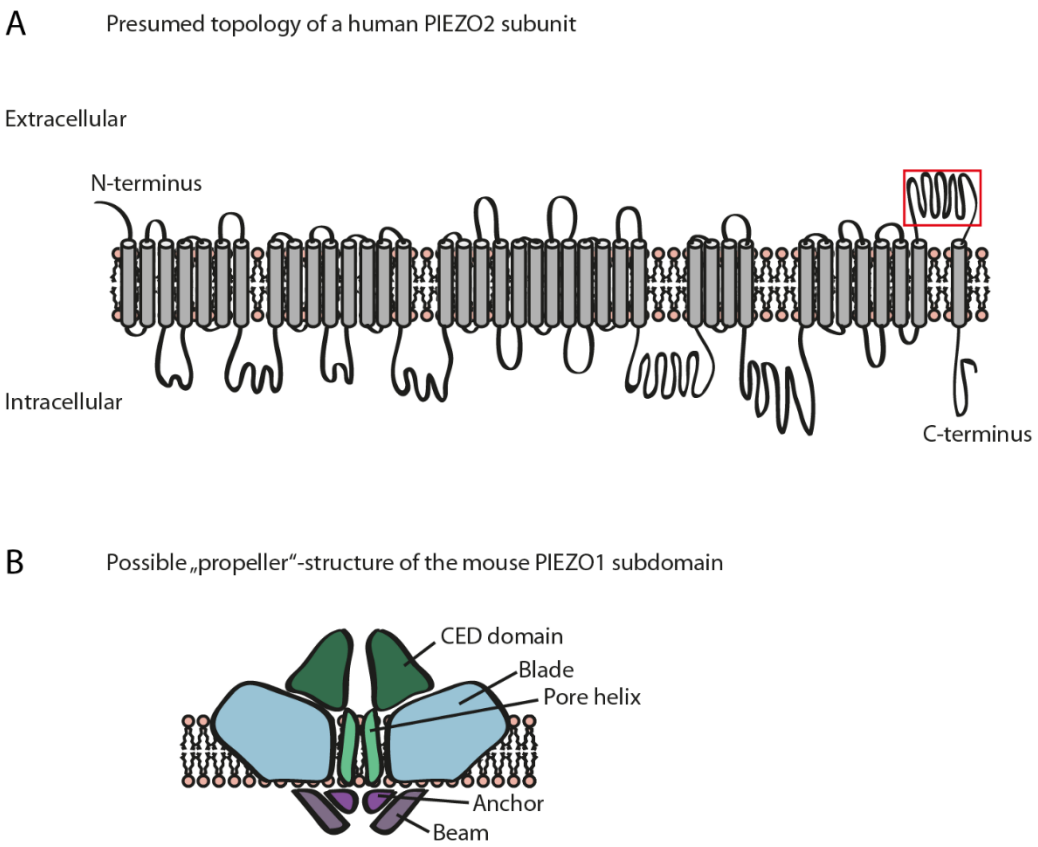

Fig. 6: The PIEZO protein

(A) Schematic representation of the initially presumed topology of the human PIEZO2 subunit and its several transmembrane domains. The red box represents the CED domain. (Redrawn and modified from Review Soattin et al., 2016).
(B) Possible structural domains of the mouse PIEZO1 channel that potentially play a role in channel gating and mechanotransduction (Redrawn and modified Wu et al., 2017).

Structural analysis for PIEZO2 is mainly based on hypothetical prediction programs (and different topology prediction models can give different results: while analysis using the Phobius program clearly showed a human PIEZO2 N-terminal signal peptide, the Signal P4.1 prediction program displayed inconclusive results). However, recently Ge *et al.* described the first overall structure of the mouse PIEZO1 channel (Ge et al., 2015a). In this study, X-ray crystallography and cryo-electron microscopy investigations showed that mPIEZO1 channels assemble as homotrimers in "propeller-like" structures (Fig. 6B). The central pore is encircled by three "blades", the intracellular beam structures (mechanically combining blades and distal ends of the transmembrane domains), the anchor-domain and the C-terminal extracellular domain (CED). Across species, the CED structure, located between the last two transmembrane domains, is highly conserved and involved in gating properties and most likely associated with the pore (Coste et al., 2015; Kamajaya et al., 2014). Based on these findings, the assumed number of transmembrane domains is markedly lower than previously predicted by topology programs and only 10-18 α-helices within PIEZO subunits seem to span the cell membrane. If a similar structure is adopted by human PIEZO2 is currently unknown.

Most ion channels are directly or indirectly coupled to interaction partners and other signaling molecules to form functional, multimeric complexes. However, initial studies with tagged-PIEZO1 showed no evidence of PIEZO-associated proteins (Coste et al., 2012). In contrast, recent findings demonstrated that the stomatin-like protein 3 (STOML3), bound to cholesterol, is involved in PIEZO channels sensitization and enhances mechanosensitivity (Poole et al., 2014; Qi et al., 2015).

Furthermore, an antibody-based purification assay of native mPIEZO2 coupled to mass spectrometry analysis identified 36 possible binding partners, and suggested pericentrin (PCNT), a protein involved in microtubule network formation, as a modulator of PIEZO2 (Narayanan et al., 2016).

The role of PIEZO2 in mouse and human primary sensory neurons

PIEZO2, displaying a rapidly-adapting ion current when mechanically stimulated, is mostly expressed in sensory tissue and shown to be involved in various physiological mechanotransduction processes. While a global PIEZO2-KO is lethal and newborn mice die shortly after birth (most likely because of respiratory defects), multiple conditional PIEZO2-KO lines have been generated and analyzed (Nonomura et al., 2017; Ranade et al., 2014b). Ranade *et al.* characterized an inducible PIEZO2-Knock-down in primary sensory neurons and in Merkel cells of adult mice. In this study, they demonstrated that PIEZO2 is the main transducer of innocuous mechanical forces with rapidly-adapting (RA) mechanically-activated currents mostly absent, and behavioral assays revealed deficits in light-touch sensation (Ranade et al., 2014b). Furthermore,

Schrenk-Siemens *et al*. confirmed that PIEZO2 is required for transducing innocuous mechanical forces and mechanically-activated currents where completely absent in human stem cell-derived low threshold mechanoreceptors (LTMRs) (Schrenk-Siemens et al., 2015).

In addition to its involvement in mechanotransduction of mechanoreceptors, it was also proposed that PIEZO2 plays a role in mediating mechanical stimuli in proprioceptors. Two independent PIEZO2-depletion studies, one in PIEZO2-deficient proprioceptive neurons of the DRG and one in neurons of the mesencephalic trigeminal nucleus (MTN) of the brainstem, revealed PIEZO2-dependent mechanically-activated currents and behavioral defects in limb coordination and balance (Florez-Paz et al., 2016; Woo et al., 2015). Moreover, Wang *et al*. implicated a role for PIEZO2 as a mechanosensor and transducer in gastrointestinal enterochromaffin cells. The inhibition or knock-down of PIEZO2 resulted in a decrease of mechanically-activated currents and thereupon in a diminished release of serotonin (Wang et al., 2017).

Although these studies revealed the crucial role PIEZO2 plays in mediating innocuous mechanical stimuli, only one study shows indications that PIEZO2 is also involved in mediating noxious mechanical stimuli (Dubin et al., 2012a). Knock-down of PIEZO2 in adult sensory neurons and Merkel cells (with a 90% reduction of the overall *Piezo2* transcript) led to a specific loss of rapidly-adapting mechanically-activated currents, whereas intermediately-adapting or slowly-adapting currents (a marker for nociceptive neurons) were not significantly affected (Ranade et al., 2014b).

PIEZO2 was not only described as being involved in rodent sensory mechanotransduction but was also associated with multiple hereditary forms of human disorders such as the Marden-Walker Syndrome, the Distal Arthrogryposis Type 5 or the Gordon Syndrome (Alisch et al., 2017; Chesler et al., 2016; Coste et al., 2013; McMillin et al., 2014; Okubo et al., 2015). Whole-exome sequencing studies of several patients with congenital contractures of the extremities, cleft palates or restricted eye movements detected various mutations in the *hPIEZO2* gene.

1.3 Model systems to study signaling of painful stimuli

1.3.1 Animal models of pain

Pain, or the sensation of pain, is described as an unpleasant experience that in general is emerged from a sensory stimulus, detected by specialized sensory neurons. The primary input itself can be modified at different levels of the pain pathway (at spinal or supraspinal levels) and, in combination with emotional experiences, pain reflects a complex, subjective feeling, which has made it challenging to specify targets for effective analgesic medications (Gangadharan and Kuner, 2013; Percie du Sert and Rice, 2014).

For many years, lower organisms and especially rodents have been used as attractive model systems to study various aspects of sensory transduction and pain, and most of the current knowledge is based on animal studies (Mogil, 2009a). Although these models serve as an indispensable tool, that helped us to provide basic insights into molecular mechanisms and the analysis of diverse pain phenotypes, not only during early development but also in the adult organism, only minor success has been achieved by translating scientific results from animal studies into clinical trials (Burma et al., 2017a; Hill, 2000; Percie du Sert and Rice, 2014). Even though opioids, one class of analgesics, are one of the most frequently prescribed and most effective compounds, they are also associated with adverse effects such as tolerance, dependence and at higher doses also with hypoventilation (Yekkirala et al., 2017). While there is no doubt that preclinical animal trials are required for initial drug development, one has to consider that prognosticated analgesic effects, apparent in rodent model system, are not necessarily detectable in humans. The voltage-gated sodium channel Nav1.8, which is almost exclusively expressed in small-diameter nociceptive neurons was selectively blocked by the compound PF-04531083, leading to analgesic effects in inflammatory and neuropathic preclinical animal pain models, whereas the human clinical trial was not as effective as previously expected and failed on dental pain (Bagal et al., 2014). These frequently described side effects and the failure of many clinical trials raised the claim for refined pain model systems that improve translational research.

As already described, pain represents an emotional experience that can only be indirectly measured in animal models by pain-correlated withdrawal or avoidance behaviors. Furthermore, more recent and more sophisticated techniques also observed contradictions between human and mouse pain phenotypes that may account for translational failures (Burma et al., 2017a; Hill, 2000; Percie du Sert and and Rice, 2014).

To circumvent crucial species differences and to prevent critical analgesic side effects in the human organism, it is advantageous to combine animal studies with human-based model systems for primarily testing analgesic drugs.

1.3.2 Human stem cells as a model system to study responses to stimuli that can elicit pain

The PNS, and in particular DRGs, where the cell bodies of primary sensory nociceptors are located, are not accessible from living patients and even difficult to receive post-mortem. Therefore, the approach to work with hESCs and hiPSCs, that can be differentiated into sensory neuron-like cells, was a fundamental milestone for various fields of research, particularly pain, allowing us to study human-derived material (Blanchard et al., 2015; Chambers et al., 2012; Schrenk-Siemens et al., 2015; Wainger et al., 2015).

Unique properties of stem cells

Stem cells (embryonic stem cells [ESCs] or adult stem cells [ASCs]) are specific types of cells with unique properties and capabilities. Compared to many other specified and determined cells of the body, such as nerve cells of the central (CNS) and peripheral nervous system (PNS), skin, muscle or blood cells, stem cells are undefined or uncommitted until they obtain internal and external cues to differentiate and give rise to many different mature cell types. In general, stem cells, irrespective of their origin, are defined by three basic aspects: 1) their ability to indefinitely proliferate and therefore the capability for long-term self-renewal, 2) their unspecialized, immature phenotype, and 3) their capacity to differentiate into mature cells with tissue-specific functions. Pluripotent ESCs derived from the early developing embryo have the ability to develop cells from all three somatic lineages plus the germline (Amit et al., 2000; Itskovitz-Eldor et al., 2000; Reubinoff et al., 2000). On the contrary, multipotent ASCs, found in mature organs such as brain (Temple, 1989; Vescovi et al., 2001), cornea (Bednarz et al., 1998; Tseng, 1996) , liver (Faris et al., 2001; Overturf et al., 1997), heart muscle (Beltrami et al., 2003), and bone marrow (Becker et al., 1963; Prockop, 1997; Simmons and Torok-Storb, 1991), only renew specialized cell types within the tissue of origin. Due to the great potential of these cells, stem cell research became a focal point of interest for cell-based regeneration therapies such as degenerative diseases, spinal cord injury diabetes or heart diseases.

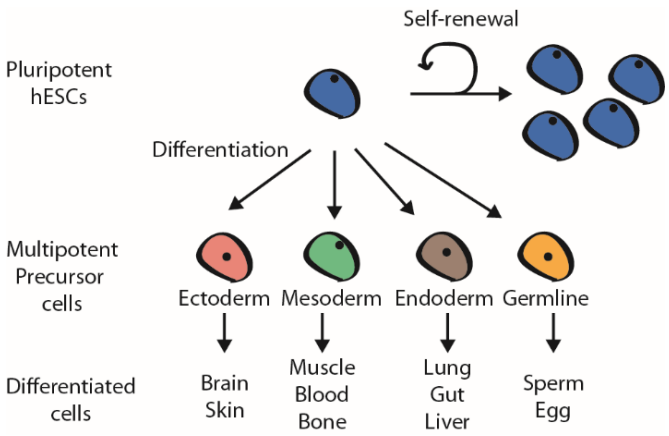

Fig. 7: Properties of embryonic and adult stem cells

Embryonic stem cells (in blue) have an uncommitted, pluripotent phenotype and the ability to indefinitely proliferate for long-term renewal or to differentiate into more defined multipotent precursor cells (red, green, brown or yellow). More defined multipotent stem cells are found in mature organs and renew specialized cell types within the organ of origin.

Although the concept of embryonic stem cells was already provided in 1964 by Kleinsmith and Pierce (describing mouse teratocarcinoma cells, tumors developed from mouse germ cells that are able to differentiate into various types of cells from different somatic lineages (Kleinsmith and

Pierce, 1964)), the first protocols for isolating and culturing mouse ESCs were only reported in 1981 (Evans and Kaufman, 1981; Martin, 1981) and, almost 20 years later, a similar success was made for the isolation of human ESCs (Thomson et al., 1998).

Human embryonic stem cells and induced pluripotent stem cells

Human embryonic stem cells (hESCs), used for scientific purposes, derive from the inner cell mass of an early developing embryo, usually generated from spared fertilized eggs of *in vitro* fertilizations.

Approximately 3-4 days after impregnation, *in vivo* as well as *in vitro* fertilized eggs undergo a series of cleavage divisions and form an 8-32 cell mass, the morula. Blastocyst formation is initiated 4-5 days after fertilization when the morula starts to open and a fluid-filled hollow (blastocoel) is formed. At this developmental stage, the blastocyst consists of three different structures: 1) the trophoblast, the outer layer of the blastocyst that supplies essential nutrients, 2) the blastocoel and 3) the inner cell mass, also called embryoblast, containing around 30 pluripotent cells. The inner cell mass is isolated from the trophoblast and can be cultured and expanded *in vitro* as human hESCs without losing their capability of self-renewal and pluripotency (Fig. 8A, Thomson et al., 1998).

Although isolated hESCs can differentiate into any somatic cell type within the human body, they are not able to form “extraembryonic” tissue, such as the placenta, and therefore cannot develop into complete and viable human beings, compared to totipotent fertilized eggs.

Nevertheless, not only the great potential of these undifferentiated, immortal cells but also the ethical issues regarding the destruction of human embryos is controversially discussed in politics and society. According to the article 50G StZG (the German stem cell law from March 2017) human embryonic stem cell research is only permitted if hESCs were isolated regularly in the country of origin prior to May 2007 (§ 4 Abs. 2 StZG).

The groundbreaking findings from Yamanaka and colleagues, demonstrating that mouse and human embryonic fibroblasts (MEFs and HEFs) can be reprogrammed by retroviral overexpression of four distinct transcription factors (OCT3/4, SOX2, c-MYC and KLF4) to become induced pluripotent stem cells (iPSCs, Fig. 8B) (Takahashi and Yamanaka, 2006; Takahashi et al., 2007), provided not only the possibility to circumvent ethical conflicts about hESC research but also to generate patient-specific or disease-specific human material.

The analysis of disease-specific iPSCs (*e.g.* from Parkinson (PD), Huntington (HD) or Down syndrome (DS)/trisomy 21-patients) indicates that the reprogramming methods offer a great

potential to compare diseased and non-diseased cell differentiation *in vitro*, which is essential for drug discovery and clinical therapies (Park et al., 2008).

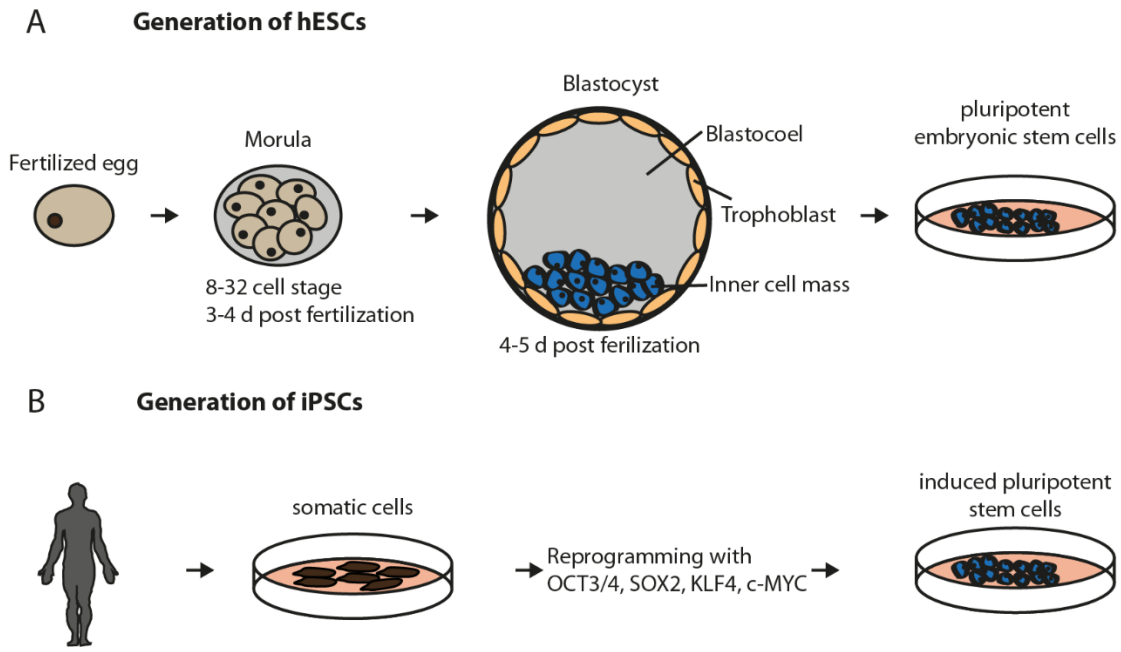

Fig. 8: Generation and isolation of hESCs and hiPSCs

(A) Schematic representation of the generation and isolation of hESCs. 3-4 days after fertilization, fertilized eggs form an 8-32 cell mass, the morula. Blastocyst formation is initiated 4-5 days after fertilization when the morula starts to open and a fluid-filled hollow is formed. The inner cell mass of the blastocyst consists of roughly 30 embryonic pluripotent stem cells. Isolated stem cells can be cultured and expanded *in vitro* without losing their capability of self-renewal and pluripotency.

(B) Schematic representation of the generation and isolation of hiPSCs. Reprogramming of somatic cells is done by retroviral overexpression of four distinct transcription factors (OCT3/4, SOX2, c-MYC and KLF4) and results in induced pluripotent stem cells.

1.3.3 Human DRG tissue as a model system to study molecular components of pain

To eliminate doubts whether *in vitro* cell culture systems recapitulate the complex and heterogeneous *in vivo* sensory system, and to validate whether stem cell-derived neurons are physiologically relevant and reflect their native human counterparts, it is important to compare the *in vitro* differentiated cells to human DRG tissue, located between each pair of vertebra along the spinal cord.

Organization of the human spinal cord and the human dermatome

The human spinal cord is segmented in 30 vertebrae. Each part consists of a pair of dorsal and ventral roots, conjoining on each side of the spinal cord to form the spinal nerve. While the dorsal roots include the axons of primary sensory neurons, ventral roots consist of the axons of motor neurons, with their cell bodies in the grey matter of the spinal cord. Spinal nerves of each segment exit the vertebral canal through bone openings (also known as neuroforamina) and they are designated by the segment of the spinal cord from which they emerge. The different parts of the spinal cord can be grouped from rostral to caudal into four classes: the cervical parts (C1-C8), the thoracic parts (T1-T12), the lumbar parts (L1-L5) and finally the sacral parts (S1-S5) (Fig. 9).

In addition to the correlation of the spinal cord segments to different spinal nerves, the organization of spinal nerves and target innervation is also related and referred to as dermatomes. A human dermatome is a specific region of the skin innervated by a distinct pair of dorsal roots that emerge from a specific part of the spinal cord (Bear et al., 2006; Foerster, 1933; Keegan and Garrett, 1948) (Fig. 9).

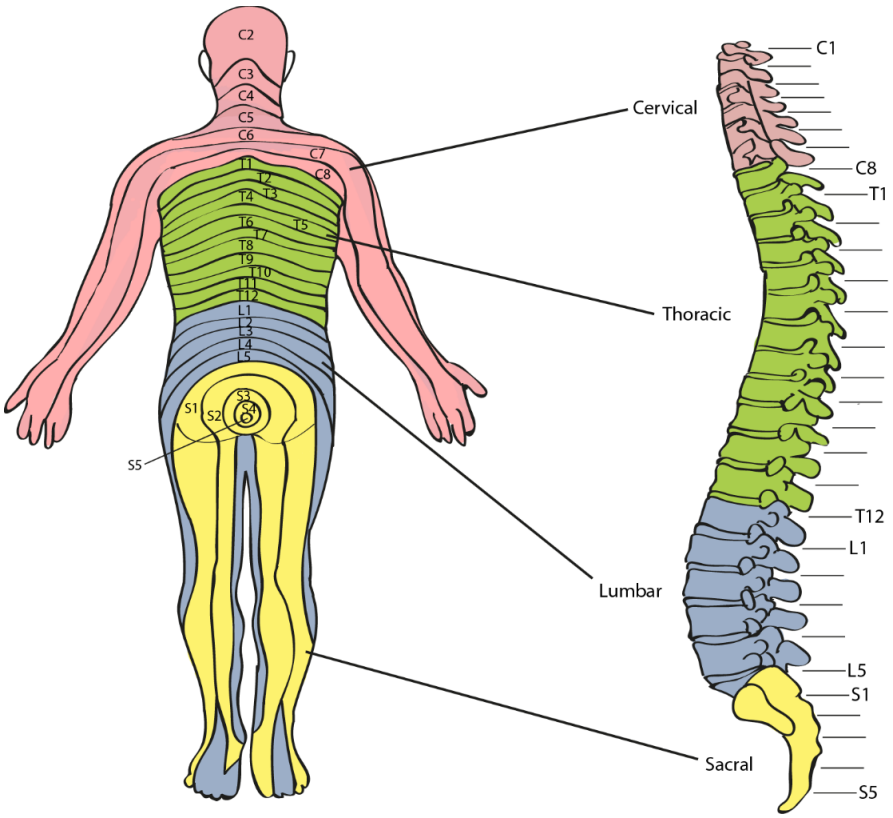

Fig. 9: Organization of the human spinal cord and the dermatome

Schematic representation of the segmented human spinal cord into four classes (cervical, thoracic, lumbar and sacral) and the spinal nerve representation on the human skin, referred to as dermatomes. Each part of the spinal cord is linked to a specific pair of spinal nerves that innervate specific areas of the human body (Redrawn and modified from Gan Quan Fu, PT).

The proof that a specific area of the human skin is mainly innervated by one specific pair of dorsal roots came from shingles pain. Neurons from a specific DRG got infected by the herpes zoster virus that remained in the DRG and, after reactivation of the virus, symptoms where only detectable in dermatomes that where innervated by the infected DRG (Ruocco et al., 2012)

2 Aims of the study

Although, for many years, lower vertebrates have been used as an invaluable model system to study various aspects of sensory transduction mechanisms and the perception of pain (Mogil, 2009), more advanced and highly developed techniques also observed contradictions between human and mouse pain phenotypes (Burma et al., 2017; Hill, 2000; Percie du Sert and Rice, 2014). To circumvent translational inconsistencies between rodent model systems and human patients, unraveling the question of how human pain-sensitive neurons are generated and how human painful stimuli are transmitted is an essential milestone for the development of new analgesic drugs.

Therefore, the **1st aim** of the thesis was to establish a protocol for the differentiation of human embryonic stem cells into functional nociceptive neurons by virally-induced overexpression of distinct proteins and transcription factors, known to be crucial during mouse nociceptor development. To assess whether differentiated neurons feature characteristic hallmarks of nociceptors a **2nd aim** was to characterize differentiated cells by Ca^{2+}-imaging, immunohistochemistry, *in situ* hybridization, quantitative RT-PCR and electrophysiological recordings. In order to validate whether (and to what degree) derived nociceptor-like cells correlate with *in vivo* nociceptors, I furthermore compared cultured neurons to human *post-mortem* DRG tissue (**3rd aim**). This comparative study highlighted molecular similarities and differences, that already exist at the level of primary sensory neurons.

In addition, we also investigated the role of PIEZO2 in human stem cell-derived nociceptors (**4th aim**). Piezo proteins were recently identified as mechanically activated ion channels that are required for innocuous mechanotransduction. However, it is not yet clear if PIEZO2 plays also a role in mechanically activated pain sensation. As a side project, we also wanted to look for possible interaction partners of PIEZO2 by expressing and biochemically purifying huPIEZO2 (**5th aim**).

Specific aims of the study were:

- Establish a differentiation protocol for the generation of hESC-derived nociceptors;
- Characterize differentiated nociceptor-like cells;
- Compare stem cell-derived nociceptors to human and mouse DRG tissue;
- Investigate the role of PIEZO2 in stem cell-derived nociceptors;
- Search for possible interaction partners of PIEZO2.

3 Materials

3.1 General Chemicals

Name	Supplier
4`,6-diamidino-2-phenylindole (DAPI)	Sigma
Accutase	Sigma
Acetic acid	Carl Roth
Acetic anhydride	Sigma
Agarose	Biozym Scientific
Amersham Hybond-XL	GE Healthcare Bio Science
Ammonium acetate	Carl Roth
Ampicillin	Sigma
B27 supplement	Thermo Fisher Scientific
Bacto Tryptone	BD
Bacto Yeast Extract	BD
BCIP (5-bromo-4chloro-3-indolyl-phosphate)	Sigma
Beta-Mercaptoethanol	Carl Roth
Bicine	Sigma-Aldrich
Biotin-NHS	Sigma
Bis-Tris pufferan >99%	Carl Roth
Blocking Reagent	Roche
Calcium chloride dihydrate	Sigma
Capsaicin	Sigma
Carbenecillin	Carl Roth
Chloroform ≥ 99.8%	Sigma
Collagenase	Sigma
DIG RNA labeling mix	Sigma
Dimethylformamid	Sigma
Dimethyl sulfoxide (DMSO)	Carl Roth
D-(+) –Glucose ≥ 99.5%	Sigma
DMEM/F12	Thermo Fisher Scientific
DMEM high glucose	Thermo Fisher Scientific

dNTPs (10 mM)	New England Biolabs
Doxycycline	Sigma
DPBS	Sigma
E8 media	Thermo Fisher Scientific
EDTA	Carl Roth
Ethanol absolute	Sigma
Ethidium bromide solution 1%	Carl Roth
Fast Start Essential DNA Green Master	Roche
Fibronectin	Thermo Fisher Scientific
Ficoll400	Sigma
Flag M2 magnetic beads	Sigma
Fluorescein RNA labeling mix	Sigma
Foetal Bovine Serum Origin: EU approved	Thermo Fisher Scientific
Formamide ≥ 98%	Carl Roth
Formamide ≥ 99.5%	Sigma
Fura-2-AM	Thermo Fisher Scientific
Glycerol	Carl Roth
Goat serum	PAN Biotech
Hepes 1M	Thermo Fisher Scientific
HEPES pufferan >99.5% p.A.	Carl Roth
Human BDNF	Peprotech
Human EGF	Peprotech
Human FGF	Peprotech
Human GDNF	Peprotech
Human NGF	Peprotech
Hydrochloric acid solution 1 M	Fluka
Hydrochloric acid p.a. 37%	Sigma
Hydrogen peroxide 30%	AppliChem
Imidazole	Merck Millipore
Immu-Mount	Thermo Fisher Scientific
Insulin from bovine pancreas	Sigma
Isopropanol	Sigma

Laminin	Sigma
L-Glutamine	Thermo Fisher Scientific
Lipofectamine 2000	Thermo Fisher Scientific
Loading dye (6x)	New England Biolabs
Magnesium chloride hexahydrate	Sigma
Maleic acid	Sigma
Matrigel	BD
Menthol	Sigma
Methanol p.a.	Sigma
MF-Millipore-Membrane Filter 0.025 µM	Merck Millipore
Milk powder	Carl Roth
Mitomycin C	Sigma
Mowiol 4-88	Carl Roth
mTeSR1 media	Stem Cell Technologies
Mustard oil	Sigma
N2 supplement	Thermo Fisher Scientific
NBT (nitro blue tetrazolium)	Roche
Neurobasal Media	Thermo Fisher Scientific
N-Lauroylsarcosine sodium salt	Sigma
O.C.T Compound Tissue Tek	Sakura
Pap Pen	Dako
Paraformaldehyde	Aldrich
Penicillin-Streptomycin	Thermo Fisher Scientific
Phenylmethylsulfonylfluoride (PMSF)	Carl Roth
Plasmocin prophylactic	Carl Roth
Pluronic F-127	Invivogen
Poly (ethylene glycol) 8000	Thermo Fisher Scientific
Polyvenylpyrolidone	Sigma
Potassium acetate	Sigma
Potassium chloride	Carl Roth
Potassium dihydrogen phosphate	AppliChem
Random Hexamers	Carl Roth

Recombinant Rnasin Ribonuclease Inhibitor	Roche
Rhodamine-NHS	Promega
RNase A	Sigma
Rock-Inhibitor Y-27632	Carl Roth
Roti-Phenol/Chloroform/Isoamylalkohol	Calbiochem
Salmon sperm DNA	Carl Roth
Sephadex G50 Coarse	GE Healthcare Bio Science
Sodium chloride	Sigma
Sodium citrate tribasic dihydrate	Sigma
Sodium hydroxide pellets	Sigma
Sodium hydroxide solution 1M p.a.	Sigma
Superscript III Reverse Transcriptase	Fluka
Taq man probe NTRK1	Thermo Fisher Scientific
Taq man probe NTRK2	Thermo Fisher Scientific
Taq man probe NTRK3	Thermo Fisher Scientific
TesR-E8	Stem Cell Technology
Triethanolamin ≥ 99%	Thermo Fisher Scientific
Triethylamine	Carl Roth
Tris Pufferano ≥ 99.9% p.a.	Sigma
Triton-X-100	Carl Roth
TRIzol Reagent	Merck
Tween-20	Thermo Fisher Scientific
Tyramine-HCl	Carl Roth
Yeast tRNA	Sigma

3.2 Buffers and Solutions

Molecular Biology

Agar Ampicillin/Carbenicillin-Plates	1.5% Agar 100 µg/ml Ampicillin/Carbenicillin in LB medium

Alkaline Lysis Solution P1	50 mM Glucose 25 mM Tris-HCl (pH 8.0) 10 mM EDTA (pH 8.0)
Alkaline Lysis Solution P2	200 mM NaOH 1% SDS
Alkaline Lysis Solution P3	3 M potassium acetate 5 M glacial acetic acid
2xHBS (Hepes Buffered Saline) buffer	274 mM NaCl 10 mM KCl 1.4 mM Na_2HPO_4 15 mM D-Glucose 42 mM Hepes (free acid)
LB (lysogeny broth) Medium	1% Bacto-Trypton 0.5% Bacto Yeast Extract 1% NaCl
50 x TAE buffer	242 g/l Tris Base 5.71% (v/v) Glacial acetic acid 0.05 M EDTA pH 8.0
TE buffer pH 8.0	10 mM Tris 1 mM EDTA

***In Situ* Hybridization**

Acetylation buffer	100 mM Triethanolamine 0.05% HCL
Denhardt´s Solution (100x)	2% Ficoll400 2% polyvenylpyrolidone 2% BSA
Hybridization buffer	5x SSC 50% Formamide 5x Denhardt´s 250 µg/ml yeast tRNA

	500 µg/ml Salmon sperm
NTMT buffer	100 mM Tris pH 9.5 100 mM NaCl 50 mM $MgCl_2$ 0.1% Tween 20
RNAse buffer	0.1 M Tris pH 8 1 mM EDTA 500 mM NaCl
TSA Buffer	10 mM Imidazole in PBS
5x MAB pH 7.5	500 mM Maleic acid 745 mM NaCl Adjust to pH 7.5 with NaOH
1x MAB	1x MAB 0.1% Tween 20
1xMABT^{++}	1x MABT 10% goat serum 1% Blocking reagent
20x SSC	3 M NaCl 0.3 M Sodium citrate
10x PBS	1.37 M NaCl 27 mM KCl 100 mM Na_2HPO_4 20 mM KH_2PO_4 Adjust to pH 6.8 (HCl)
PBST	0.1% Tween 20 in 1xPBS
4% PFA in PBS	4% PFA 250 nM NaOH

Ca^{2+}-imaging

Ringer´s solution	140 mM NaCl 5 mM KCl 2 mM $CaCl_2$*$2H_2O$ 2 mM $MgCl_2$*$6H_2O$ 10 mM Glucose 10 mM Hepes
High K^+ solution	45 mM NaCl 100 mM KCl 2 mM $CaCl_2$*$2H_2O$ 2 mM $MgCl_2$*$6H_2O$ 10 mM Glucose 10 mm Hepes

Southern Blot

Church buffer	200 mM Na-PO_4 pH 7.2 1 mM EDTA 1% BSA 7% SDS
TE Puffer pH 8.0	10 mM Tris 1 mM EDTA
Depurination solution	0.8% HCl in ddH_2O
Denaturation solution	1 M NaCl 0.5 M NaOH
DNA isolation buffer	100 mM Tris pH 8.0 5 mM EDTA 0.2% SDS 200 mM NaCl 100 µg/ml Proteinase K

Immunoprecipitation

DDM buffer (Solubilization buffer)	30 mM Tris-Cl, pH 7.4 150 mM NaCl 10 % Glycerol 0.5 % DDM 0.1 mM $CaCl_2$ 1 mM $MgCl_2$ 2 mM KCl Add freshly: 1 mM PMSF 5 mM NaF 1 mM NaOV 20 mM beta-glycerophosphate
Sucrose buffer (Homogenization buffer)	0.32 M Sucrose 30 mM Tris 2 mM KCl 1 mM $MgCl_2$ 0.1 mM $CaCl_2$ Add freshly: 1 mM PMSF 5 mM NaF 1 mM NaOV 20 mM beta-glycerophosphate
20 x Tris-Acetate Running buffer	50 mMTricine 50 mMTris base 0.1% SDS pH 8.24
20 x Transfer buffer	25 mM Bicine 25 mM Bis-Tris (free base) 1 mM EDTA
Washing buffer	30 mM Tris-HCl pH 7.4 150 mM NaCl

3.3 Enzymes and Molecular Weight Markers

Name	Company
Restriction Enzymes	New England Biolabs
Phusion High-Fidelity Polymerase	New England Biolabs
T4 DNA Ligase	New England Biolabs
T3 RNA Polymerase	New England Biolabs
T7 RNA Polymerase	New England Biolabs
SP6 RNA Polymerase	New England Biolabs
Shrimp Alkaline Phosphatase (rSAP)	New England Biolabs
Superscript III Reverse Transcriptase	Thermo Fisher Scientific
Proteinase K	Carl Roth
Collagenase	Thermo Fisher Scientific
Trypsin-EDTA (0.05%)	Thermo Fisher Scientific
1kb plus ladder	New England Biolabs
100bp ladder	New England Biolabs
PageRuler™ Prestained Protein Ladder	Thermo Fisher Scientific

3.4 Bacteria Strains

Strain	Company
E. coli DHB10 (Electrocompetent bacteria)	Thermo Fisher Scientific

3.5 Plasmids and Vector Backbones

Name	Company/Producer
pBlueScript II SK(+)	Stratagene
pCDNA3.1 (+)	Thermo Fisher Scientific
pMDL/pRRE viral helper plasmid	Dr. Alexander Loewer (MDC Berlin)
pRSV-REV viral helper plasmid	Dr. Alexander Loewer (MDC Berlin)

VSV-G viral helper plasmid	Dr. Alexander Loewer (MDC Berlin)
TetO-NGN2-EGFP-Puro viral plasmid	Prof.Thomas C. Südhof (Stanford)
ELFa RUNX1 IRES-GFP viral plasmid	Dr. Katrin-Schrenk Siemens
ELFa TRKA IRES-GFP viral plasmid	Dr. Katrin-Schrenk Siemens
ASCL1 viral plasmid	Clifford J. Woolf (Harvard stem cell institute)
ISL2 viral plasmid	Clifford J. Woolf (Harvard stem cell institute)
KLF7 viral plasmid	Clifford J. Woolf (Harvard stem cell institute)
MYT1L viral plasmid	Clifford J. Woolf (Harvard stem cell institute)
NGN1 viral plasmid	Clifford J. Woolf (Harvard stem cell institute)

3.6 Cell Lines

Cell line	**Description**
Hues7	Human embryonic stem cell line 7, Harvard university
HEK 293	Human embryonic kidney 293 cells
HEK 293TN	Pseudoviral Particle Producer Cell Line, Biocat

3.7 Cell Culture Media

Neurosphere medium	50% DMEM/F12 50% Neurobasal medium 5 µg/ml Insulin 1x B27 supplement 0.5x N2 supplement 1x Glutamine
Differentiation medium nociceptors	95% neurosphere medium 5% FCS 1x P/S 10 ng/ml BDNF 10 ng/ml GDNF

	10 ng/ml NGF
Differentiation medium mechanoreceptors	100% neurosphere medium 1xP/S 10 ng/ml BDNF 10 ng/ml GDNF 10 ng/ml NGF 10 ng/ml NT-3 100 nM Retinoic acid
Freezing medium stem cells	89% mTeSR1 medium 10% DMSO
Freezing medium NCLCs	89% Neurosphere medium 10% DMSO
HEK293TN medium	90% DMEM high Glucose 10% FCS 1x P/S

3.8 Oligonucleotides

Name	**Sequence (5`→ 3`)**	**Usage**
hu*TRKA* fwd	gacctcgagtctggagctccgtgatctga	*In situ* probe
hu*TRKA* rev	gacgcggccgcccgttgttgacgtgggtg	*In situ* probe
hu*TRKB* fwd	attactcgagtggagcctaacagtgtagatcctgagaac	*In situ* probe
hu*TRKB* rev	atatgcggccgctggtactccgtgtgattggtaacatg	*In situ* probe
hu*TRKC* fwd	attactcgagtggatgtctctctttgcccagc	*In situ* probe
hu*TRKC* rev	atatgcggccgcattcaccagcgtcaagttgatgg	*In situ* probe
hu*Nav1.6* fwd	gacctcgagtcgcaagcaggaggaggtatct	*In situ* probe
hu*Nav1.6* rev	attagcggccgccacctgcccaagcattaga	*In situ* probe
hu*Nav1.7* fwd	attactcgagaaggtgggcagcattagcagat	*In situ* probe
hu*Nav1.7* rev	attagcggccgcttgccaaacacgggattgt	*In situ* probe
hu*Nav1.8* fwd	atatctcgagtggattctctgaaggcaa	*In situ* probe
hu*Nav1.8* rev	atatgcggccgcatctgcaatgggaaagagtt	*In situ* probe

hu*Nav1.9* fwd	attactcgagcctagatagtatgaaagcaatga	*In situ* probe
hu*Nav1.9* rev	attagcggccgcAcagtccttcctggtgtcttc	*In situ* probe
huNGN1 fwd	taccgagctcggatcgaattcgccaccatgccagc	NGN1-viral construct
huNGN1 rev	tgcttgcttcgtggcgtggtaaggaatgaaacagggcgttg	NGN1-viral construct
EGFP fwd	gccacgaagcaagcagga	NGN1-viral construct
EGFP rev	actcgagtcgcggcctctagacttgtacagctcgtccatgc	NGN1-viral construct
5`arm fwd	agaaggtaccgagggagggactcgcagcg	PIEZO2 targeting
5`arm rev	gagagtcgacagaccatggcgtcggtccggcgag	PIEZO2 targeting
ATG-3xFlag-His-tag fwd	gacccatgcactacaaagaccatgacggt	PIEZO2 targeting
3xFlag-His-tag rev	gacgtcgacgaagtgagagagccaggctgt	PIEZO2 targeting
-ATG-Exon1-Intron fwd	gacacgcgtgcctcagaagtggtgtgcggg	PIEZO2 targeting
Exon-Intron rev	ataactgcagcccgtcccgagcatcctgt	PIEZO2 targeting
3`arm fwd	aggaggatcccatgtgctggaaactgtttatgttga	PIEZO2 targeting
3`arm rev	attagcggccgcgagactagtggactaggtgttgggggtctatagc	PIEZO2 targeting
Puro fwd	caaggtaccgaactagatgatccggctgtg	PIEZO2 targeting
Puro rev	ttctgcgcctgcagcaat	PIEZO2 targeting

3.9 Commercial Kits

Name	Company
Amersham megaprime DNA Labeling system	GE Healthcare Life Science
Amersham ECL Prime Western Blotting Detection Kit	GE Healthcare Life Sciences
QIAquick PCR Purification Kit	Qiagen
Zymo PURE Midiprep Kit	Zymo Research
Zymo PURE Maxiprep Kit	Zymo Research
Zymoclean Gel DNA Recovery Kit	Zymo Research

3.10 Antibodies

1st Antibody	Dilution	Company
Digoxigenin-POD Fab fragments	1:1,000	Roche
Digoxigenin-AP Fab fragments	1:1,000	Roche
Fluorescein-POD Fab fragments	1:2,000	Roche
Fluorescein-AP Fab fragments	1:1,000	Roche
c-MAF, gp	1:5,000	Dr. Hagen Wende
FLAG M2, ms	1:3,000	Sigma-Aldrich
ISLET-1, ms, IgG2b	1:100	DSHB
NF200 (200-220 kDa), ch	1:25,000	Millipore
NF200, clone N52, ms	1:600	Sigma-Aldrich
RFP, rb	1:500	Rockland
TUJ1 (Tubulin β3), ms	1:750	Covance

2nd Antibody	Dilution	Company
Alexa Fluor 488 donkey α- mouse IgG	1:1,000	Dianova
Alexa Fluor 488 goat α-guinea pig IgG	1:1,000	Dianova
Alexa Fluor 555 donkey α- rabbit IgG	1:1,000	Dianova
Alexa Fluor 647 donkey α- chicken IgG	1:1,000	Dianova
Goat anti-rabbit-HRP	1:2,000	Jackson Immuno Research
Streptavidin-Cy2	1:1,000	Dianova

3.11 Equipment

4D- Nucleofactor (core, X and Y unit)	Lonza
Bacteria shaker certomat BS1	Sartorius
Biological safety cabinets Safe 2020	Thermo Fisher Scientific
Cell incubator	Binder
Centrifuge 5417R	Eppendorf
Centrifuge 5804R	Eppendorf
Centrifuge 5424	Eppendorf
Centrifuge, Maxima Ultracentrifuge Coulter GmbH,	Beckman
ChemiDoc™ XRS+ System	Bio-Rad
Contamination monitor LB122	Berthold
coolSNAP HQ2 CCD camera	Photometrics
Cryostat CM3050S	Leica
Dissection Microscope	Olympus SZ61
Duomax 1030 shaker	Heidolph
Fla Image Eraser	GE Healthcare Life Sciences
Gene Pulser X Cell	Bio-Rad
Image Quant LAS 4000	GE Healthcare Life Sciences
Intelli-mixer RM-2l	Elmi
Inverted fluorescent microscope	Carl Zeiss
Lambda DG-4 light source	Sutter instruments
Large Sky Line Digital Orbital Shaker DOS10-20L	Elmi
Light Cycler 96	Roche
Liquid nitrogen tank GT40	Air Liquide
Megafuge 1.0R	Heraeus Sepatech
Microwave	Severin
Mili-Q Reference system	Merck-Millipore
Nanodrop ND-1000	Peqlab
Power Source (250V)	VWR
Primovert microscope	Zeiss
Scale BJ410C	Precisa

Thermal cycler C1000	Bio-Rad
Thermomixer comfort	Eppendorf
Typhoon Fla 7000	GE Healthcare Life Sciences
Waterbath TW20	Julabo
X Cell Sure Lock	Thermo Fisher Scientific

4. Methods

4.1 Molecular Biology

4.1.1 Preparation of Genomic DNA

The preparation of genomic stem cell DNA was performed in a 96-well format. Cells were washed once with PBS and lysed with 50 µl DNA isolation buffer (Proteinase K freshly added) in a humidity chamber overnight at 55 °C.

Afterwards DNA was precipitated for 30 min at room temperature by adding 2.5x volume of 100% ethanol and 1/10 volume of 3 M sodium acetate, washed once with 70% ethanol and air-dried until the ethanol was evaporated. For Southern Blot analysis, precipitated DNA of a 96 well plate was digested with HindIII over night at 37 °C.

4.1.2 Polymerase Chain Reaction (PCR)

The Polymerase chain reaction is a revolutionary technique that is used for amplifying specific DNA templates, generating thousands of copies *in vitro* (Saiki et al., 1986).

A general PCR master mix for one reaction included 1x Phusion HF or GC buffer (for GC rich amplicons), 200 µM dNTPs, 0.5 µM forward and reverse primer, approximately 50-250 ng genomic or 10 ng plasmid template DNA, 1.0 unit/50 µl PCR Phusion DNA Polymerase and according to the DNA concentration deionized water. The PCR reaction was performed in a temperature gradient thermocycler, programmed as follows

98 °C	30 sec	
98 °C	10 sec	30 x
45-72 °C	25 sec	
72 °C	15-30 sec/kb	
72 °C	10 min	
4 °C	hold	

4.1.3 Restriction Digest

For the digestion of plasmid or genomic DNA the standard restriction enzymes that cut DNA sequences at a specific restriction site were used. A general protocol included a distinct amount of DNA (1-30 µg), 10 U enzyme per µg DNA (generally 1 µl was used), 1x NEB enzyme buffer and according to the reaction volume deionized water. Depending on the amount of digested DNA and the restriction enzyme that was used, the reaction was incubated for 1 hr/µg at an enzyme-dependent temperature (most likely 37 °C). The reaction was stopped by heat inactivation.

4.1.4 Gel purification

To separate DNA fragments according to their molecular weight, an agarose gel electrophoresis was performed. Depending on the size of the DNA fragments a 1-2% agarose gel was prepared in 1x TAE buffer and for visualization of the DNA ethidium bromide was added. To compare different DNA fragments, a 100 bp or 1 kb DNA ladder from NEB was also loaded on the gel. DNA bands, visualized with a ChemiDoc™ XRS$^+$ System from Bio-Rad, were cut out of the gel and DNA was extracted with the Zymoclean Gel DNA Recovery Kit as described in the instruction manual.

4.1.5 Ligation

Prior to ligation, to hamper relegation of the vector backbone, vector dephosphorylation was performed. Therefore, 1 µl Shrimp Alkaline Phosphatase (rSAP) and 1x rSAP Reaction Buffer was added to the DNA and incubated for 30 min at 37 °C. The reaction was stopped by heat inactivation at 65 °C and purified with the QIAquick PCR Purification Kit from Qiagen.

A general 20 µl ligation reaction contained 50 ng vector backbone, a threefold molar excess of insert DNA, 1x T4 DNA Ligase Buffer, 1 µl T4 DNA Ligase and according to the DNA concentration deionized water. After 20 min incubation at room temperature, the reaction was purified by a Phenol/Chloroform/Isoamylalcohol extraction and microdialysis.

4.1.6 Phenol/Chloroform/Isoamylalcohol extraction and microdialysis

To purify ligated DNA constructs prior to transformation a Phenol/Chloroform/Isoamylalcohol (PCI) extraction and microdialysis were performed. Therefore, an equal volume of PCI was added to the ligation reaction and mixed extensively. By a centrifugation step at full speed (≥13000 rpm) for 3 min the two phases were separated and the upper, aqueous phase, containing the DNA, was transferred for 30 min on a MF-Millipore-Membrane filter that was placed on deionized water. After desalting, the DNA containing phase was collected and used for transformation.

4.1.7 Transformation of Electrocompetent E. coli

For multiplication of plasmid DNA, electrocompetent *E. coli* of strain DHB10 were transformed with 10-50 ng vector DNA. *E. coli*, stored at -80 °C, were thawed on ice and a 25 µl aliquot was mixed with 5 µl of the purified ligation reaction.

The plasmid-cell mixture was transferred into a 1 mm cuvette (Bio-Rad) and exposed to electrical current (1800 V, 25 µF, 200 Ω), which results in opening pores in the cell so that the plasmid is able to enter the cell membrane. Afterwards, bacteria were collected with 1 ml of LB medium and incubated at 37 °C for 30 minutes on a shaker. Finally, the bacteria suspension was plated on a bacteria agar plate containing 100 µg/ml ampicillin or carbenicillin or any other antibiotics, depending on the resistance cassette of the plasmid and incubated overnight at 37 °C. Lentiviral constructs, were incubated at 30 °C to prevent recombineering.

4.1.8 Minipreparation of Plasmid-DNA

To test if the cloning was successful (if the right DNA fragment was inserted into the vector backbone), a DNA-minipreparation was performed. For this, 2 ml LB medium (containing 100 µg/ml ampicillin or carbenicillin) was inoculated with one bacterial clone and cultured with vigorous shaking at 37 °C for 14-15 hrs. Afterwards cultures were pelleted by a centrifugation step for 10 min at full speed (≥13000 rpm) and supernatant was discarded. After resuspending bacterial pellets in 200 µl buffer P1, the same amount of lysis buffer P2 and neutralization buffer P3 were added consecutively and mixed by inverting the tube several times. After the samples were centrifuged at full speed for 15 min, clear supernatant was transferred into a new tube and DNA was precipitated by 500 µl isopropanol and centrifuged again at full speed for 15 min. DNA pellet was washed once with 70%

ethanol and air-dried until the ethanol was evaporated. Finally, the pellet was resuspended in 30 µl TE-buffer and used for a test restriction digest.

4.1.9 Midipreparation of Plasmid DNA

The midipreparation of plasmid DNA was performed as described in the instruction manual of the ZymoPURE Plasmid Midiprep Kit from Zymo.

4.1.10 Sequencing

Sequencing of DNA constructs was done by Eurofins Genomics. For plasmid DNA sequencing, a 15µl sample of 50-100 ng/µl was submitted and analyzed.

4.1.11 Riboprobe synthesis (In situ probe synthesis)

For the detection of specific RNA sequences within mouse or human DRG tissue, as well as in differentiated neurons, complementary, fluorescent-labelled RNA probes (riboprobes) were generated by RNA *in vitro* transcription. For the *in vitro* transcription a purified, linearized plasmid was used as a template, containing the sequence of the RNA probe and phage polymerase promoters T3, T7 or SP6, one or two on each site of the multiple cloning site, allowing the transcription from both sites of the inserted RNA sequence.

Fluorescent labeling was achieved by Digoxigenin (DIG, Sigma) or Fluorescein (FITC) conjugated nucleotides that were incorporated into the synthesized RNA probes. A general 20 µl RNA transcription reaction contained 1 µg of the linearized and boiled plasmid, 1x (FITC or DIG) RNA labeling mix, 1x RNA polymerase buffer, 50 U (2 µl) RNA polymerase (T3, T7 or SP6), 40U (1 µl) of ribonuclease inhibitor (RNAsin), and 2 µl DTT (10 mM). The reaction was incubated for 2 hrs at 37 C. For better penetration of human and mouse DRG tissue *in situ* probes were hydrolyzed. Therefore, 21 µl deionized water and 5 µl 0.6 M Na_2CO_3 and 5 µl 0.4 M $NaHCO_3$ were added to the RNA synthesis reaction and incubated for 10 min at 60 °C. Hydrolyzed as well as non-hydrolyzed probes were purified and precipitated with sodium acetate and ethanol. For this the amount of DNA solution was filled up to 200 µl with deionized water, 100 µl of 7.5 M Sodium acetate and 600 µl ethanol was added and DNA was precipitated for 30 min at room temperature. After a centrifugation step at full speed for 20 min, DNA pellet was washed once with 70% ethanol and air-dried until the

ethanol was evaporated. The pellet was resuspended in 50 µl pure formamide and 50 µl deionized water and stored at -80 °C until further use.

4.1.12 RNA extraction and cDNA synthesis

For RNA isolation, cells on 6-well plates were washed once with PBS, lysed and resuspended in 500 µl cold Trizol until cell clumps were dispersed. From this step on, RNA extraction and cDNA synthesis were carried out at 4 °C. After the addition of 100 µl chloroform, samples were briefly vortexed until the mixture became foamy and incubated on a shaker at room temperature for 10 min at 400 rpm. Afterwards samples were centrifuged at full speed (≥13000 rpm) for 10 min at 4 °C and the upper, aqueous phase, containing the RNA, was transferred into a new tube. For RNA precipitation, an equal volume of isopropanol was added, and samples were incubated on ice for 10 min. After an additional centrifugation step at full speed for 10 min at 4 °C, RNA was washed once with 70% ethanol and air-dried until the ethanol was evaporated. The RNA pellet was resuspended in 30 µl deionized water. For cDNA synthesis, RNA was reverse transcribed by using the SuperScriptTM III Reverse transcriptase kit (Invitrogen). A 10 µl reaction included 2.5 µg of the extracted RNA, 1 µl oligo (dT) (50 µM), 1 µl dNTP mix (10 mM) and according to the RNA concentration deionized water. Reaction was incubated at 65 °C for 5 min and afterwards 1 µl SuperScriptTM III Reverse Transcriptase, 2 µl DTT (0.1 M), 1 µl RNasin, 2 µl $MgCl_2$ (50 mM) and 4 µl First-Strand buffer was added. The reaction was heated up at 50 °C for 50 min followed by an incubation of 85 °C for 5 min. Extracted RNA and cDNA were stored at -80 °C until further use for qPCR analysis.

4.2 Cell Culture

Table 1: Overview of cell culture dishes and plates

Plate/Well	Area per plate/well [cm^2]	Medium per plate/well [ml]	Trypsin/EDTA per plate/well [cm2]
96-well	0.5	150	0.05
48-well	1.0	0.25	0.1
24-well	2.1	0.5	0.25
12-well	3.8	1	0.5
6-well	9.6	2	1
35-mm dish	10	2	1
10-cm dish	60	10	4

4.2.1 Cultivation and Splitting of human embryonic stem cells (hESCs)

Hues7 cells were cultivated and passaged on extracellular matrix proteins in TesR-E8 medium. Depending on the morphology and the density of seeded colonies, stem cells were usually passaged every 3-5 days. Colonies on a 10-cm dish were splitted by washing once with PBS followed by an incubation for 5 min in 0.5 mM EDTA. Cells were gently detached by rinsing them off with cell culture medium and transferred onto new Matrigel pre-coated culture dishes.

4.2.2 Genetic modification of human embryonic stem cells by the tag-PIEZO2 targeting vector

For the electroporation of human embryonic stem cells, 30 µg of the tag-PIEZO2 targeting vector was digested with SacI and KpnI to isolate the targeting sequence. To check for successful digestion, digested and undigested vector DNA was run side-by side on an agarose gel.

ES cells, grown on a 10-cm dish, this time in mTesR1 medium, were washed once with PBS, incubated with Accutase (a gentle detachment reagent) for 5 min at 37 °C, and collected with pre-warmed DMEM/F12 medium. After centrifugation, for 3 min at 1000 rpm, cells were resuspended and triturated in mTesR1 medium. 2.4×10^6 cells were centrifuged again and resuspended in 150 µl Ingenio Electroporation Solution. The homogenous single cell suspension was mixed with 7.5 µg of linearized SacI/KpnI tag-Piezo2 targeting vector and 7.5 µf of CRISPR plasmid, dissolved in 150 µl Ingenio Electroporation Solution and transferred into Amaxa cuvettes (100 µl/cuvette). After incubation for 4 min on ice, cells were electroporated with a Lonza 4D-Nucleofactor (pulse program

DC100), and plated on Matrigel-coated 10-cm dishes, containing stem cell medium mTesR1 plus ROCK Inhibitor (10 µM, Y-27632).

Depending on cell density and morphology, puromycin selection (tagged Piezo2 targeting construct contains a puromycin resistance cassette) was started 48 or 72 hrs later. Medium was changed daily.

4.2.3 Picking of Embryonic Stem Cell Clones

Approximately 10-14 days after the electroporation, ES cell clones resistant to puromycin treatment were picked semi-sterile under a cell culture microscope. For this, clones were scratched off and taken up with a 10 µl tip and transferred in a 96-well plate, containing 100 µl stem cell medium 1x penicillin/streptomycin and ROCK Inhibitor (10 µM). Depending on cell density, colonies in a 96-well were splitted 3-7 days later onto two 96-wells by treating them with 50 µl Accutase for 3 min and scratching them off with a 10 µl tip. One well was used for genomic DNA extraction and Southern Blot screening, whereas the other well was expanded.

*4.2.*4 Southern Blot

To screen for positively targeted stem cell clones, Southern Blot analysis was performed. For this, HindIII digested genomic DNA from a clone grown in a 96-well was loaded on a 0.7% agarose gel. After an overnight run (~ 16 hrs) at 30 Volt, the gel was first incubated in depurination buffer (0.8% HCl) for 8 min, twice in denaturation buffer (1M NaCl, 0.5 M NaOH), 20 min each, and then washed for 5 min with 20 x SSC buffer (3 M NaCl, 0.3 M sodium citrate). The Southern blot was built up as follows: a glass plate, agarose gel, transfer Hybond membrane (GE Healthcare), 3 pieces of Whatmann paper and a stack of paper towel, all covered with another glass plate. After an overnight incubation, to allow the transfer of the DNA from the agarose gel to the membrane, the blot was dismantled and different gel chambers were labelled on the membrane. Prior to pre-hybridization in 8ml church buffer (200 mM Na-PO_4 pH 7.2, 1 mM EDTA, 1% BSA, 7% SDS) for 1 hr at 65 °C in a hybridization oven, the membrane was washed with 2x SSC buffer. The 3` and the 5` probes, used for the hybridization reaction were a kind gift from Dr. Katrin Schrenk-Siemens and were already used for previous Piezo2 targeting experiments. The Amersham Megaprime DNA Labeling System Kit (GE Healthcare Life Science) was used for labelling DNA probes. Therefore, 5 µl primer solution was mixed with 25 ng probe DNA and incubated at 95 °C for 5 min. After the addition of 10 µl labeling buffer, 5 µl [α-32P] dCTP radioactivity and 2 µl Klenow enzyme the reaction was incubated at 37 °C for 30 min. The reaction was stopped with 5 µl EDTA (0.2 M) and 25 µl salmon sperm. To get rid of unbound radioactive nucleotides and to test if the labeling of the probe was successful, the reaction

was purified by using a G50 sephadex column cleanup and incorporation rate was measured with a beta counter before and after the purification. Probes were used if the incorporation rate of purified and unpurified probes was around 50%. Purified probes were mixed with 50 µl genomic mouse DNA (10 µg) as blocking DNA and incubated at 95 °C for 5 min. After the addition of 1 ml church buffer and an incubation again at 95 °C for 10 min, reaction was pre-hybridized for 1hr at 65 °C in the hybridization oven. After a short centrifugation step, radioactive labeling mix was added to the membrane in the hybridization tube and incubated overnight at 65 °C. The next day, the radioactive solution was discarded, and membrane was washed once in 1x SSC + 1% SDS for 5 min and once in 1x SSC + 0.1% SDS for 20 min both washing steps at 65 °C. Afterwards, membrane was washed with 0.5x SSC + 0.1% SDS and 0.2x SSC + 0.1% SDS for 20 min and 5 min respectively. Finally, membranes were placed in an X-ray film cassette with a screen on top of it and after different exposure times developed with a phosphor-imager Typhoon Fla 7000.

4.2.5 Differentiation of hESCs into NCLCs

For the first differentiation step into neuronal precursor cells, splitted Hues7 cells were transferred onto uncoated dishes and cultured in neurosphere medium, that was changed every second day. Cells started to form globular structures, that we named neuroectodermal spheres. After 6-12 days, neurospheres spontaneously attached to the bottom of the cell culture plate and NCLCs started to delaminate and migrate out. Migrating NCLCs were collected by removing the remnants of the attached neurospheres mechanically with a 10 µl pipette tip and incubation with Accutase for 3 min. Afterwards cells were resuspended in differentiation medium and plated on Polyornithin/Laminin/Fibronectin coated dishes or chambers. For nociceptor differentiation, cells were cultured in nociceptor differentiation medium.

4.2.6 Lentivirus production and Lentiviral infection of NCLCs

In brief already described in Schrenk-Siemens et al., 2015. Lentiviral particles of the third generation, using only a fractional set of HIV genes, were produced in HEK293TN cells by performing Calcium-Phosphate co-transfection of three viral helper plasmids (pRSV-REV, pMDLg/pRRE and the VSV-G virus envelope protein) plus the expression vector with the gene of interest. 24 hours prior to transfection, HEK cells were splitted and $2.5x10^6$ cells were plated per 10 cm and dish. For each transfection reaction per 10 cm dish 450 µl deionized water was mixed with 50 µl $CaCl_2$ (2.5 M) and plasmid DNA (1.8 µg pMDL/pRRE, 0.7 µg pRSV-REV, 0.3 µg VSV-G and 3.2 µg expression vector), and then added to 500 µl 2x HBS buffer. After 20 min incubation at room temperature,

transfection reaction was added to the cells. The lentivirus supernatant was harvested 48 and 72 hrs after transfection and concentrated by adding 50% PEG-8000 and two consecutive centrifugation steps at 2500 g for 20 min and 1200 g for 5 min. Depending on the size of the concentrated viral pellet, virus was resuspended in an appropriate volume of PBS and stored at -80 °C.

For the infection of neuronal precursor cells, approximately 60.000 neural crest cells were plated on Laminin/Fibronectin/Polyornithin coated 3.5 cm dishes and incubated for 6 hrs with different amounts of the concentrated virus. For a better virus uptake, protamine sulfate (8 µg/ml) was added to the medium. Afterwards, virus-containing medium was aspirated, cells were washed twice with PBS and fresh medium was added. Gene expression was activated 24 hrs post infection with a 10-day doxycycline treatment (5 µg/ml).

4.2.7 Differentiation of infected NCCs into nociceptive neurons

For the differentiation of neural crest cells into nociceptors, infected cells were kept in culture for at least 20 days in a special differentiation medium, mentioned as nociceptor differentiation medium. Depending on cell debris, medium was changed every 1-2 days. For Ngn1 gene induction, cells were treated with doxycycline (5 µg/ml).

4.2.8 Splitting of differentiating sensory neurons

One week after gene induction (when cells started to show neuronal morphologies), differentiating neurons were splitted by washing once with PBS and incubating in collagenase (Sigma) for 5 min at 37 °C. The cell monolayer came loose, and the collagenase-cell mix was transferred into a falcon tube. To further digest neuronal clumps, cells were triturated with a 1 ml pipette tip and centrifuged afterwards for 3 min at 1000 rpm. Resuspended cells were splitted according to their initial density most of the time in a ratio of (1:3-1:5) and transferred to fresh pre-coated culture plates.

4.2.9 Transient transfection of HEK 293T cells

To test and optimize purification conditions for the isolation of the 3xFlag-His-tagged Piezo2 protein, a tagged mouse Piezo1 construct was generated and transiently transfected into HEK293T cells by using Lipofectamine 2000. 24 hours prior to transfection, HEK cells were splitted and $0.5x10^6$ cells were plated per 6-well, resulting in a 70-90% confluency at the day of transfection. For each

transfection reaction, 250 µl Opti-MEM medium was mixed with 5 µl Lipofectamine 2000 (Thermo Fisher Scientific) and in an additional tube, 250 µl Opti-MEM medium was mixed with distinct amounts of plasmid DNA (1 µg-3 µg). After 5 min incubation at room temperature, diluted DNA was combined with diluted Lipofectamine and incubated again for 20 min at room temperature. Finally, transfection reaction was added to HEK cells. Medium was changed 24 hrs after transfection.

4.2.10 Immunoprecipitation

To test and optimize purification conditions for the isolation of the 3xFlag-His-tagged Piezo protein, an expression vector, containing the full length mPiezo1 sequence with a 3xFlag-His-tag at the N-terminus, was generated, transiently transfected into HEK 293 cells and purified by performing an immunoprecipitation with Flag-antibody coupled magnetic beads. As previously described, HEK 293 cells on a 6-well were transfected with 1 µg of plasmid DNA using Lipofectamine 2000. 24 hrs after the transfection, cells were lysed in 500 µl homogenization buffer (0.32 M Sucrose, 30 mM Tris, 2 mM KCl, 1 mM $MgCl_2$, 0.1 mM $CaCl_2$, 1 mM PMSF, 5 mM NaF, 1 mM NaOV, 20 mM beta-glycerophosphate) and centrifuged at 1000 g for 10 min at 4 °C to remove the nuclear fraction and cell debris. Supernatant was then ultracentrifuged for 1 hr at 100,000 g to separate cytosolic and plasma membrane protein fraction. Plasma membrane enriched fraction (the pellet of the ultracentrifugation step) was solubilized in 600 µl solubilization buffer (30 mM Tris-Cl, pH 7.4, 150 mM NaCl, 10 % Glycerol, 0.5 % DDM, 0.1 mM $CaCl_2$, 1 mM $MgCl_2$, 2 mM KCl, 1 mM PMSF, 5 mM NaF, 1 mM NaOV, 20 mM beta-glycerophosphate) for 2 hrs at 4 °C. Insolubilized material was removed by an additional centrifugation step at 17,000 g for 10 min. 35 µl of solubilized total lysate (supernatant of the ultracentrifugation step) and membrane lysate were saved, mixed with 1x laemmli and used as samples “before the IP”. The remaining samples were added to 30 µl of washed M2-Flag antibody-coated magnetic beads and immunoprecipitation was performed by an incubation step for 2.5 hrs at 4 °C. Afterwards, tubes were put in a magnetic manifold and flow through was collected. After three washing steps with washing buffer (30 mM Tris-HCl pH 7.4, 150 mM NaCl), proteins were eluted by adding 50 µl of 2x laemmli with 10% ß-mercaptoethanol and incubating samples for 10 min at 50 °C. Eluates were diluted 1:1 in laemmli buffer and loaded on a 3-8% Tris-Acetate gradient SDS-PAGE gel together with already collected supernatant lysates “before the IP”. 15 µl of the total lysate supernatant and 5 µl of the eluate were loaded onto the gel together with a PageRuler™ Prestained Protein Ladder. The SDS-PAGE gel was run for 2 hrs at 120 V and blotted for 2 hrs at 30 V. Membranes were removed from the Blot and blocked in 5% Milk in PBST for 1 hr at room temperature. Primary antibody was diluted 1:3000 in 5% Milk in PBST and applied overnight at 4 °C. After rinsing 3 times with PBST for 10 min each, membrane was incubated with the secondary antibody (diluted 1:1000 in

5% Milk in PBST) for 3 hours at room temperature. Finally, membrane was washed with PBST and protein levels were detected by a chemiluminescent Western Blot detection reagent.

4.3 Animals

As previously described (Rostock et al., *in press*), animal housing and experimental design was implemented according to the local animal welfare and their protocols (Regierungspräsidium Karlsruhe, Germany). Male and female mice (8-11 weeks) of a C57BL/6 background were used for the experiments. Mice were deeply anesthetized with isoflurane and DRG from L2–L6 were freshly dissected, embedded in OCT (Sakura) and frozen on dry ice.

4.4 Human Donors

Human DRGs were received from a profitless organization, that collects human tissue, the Netherlands Brain Bank (NBB). Depending on *post-mortem* parameters such as age, time delay between death and tissue preparation or pH ≥ 6.3 (measured from cerebrospinal fluid), human DRG of non-diseased donors were selected. Fresh frozen tissue was shipped on dry ice and stored at –80 °C for at least 96 hours.

Table 2: Different human DRG used for *in situ* hybridizations or immunohistochemistry

DRG Location	Sex/Age	Cause of death
L4	F/77	Pulmonary metastasis of vulva carcinoma
L5	F/71	Renal insufficiency by hypertensive nephropathy
T6	M/51	Suicide by refusing food and water
T8	F/78	Cardiac insufficiency
T12	F/75	Myocardial infarct

(L= lumbar; T=thoracic)

4.5 Experimental analyses of differentiated neurons or human and mouse tissue

4.5.1 Immunohistochemistry

As already described in Rostock et al., (*in press*), 20 µm thick mouse and human DRG slices were cut on a Leica cryostat, washed with PBS and fixed with 4% PFA for 30 min. Cultured cells were only fixed for 10 min. Afterwards samples were blocked with 10% goat serum + 0.1% TritonX-100 in PBS for 1 hour at room temperature.
Primary antibodies, diluted in 3% goat serum + 0.1% TritonX-100 in PBS were applied overnight at 4°C. After 3 washing steps with 0.1% Triton in PBS for 10 min, samples were incubated with secondary antibodies and DAPI (diluted in 3% goat serum + 0.1% TritonX-100) for 2 hours at room temperature. Finally, tissue and cells were rinsed with 0.1% TritonX-100 in PBS for 3 times and once in PBS and mounted with ImmuMount.

4.5.2 In Situ Hybridization

In situ hybridization was performed as previously described (Wende *et al*., 2012; Rostock et al., *in press*) and optimized for human DRG samples. Human and mouse cryo-sections of 20 µm thickness or differentiated cells were fixed in 4% PFA for 30 min, acetylated with acetylation buffer (100 mM Triethanolamine, 0.05% HCl) for 10 min at room temperature and afterwards permeabilized in 0.3% TritonX100 in PBS for 20 min at 4 °C. After pre–hybridization for 1 hr at room temperature, DIG and/or FITC-labeled cRNA probes (for human and mouse tissue, probes were hydrolyzed) were diluted 1:50 in hybridization buffer (5x SSC, 50% Formamide, 5x Denhardt´s, 250µg/ml yeast tRNA, 500 µg/ml Salmon sperm), added to the samples and hybridization was performed over night at 60 °C for human and mouse tissue or at 65 °C for differentiated cultures. The next day samples were washed twice in 2 x SSC, 50% Formamide, 0.1% N-Lauroylsarcosine at 60 °C and then treated with 20 µg/ml RNase A in RNAse buffer for 15 min at 37 °C. After washing twice in 2 x SSC + 0.1% N-Lauroylsarcosine and 0.2 x SSC + 0.1% N-Lauroylsarcosine at 37 °C for 20 minutes each, cell culture dishes and slices were blocked in $MABT^{++}$ (1x MABT [100 mM Maleic acid, 149 mM NaCl, 0.1% Tween 20, pH 7.5], 10% goat serum, 1% blocking reagent).
For a monomeric, colorimetric NBT/BCIP staining, samples were incubated overnight with anti-DIG-AP-Fab (1:1000) in $MABT^{++}$. After several washing steps with MAPT the color reaction was performed using NBT and BCIP 1:1000 in NTMT buffer (100 mM Tris pH 9.5, 100mM NaCl, 50 mM MgCl2, 0.1% Tween-20).
For a double fluorescent *in situ* hybridization, differentiated cells or DRG sections were stained by two sequentially rounds of Thyramide signal amplification (TSA) steps with an intermediate peroxidase inactivation step with 3% H_2O_2 for 2 hrs and 4% PFA for 30 min. Samples were incubated with anti-

FITC-POD (1:2000) or anti-DIG-POD (1:1000) in $MABT^{++}$ overnight at 4 °C. After intensive washing in MABT, the TSA reaction was performed by applying either Thyramide-Biotin or Thyramide-Rhodamine for 30 min at room temperature. For the detection of Thyramide-Biotin a streptavidin–cy2 antibody (1:1000) was applied, whereas nuclei were stained with DAPI. Finally, samples were washed five times with PBS + 0.1% Tween-20 and PBS and mounted with Immu-Mount.
In situ probes were generated based on the sequences used by the Allen brain atlas (for m*TrpV1*, m*TrkA* and *mNav1.6-1.9*) or were a kind gift from Dr. Hagen Wende (m*TrkB*, m*TrkC*, m*Ret*, m*Piezo2* and h*PIEZO2* and h*RET*). Full length clones for hTRPV1 and hTRPA1 were provided by Dr. David Julius (University of California, San Francisco), and *in situ* probes covered the complete open reading frame. Other *in situ* probes were amplified using the primers shown in the section 3.8 and cloned into pBluescript SK (+).

4.5.3 Calcium Imaging

To test functional properties of differentiated neurons, Ca^{2+}-imaging experiments were performed. When a neuron gets activated by a certain stimulus, in the case of a sensory neuron, this could be for example by capsaicin, mustard oil or in general by high potassium its membrane gets depolarized and allows Ca^{2+} ions to enter. Intracellular calcium changes can be measured with Fura-2 AM, a ratiometric, fluorescent Ca^{2+} indicator dye. Measuring calcium changes with a ratiometric calcium indicator compared to a non-ratiometric dye (*e.g*. Cal525 AM) diminishes the effects of photobleaching or inhomogeneous loading, resulting in more reproducible performances.

Differentiated cells were washed once with PBS and Ringer solution, and loaded with the Fura-2 loading buffer (10 µM Fura-2, 50 µg/ml Pluronic Acid [F-127] in Ringer solution) for 1 hour at room temperature in the dark.

After washing once with Ringer solution, glass cover slips were placed in a perfusion chamber installed on an inverted fluorescent microscope. Every 3 seconds, cells were excited at wavelengths of 340 nm and 380 nm using a Lambda DG-4 light source from Sutter instruments, whereas emitted light was captured at a wavelength of 510 nm using a coolSNAP HQ2 CCD camera (Photometrics).

To analyze cell responses, Fura2-loaded cells were successively stimulated and perfused with capsaicin (1 µM), mustard oil (200 µM) or menthol (0.1 µM). Different stimuli were intensively washed away by perfusing with Ringer solution. A final high potassium stimulus activated and indicated all neuronal cells in culture. For the analysis, regions of all neurons were set and the fluorescent signal of regions of interest were recorded over time by using MetaFluor 7.1 software. Further analysis was done with Excel 2016 and Graphpad Prism5 software. The cut-off value for a responding cell was calculated according to the basal ratio (R_0) during Ringer perfusion and the peak

ratio during the different stimuli (R_S). A cell was counted as a responder if the R_S ratio was higher than the mean plus 3-times Standard Deviation of the mean R_0 value. Values are shown as mean +/- SEM.

4.5.4 Real-Time (quantitative) PCR

The real-time polymerase chain reaction (RT-PCR), which is also known as quantitative PCR (qPCR), is a technique that allows the observation of specific amplified target DNA over time and can therefore be used for the quantitative analysis of different amplicons. In a qPCR experiment, the accumulation of the fluorescent signal is measured and in general there are two different ways how one can detect and classify PCR amplifications. A non-specific fluorescent dye, in our experiments SYBR Green, binds to any double-stranded DNA and an increase in DNA, after each PCR cycle, leads to an increase in fluorescent signal intensity. However, a TaqMan probe, an example for the specific detection of amplified DNA, is based on a designed probe, consisting of a fluorophore attached to the 5`-end and a quencher that is attached to the 3`-end of the probe quenching the fluorescent signal, emitted by the fluorophore. After extension of DNA molecules by the Taq polymerase, the annealed TaqMan probe is degraded and the fluorophore is released and no longer quenched by the quenching molecule, allowing the fluorescence to be detected. The cycle number at which the fluorescent signal intensity exceeds a certain threshold above background intensity, is called threshold cycle value (C_t value) and can be used for comparing different samples. For normalization purposes, at least two housekeeping genes (genes that are stably expressed in all cell types investigated) such as Glyceraldehyde 3-phosphate dehydrogenase (*GAPDH*), Hypoxanthine-guanine phosphoribosyltransferase (*HRPT*) or β-2 microglobulin (*B2M*) were used for the evaluation. For gene expression analysis delta C_t values were calculated as follows: Ct values of genes of interest (GOI) of differentiated nociceptors were first normalized to the housekeeping gene (HKG) and in a next step to undifferentiated NCLCs, serving as calibrators (1. HKG-GOI; 2. Differentiated cells-NCLCs). For analyzing gene expression of differentiated nociceptors, cDNA synthesized from RNA extracted from neurons was used as a template for qPCR analysis using the SYBR Green dye or TaqMan probes (Thermo Fisher Scientific). Each qPCR reaction using SYBR Green included 10 µl 2x Fast SYBR® Green Master Mix, 1 µl 10 µM forward and reverse primer, 1 µl of a 1:10 dilution of the 20 µl synthesized cDNA reaction and 7 µl deionized water. Reactions with TaqMan probes included 7.5 µl 2x Fast Start Essential DNA Probe Master, 0.75 µl of the 20 x primer-probe-mix, 1 µl of a 1:10 dilution of the 20 µl synthesized cDNA reaction and 5.75 µl deionized water. For normalization purposes, at least two housekeeping genes (*GAPDH* and *HRPT*) were analyzed in parallel and used for normalization of the C_t values of the gene of interest (GOI). The qPCR reaction was performed in a Light Cycler 96 from Roche, programmed as follows

SYBR Green-program

Preincubation	95 °C	10 min	
3 Step amplification	95 °C	10 sec	40 x
	60 °C	10 sec	
	72 °C	30 sec	
Melting	95 °C	10 sec	
	65 °C	60 sec	
	97 °C	1 sec	

Taq-Man program

Uracil-DNA Glycosylase (UDG) incubation	50 °C	2 min	
Polymerase activation	95 °C	10 min	
Amplification	95 °C	15 sec	45 x
	60 °C	1 min	

4.5.5 Electrophysiological Recordings done by Dr. Jörg Pohle

Neurons were visually identified using differential interference contrast microscopy with a 20X objective at an inverse microscope (Zeiss Observer A1). Only TRKA-positive cells were considered and identified with red fluorescence. With a borosilicate patch pipette filled with a KCl-based patch pipette solution cells were patched in a 3.5-cm dish in an extracellular HEPES-buffered physiological solution at room temperature. Electrophysiological traces were recorded with an Axopatch 200B amplifier and a Digidata 1440A converter using Clampex 10.6. Whole cell capacitance and pipette resistance were actively compensated. Action potentials were recorded in current clamp. Current was injected to keep baseline at -65 mV. From this, positive current steps were injected for 500 ms to evoke action potentials. Mechanical currents were recorded in voltage clamp at -65 mV. To evoke mechanical currents, cells were indented with increasing step size with the help of a polished borosilicate patch pipette fastened to a Kleindieck manipulator. Currents measured at an indentation of 20 µm were used to identify responsive cells.

4.6 Data Analysis

Data analysis was done as described in Rostock et al., (*in press*).

4.6.1 Image acquisition and quantification analysis

Fluorescent images were taken on a Nikon A1R or C2 point scanning confocal microscope, whereas bright field picture acquisition was done on a Ni–E wide field microscope (Nikon Imaging Center, University of Heidelberg). Further images analysis was done by using NIS–Element AR (Nikon), ImageJ/Fiji, Adobe Photoshop and Illustrator software.
Quantification analysis of each marker gene was performed by examining positive neurons from at least 3 different differentiations, 3-10 DRG sections per mouse (3-4 mice in total) and 3-4 sections per human DRG (3 human donors in total). Positive cells were counted manually using Adobe Photoshop software.

4.6.2 Area distribution analysis

For the analysis of the soma area distribution of *TrkA, TrkB and TrkC* positive cells, 3 DRG slices of 3 different donors were randomly selected for each marker gene and analyzed by ImageJ/Fiji software. Regions of interest (ROI) were first set automatically by analyzing particles according to their pixel

size in a thresholded, “binary”, black and white image. All pixels with values below a defined threshold were converted to white and pixels with values above a defined threshold were converted to black and included into the analysis. ROIs were also manually checked to refine automatically selected ROIs. Values were first measured and indicated in pixels and then converted in for displaying cell soma area. Graphpad Prism software was used for plotting the data.

4.6.3 Signal intensity analysis

Signal intensity analysis of *TrkA* or *Ret* positive cells was analyzed in 5 randomly chosen DRG slices from mouse and human tissue, respectively, by using ImageJ/Fiji software. ROIs for both *TrkA* and *Ret* were set, by analyzing particles (as described for the area distribution analysis) and values were measured according to their mean grey value. For normalization of each slice, single mean grey values for *TrkA* or *Ret* were divided by the maximum mean grey value of each slice and multiplied by 100. Graphpad Prism software was used for plotting all *TrkA* and *Ret* ratios in percent.

4.6.4 Statistical analysis

For quantifications the mean and the standard error of the mean (SEM) of 3 unrelated human individuals and 3-4 mice were considered. In *TrkA*-positive cells, fractions of double-positive cells in individual slices were determined. The dependence of fractions within slices from a certain subject (single human or mouse) was taken into account by applying a linear, mixed–effects model of the relationship between the fraction of double–positive cells and species as fixed effects. An additive random effect for each subject’s fraction level was introduced as random intercept. For this purpose, the software R (version 3.3.2) was used, with the lme function from the package nlme (version 3.1–131). The model was expressed in R as: lme(Fraction ~ Species, random = ~1 | Subject) using default restricted maximum likelihood criterion. Residual plots provided no obvious discrepancies from homoscedasticity or normality.

5. Results

The ability to perceive and transduce sensory stimuli is a fundamental property of the body and influences our sense of well-being immensely. Aside from pleasant mechanical stimuli (for example, a gentle hug from a friend), painful stimuli, such as a pinprick, serves as a warning signal to change our behavior and to protect us from tissue damage.

Vertebrates can detect these stimuli via specialized cells, the somatosensory neurons. It is known that the peripheral nervous system consists of many different types of sensory neurons, but how they are generated and the mechanisms by which they transduce the different types of stimuli is at present not fully understood. Therefore, the initial aim of this Ph.D. thesis was to differentiate human embryonic stem cells (hESCs) first into precursor cells of peripheral neurons, and afterwards into pain-sensitive nociceptors. Differentiated nociceptors were characterized by using Ca^{2+}-imaging, immunohistochemistry, *in situ* hybridization, quantitative RT-PCR and electrophysiological recording techniques (work done by Dr. Jörg Pohle). To validate whether hESC-derived nociceptors are physiologically relevant, we also compared them to mouse and human *post-mortem* DRG tissue and analyzed if they had a similar marker gene profile.

Furthermore, we were also interested in exploring the role of PIEZO2 in sensory neurons. PIEZO2 is a large transmembrane protein identified as a main transducer of innocuous mechanical stimuli, but so far it is uncertain whether it also plays a role in transducing noxious mechanical stimuli to trigger the sensation of pain. This question can be answered by comparing mechanically-activated currents from wild-type (WT) and PIEZO2-knockout (KO) nociceptors. Additionally, we also looked for accessory proteins of Piezo2 that could be involved in human PIEZO2-mediated sensory transduction, mediating innocuous mechanical stimuli.

Specifically, my thesis project consists of 5 parts:

1. Establish a differentiation protocol for the generation of nociceptive-like neurons using hESCs;
2. Characterize differentiated nociceptor-like cells;
3. Compare stem cell-derived nociceptors to human and mouse DRG tissue;
4. Investigate the role of PIEZO2 in stem cell-derived nociceptors;
5. Search for possible interaction partners of PIEZO2.

The outcome of this study would help us to identify differences between human and mouse nociceptors and to use this differentiation protocol as a basis for the generation of other distinct human nociceptive subpopulations, to finally provide a model system to study human pain and pain transduction *in vitro*.

5.*1* Establishing a differentiation protocol for stem cell-derived nociceptors

5.1.1 TRKA overexpression

From animal studies, it is known that shortly after neurogenesis induction (E9-E10.5), developing sensory neurons start to express sensory-specific gene programs and have characteristic molecular patterns. One of the best studied gene family markers are the tropomyosin-receptor kinases TRKA, TRKB and TRKC. These neurotrophin receptors are classically used to categorize sensory neurons into three main subpopulations, TRKA-expressing nociceptors, TRKB-positive mechanoreceptors and TRKC-positive proprioceptors (Chen et al., 2006; Perez-Pinera et al., 2008; Snider, 1994). Various studies in rodents and chicken demonstrated that TRKA, the high affinity receptor for NGF, is essential for differentiation and survival of small peptidergic DRG neurons and the absence of NGF/TRKA-signaling results in the loss of 70-85% of DRG neurons (Crowley et al., 1994; Silos-Santiago et al., 1995b). During development (at around E13), 80% of all differentiating DRG neurons express TRKA, whereas in adult mice TRKA expression is restricted to small diameter peptidergic nociceptors. TRKA-positive cells represent the largest group of sensory neurons (in mice ~ 40% of all DRG neurons), that mediate the detection of heat or noxious mechanical stimuli (Ernsberger, 2009; Molliver and Snider, 1997b).

Based on these findings, and due to the fact that in our laboratory a differentiation protocol for the generation of mechanoreceptors was already developed (Schrenk-Siemens et al., 2015), we wanted to modified the already existing protocol and establish a differentiation protocol for the generation of stem cell-derived nociceptors. Considering that TRKA seemed to be a major player for the generation of small diameter nociceptors, we started to virally overexpress the TRKA receptor and investigated if the overexpression could drive neural crest-like cells (NCLCs), the progenitors of primary sensory neurons to become nociceptors. For this we used a two-step differentiation protocol that recapitulates the *in vivo* sensory neuron development and is first based on the production of NCLCs. Some NCLCs are already predisposed to become sensory neurons and, considering what is known from mouse literature, we assumed that the viral-induced overexpression of TRKA would drive NCLCs towards a nociceptive lineage. Stem cell-derived NCLCs were infected with concentrated TRKA lentiviral particles, to constantly overexpress the neurotrophin receptor, and cultured for further differentiation in a differentiation medium, already proved to be successful for the differentiation of stem cell-derived mechanoreceptors (containing different growth factors such as BDNF, GDNF, NGF, NT-3 and retinoic acid) (Fig. 10A). The cell death rate of infected, differentiated cells was high and only few cells with neuron-like morphologies survived the differentiation procedure and could be analyzed by Ca^{2+}-imaging (Fig. 10B-D). To identify nociceptive neurons in culture, differentiated cells were stimulated with capsaicin (Caps, 1 µM), mustard oil (MO, 200 µM) or high potassium (HK, 100 mM) and tested

for their response by Ca^{2+}-imaging recordings. Only HK-excitable cells, defined as neurons, were included in the analysis.

Ca^{2+}-imaging experiments of TRKA-infected NCLCs, differentiated for 2-3 weeks, showed that a permanent TRKA overexpression was not sufficient and effective for the differentiation of nociceptive neurons. Images of pseudo-color Ca^{2+}-responses of cells within the field of view (Fig. 10B) and representative traces of one experiment (Fig. 10C) indicated, that the stimulation with 1 µM capsaicin (Fig. 8B-b and Fig. 8C), an agonist of the nociceptor-specific ion channel TRPV1, did not activate TRKA-infected cells in comparison to unstimulated cells in Ringer solution as a baseline (Fig. 10B-a). Quantification analysis demonstrated that, in 2 out of 3 analyzed cultures, differentiated cells showed a slight response to 200 µM allyl isothiocyanate, the pungent ingredient in mustard oil (Fig. 10B-c, Fig. 8C, Fig. 8D), activating TRPA1, an ion channel that is expressed by a subset of peptidergic, capsaicin-sensitive neurons.

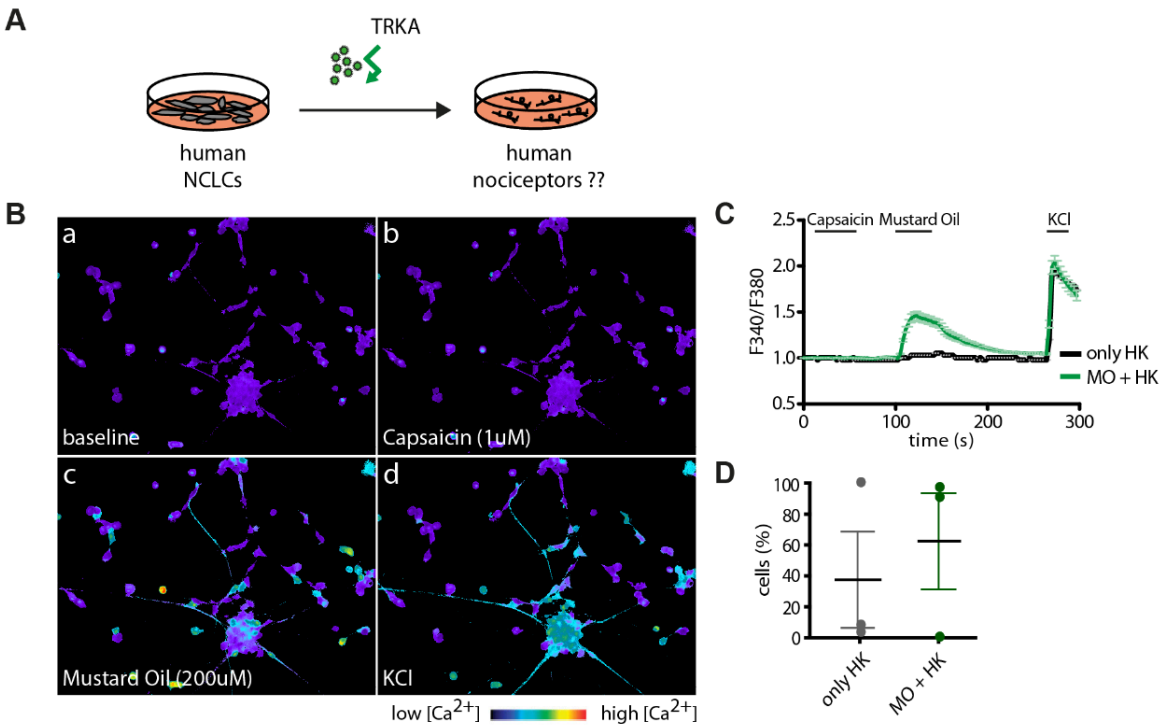

Fig. 10: Lentiviral TRKA overexpression and Ca^{2+}-imaging experiment of differentiated neurons

(A) Schematic representation of TRKA overexpression experiments, showing the transfection of human NCLCs with TrkA lentiviral particles and the differentiation into sensory neurons.

(B) Pseudo-color images of TRKA-infected, differentiated neurons, loaded with the fluorescent calcium indicator Fura-2 before stimulation (a) after capsaicin (b, 1 µM, Caps), mustard oil (c, 200 µM, MO) or high potassium (d, 100 mM, HK) treatment. Pseudo-color scale bar represents intracellular calcium concentrations.

(C) Representative traces of one experiment, shown in (B). While none of the neurons responded to capsaicin, some of them showed a response to mustard oil stimulation (in green). Average of responding neurons is given as mean ± SEM (n=32 cells).

(D) Quantification of three independent experiments, indicating that in one experiment all neurons only responded to high potassium (HK, in black), whereas in 2 experiments nearly all neurons showed a slight response to mustard oil (in green). None of the neurons responded to capsaicin. Percentage of responding neurons was calculated per experiment and reported as mean ± SEM (N=3 experiments).

Due to the fact that TRKA-infected differentiated cells only showed a slight response to mustard oil but no response to capsaicin and that only few cells survived the differentiation procedure, I concluded that constitutive TRKA overexpression did not generate stem cell-derived nociceptors.

5.1.2 RUNX1 overexpression

Another factor also known to play a crucial role in differentiation and specification of nociceptive sensory neurons is RUNX1, a Runt domain transcription factor. During development, RUNX1 is expressed in most nociceptors from E14.5-P0, more than 80% of TRKA-positive neurons also express low or high levels of RUNX1. In adult mice, RUNX1 becomes restricted to non-peptidergic nociceptors, cells that shut down TRKA expression and instead express the neurotrophic factor receptor RET (Chen et al., 2006). Furthermore, RUNX1 expression is essential for further ion receptor expression such as TRP channels or Nav channels and is also involved in controlling lamina-specific termination in the dorsal spinal cord (Chen et al., 2006). Based on these findings, we decided to test whether a viral-induced overexpression of RUNX1 is sufficient to drive NCLCs towards a nociceptive lineage.

As already described for TRKA overexpression experiments, NCLCs were infected with RUNX1 lentiviral particles to continuously overexpress the transcription factor and differentiated for additional 2-3 weeks in a differentiation medium that was established for the generation of stem cell-derived mechanoreceptors (Fig. 11A). Ca^{2+}-imaging experiments, of differentiated RUNX1-infected cells showed similar results as for TRKA-infected neurons: a permanent RUNX1 overexpression seemed not to be sufficient and effective for the differentiation of nociceptive neurons. The cell death rate of infected, differentiated cells was also high and only few cells with neuron-like morphologies survived the differentiation procedure and could be analyzed by Ca^{2+}-imaging (Fig. 11B-D).

A 1 µM capsaicin stimulus (Fig. 11B-b and Fig.11 C) did not activate RUNX1-infected, differentiated neurons in comparison to the baseline (Fig. 11B-a; cells in Ringer). A 200 µM mustard oil stimulus caused only a slight response in 85% of differentiated HK responders (Fig. 11B-c and C or D).

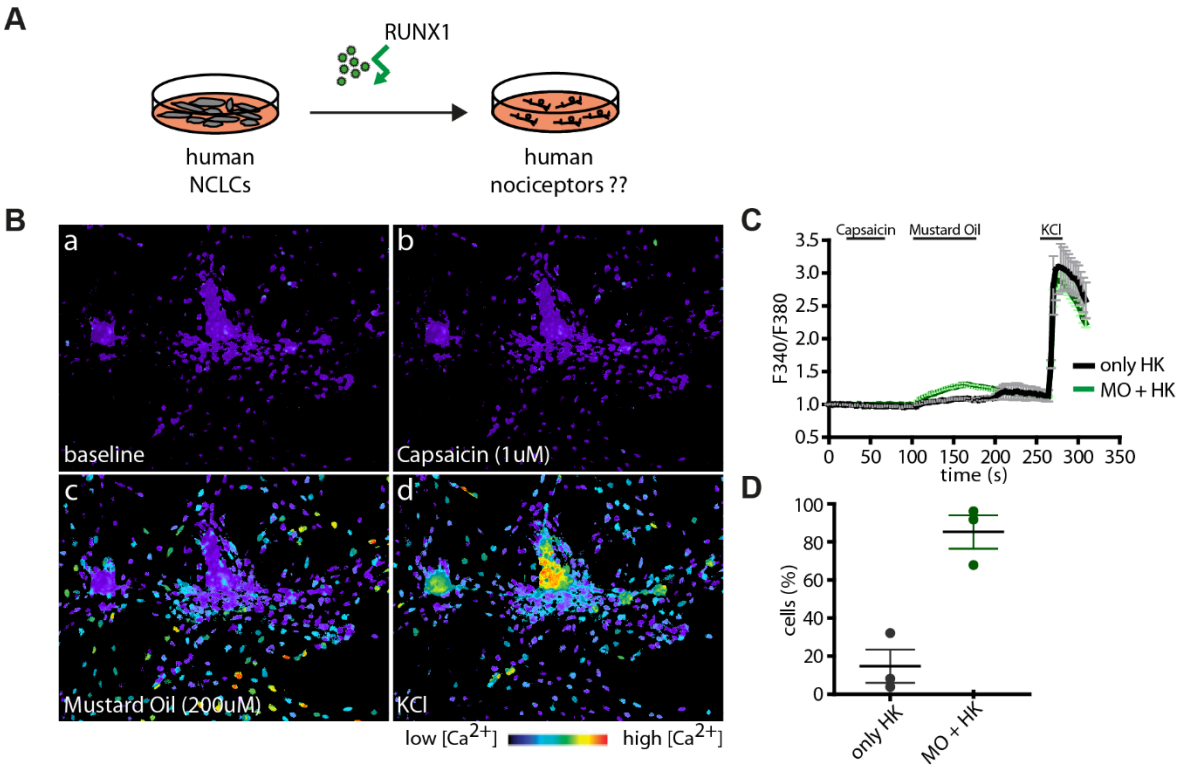

Fig. 11: Lentiviral RUNX1 overexpression and Ca^{2+}-imaging experiment of differentiated neurons

(A) Schematic representation of RUNX1 overexpression experiments, showing the transfection of human NCLCs with Runx1 lentiviral particles and the differentiation into sensory neurons.

(B) Pseudo-color images of RUNX1-infected, differentiated neurons, loaded with the fluorescent calcium indicator Fura-2 before stimulation (a) after capsaicin (b, 1 µM, Caps), mustard oil (c, 200 µM, MO) or high potassium (d, 100 mM, HK) treatment. Pseudo-color scale bar represents intracellular calcium concentrations.

(C) Representative traces of one experiment, shown in (B). While none of the neurons responded to capsaicin, some of the neurons showed a slight response to mustard oil stimulation (in green). Average of responding neurons is given as mean ± SEM (n=73 cells).

(D) Quantification of three independent Calcium-imaging experiments, indicating that in all three analyzed experiments a vast majority of neurons showed a slight response to mustard oil (in green). None of the neurons responded to capsaicin. Percentage of responding neurons was calculated per experiment and reported as mean ± SEM (N=3 experiments).

Since RUNX1-infected, differentiated cells only showed a slight response to mustard oil and did not respond to capsaicin and additionally only few cells survived the differentiation procedure, a permanent RUNX1 overexpression also seemed not to be efficient for the generation of stem cell-derived nociceptors.

5.1.3 NGN1 overexpression

At the same time, when we tried to establish a functional differentiation protocol for the generation of nociceptors by overexpressing TRKA or RUNX1, Südhof and colleagues published a study in which they demonstrated that the forced overexpression of a single transcription factor, NGN2, led

to the direct conversion of hESCs or induced pluripotent stem cells (iPSCs) into neuronal cells in less than 2 weeks, with an efficiency of nearly 100% (Zhang et al., 2013b). NGN1 and NGN2 are basic helix-loop-helix (bHLH) transcription factors known to determine specific neuronal progenitor populations in the developing CNS as well as in the PNS and furthermore to induce neurogenesis in mice (Ma et al., 1999b; Sommer et al., 1996). While in the PNS NGN2 seems to trigger neuronal diversification of mainly large diameter mechanoreceptive or proprioceptive neurons, NGN1 seems to mediate the differentiation of small diameter, TRKA-positive nociceptive neurons (Ma et al., 1998, 1999a).

To unravel the question if NGN1 overexpression is critical to drive NCLCs into a nociceptive lineage, we cloned the human *NGN1* into a tetracycline-inducible lentiviral backbone, already used by Zhang *et al*., to obtain an inducible Tet-on lentiviral construct. Theoretically, this system allows reversible transgene expression upon application of the antibiotic doxycycline. Only in the presence of doxycycline, the reverse tetracycline transactivator protein (rtTA) can bind the TetO operator and thus induce NGN1-EGFP gene expression. If doxycycline treatment is stopped, the transactivator cannot bind the operator anymore and gene expression and therefore also the coupled EGFP signal is switched off (Fig. 12A).

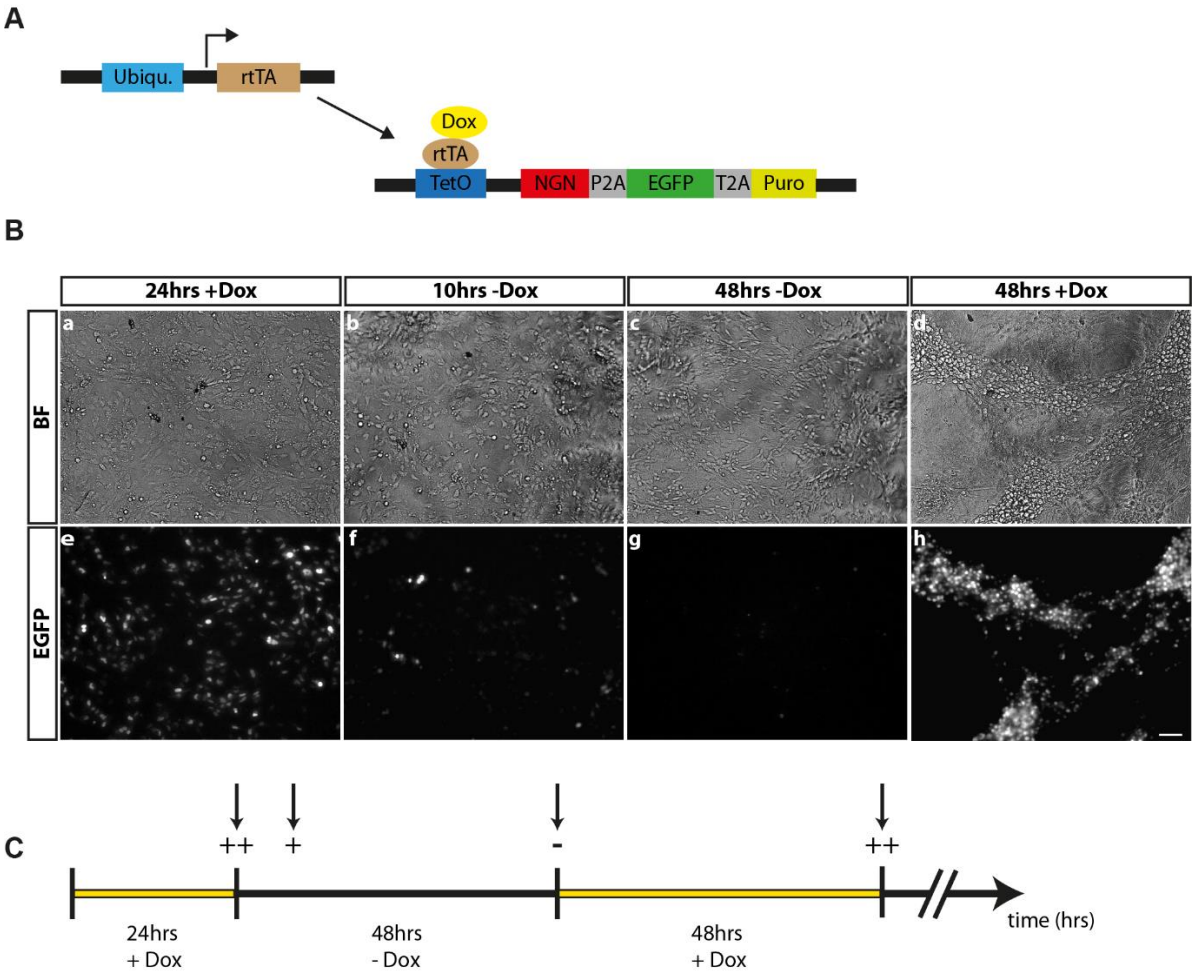

Fig. 12: Lentiviral Tet-on-system

(A) Schematic representation of the lentiviral Tet-On system for NGN1/rtTA overexpression experiments. Cells were transfected with a virus expressing the reverse tetracycline transactivator (rtTA) and a virus expressing a NGN1-EGFP-Puromycin -resistance fusion protein, linked by P2A and T2A sequences.
(B) Time course experiments, checking for virally-induced NGN1-EGFP expression in hESC-derived NCLCs. (a-d) Phase contrast images and (e-h) GFP-fluorescent images of NGN1/rtTA-infected NCLCs after doxycycline treatment (e, h) and without the antibiotic (f-g). Scale bar 50 µm.
(C) Time-line illustrating the Dox treatment (yellow regions) and analysis of NGN1-EGFP expression in NCLCs at different timepoints (↓). Strong EGFP signal (++) , slight EGFP signal (+), no EGFP signal (-).

To test if we are able to control NGN1 gene expression, I performed time-course experiments to check for virally induced NGN1-EGFP expression in hES cell-derived NCLCs in the presence or absence of doxycycline (Fig. 12C). As expected, NGN1 expression could be induced 24 hours after doxycycline treatment, as indicated by the strong EGFP signal (Fig. 12B-e). Gene expression was already reduced after 10 hours without doxycycline (Fig. 12B-f) and was no longer detectable after 48 hours without the antibiotic (Fig. 12B-g). Gene expression could also be reliably induced and inhibited multiple times as shown by the EGFP signal after repetitive doxycycline treatment (Fig. 12B-h).

In order to explore whether introducing such a central transcription factor is crucial for sensory neuron development and would drive more NCLCs cells to adopt a nociceptive phenotype, we infected NCLCs with NGN1 and rtTA lentiviral particles and analyzed them by immunostaining and Ca^{2+}-imaging experiments. It is generally accepted that, shortly after neurogenesis induction, post-mitotic sensory neurons start to express the insulin gene enhancer protein ISLET1 and the brain-specific homeobox/POU domain protein 3A, BRN3A (Anderson, 1999). Additionally, these proteins are important for further sensory specific gene expression patterns, as TRKA and RUNX1-positive cells are almost lost in *Ilset1* mutants, while TRKC and RUNX3-positive, proprioceptive neurons are not affected (Eng et al., 2001, 2004, 2007; Sun et al., 2008).
To test if NGN1/rtTA overexpression induces neurogenesis in infected NCLCs, immunostainings of GFP-infected control cells (Fig. 13A-C) and NGN1/rtTA-infected cells (Fig. 13D-F) were performed 3 days after gene induction. Quantifications demonstrated that the number of ISLET1-positive sensory neuron precursors was increased in NGN1/rtTA-infected NCLCs compared to control GFP-infected cells: only 3% of the GFP-infected control population (Fig. 13A-C) was ISLET1-positive, while in NGN1/rtTA-infected cells 75% of all cells showed an ISLET1 staining (Fig. 13D-F).

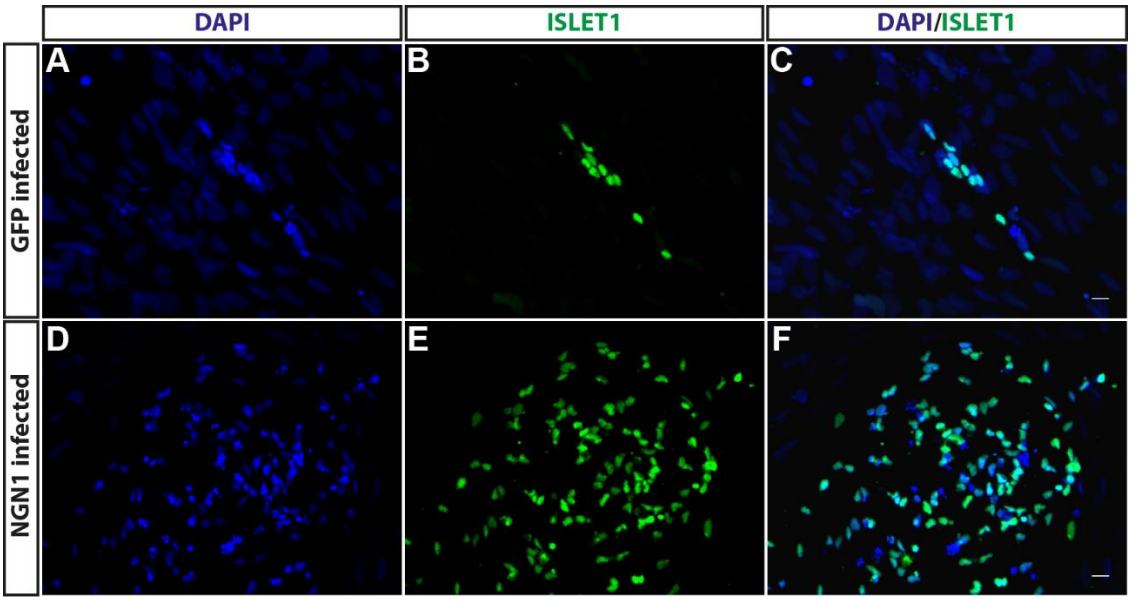

Fig. 13: Induction of sensory neuron development after Ngn1 overexpression

Immunostaining of GFP and NGN1 infected NCLCs (3 days after gene induction) for ISLET1 (ISL1), a marker for post-mitotic developing sensory neurons. Only 3% of all $DAPI^+$ cells were ISL1-positive in the GFP-infected cell population (A-C), while 75% of all cells showed an ISL1 staining in NGN1-infected cells (D-F). Scale bar 20µm.

Ca^{2+}-imaging experiments of NGN1/rtTA-infected NCLCs (Fig. 14A-D), stimulated with capsaicin (1 µM) or mustard oil (200 µM) after 3 weeks of differentiation, showed that a transient overexpression of NGN1 (induction of 3 days) seemed not to be sufficient and effective for the differentiation of nociceptive neurons (Fig. 14A-D). However, compared to what we have seen with TRKA or RUNX1 overexpression experiments, the mortality rate was lower, and most of the cells survived the differentiation procedure and developed neuron-like morphologies (Fig. 14 B).

However, a 1 µM capsaicin stimulus did not activate NGN1-infected cells (Fig. 14B-b and Fig. 14C), and mustard oil either provoked a slight or no response (depending on the experiment analyzed, Fig 14B-c and Fig. 14C-D). On average, 32% of differentiated NGN1-infected cells responded to mustard oil and to a high K^+ (HK) stimulus, whereas 68% of the neurons showed only a response to HK. None of the cells responded to a 1 µM capsaicin stimulus (Fig. 14 B-D).

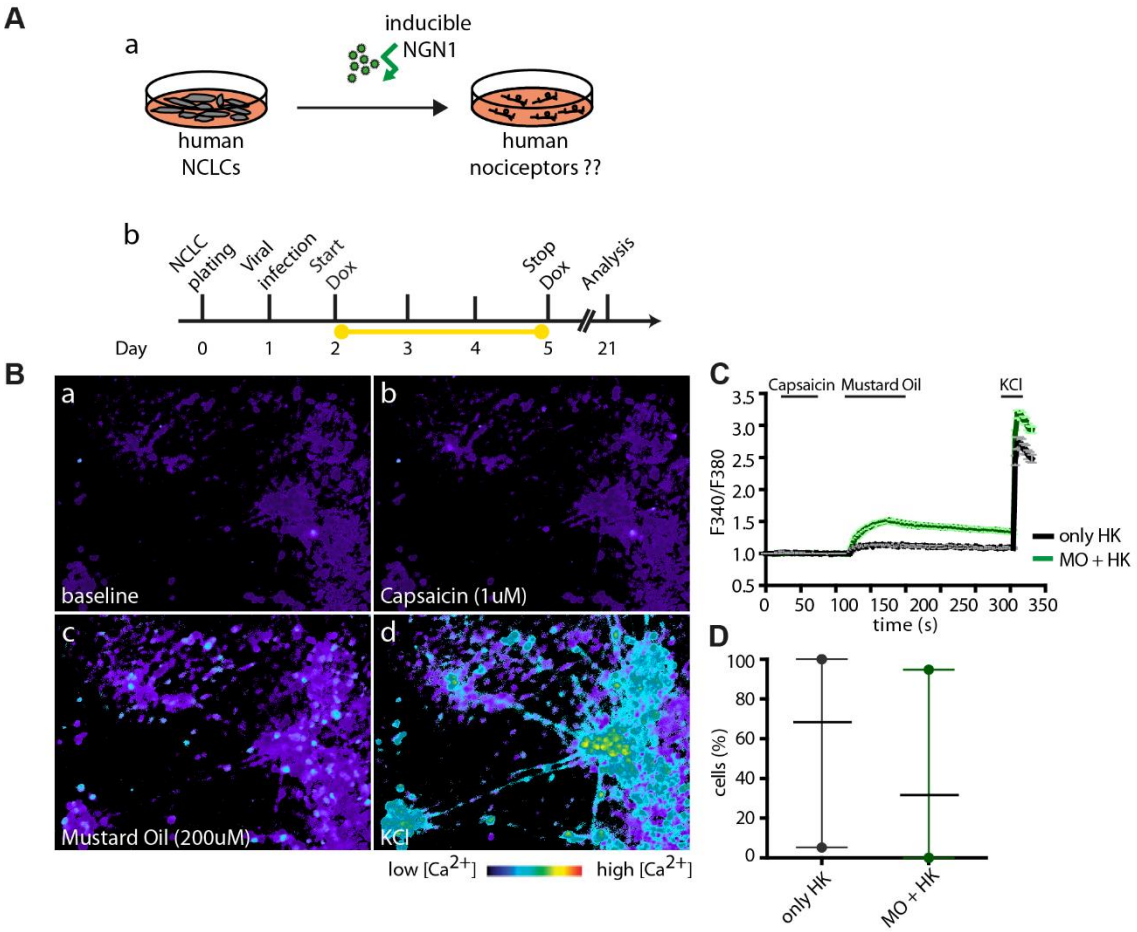

Fig. 14: Lentiviral NGN1 overexpression and Ca^{2+}-imaging experiment of differentiated neurons

(A) Schematic representation of NGN1 overexpression experiments, showing the transfection of human NCLCs with NGN1 lentiviral particles and the differentiation into sensory neurons (b) and time-flow diagram of lentivirus infection, doxycyclin treatment and functional analysis of differentiated neurons.

(B) Pseudo-color images of NGN1 infected, differentiated neurons, loaded with the fluorescent calcium indicator Fura-2 before stimulation (a) after capsaicin (b, 1 µM, Caps), mustard oil (c, 200 µM, MO) or high potassium (d, 100 mM; HK) treatment. Pseudo-color scale bar represents intracellular calcium concentrations.

(C) Representative traces of one experiment, shown in (B). While none of the neurons responded to capsaicin, some of the neurons showed a slight response to mustard oil stimulation (in green). Average of responding neurons is given as mean ± SEM (n=96 cells).

(D) Quantification of two independent Calcium-imaging experiments, indicating that in one experiments a vast majority of neurons showed a response to mustard oil and HK (in green), whereas in the second experiment neurons only responded to HK stimulation (in black). None of the neurons responded to capsaicin. Percentage of responding neurons was calculated per experiment and reported as mean with range (N=2 experiments).

In summary, although overexpression of NGN1 led to a marked increase in the number of ISLET1-positive cells, and the number of developing sensory neurons was also increased, this was not sufficient to differentiate the developing sensory neurons further into a distinct nociceptive lineage.

5.1.4 NGN1/RUNX1 overexpression

Since overexpression of single proteins (TRKA, RUNX1 or NGN1) was not effective to drive NCLCs towards a nociceptive fate, and due to the fact that developing sensory neurons express a full set of sensory specific genes in a time-dependent manner, we decided to change our strategy and combine viral-induced overexpression of NGN1 and RUNX1. NCLCs were first infected with NGN1 and tTA lentiviral particles and gene expression was induced by doxycycline for 3 days until infected EGFP-positive cells started to change their morphology. In a following step, differentiating cells were infected with RUNX1 lentiviral particles, trying to recapitulate the *in vivo* sensory neuron development. Studies investigating the development of nociceptors in mice have shown that NGN1 is important for sensory neurogenesis and mediates the differentiation of TRKA-positive nociceptors (Ma et al., 1999a) and, later during development, RUNX1 is broadly expressed in differentiating nociceptors and becomes restricted to the non-peptidergic subpopulation (Chen et al., 2006).

Ca^{2+}-imaging experiments with NGN1/tTA and RUNX1-infected NCLCs, after 3 weeks of differentiation, showed that 13% of the neurons responded uniquely to the HK stimulus, and most neurons got activated by both mustard oil and HK (Fig. 15). Additionally, a small fraction of all analyzed neurons (4%) showed a slight response to capsaicin, mustard oil and HK stimuli, suggesting that this small fraction of cells became functional nociceptor-like neurons.

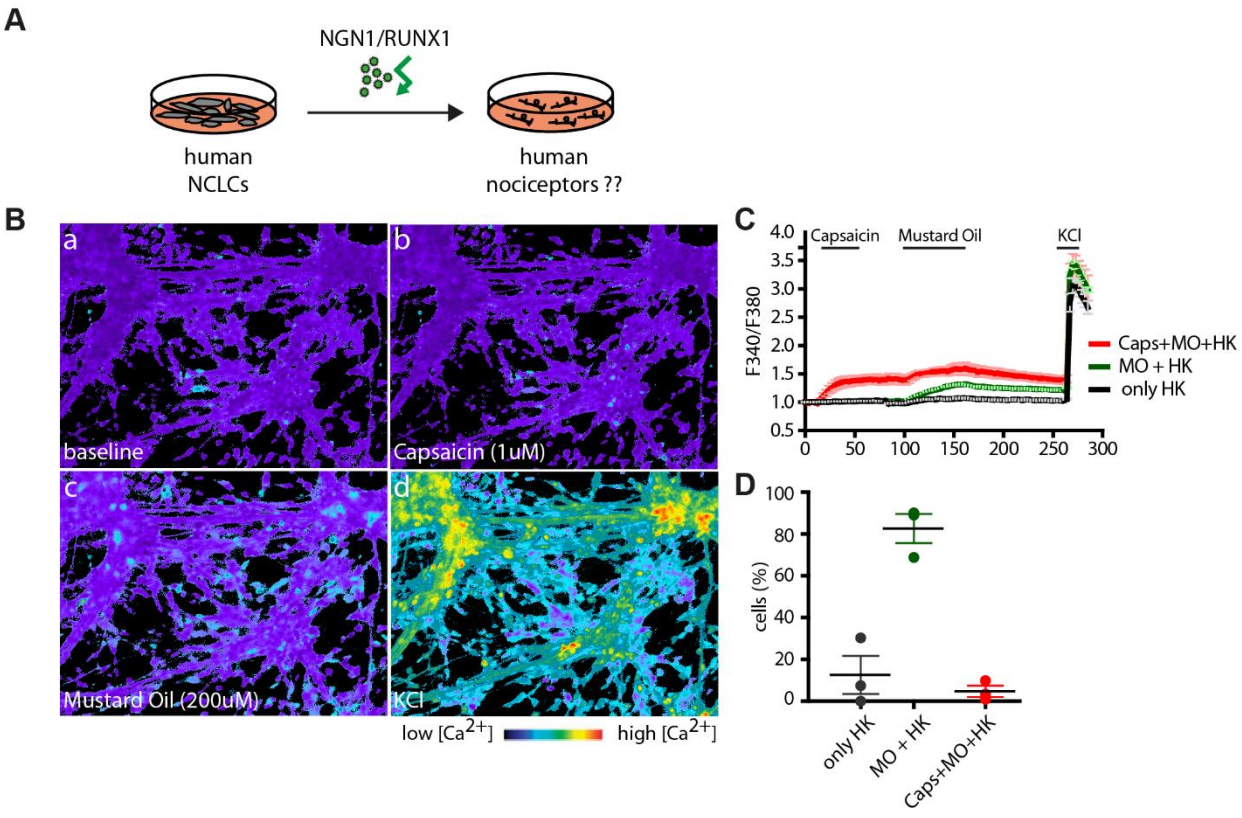

Fig. 15: Lentiviral NGN1/RUNX1 overexpression and Ca^{2+}-imaging experiment of differentiated neurons

(A) Schematic representation of NGN1/RUNX1 overexpression experiments, showing the transfection of human NCLCs with NGN1/RUNX1 lentiviral particles and the differentiation into sensory neurons.
(B) Pseudo-color images of NGN1/RUNX1-infected, differentiated neurons, loaded with the fluorescent calcium indicator Fura-2 before stimulation (a) after capsaicin (b, 1 µM, Caps), mustard oil (c, 200 µM, MO) or high potassium (d, 100 mM, MO) treatment. Pseudo-color scale bar represents intracellular calcium concentrations.
(C) Representative traces of one experiment, shown in (B), showing that some cells showed a slight response to capsaicin, mustard oil and HK (in red), some to mustard oil and HK (in green) and also cells that only responded to the HK stimulus (in black). Average of responding neurons is given as mean ± SEM (n=174 cells).
(D) Quantification of three independent Calcium-imaging experiments indicated that a vast majority of neurons showed a slight response to mustard oil and HK (in green), whereas 13% of the neurons responded to HK only and a minority of neurons to all stimuli, capsaicin and mustard oil and HK (in red). Percentage of responding neurons was calculated per experiment and reported as mean ± SEM (N=3 experiments).

Since our initial analysis was only based on visual detection of responding cells and only a very small fraction of cells showed a weak response to capsaicin (compared to what is known from literature and what we have seen from cultured mouse DRG neurons), we assumed that the combined overexpression of NGN1 and RUNX1 was not sufficient for the generation of a good number of stem cell-derived nociceptors. One hypothesis to explain such results could be that some other important factors are missing or something in the differentiation medium such as growth factors, or neurotrophins are lacking and hindering further differentiation.

5.1.5 Overexpression of 5 transcription factors (based on Wainger et al., 2015)

Subsequent to asserting that the overexpression of single developmental factors (TRKA, RUNX1 and NGN1) or the combination of two (NGN1/RUNX1) seemed not to be sufficient for the generation of nociceptive neurons, a work by Clifford Woolf and colleagues demonstrated that permanent viral-induced overexpression of a set of transcription factors (neurogenin 1 [NGN1], Islet-2 [ISL2], Kruppel-like factor 7 [KLF7], myelin transcription factor 1-like [MYT1L], and Achaete-scute homolog 1 [ASCL]) is able to reprogram mouse and human fibroblasts into functional nociceptors (Wainger et al., 2015).

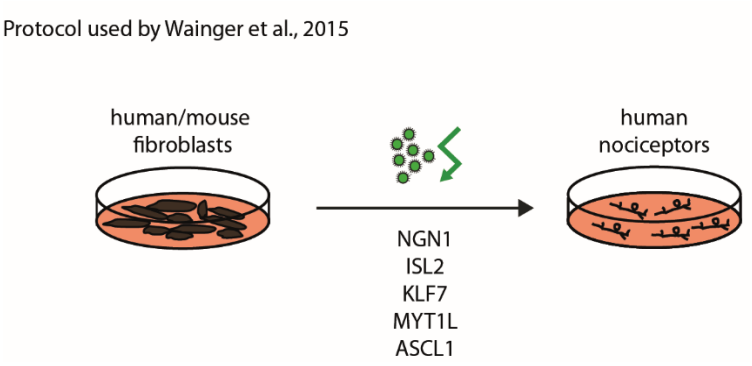

Fig. 16: Schematic representation of the reprogramming protocol used by Wainger et al., 2015

Scheme of the reprogramming protocol to convert human/mouse fibroblasts into pain-sensitive sensory neurons, used by Wainger et al., 2015. The combined stable overexpression of five transcription factors (NGN1, ISL2, KLF7, MYT1L and ASCL1) converted fibroblats and generated sensory neurons with a nociceptive phenotype.

Due to the fact that we were still interested in generating and characterizing hESC-derived nociceptors, we decided to adopt and modify this protocol for use in our cell culture system.

Different to the Wainger *et al*. study (henceforth referred to as "Woolf protocol"), we did not use human and mouse fibroblasts as a starting cell population, but instead our stem cell-derived NCLCs, as they are very similar to the *in vivo* progenitors of sensory neurons. Furthermore, the differentiation cocktail used by Wainger *et al*. contained a reduced number of growth factors (only NGF, BDNF and GDNF) but also included fetal bovine serum, a widely used undefined growth supplement for cell culture media. By recapitulating the published protocol with our cellular system, NCLCs were infected with lentiviral particles of all 5 transcription factors (NGN1, ISL2, KLF7, MYT1L and ASCL) resulting in their stable overexpression over the entire differentiation period (at least 3 weeks). While the transcription factors ASCL1 and MYT1L are important for reprogramming cells, to drive them towards the neuronal lineage, KLF7 or NGN1 are rather relevant for further sensory neuron diversification of TRKA-expressing nociceptors (Lei et al., 2005; Ma et al., 1999a; Vierbuchen et al., 2010).

Ca^{2+}-imaging experiments of NGN1/ISL2/KLF7/MYT1L/ASCL1-infected NCLCs (differentiated for at least 3 weeks), stimulated with capsaicin (1 µM), mustard oil (200 µM) or menthol (0.1 µM), an organic compound activating the cold-receptor TRPM8, showed that a persistent overexpression of these 5 factors seemed to be sufficient and effective for the differentiation of nociceptive neurons (Fig. 17). Strikingly, a large proportion of cells responded to capsaicin, pointing out their nociceptive properties.

On average, approximately 70.5% of the derived excitable cells (determined by a HK stimulus and therefore defined as neurons) showed a response to capsaicin plus HK (Fig. 17B-b, C, D), 20% to capsaicin and mustard oil, and only a small percent of neurons responded to mustard oil only (Fig. 17C, 1.1%), menthol plus capsaicin (Fig. 17D, 0.8%) or HK only (7.6%).

In summary, a persistent viral-induced overexpression of 5 transcription factors, as already used by Wainger *et al*. was finally able to generate functional stem cell-derived nociceptors, even when fibroblasts as the starting material were replaced by stem cell-derived NCLCs.

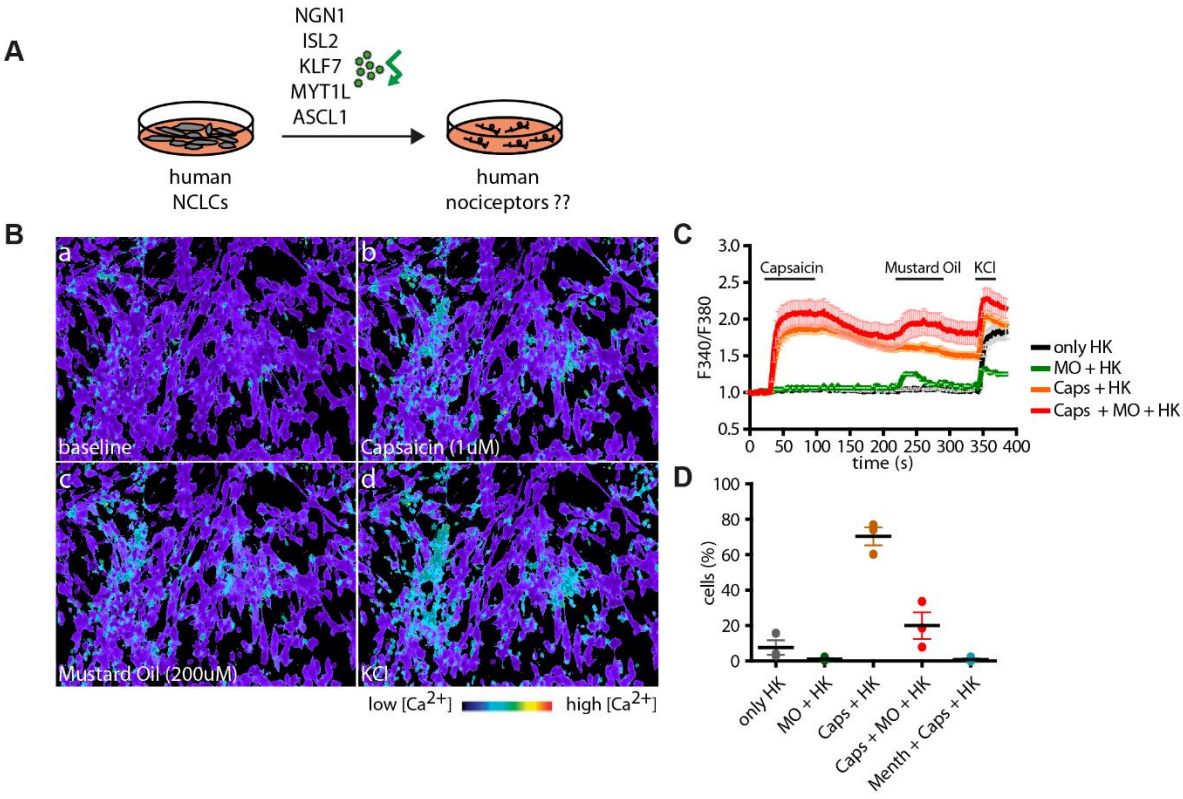

Fig. 17: Lentiviral overexpression of "5 Woolf factors" and Ca^{2+}-imaging experiment of differentiated neurons

(A) Schematic representation of overexpression experiments, showing the transfection of human NCLCs with lentiviral particles of all five "Woolf factors" and the differentiation into sensory neurons.

(B) Pseudo-color images of infected, differentiated neurons after at least 21 days in culture, loaded with the fluorescent calcium indicator Fura-2 before stimulation (a) after capsaicin (b, 1 µM, Caps), mustard oil (c, 200 µM, MO) or high potassium (d, 100 mM, HK) treatment. Pseudo-color scale bar represents intracellular calcium concentrations.

(C) Representative traces of one experiment, shown in (B) indicated that differentiated neurons showed a proper response to capsaicin and HK (in orange) and capsaicin and mustard oil (in red). A fraction of cells responded to mustard oil /HK (in green) or HK only (in black). Average of responding neurons is given as mean ± SEM (n=95 cells).

(D) Quantification of three independent Calcium-imaging experiments indicated that a vast majority of neurons, about 70% showed a response to capsaicin and HK (in orange), about 20% of the neurons responded to capsaicin/mustard oil/HK (in red) and a minority of neurons got activated by mustard oil/HK (in green), menthol/capsaicin/HK (in blue) or HK only (in black). Percentage of responding neurons was calculated per experiment and reported as mean ± SEM (N=3 experiments).

5.1.6 Simplification I of the Woolf protocol: overexpression of 3 factors

Contrary to the "Woolf protocol" using fibroblasts as starting material, stem cell-derived NCLCs, the progenitors of the primary sensory neurons, are more prone to become sensory neurons. While the transcription factors ASCL1 and MYT1L are more important for reprogramming cells in order to drive them towards the neuronal lineage, KLF7 or NGN1 are rather relevant for further sensory neuron diversification of TRKA-expressing nociceptors (Lei et al., 2005; Ma et al., 1999a; Vierbuchen et al., 2010) (Fig. 18A). Since Wainger *et al*. started with a completely different cell type compared to us, we hypothesized that not all five transcription factors were necessary to obtain stem cell-derived nociceptors. To test our hypothesis, that only 3 virally-expressed

transcription factors in the differentiation cocktail are required to generate functional nociceptors, NCLCs were infected with lentiviral particles of only the 3 transcription factors NGN1, ISL2 and KLF7 and differentiated for at least 3 weeks.

Ca^{2+}-imaging experiments of these differentiated cells, stimulated with capsaicin (1 µM), mustard oil (200 µM) or menthol (0.1 µM) (Fig. 18B-E), demonstrated that a persistent overexpression of only 3 "Woolf factors" seemed sufficient and effective for the differentiation of TRKA-positive nociceptive neurons: 41.4 % of the derived tomato-positive neurons showed a response to capsaicin and HK (indicated by the orange trace), 34.3% of the neurons got activated by capsaicin and mustard oil (shown by the red trace) and only a small percent of cells responded to mustard oil plus HK (7 %; green trace), menthol plus capsaicin (0.3% blue trace) or HK only (black trace).

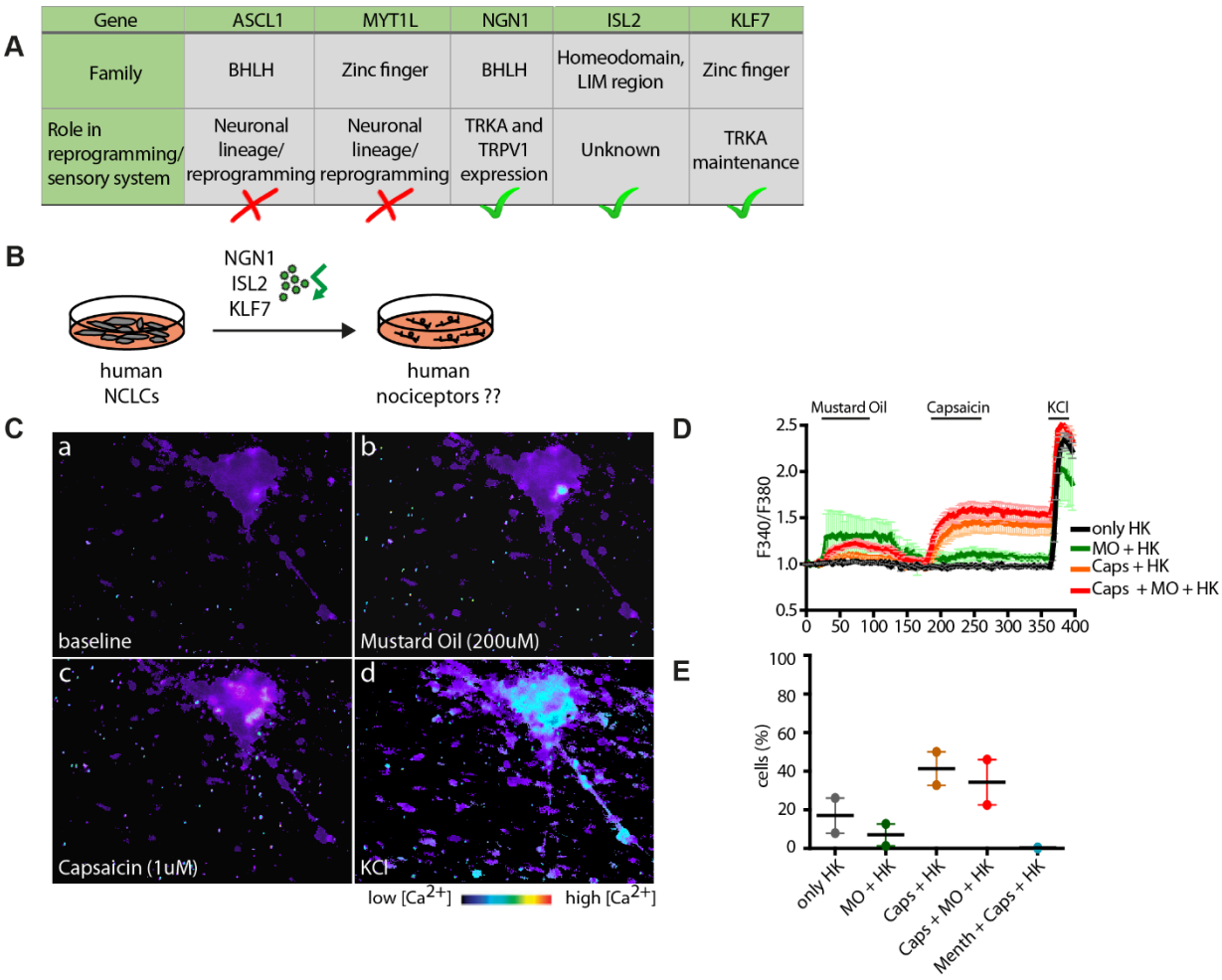

Fig. 18: Lentiviral overexpression of "3 Woolf factors" and Ca^{2+}-imaging experiment of differentiated neurons

(A) Transcription factors, used by Wainger *et al*., 2015 and their role in the sensory system.
(B) Schematic representation of overexpression experiments, showing the transfection of human NCLCs with lentiviral particles of three "Woolf factors" and the differentiation into sensory neurons.
(C) Pseudo-color images of infected, differentiated neurons, loaded with the fluorescent calcium indicator Fura-2 after at least 21 days in culture, before stimulation (a) after capsaicin (b, 1 µM, Caps), mustard oil (c, 200 µM, MO) or high potassium (d, 100 mM, HK) treatment. Pseudo-color scale bar represents intracellular calcium concentrations.
(D) Representative traces of one experiment, shown in (B) indicated that differentiated neurons showed a proper response to capsaicin and HK (in orange) and capsaicin and mustard oil (in red). A fraction of cells responded to mustard oil/HK (in green) or high HK (in black). Average of responding neurons is given as mean ± SEM (n=36 cells).
(E) Quantification of two independent Calcium-imaging experiments indicated that about 41% of neurons showed a response to capsaicin and HK (in orange), about 34% of the neurons responded to capsaicin/mustard oil/HK (in red) and a minority of neurons got activated by mustard oil/HK (in green), menthol/capsaicin/HK (in blue) or HK only (in black). Percentage of responding neurons was calculated per experiment and reported as mean with range (N=2 experiments).

These experiments showed that the viral-induced overexpression of only 3 transcription factors is sufficient to obtain functional stem cell-derived nociceptors when using already primed neuronal precursor cells as the starting population.

5.1.7 Simplification II of the Woolf protocol: overexpression of 1 factor

Although preliminary Ca^{2+}-imaging results of differentiated nociceptors generated according to the modified "Woolf protocol" were promising and virally-induced overexpression experiments with only 3 transcription factors seemed to be effective for the differentiation of stem cell-derived nociceptive neurons, we could not reliably reproduce these findings.

Several rounds of lentivirus production did not result in infectious lentiviral particles or in the generation of nociceptors. Also, the lack of a fluorescent protein within the viral constructs fused to the gene of interest prevented us from controlling the virus production or viral infection rates. To elucidate which virus was actually infectious and, more importantly which factor was essential for the generation of stem cell-derived nociceptors, RT-PCR analyses were performed with ISL2, KLF7 or NGN1-infected NCLCs after different times of differentiation (uninfected NCLCs were used as negative control and mouse spinal cord samples as positive control) (Fig. 19).

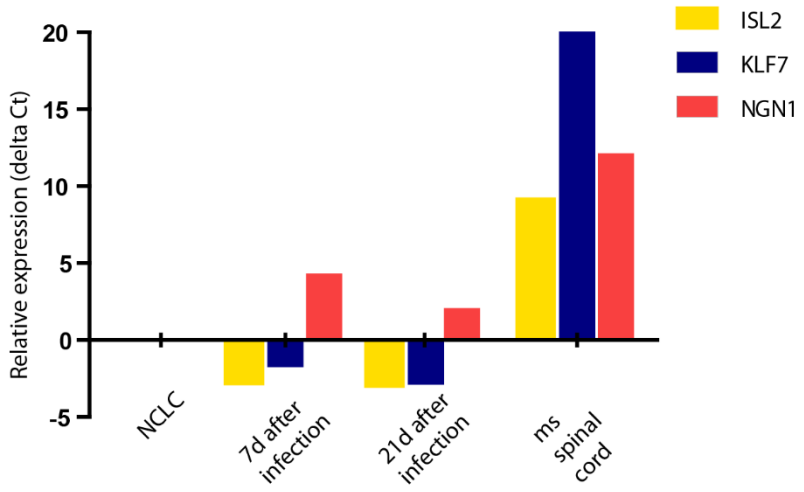

Fig. 19: Verification of "Woolf virus" expression

qRT-PCR analysis, representing the relative expression level of *ISLET1* (yellow), *KLF7* (blue) and *NGN1* (red) in stem cell-derived nociceptors after different time points of differentiation, normalized to the housekeeping gene *B2M* and compared to uninfected NCLCs as a negative control and mouse spinal cord samples as a positive control. In infected differentiated nociceptors only *Ngn1* induction was detectable. The delta Ct values of one experiment are shown.

Expression analysis (normalized to the housekeeping gene *B2M* and the uninfected NCLCs), demonstrated that infection of ISL2 (shown in yellow) or KLF7 (shown in blue) did not promote a detectable gene induction (7 or 21 days after viral infection), when compared to spinal cord samples, where gene expression was increased. Only in NGN1-infected NCLCs (shown in red) gene expression was induced after 7 or 21 days, compared to uninfected control cells (Fig. 19).

These results suggest that not all 3 transcription factors are required for the generation of nociceptive neurons, but that only NGN1 expression was effective to drive NCLCs into a nociceptive lineage. In line with this finding, Südhof and colleagues also demonstrated that the forced overexpression of NGN2 alone, another member of the bHLH transcription factor family, is sufficient to directly convert hESCs or iPSCs into neuronal cells (Zhang et al., 2013b). To test the hypothesis that only NGN1 is effective to drive NCLCs into a nociceptive lineage, NCLCs were infected with NGN1 lentiviral particles and differentiated for at least 3 weeks.

Ca^{2+}-imaging experiments of NGN1-infected, TRKA-positive neurons, stimulated with capsaicin (1 µM), mustard oil (200 µM) or menthol (0.1 µM), indicated that a persistent overexpression of NGN1 alone seemed to be sufficient for the differentiation of nociceptive neurons (Fig. 20 B-D).

Quantification analysis revealed that, on average, 29.5% of the derived neurons showed a response to capsaicin and HK (indicated by the orange trace, Fig. 20 B-c, C, D), 16.6% of the neurons got activated by capsaicin and mustard oil (shown by the red trace) and only a small percentage of cells

responded to mustard oil plus HK (8%; green trace) or menthol plus capsaicin (0.2%) (Fig. 20 B-D). Although the variability of different experiments was high and the number of capsaicin sensitive neurons fluctuated (as indicated by the marked error bars in Fig. 20 D), there was clear evidence that a permanent viral-induced overexpression of NGN1 drives NCLCs towards the sensory lineage with characteristic hallmarks of functional nociceptors.

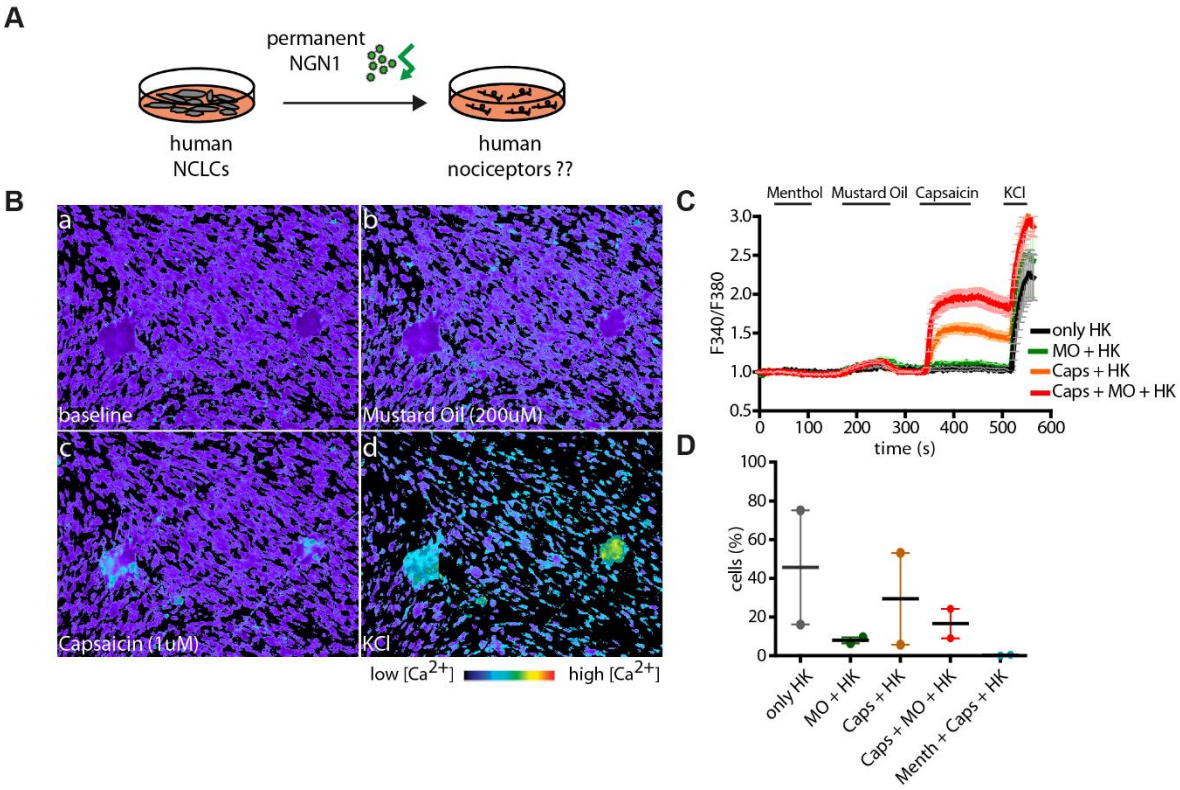

Fig. 20: Lentiviral overexpression of "Woolf-NGN1" and Ca^{2+}-imaging experiment of differentiated neurons

(A) Schematic representation of overexpression experiments, showing the transfection of human NCLCs with lentiviral particles of "Woolf-NGN1" and the differentiation into sesnory neurons.

(B) Pseudo-color images of infected, differentiated neurons, loaded with the fluorescent calcium indicator Fura-2 before stimulation (a) after mustard oil (b, 200µM, MO), capsaicin (c, 1 µM, Caps) or high potassium (d, 100 mM, HK) treatment. Pseudo-color scale bar represents intracellular calcium concentrations.

(C) Representative traces of one experiment, shown in (B) indicated that differentiated neurons showed a proper respons to capsaicin and HK (in orange) and neurons that got activated by both stimuli, capsaicin and mustard oil (in red), a fraction of cells responded to mustard oil/HK (in green) or HK only (in black). Average of responding neurons given as mean ± SEM (n=34 cells).

(D) Quantification of two independent experiments indicated that about 30% of neurons showed a response to capsaicin and HK (in orange), about 17% of the neurons responded to capsaicin/mustard oil/HK (in red) and a minority of neurons got activated by mustard oil/HK (in green), menthol/capsaicin/HK (in blue). Percentage of responding neurons was calculated per experiment and reported as mean with range (N=2 experiments).

Due to the fact that we were not able to reproducibly control "Woolf"-virus production and virus infection and that only NGN1 seemed to be infectious and essential for the generation of functional nociceptors, we decided to change our strategy and go back to the doxycycline-inducible NGN1 viral construct (already used in previous experiments). This is a major benefit as it facilitates the differentiation procedure, depending on the exogenous expression of only one transcription factor, and virus production and infection can be controlled by the EGFP signal, increasing the reproducibility of differentiated nociceptors.

In Table 3, different NGN1 overexpression systems and culturing properties are summarized, indicating that the inducible NGN1 overexpression for 3 days in "mechano"- differentiation medium (containing NGF, BDNF, GDNF and RA) was not sufficient to generate stem cell-derived nociceptors, compared to an inducible NGN1-overexpression for 10 days (final protocol shown in chapter 5.2) or a permanent NGN1 induction, in a differentiation medium containing FCS, NGF, BDNF and GDNF, where differentiated TRKA-positive neurons showed characteristic features of stem cell-derived nociceptors.

Virus	Gene induction	Culturing medium	Nociceptive properties
Inducible NGN1	3 days	"Mechano"-differentiation medium	↓
Woolf-NGN1	permanent	"Nociceptor"- differentiation medium	↑
Inducible-NGN1	10 days	"Nociceptor"- differentiation medium	↑

Table 3: Different NGN1 overexpression systems and experimental setups used for the generation of stem cell-derived nociceptors. Two different NGN1 lentiviral particles (either an inducible or a permanent NGN1 expression construct) were used for infection experiments. Gene overexpression was either only for 3 and 10 days or for the whole differentiation period. Infected cells were kept either in a differentiation medium, established for the generation of stem cell-derived mechanoreceptors ("mechano"-differentiation medium) or a differentiation medium used in the Wainger et al., 2015 study ("Nociceptor"-differentiation medium"). Different experimental setups generated neurons with (↑) or without (↓) nociceptive properties.

5.1.8 Verification of the TRKA-tomato reporter line

To enable the identification and analysis of developing small diameter nociceptive neurons, an extremely heterogeneous population, a TRKA-tomato reporter line, generated in our laboratory, was used for further differentiation experiments. With the help of the CRISPR-Cas9 technology (Ran et al., 2013; Xiao-Jie et al., 2015), the tomato red fluorescent marker was incorporated into the endogenous *TRKA* locus, coupled with a T2A linker sequence in front of the stop codon (and therefore expressed under the *TRKA* promotor, Fig. 21A). As soon as developing nociceptive neurons start to express TRKA, differentiating cells co-express the fluorescent marker and the endogenous tomato signal is detectable (Fig. 21B). To demonstrate that the tomato signal indeed reflects the endogenous TRKA expression, *in situ* hybridization experiments for *tomato* and human *TRKA* were performed on stem cell-derived nociceptors (Fig. 21C-E). Quantification analysis demonstrated that 98.7% of *tomato*-positive neurons were also positive for *TRKA* (Fig. 21F). This experiment showed that the tomato signal reflects the endogenous TRKA expression and furthermore that the TRKA-tomato reporter line could be used for the identification and classification of differentiating nociceptive subpopulations.

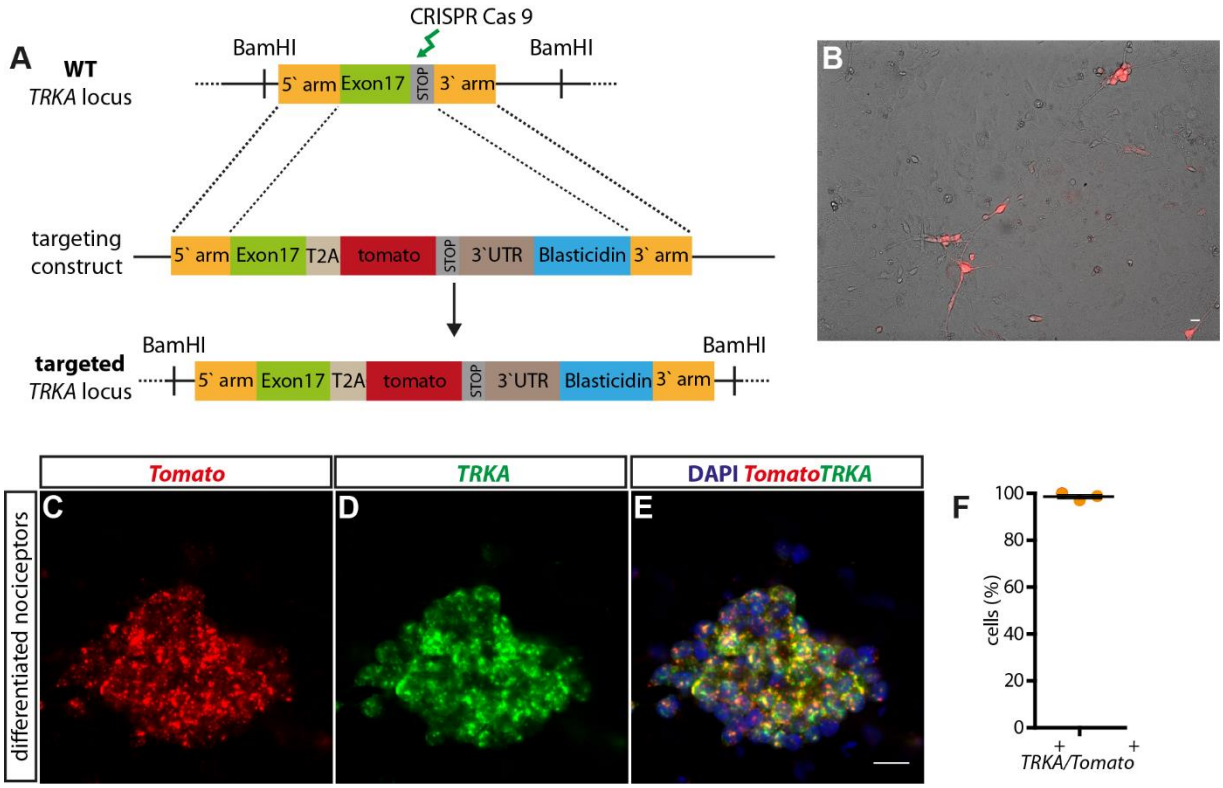

Fig. 21: Verification of the TRKA-tomato hESC reporter line

(A) Scheme of TRKA-tomato targeting construct for the generation of a TRKA-tomato reporter line generated by Dr. Katrin Schrenk-Siemens in our laboratory, where tomato is inserted into the endogenous *TRKA* locus.
(B) Differentiating TRKA-tomato hESCs, showing an endogenous TRKA-tomato signal.
(C-E) Verification of the TRKA-tomato reporter line by *in situ* hybridization experiments. Nearly all *tomato* positive neurons (C) are also positive for *TRKA* (D). (E) Overlay of both markers, *tomato* in red and *TRKA* in green. Scale bar 20 µm.
(F) Quantification of three independent *TRKA-tomato in situ* hybridization experiments, showing that the overlap is almost 100%.

5.2 Final differentiation protocol and characterization of stem cell-derived nociceptors

5.2.1 Final differentiation protocol

Since *in vivo* primary sensory neurons derive from the neural crest, we tried to generate stem cell-derived nociceptors by recapitulating sensory neuron development, using a two-step differentiation protocol that relies on the generation of NCLCs as an intermediate cell population (Fig. 22). As a starting cell line, hESCs, growing in colonies, were cultured and expanded on matrigel-coated dishes (Fig. 22A), a basement membrane matrix that is essential for anchorage-dependent cell types. The first differentiation step to produce NCLCs was an already established protocol in our laboratory (Schrenk-Siemens et al., 2015a). For this, hESCs are cultured in uncoated dishes, where they start to form neuroectodermal spheres (Fig. 22B). Under the influence of intrinsic and extrinsic signals, neuroectodermal spheres spontaneously attach to the cell culture dish, and cells undergo an epithelial-to-mesenchymal transition to become highly motile, and neuronal precursors start to migrate out (Fig. 22B-C). For the second differentiation step, to further differentiate NCLCs into mature sensory neurons, NCLCs are harvested and infected with inducible NGN1 and rtTA lentiviral particles (Fig. 22C).

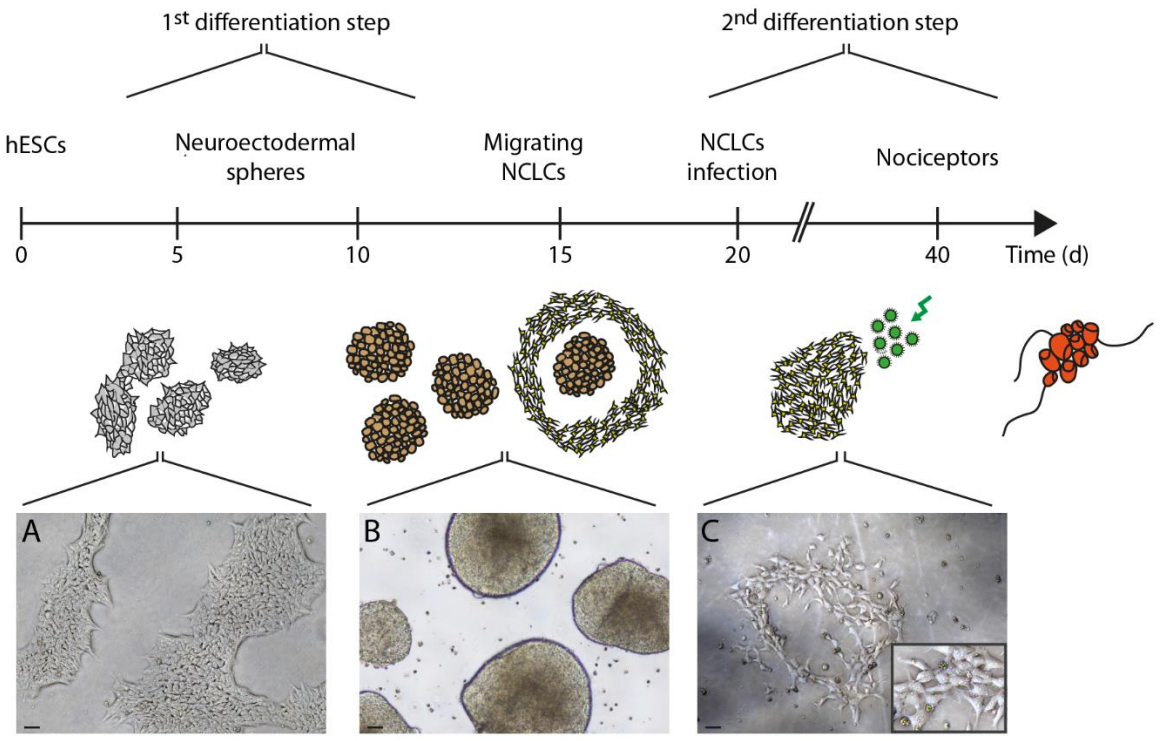

Fig. 22: Two-step differentiation protocol

Time-course illustration of the two-step differentiation protocol (top) and images of different cell populations at different stages of differentiation (bottom). As a starting cell population the hESCs growing in colonies (A), stem cell-derived neuroectodermal spheres (B) and delaminating NCLCs (C), precursor cells of primary sensory neurons, used for viral-induced overexpression experiments. Scale bar 50µm.

According to our new established, final differentiation protocol, migrated NCLCs were infected with the NGN1/rtTA virus 1 day after plating, and doxycycline-induced gene expression was started 24 hours post-infection. For the differentiation of TRKA-positive nociceptive neurons, NGN1 was induced for a transient period of 10 days followed by additional 10-14 days in culture, allowing the cells to mature into functional neurons (Fig. 23A).

Time-course analysis demonstrated that already 24 hours after gene induction the majority of cells were GFP-positive, meaning that most cells were infected and overexpressing NGN1 (Fig. 23B). Due to proliferation aspects and high cell density, differentiating cells were splitted after 6-8 days of gene induction. At this developmental stage cells started to migrate and form nest-like structures (Fig. 23B d-f). Approximately 11-14 days after gene induction, the NGN1 signal decreased and was completely absent 15 days after splitting, while the tomato signal (indicating TRKA expression) increased gradually (Fig. 23B g-i).

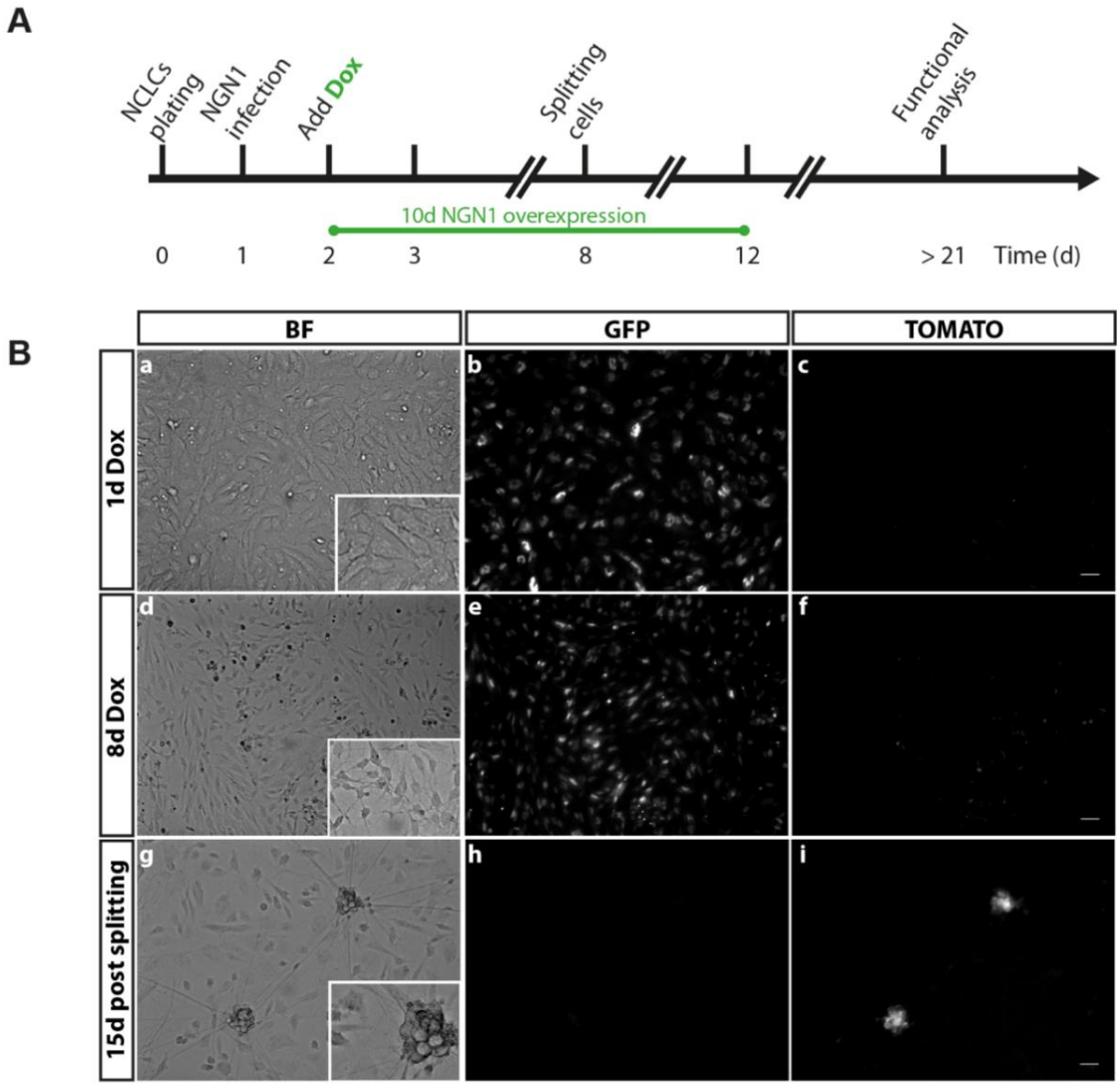

Fig. 23: Generation of stem cell-derived primary sensory neurons based on NGN1 overexpression

(A) Time-line illustrating the NCLC infection and differentiation into primary sensory neurons.
(B) Images of distinct cell populations at different stages of differentiation. As a starting cell population the NCLCs one day after doxycycline (Dox) treatment are shown (a). Note the induced NGN1 expression as identified by the EGFP signal (b). The tomato-TrkA signal is not yet detectable (c). 8 days after gene induction, cells start to migrate and form neuron-like morphologies (d). NGN1 is still induced (e), tomato-TRKA is not yet detectable (f). 15 days post splitting, differentiated neurons formed cell clusters (g) and started to express tomato-TRKA (i). NGN1 overexpression is not detectable any longer (h). Scale bar 50 µm.

Ca^{2+}-imaging experiments revealed that a transient NGN1 overexpression alone (10 days) was sufficient to differentiate NCLCs into primary sensory neurons with nociceptive properties, when culturing them in the differentiation cocktail of the Wainger *et al*. study (Fig. 24). Although only a small fraction (7%) of tomato-positive neurons showed a response to capsaicin and HK (indicated by the orange trace), and 2% of the neurons got activated by capsaicin and mustard oil (shown by the red trace, Fig. 24B-D), we decided to maintain this controllable protocol and characterize differentiated TRKA-positive neurons in more details.

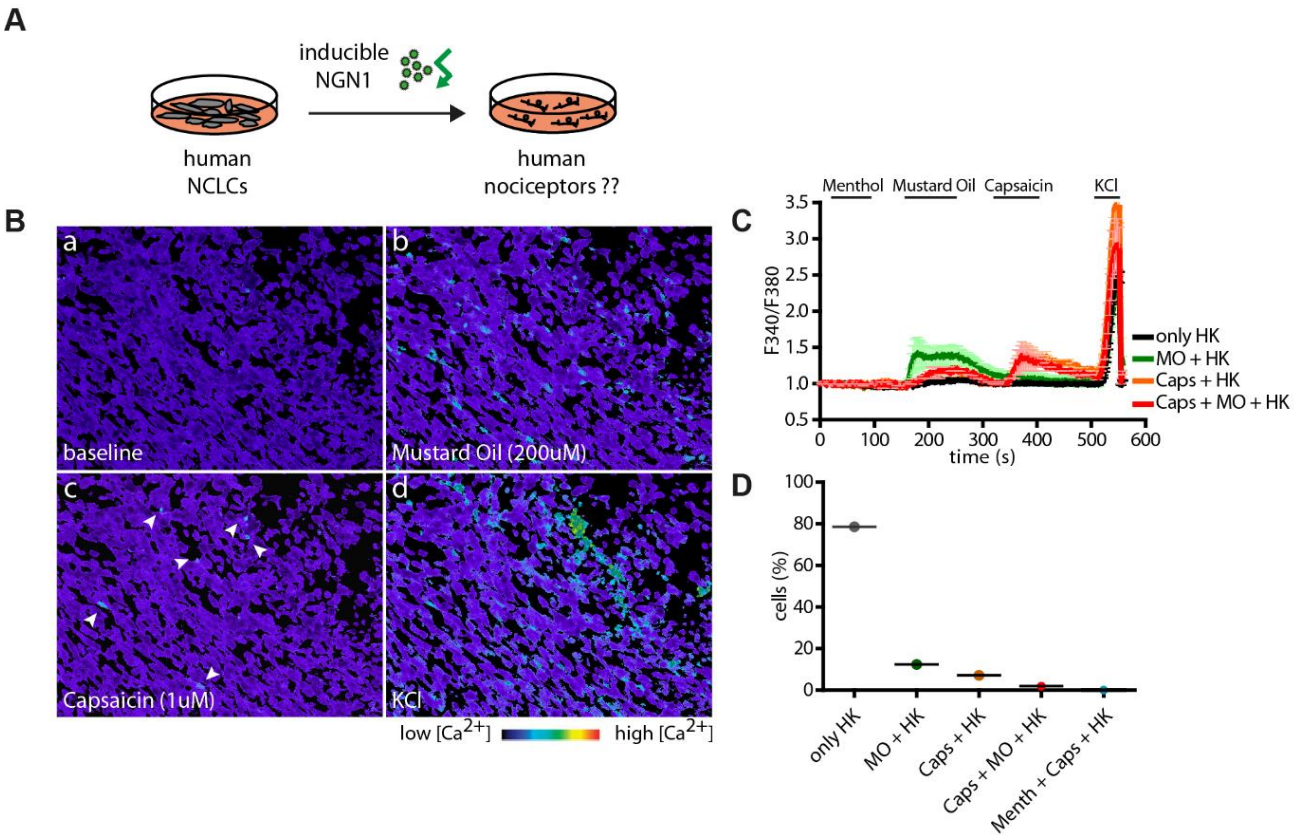

Fig. 24: Lentiviral overexpression of "inducible NGN1" and Ca^{2+}-imaging experiment of differentiated neurons

(A) Schematic representation of overexpression experiments, showing the transfection of human NCLCs with lentiviral particles of the inducible NGN1 and the differentiation into sensory neurons.
(B) Pseudo-color images of infected, differentiated neurons after at least 21 days in culture, loaded with the fluorescent calcium indicator Fura-2 before stimulation (a) after mustard oil (b, 200 µM), capsaicin (c, 1 µM) or high potassium (d, 100 mM) treatment. Pseudo-color scale bar represents intracellular calcium concentrations.
(C) Representative traces of one experiment, shown in (B) indicated that differentiated neurons showed a proper response to capsaicin and HK (in orange) and neurons that got activated by both stimuli, capsaicin and mustard oil (in red). A fraction of cells responded to mustard oil/HK (in green) or HK only (in black). Average of responding neurons is given as mean ± SEM (n=59 cells).
(D) Quantification of one Calcium-imaging experiment indicated that about 7% of neurons showed a response to capsaicin and HK (in orange), about 2% of the neurons responded to capsaicin/mustard oil/HK (in red) and a minority of neurons got activated by mustard oil/HK (in green), menthol/capsaicin/HK (in blue). Percentage of responding neurons was calculated per experiment (N=1 experiment).

The modified differentiation procedure - the inducible overexpression of NGN1 alone - has a great advantage compared to the already published Wainger *et al*. study, since it facilitates the differentiation protocol (only one virus is needed) and increases the reproducibility by controlling viral infection with an EGFP fluorescent reporter. Furthermore, if one tries to recapitulate *in vivo* sensory neuron development, where NGN1 is essential to drive neural crest cells towards a TRKA lineage (Ma et al., 1999a), a transient NGN1 overexpression during a distinct period of differentiation seemed to be more *in vivo*-like compared to a stable NGN1 overexpression.

5.2.2 Characterization of stem cell-derived nociceptors - Immunostainings

Following the Ca^{2+}-imaging experiments, showing that the induced NGN1 expression drives sensory neuron development, we wanted to characterize differentiated TRKA-positive neurons in more detail. Therefore, to assess how many NCLCs in culture adopted a sensory neuron phenotype, immunostainings for ISLET1 (a marker for post-mitotic sensory neurons) and RFP (which labels tomato-positive, TRKA expressing cells) were performed. Protein expression analysis demonstrated that differentiation efficiencies varied between different cultures. In two out of three analyzed cultures, differentiated neurons grew in big clusters (Fig. 25A-a), whereas in one experiment differentiated cells grew only in small clusters or even as single cells (Fig. 25A-b). Quantification analysis revealed that 24.4% of DAPI-positive cells were also positive for ISLET1, indicating their sensory phenotype (Fig. 25B). Furthermore, immunohistochemistry analysis of differentiated cells showed that 99% of the ISLET1-positive sensory neurons were also positive for RFP, and therefore also expressed TRKA (Fig. 25C a-b, D).

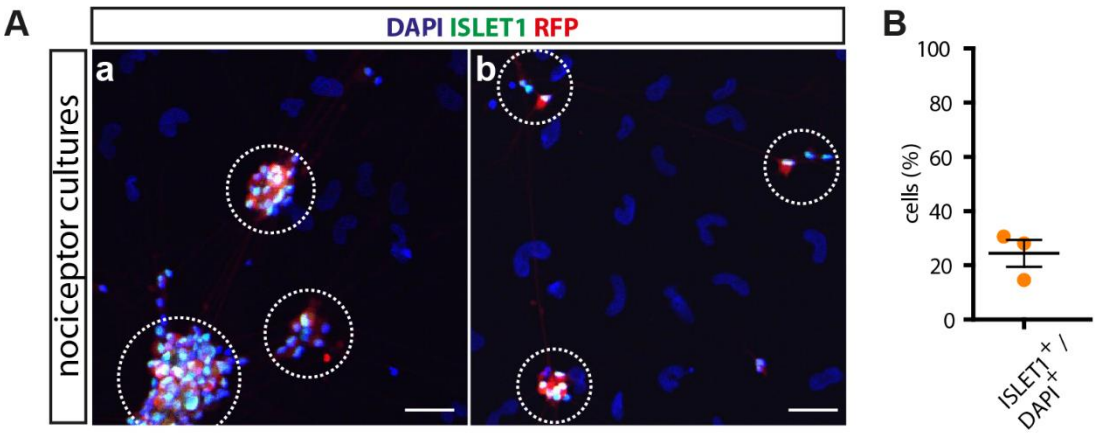

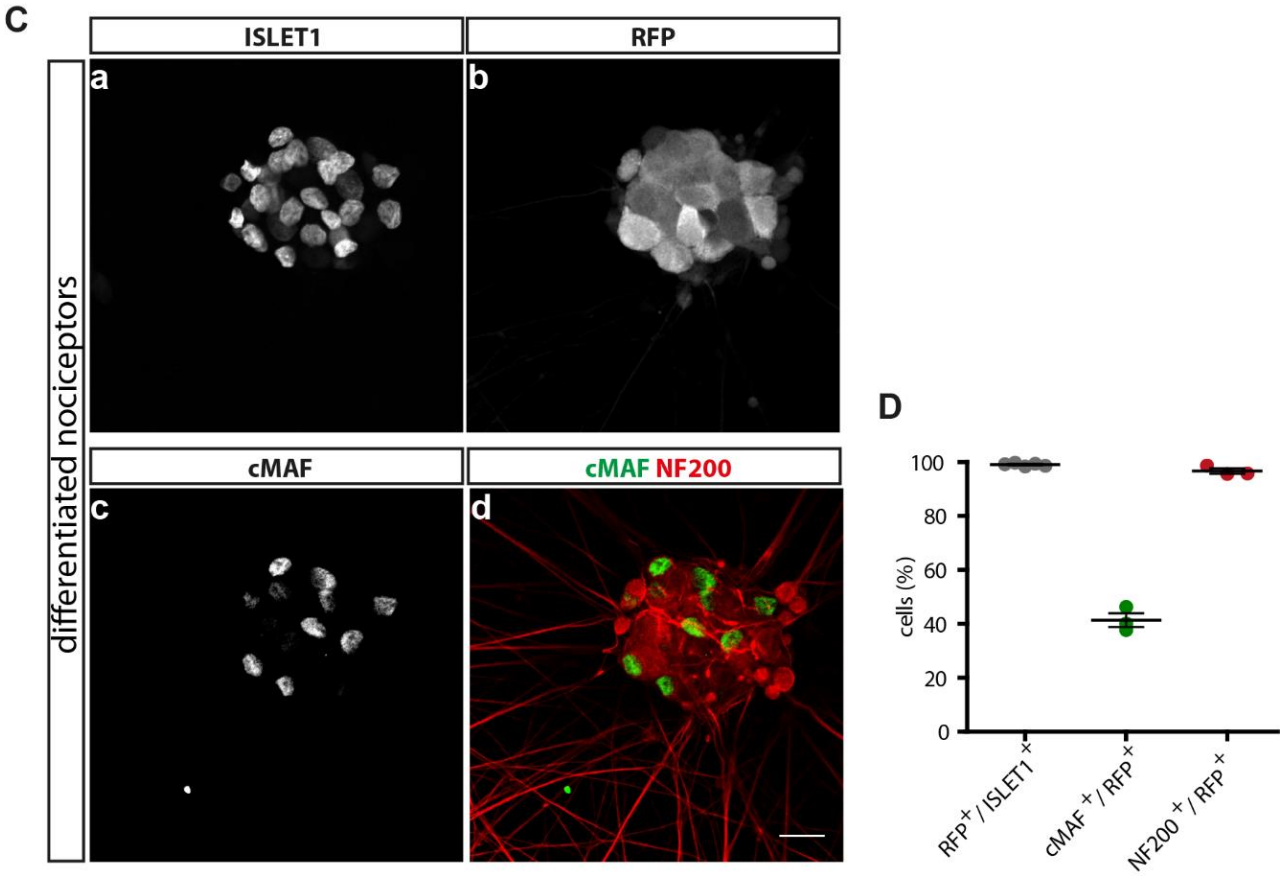

Fig. 25: Immunohistochemistry analysis of differentiated TRKA positive nociceptor

(A) Immunohistochemical staining of differentiated hESC-derived sensory neurons for ISL1, a marker of post-mitotic sensory neurons and for RFP, the red fluorescent protein, labeling the TRKA-tomato positive neurons. Differentiation efficiencies varied between cultures. Either differentiated cells grew in big clusters (a), or only in smaller clusters or even single cells (b). Scale bar 50 µm.

(B) Quantification analysis showing that on average around 24.4% of DAPI positive cells are also positive for ISLET1, indicating their sensory phenotype.

(C) Immunohistochemical staining of differentiated hESC-derived nociceptor clusters for ISL1 (a), RFP (b), cMAF (c) and NF200 (d). Scale bar 20 µm.

(D) Quantification analysis of 3-4 separate differentiations showing that almost all ISL1 positive neurons are also positive for the red fluorescent protein RFP. Nearly all RFP positive neurons co-express NF200 and about 41.4% of the RFP positive neurons are also positive for cMaf.

The ability to perceive various sensations relies on the conversion of distinct stimuli into an electrical signal, conveyed from primary sensory neurons in the periphery to specific target regions in the brain. Primary sensory neurons can be functionally classified into Aβ, Aδ and C-fibers. Whereas heavily myelinated, fast-conducting Aβ-fibers are large diameter low-threshold mechanoreceptors, lightly myelinated Aδ fibers and unmyelinated, slowly conducting C-fibers are mainly small diameter nociceptors (Julius and Basbaum, 2001).

Additionally, it was shown that, in animal models, different fiber-types can also be categorized by the presence of different neurofilament subunits. According to their molecular weight, three different neurofilament subtypes have been identified: the heavy, the medium and the light

neurofilament (Lariviere and Julien, 2004; Shelanski et al., 1994). NF200, the heavy neurofilament subunit, is a molecular marker of fast-conducting A-fibers. To investigate whether this marker can also be used to characterize stem-cell-derived TRKA-positive neurons, NF200 immunostainings were performed. Interestingly, almost all (96.7%) TRKA-positive cells were also positive for NF200 (Fig. 25C-d, D).

Nociceptors are an extremely heterogeneous cell population, and can be activated not only by heat, cold or chemical irritants, but also by noxious mechanical stimuli that would lead to tissue damage, compared to the innocuous mechanical stimuli transduced by low-threshold mechanoreceptors (Basbaum et al., 2009). To further classify differentiated sensory neurons, we also stained them with an antibody recognizing cMAF, a transcription factor known to be essential for mechanosensory function in human and mice (Wende et al., 2012). Quantification analysis demonstrated that 41.4 % of TRKA-expressing neurons are also positive for cMAF, pointing out their mechanosensitivity (Fig. 25C c-d, D).

5.2.3 Neurotrophin receptor expression in differentiated nociceptors

To further characterize differentiated TRKA-positive neurons, and due to the lack of human specific antibodies of sufficient quality, we performed dual-color *in situ* hybridizations, analyzing the RNA transcripts of differentiated neurons. In addition to classifying primary sensory neurons according to their cell body size or axon fiber conduction velocity, they can classically also be separated by their expression of one member of the neurotrophin receptors that are mutually exclusive (Chen et al., 2006; Ernsberger, 2009; Perez-Pinera et al., 2008; Snider, 1994).

Studies in rodents or chicken have observed that TRKA is primarily expressed in small diameter peptidergic nociceptors that mainly respond to heat or noxious mechanical forces (Averill et al., 1995), whereas TRKB-positive neurons, mainly low threshold mechanoreceptors, get activated by innocuous mechanical stimuli (Perez-Pinera et al., 2008). Large diameter TRKC-expressing neurons, classified as proprioceptors, are known to be important for transducing muscle spindle tension (Snider, 1994). In order to assess whether our stem cell-derived neurons reflect what is known from animal studies and express TRK receptors in a mutually-exclusive manner, we performed double fluorescent *in situ* hybridizations for *TRKA* in combination with one of the other neurotrophin receptors.

In situ hybridizations for *TRKA/TRKB* showed only a small amount of *TRKA/TRKB* double positive neurons (shown by arrowheads in Fig. 26A-D). Quantification analysis of three independent differentiations revealed that only 3.8% of the *tomato-TRKA*-positive cells were also positive for *TRKB* (Fig. 26E).

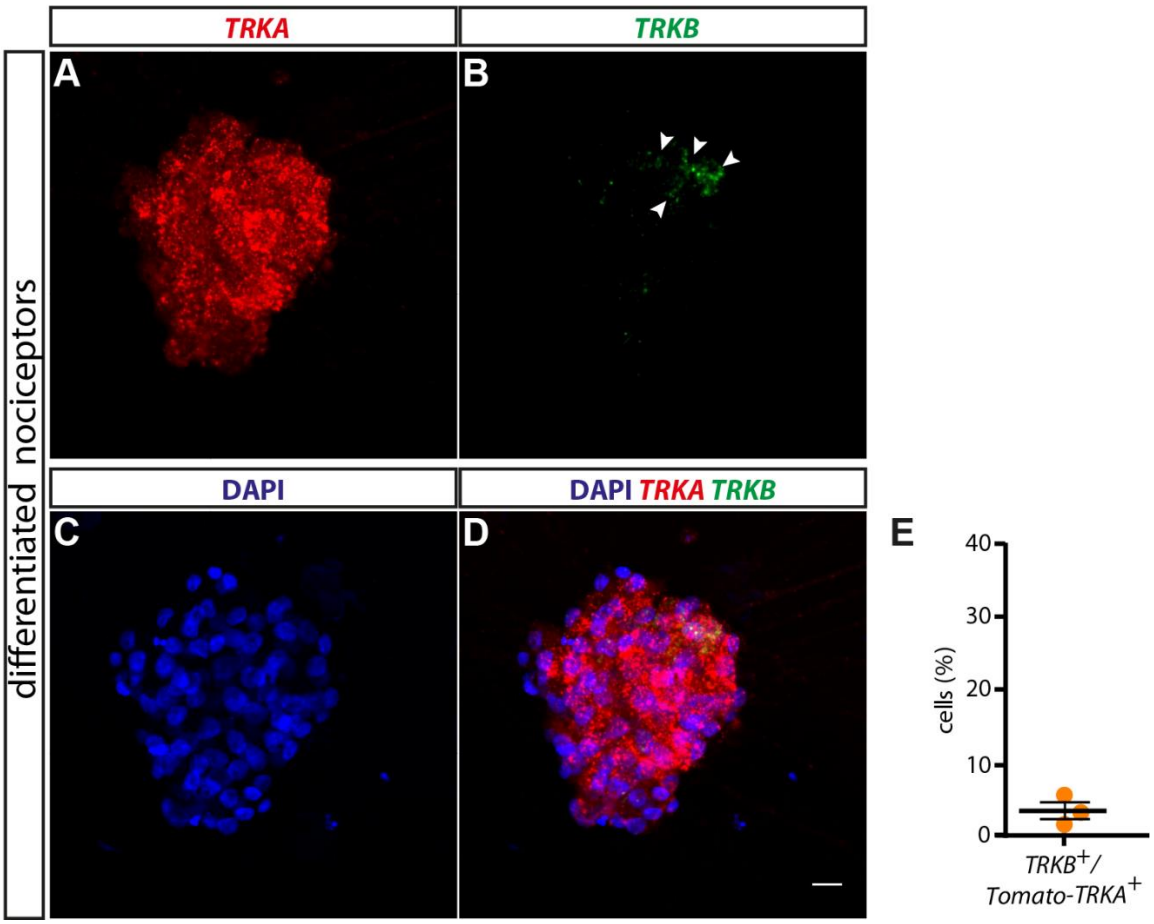

Fig. 26: Dual color *in situ* hybridization analysis of stem cell-derived nociceptors for *TRKA/TRKB*

Double fluorescent *in situ* hybridizations of differentiated nociceptors indicated that a small fraction of *TRKA*-positive neurons (A) are also positive for *TRKB* (B, indicated by arrowheads). DAPI staining showed all cells in the field of view (C). (D) Overlay of all three markers, DAPI in blue, *TRKA* in red and *TRKB* in green. (E) Quantification analysis of 3 separate differentiations showing that on average around 3.8% of *TRKA*-positive nociceptors also express *TRKB*. Scale bar 20 µm.

Quantifications of 3 separate *TRKA/TRKC* double fluorescent *in situ* hybridization experiments showed that a higher proportion (19.2%) of the *TRKA* population (shown in red in Fig. 27A) co-express *TRKC* (indicated by arrowheads; Fig. 27B, E).

These findings demonstrated, similar to what is known from animal studies, that stem cell-derived nociceptors selectively express the neurotrophin receptors and only smaller fractions of *TRKA*-positive neurons co-express *TRKB* or *TRKC*, receptors that are mainly expressed in mechanoreceptors or proprioceptors, respectively.

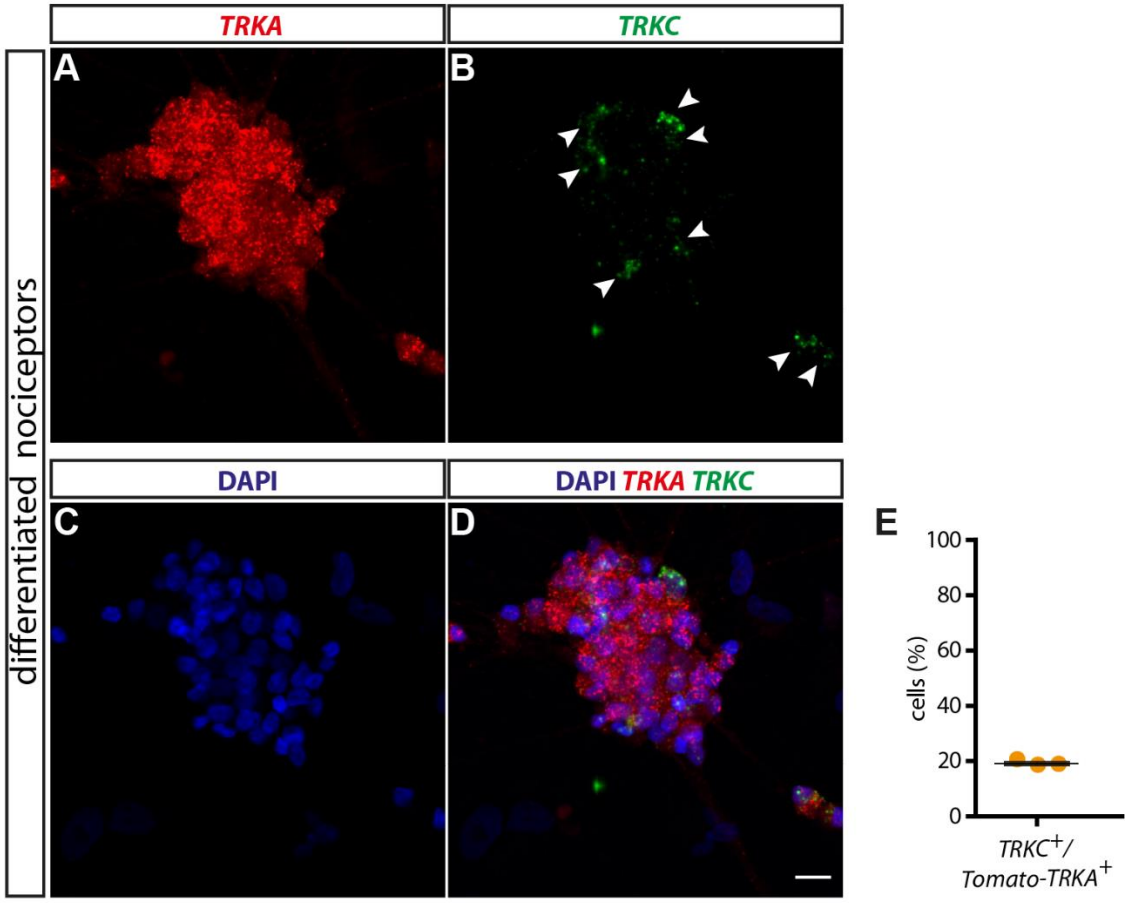

Fig. 27: Dual color *in situ* hybridization analysis of stem cell-derived nociceptors for *TRKA/TRKC*

Double fluorescent *in situ* hybridizations of differentiated nociceptors indicated that a small fraction of *TRKA*-positive neurons (A) are also positive for *TRKC* (B, indicated by arrowheads). DAPI staining showed all cells in the field of view (C). (D) Overlay of all three markers, DAPI in blue, *TRKA* in red and *TRKC* in green. (E) Quantification analysis of 3 separate differentiations showing that on average around 19.2% of *TRKA*-positive nociceptors also express *TRKC*. Scale bar 20 µm.

5.2.4 RET expression in differentiated nociceptors

Based on what is known from animal studies, neurotrophin receptors are broadly expressed during development (Ernsberger, 2009). Later during differentiation, neurotrophin receptor expression gets more defined and at postnatal stages TRK receptors can even be used for categorizing different neuronal subpopulations. During development, differentiating TRKA-positive neurons separate into two major nociceptive subpopulations. Peptidergic nociceptors continuously express TRKA and signaling molecules such as Substance P or CGRP, whereas the non-peptidergic nociceptor subpopulation downregulates TRKA expression and upregulates the tyrosine receptor kinase RET (Molliver et al., 1997). Although all primary sensory neurons can be classified by the expression of the neurotrophin receptors TRKA, TRKB, TRKC and of the tyrosine receptor kinase RET (mainly

expressed in non-peptidergic nociceptors as well as in some TRKB, TRKC-positive cells), it was also demonstrated that a small group of 5-10% of sensory neurons co-express TRKA and RET (Golden et al., 2010; Molliver et al., 1997). Subsequently, TRKA/RET-double positive neurons have been identified as itch-sensitive neurons (Stantcheva et al., 2016a).

Surprisingly, *in situ* hybridization analysis, with probes detecting human *RET* and the endogenous *tomato-TRKA* RNA, showed a strong overlap of both populations: 77.6% of *TRKA*-positive neurons (shown in red, Fig. 28A) co-express the tyrosine receptor kinase *RET* (shown in green, Fig. 28B). There is strong evidence to suggest that species-specific molecular differences already exist at the level of primary sensory neurons and in human stem cell-derived nociceptors the *RET/TRKA*-double positive population is higher, when compared to mouse DRG neurons.

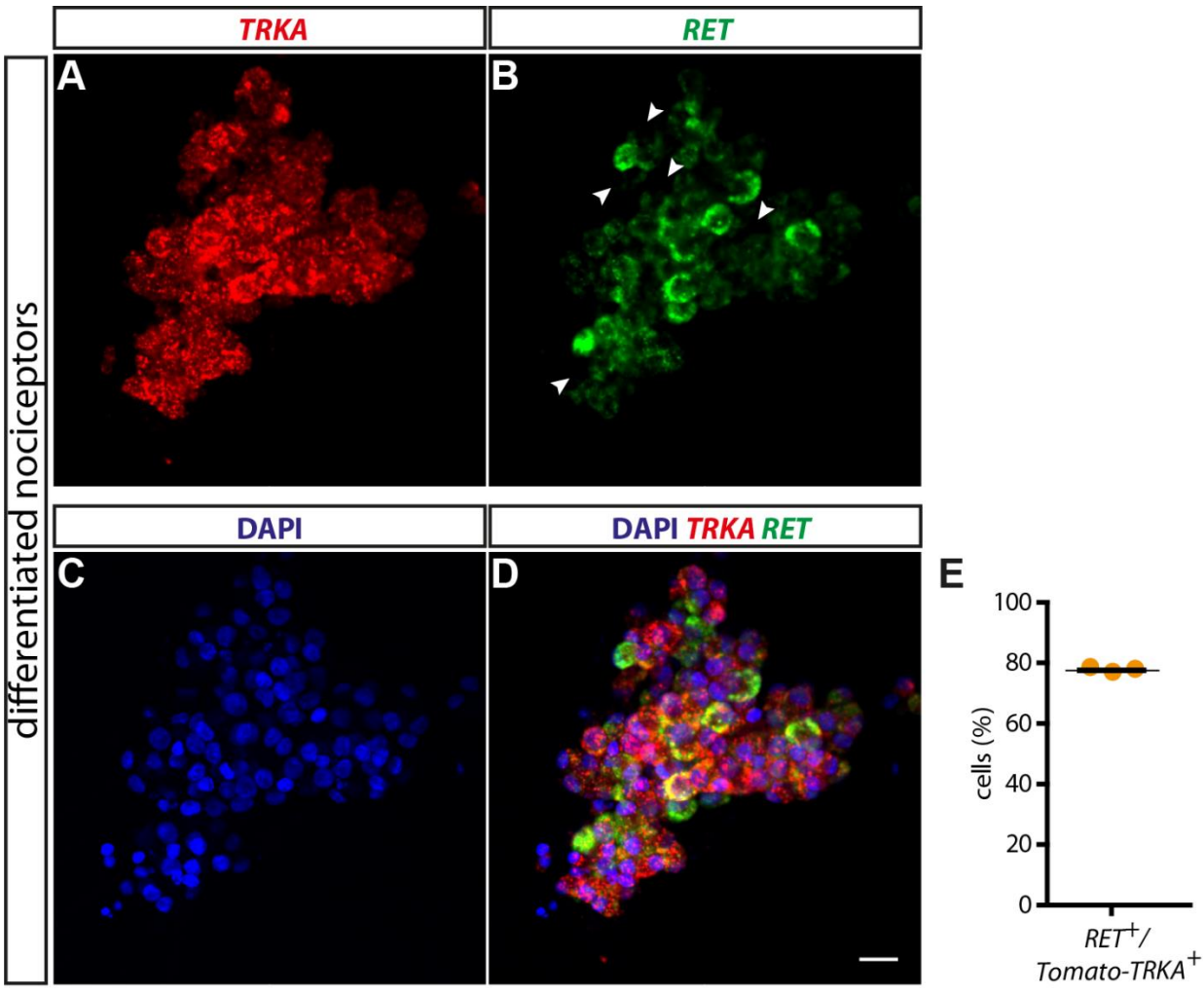

Fig. 28: Dual color *in situ* hybridization analysis of stem cell-derived nociceptors for *TRKA/RET*

Double fluorescent *in situ* hybridizations of differentiated nociceptors indicated that the majority of *TRKA*-positive neurons (A) are also positive for *RET* (B, negative cells are labelled by arrowheads). DAPI staining showed all cells in the field of view (C). (D) Overlay of all three markers, DAPI in blue, *TRKA* in red and *RET* in green. (E) Quantification analysis of 3 separate differentiations showing that on average around 77.6% of *TRKA*-positive nociceptors also express *RET*. Scale bar 20 µm.

5.2.5 Sodium channel expression in differentiated nociceptors

Another important gene family that has been linked to pain sensation, are the voltage-gated sodium channels (VGSC), large integral membrane proteins crucial for initiating and propagating action potentials. In mammals, the voltage-gated sodium channel family consists of 9 different members, referred to as Nav1.1-Nav1.9. Three channels, Nav1.7, Nav1.8 and Nav1.9, are most abundantly expressed in primary sensory neurons of the peripheral nervous system and mutations in these channels have been associated with a variety of heritable pain disorders (Cummins et al., 2007; Kanellopoulos and Matsuyama, 2016). While Nav1.7 is broadly expressed in different types of peripheral neurons, Nav1.8 and Nav1.9 are more restricted to small diameter nociceptive neurons (Amaya et al., 2000; Toledo-Aral et al., 1997).

Due to the fact that Nav1.6-Nav1.9 are known to be expressed in human and mouse DRG neurons and that Nav1.7-Nav1.9 are implicated in human pain disorders, we wanted to explore Nav channel expression in stem cell-derived nociceptors. We performed RT-PCR to analyze the distribution of Nav1.6-Nav1.9 expression in differentiated nociceptor cultures compared to stem cell-derived mechanoreceptors and uninfected NCLCs (Fig. 29).

Gene expression analysis of the three nociceptor cultures (Fig. 29; Noci #1-#3 and #pooled) and of differentiated mechanoreceptors (Fig. 29; Mechano) (normalized to the housekeeping gene *GAPDH* and the uninfected NCLCs), corroborated data from the literature: *Nav1.6* was detectable in both sensory subtypes (mechanoreceptors and nociceptors) at comparable low levels (Fig. 29; shown in yellow), *Nav1.7* (Fig. 29; shown in blue) was broadly expressed in differentiated nociceptors as well as in stem cell-derived mechanoreceptors, and *Nav1.8* (Fig. 29; shown in red) was more restricted to small diameter neurons and only detectable in differentiated TRKA-positive nociceptors.

Surprisingly, the sodium channel *Nav1.9* had higher expression in mechanoreceptors than in differentiated TRKA-positive nociceptors, contrary to previous published work that showed that Nav1.9 expression, similar to Nav1.8, is mainly expressed in small diameter nociceptive DRG neurons.

These results suggest that differentiated stem cell-derived nociceptors feature some characteristic hallmarks of native DRG nociceptors.

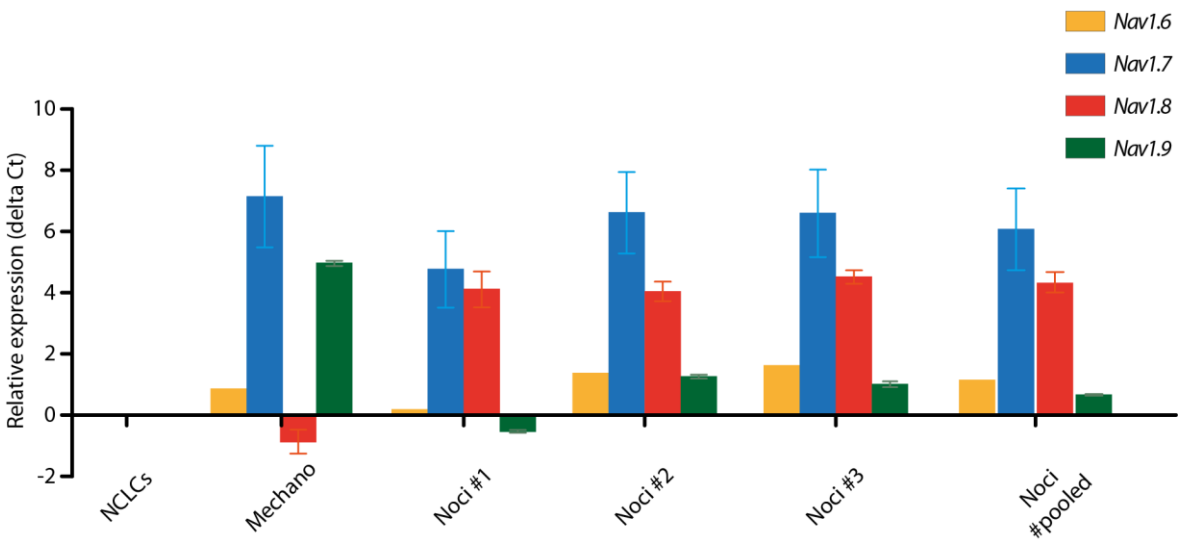

Fig. 29: Nav channel expression in stem cell-derived sensory neurons

qRT-PCR analysis, representing the relative expression level of *Nav1.6* (yellow), *Nav1.7* (blue), *Nav1.8* (red) and *Nav1.9* (green) in three different nociceptor cultures (Noci #1, Noci #2, Noci #3) and differentiated mechanoreceptors (Mechano) after 3 weeks of differentiation, normalized to the housekeeping gene *GAPDH* and compared to uninfected NCLCs as a negative control.The mean with range of the delta Ct values of two different experiments are shown. Data was pooled after substracting Ct values.

5.2.6 Electrophysiological analysis of differentiated nociceptors (done by Dr. Jörg Pohle)

We next asked whether stem cell-derived neurons also show electrophysiological properties of nociceptors. In addition to functional Ca^{2+}-imaging recordings and marker gene expression profiles, adult sensory neurons can also be categorized by their action potential characteristics. While myelinated, large diameter low-threshold mechanoreceptors are characterized by narrow action potentials, small diameter nociceptive neurons mainly elicit broad action potentials, mediated by Nav1.8 channels. Moreover, rodent studies, analyzing the action potential morphology of dissociated DRG neurons, found another nociceptor-specific marker: in response to increasing steps of current injections, primary sensory nociceptors elicited multiple action potentials, whereas non-nociceptive neurons only showed single action potentials (Viatchenko-Karpinski and Gu, 2016; Wainger et al., 2015). Interestingly, we (electrophysiological recordings were performed by a colleague in our laboratory, Dr. Jörg Pohle) found that the majority of stem cell-derived, TRKA-positive nociceptors elicited trains of action potentials in response to step-wise depolarizing currents, a feature that is characteristic of a nociceptive phenotype (Fig. 30).

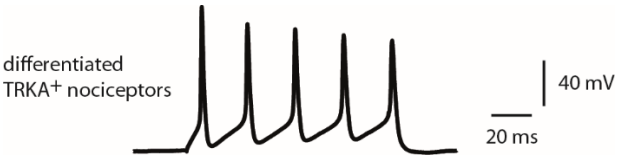

Fig. 30: Electrophysiological characterization of stem cell-derived nociceptors

In response to increasing steps of current injections hESC-derived sensory TRKA-positive neurons elicited trains of action potentials, a marker for nociceptive neurons. Work done by Dr.Jörg Pohle

As already mentioned, primary sensory nociceptors can not only be activated by extreme temperatures or chemical irritants, but also by noxious mechanical forces. Mechanosensitive neurons are characterized by their ability to sense and thereupon transduce mechanical stimuli into an electrical signal that can be measured by electrophysiological recordings. In response to membrane indentation, caused by a nanomotor-driven probe, mechanosensitive neurons elicit mechanically-activated currents, which can be measured by a patch pipette. Based on the inactivation kinetics, mechanically-activated currents can be discriminated into three different subtypes: rapidly-adapting (RA), intermediately-adapting (IA) or slowly-adapting (SA) currents. While RA mechanically-activated currents can be found in both populations, mechanoreceptors and nociceptors, IA and SA currents are exclusively present in nociceptive neurons (Drew et al., 2002; Hu and Lewin, 2006; Viatchenko-Karpinski and Gu, 2016).

In order to assess whether stem cell-derived nociceptors also show characteristic features of mechanosensitive neurons, electrophysiological stimulations were performed. In response to mechanical stimulation (10 µm indentation) by a nanomotor-driven probe, 61.8% of TRKA-positive nociceptors elicited robust mechanically-activated currents (Fig. 31A-B). Furthermore, mechanical currents increased in amplitude with rising membrane indentation intensity: the deeper the indentation, the higher the amplitude (Fig. 31C). Most importantly, elicited currents exhibited all different kinetics from RA (τ < 10 ms), IA (τ = 10-30 ms) and SA (τ > 30 ms) mechanically-activated currents (Fig. 31D), indicating that differentiated TRKA-positive neurons adapted characteristic features of a nociceptor phenotype.

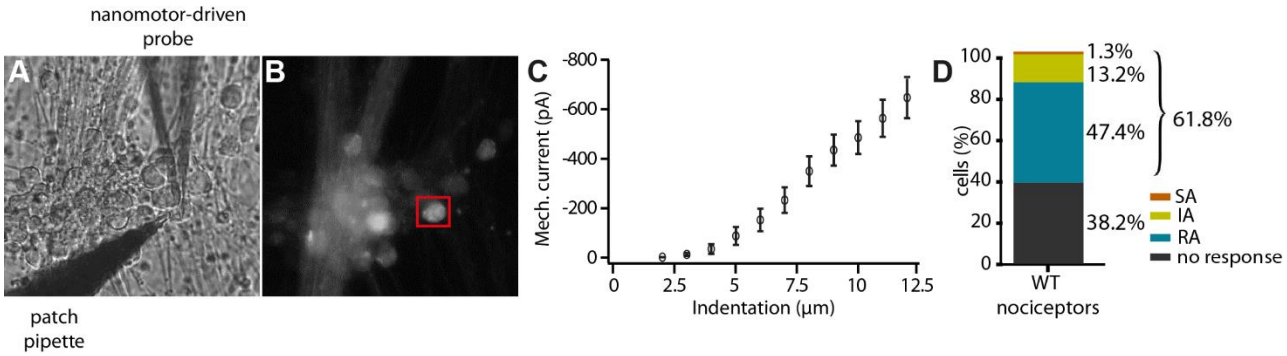

Fig. 31: Mechanical stimulation of stem cell-derived TRKA positive nociceptors. Work done by Dr.Jörg Pohle.

(A-B) Representative images (Brightfield image (A); fluorescent TRKA signal (B)) of mechanically stimulated TRKA-positive neurons by a nanomotor-driven probe.

(C) Representative current amplitude as a function of mechanical indentation of the membrane. Mechanically-activated currents increased with membrane indentation intensity.

(D) Quantification analysis of mechanically stimulated nociceptors. Approximately 61.8% of TRKA-positive nociceptors elicited robust (SA/IA/RA) mechanically-activated currents.

To conclude, not only functional Ca^{2+}-imaging recordings and marker gene expression analysis but also electrophysiological recordings demonstrated that differentiated, TRKA-positive neurons show characteristic hallmarks of peptidergic nociceptors. While not formerly proven that the hES-derived nociceptors are indeed of peptidergic origin, this is assumed based on the expression of the peptidergic marker TRKA. Nevertheless, future analysis will have to show if this is indeed the case. Furthermore, gene expression analyses of several independent nociceptor cultures showed similar results, suggesting that the differentiation protocol is reproducible.

5.3 Comparison of human and mouse DRG neurons

5.3.1 Optimizing in situ hybridization protocol for human tissue

To validate whether hESC-derived nociceptors are physiologically relevant, we analyzed the marker gene expression profile in *in vitro* differentiated neurons and human *post-mortem* DRG tissue.

In addition to the comparative study, to assess how similar *in vitro* generated nociceptors are, in contrast with their native human correspondents, we also wanted to explore differences and similarities between the animal mouse model system and the human organism. We therefore compared gene expression patterns of native human and mouse DRG tissue.

In order to compare gene expression profiles of stem cell-derived nociceptors and human dorsal root ganglia by *in situ* hybridization, we obtained human *post-mortem* DRG tissue of five unrelated individuals from the Netherlands Brain bank (www.brainbank.nl). Furthermore, not only to account

for inter-individual differences but also for gene expression differences within one individual, we acquired native DRG that innervated different human dermatomes.

The human dermatome is a distinct area of the skin innervated by a specific pair of DRG. While cervical nerves (C1-8) mainly innervate the neck, the arms and fingers, the thoracic DRG (T1-T12) mostly innervate the thorax and the lumbar nerves (L1-L5) mainly the legs.

Prior to gene expression analysis of human DRG tissue, the *in situ* hybridization protocol was optimized with an anti-sense RNA probe against human *TRKA*, known to be broadly expressed in DRG tissue. Single-color *in situ* hybridization experiments performed according to the already established protocol, using a non-hydrolyzed probe at 65 °C (Fig. 32A) showed only very few positive cells. A decreased hybridization temperature of 42 °C raised the number of positively-labeled cells, but also the background was higher (Fig. 32B). The *in situ* hybridization signal could be nicely increased by using a hydrolyzed RNA probe, which facilitates the RNA penetration, at a hybridization temperature of 60 °C (Fig 32C). Brownish deposits are most likely lipofuscin particles, that are present in the cells and can already be identified by light microscopy.

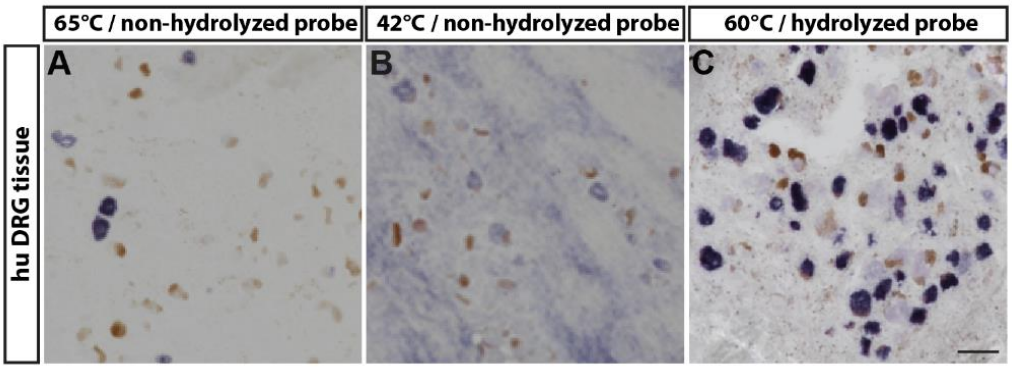

Fig. 32: Optimizing the *in situ* hybridization protocol for human DRG tissue

(A) Original protocol as previously described in Wende et al., 2012 using a non-hydrolyzed *hTRKA* RNA probe at a hybridization temperature of 65°C. Only few neurons were positively stained for *TRKA*.

(B) Modified protocol using a non-hydrolyzed *hTRKA* RNA probe at a hybridization temperature of only 42 °C. More neurons were positively stained for *TRKA* but the background was higher.

(C) Optimized protocol for human DRG tissue using a hydrolyzed *hTRKA* RNA probe at a hybridization temperature of 60°C. Many neurons were positively stained for *TRKA*. Scale bar 100 µm.

5.3.2 Neurotrophin receptor expression in human and mouse DRG tissue

From animal studies, it is known that neurotrophin receptors (TRKA, TRKB and TRKC) are broadly expressed during development and get more defined at later developmental stages and can even be used for categorizing different sensory neuronal subpopulations (Ernsberger, 2009; Molliver and Snider, 1997b; White et al., 1996). While TRKA is primarily expressed in small diameter peptidergic nociceptors (Averill et al., 1995), TRKB-positive neurons mainly belong to

low threshold mechanoreceptors (Perez-Pinera et al., 2008), and large diameter TRKC-expressing neurons mainly to proprioceptors (Snider, 1994).

Neurotrophin receptor expression analysis of differentiated *TRKA-tomato* positive neurons confirmed what was already described in animal studies and showed an almost indistinguishable expression pattern: only 3.8% of *TRKA*-positive cells co-expressed *TRKB* and 19.2% co-expressed *TRKC* (Fig. 26 and 27). To identify whether neurotrophin receptors are expressed in a similar pattern and can also be used for categorizing different sensory neuronal subpopulations in native human and mouse DRG, dual-color *in situ* hybridization experiments for *TrkA* in combination with *TrkB* and *TrkC* were performed. Quantifications indicated that 5.3± 0.7% of human *TRKA*-labelled neurons are also positive for *TRKB*, whereas in mouse DRG neurons 4.8 ± 1.7% double positive cells were detectable (Fig. 33A-C).

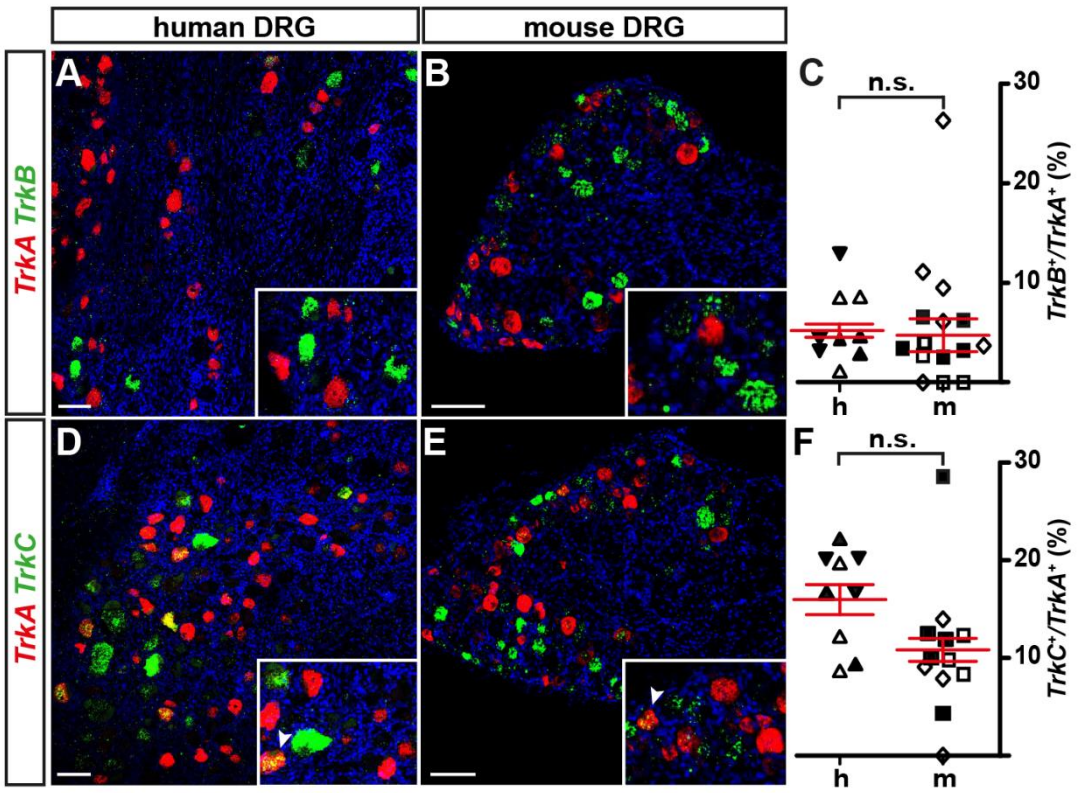

Fig. 33: Dual color *in situ* hybridization analysis of human and mouse DRG tissue for *TrkA/TrkB*

Double fluorescent *in situ* hybridization of cryo-section from a native human (A, D) and mouse (B, E) DRG, showing the presence of *TrkB* (A, B) or *TrkC* (D, E) in combination with *TrkA*. In both species, *TrkB* (green) is expressed in a small subset of *TrkA*-positive neurons (red, A, B). Quantifications of three independent individuals revealed that about 5.3± 0.7% of human *TRKA* neurons co-express *TRKB*, similar to the mouse analysis showing 4.8 ± 1.7% *TrkA/TrkB* double positive neurons (C). Gene expression analysis for *TrkA/TrkC* (D, E) indicated that in both species only a small subpopulation of *TrkA* (red) positive neurons express *TrkC* (green). Quantifications of three independent individuals revealed that about 16.0 ± 1.5% of human *TRKA* neurons co-express *TRKC*, not significantly different to the mouse analysis showing 10.8 ± 1.2% *TrkA/TrkC*-double positive neurons (F). Scale bar 100 µm.

Dual color *in situ* hybridizations for *TrkA/TrkC* demonstrated an overlap of 16.0 ± 1.5% in human tissue, similar to 10.8 ± 1.2% in *post-mortem* mouse DRG (Fig. 33D-F). Statistical analysis (using the linear mixed model) indicated that fractions derived from human DRG slices did not significantly differ from fractions derived from mouse DRG tissue (*TrkB/TrkA*, p=0.956; *TrkC/TrkA*, p=0.111). These findings show a rather identical neurotrophin receptor expression distribution of *TRKA/TRKB* and *TRKA/TRKC*-double positive sensory neurons in stem cell-derived nociceptors compared to native human DRG and furthermore also to mouse tissue.

In addition to TRK receptor distribution among different sensory neuron subpopulations, it was also demonstrated that primary sensory neurons in rodents can be classified by the size of their cell body: TRKA-positive neurons have mainly a small cell size, TRKB-positive cells mainly an intermediate area size and TRKC-expressing sensory neurons mainly larger cell bodies (McMahon et al., 1994; Molliver et al., 1997; Silos-Santiago et al., 1995b). To ascertain whether a similar cell size distribution can also be found in human and mouse DRG, we plotted the soma area of *TrkA*, *TrkB* and *TrkC*-positive cells against their relative frequency. Compared to mouse DRG neurons, we found a similar relative size distribution in native human DRG tissue. On average, *TRKA*-positive neurons have small cell bodies (400-1000 µm^2; Fig. 34A, labelled in red), compared to intermediate size *TRKB*-expressing neurons (peak around 1400 µm^2, Fig.34A, labelled in green) and to large *TRKC*-positive neurons (peak around 1600 µm^2; Fig. 34A, labelled in blue) (Fig. 34A-B). Furthermore, analysis of the overall cell size, comparing the smallest and largest neurons of each *Trk*-receptor subpopulation, showed that on average human DRG neurons are 1.5-3 times larger compared to mouse DRG neurons, an already described phenotype (Davidson et al., 2014; Vega et al., 1994). These findings confirm a similar expression pattern of *TRKA/TRKB* and *TRKA/TRKC*-double positive neurons in stem cell-derived nociceptors and human and mouse DRG tissue. Moreover, the relative size distribution of mouse and human DRG neurons is similar and nicely related to the expression of one member of the neurotrophin receptors.

In comparison, soma size of stem cell-derived TRKA-positive neurons positively correlated with increasing time of differentiation, and cells kept in culture for more than 6 weeks had cell body sizes up to 400 µm^2, reaching similar soma sizes of human native *TRKA*-expressing DRG neurons (effect was only quantified once).

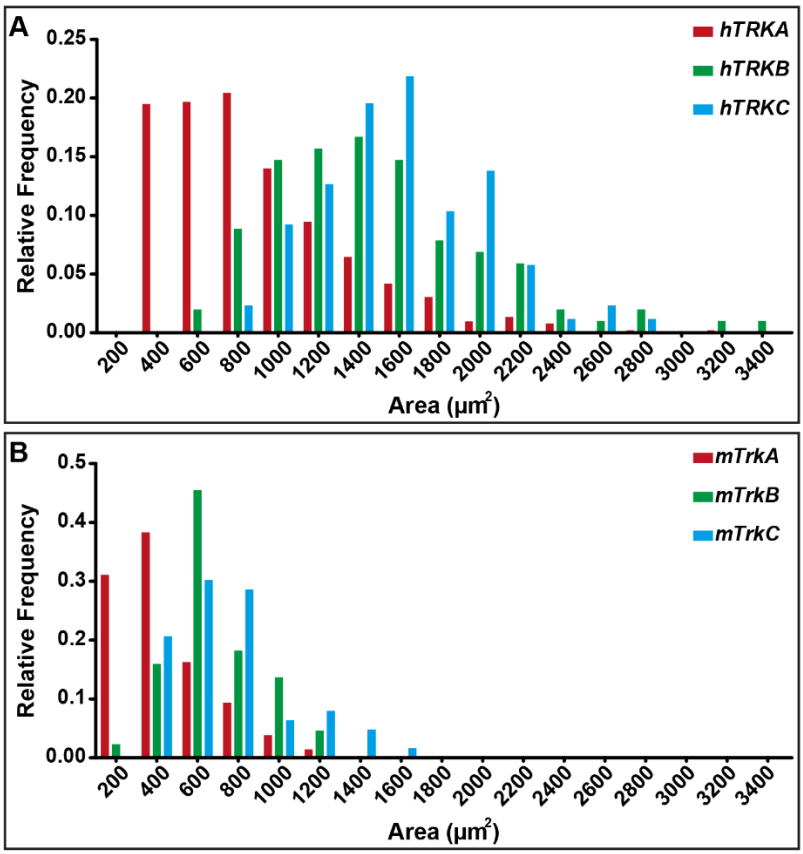

Fig. 34: Cell size distribution of TrA, TrkB or TrkC-positive human and mouse DRG neurons

(A) Soma area of *TRKA* (red), *TRKB* (green) and *TRKC* (blue) positive human DRG neurons plotted against their relative frequency.
Compared to mouse DRG neurons, a similar relative size distribution is found in native human DRG tissue with the majority of *TRKA*-positive neurons having smaller cell bodies, compared to intermediate size *TRKB*-expressing neurons and *TRKC*-positive neurons with mainly even larger cell bodies.

(B) Soma area of *TrkA* (red), *TrkB* (green) and *TrkC* (blue)positive mouse DRG neurons plotted against their relative frequency.

5.3.3 Ret expression in human/mouse DRG tissue

We next asked whether a *TrkA/Ret*-double positive subpopulation is found in human and mouse DRG. Although all primary sensory neurons can be classically categorized by the exclusive expression of TRKA, TRKB, TRKC or RET, it has also been demonstrated that a small group of 5-10 % of sensory neurons co-express TRKA and RET (Golden et al., 2010; Molliver et al., 1997).

Surprisingly, in stem cell-derived nociceptors the overlap of both populations was high, with 77.6% of *TRKA*-positive cells co-expressing *RET* (Fig. 28). *In situ* hybridization analysis with anti-sense RNA probes against *TrkA* and *Ret* showed that in both human and mouse DRG a fraction of *TrkA*-positive neurons also expressed *Ret* (Fig. 35). In human DRG slices, 45.9 ± 0.7% of *TRKA*-positive cells also expressed *RET*, whereas in mouse DRG slices the amount of *TrkA/Ret*-double positive cells was significantly lower (23.2 ± 1.8%) (Fig. 35). These findings indicate that in both species a *TrkA/Ret* population exists, but in human stem-cell derived nociceptors and in native human DRG

the population is higher compared to mouse DRG (human vs mouse DRG; p=0.002 **; linear mixed model).

Moreover, in both species, we also found different *Ret* expression levels (Fig. 35A, D), an already described phenotype in the mouse (Stantcheva et al., 2016a). Clustering analysis of *TrkA*, *Ret* or *TrkA/Ret*-double positive cells in mouse or human DRG tissue, pursuant to their *in situ* intensity levels, showed the *TrkA/Ret*-double positive population (*high TrkA/high Ret*) in analyzed human DRG (Fig. 35H), whereas in mouse DRG this population was almost undetectable (Fig. 35I). This difference in *RET* expression levels was also noticeable in human stem cell-derived nociceptors, but has not been further investigated yet.

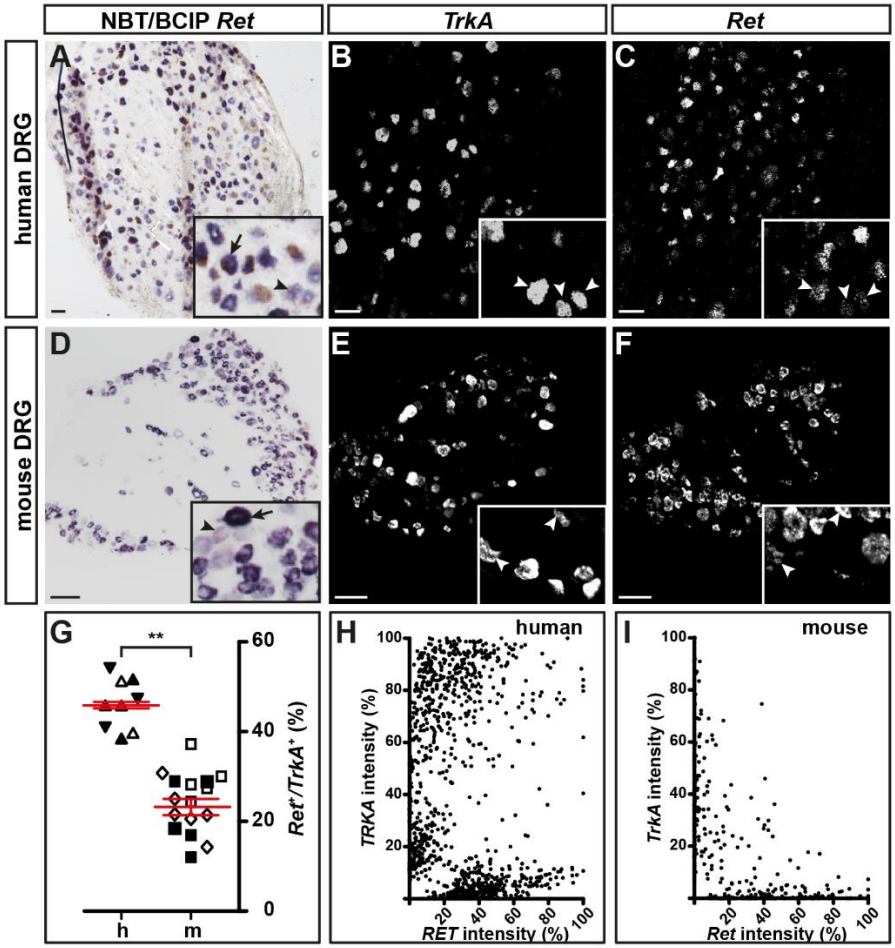

Fig. 35: *In situ* hybridizations analysis of human and mouse DRG tissue for *TrkA/cRet* expression

In situ hybridization analysis, illustrated as single channels, of cryo-section from a native human (A-C) and mouse (D-F) DRG, showing the presence of *Ret* alone (A, D) or in combination (C, F) with *TrkA* (B, E). In both species, different *Ret* expression levels were detectable in colorimetric *in situ* experiments. (A, D shown by arrows and arrowheads). Dual color *in situ* experiments revealed that *Ret* is expressed in a subset of *TrkA*-positive neurons in human (B, C) and mouse (E, F) DRG neurons (indicated by arrowheads). Quantifications of three independent individuals revealed that about 45.9 ± 0.7% of human *TRKA* neurons co-express *RET*, compared to the mouse analysis showing about 23.2 ± 1.8% *TrkA/Ret*-double positive neurons (G). Clustering analysis of *TrkA*, *Ret* or *TrkA/Ret*-positive human (H) and mouse (I) DRG neurons, according to their *in situ* intensity levels, showed again the existence of a *TRKA/RET*-double positive population in human DRG. Scale bar 100 µm.

5.3.4 NF200 expression in human and mouse DRG tissue

Additionally, we also wanted to elucidate whether human and mouse DRG neurons could be categorized by their expression of distinct neurofilament subunits and whether species-differences regarding their neurofilament expression were observable. NF200, the heavy neurofilament subunit, has been broadly used for labeling fast-conducting A-fibers and, interestingly, almost all (96.7%) of the differentiated, TRKA-positive neurons, were also positive for NF200. Quantification analysis of immunostainings with two different antibodies, recognizing NF200, showed that nearly all (97.3 ± 1.2%) neurons (defined as class III beta-tubulin (TUJ1)-positive cells), in human DRG also expressed NF200, whereas in mouse DRG slices only 61.7 ± 0.4% of all neurons co-expressed NF200 ($p < 0.001$; linear mixed model) (Fig. 36). Small diameter TUJ1-positive neurons in the mouse seemed not to be NF200-positive (indicated by arrowheads, Fig. 36D-F).

These results again suggest that our differentiation strategy seems to produce nociceptors very similar to their *in vivo* equivalents, because in stem cell-derived neurons and native human DRG almost every sensory neuron is positive for NF200, independent of different neuronal subtypes, as already described for human *post-mortem* tissue by Vega et al., 1994.

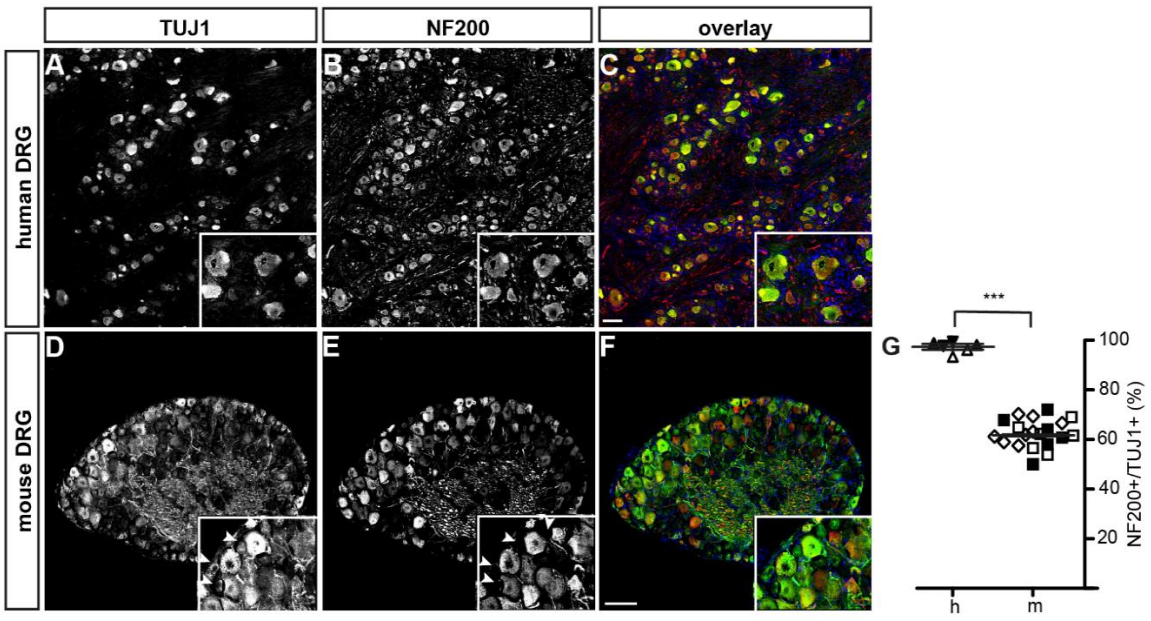

Fig. 36: Immunohistochemical analysis of human and mouse DRG tissue for TUJ1/NF200 expression

Immunostainings of cryo-sections from a native human (A-C) and mouse (D-F) DRG with antibodies recognizing the pan-neuronal marker TUJ1 (A, D) and the heavy neurofilament NF200 (B, E). In human DRG slices NF200 is broadly expressed in all TUJ1-positive neurons (A-C) compared to mouse DRG slices where NF200 is only expressed in a subset of TUJ1-positive neurons (D-F, NF200 negative cells are marked by arrowheads). Quantifications of three independent individuals revealed that almost all human DRG neurons (97.3 ± 1.2%) express NF200, compared to the mouse analysis showing about 61.7 ± 0.4% TUJ1/NF200-double positive neurons (G). Scale bar 100 µm.

5.3.5 Sodium channel expression in human/mouse DRG tissue

Since we already saw species-specific differences between human and mouse gene expression patterns when comparing hESC-derived nociceptors to native human and mouse DRG neurons (see chapter 5.2 and 5.3) we decided to expand the comparative study and focus on more classical nociceptive molecules.

As stated before, voltage-gated sodium channels (Nav1.7-Nav1.9) are important pain mediators, by initiating and propagating action potentials. Also, mutations in these genes have been associated with a variety of heritable pain disorders (Cummins et al., 2007; Kanellopoulos and Matsuyama, 2016). Although different sodium channels are known to be involved in pain mechanisms, making them interesting targets for the discovery of specific pain-relieving drugs, it has not been fully elucidated which channel isoform causes which type of pain disorder, and developmental efforts did not yield new therapeutic drugs (Cummins et al., 2004, 2007; Han et al., 2016). Moreover, it was also demonstrated that mouse and human pain phenotypes, linked to sodium channel mutations, are different (Minett et al., 2012, 2014; Nassar et al., 2004; Weiss et al., 2011).

In order to compare Nav channel expression of stem cell-derived nociceptors and native human and mouse DRG tissue, double *in situ* hybridizations for *TrkA* and *Nav1.6-1.9* were performed. Quantification analysis indicated that in human DRG about 35.2 ± 5.9% of *TrkA*-positive neurons co-express *Nav1.6*, not significantly different compared to mouse DRGs (42.9 ± 2.7% double-positive cells were detectable, p=0.204; linear mixed model) (Fig. 37). Experiments for *TrkA/Nav1.7* showed again no significant difference between human and mouse DRG (57.0 ± 2.1% in human and 53.8 ± 2.0% in mouse DRG, Fig. 37A, D, G). On the other hand, gene expression analysis for *TrkA/Nav1.8* and *TrkA/Nav1.9* displayed differences between human and mouse DRG tissue. The fraction of *TrkA/Nav1.8*-double positive cells for both species was larger than the fraction of *TrkA/Nav1.9*-double positive cells (Fig. 37B, E, H vs Fig. 37C, F, I). In addition, for both *Nav1.8* and *Nav1.9*, the fraction of double positive cells was larger in human DRG: about 50.6 ± 2.0% of mouse DRG neurons co-expressed *TrkA/Nav1.8* compared to 69.8 ± 2.0% in human DRG (p=0.009; linear mixed model; Fig. 37B, E, H), whereas *TrkA/Nav1.9* co-expression was detectable in 12.4 ± 1.6% of mouse DRG neurons compared to 25.6 ± 1.7% in human DRG (p=0.003; linear mixed model; Fig. 37C, F, I).

To conclude, this comparative study of sodium channel expression in native human and mouse sensory neurons indicated explicit species-specific differences that have to be taken into account and could be useful for the discovery of new therapeutic approaches and analgesic drugs.

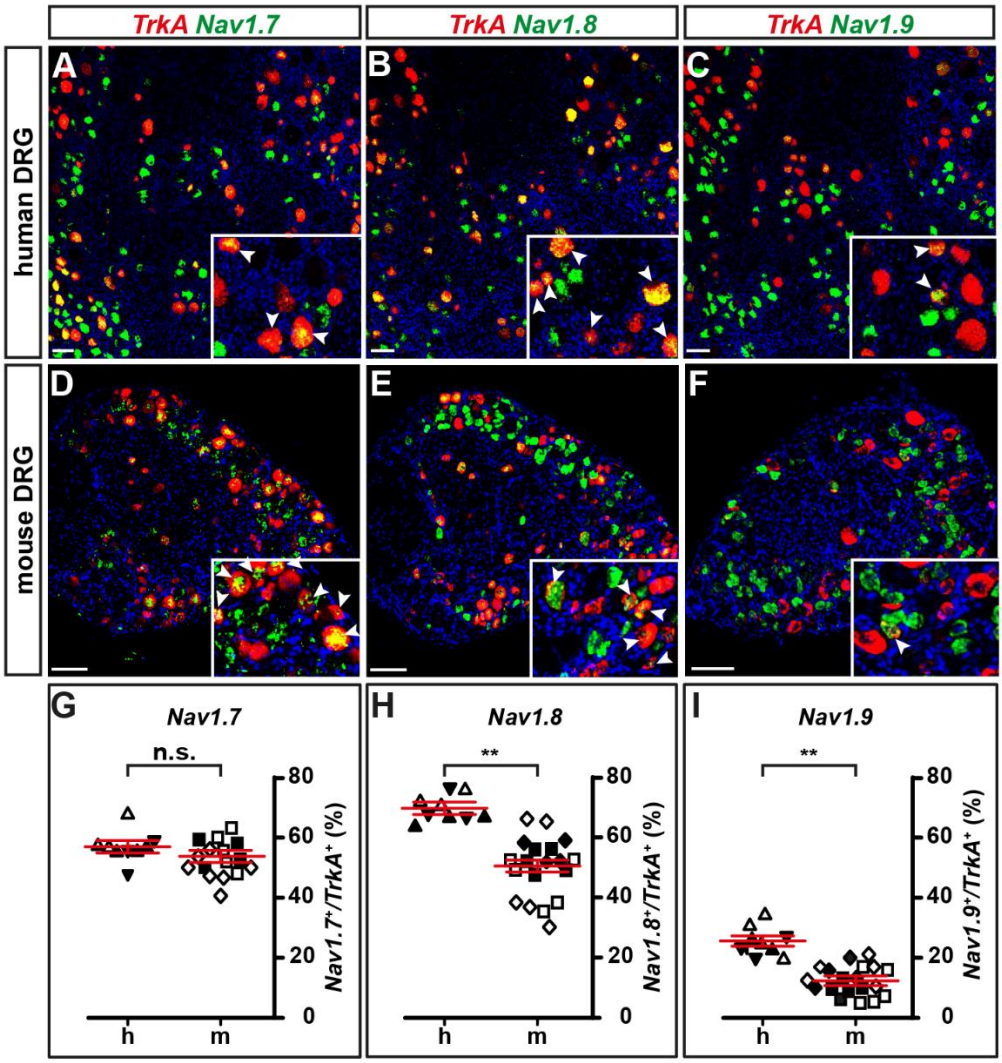

Fig. 37: Dual color *in situ* hybridizations analysis of human and mouse DRG tissue for *TrkA/Nav* channel expression

Double fluorescent *in situ* hybridization of cryo-section from a native human (A-C) and mouse (D-F) DRG, showing the presence of *Nav1.7* (A, D), *Nav1.8* (B, E) or *Nav1.9* (D, E) in combination with *TrkA*. While, in both species *Nav1.7* and *Nav1.8* (green) are expressed in a large fraction of *TrkA*-positive neurons (red), *Nav1.9* is expressed in only a small percentage of *TrkA*-positive neurons. Quantifications of three independent individuals revealed that about 57.0 ± 2.1% of human *TRKA* neurons co-express *Nav1.7*, similar to the mouse analysis showing about 53.8 ± 2.0% *TrkA/Nav1.7* double positive neurons (G). Quantifications for *TrkA/Nav1.8* (H) and *TrkA/Nav1.9* (I) indicated that for both markers the percentage of *TrkA/Nav*-double positive cells is higher in human DRG neurons than in mouse sensory neurons. Scale bar 100 µm.

5.3.6 TRP channel expression in human/mouse DRG tissue

Most primary sensory neurons can also be functionally categorized by the existence of a member of the cationic Transient Receptor Potential (TRP) channel family. TRPV1, originally identified as the receptor for capsaicin, is one of the best studied family members. In addition to its activation by a noxious heat stimulus, more recent studies demonstrated that TRPV1 gets sensitized under inflammatory conditions or injury and is therefore in focus of pain research and therapeutic approaches (Carnevale and Rohacs, 2016; Caterina et al., 1997; Yarmolinsky et al., 2016). From

animal studies, it is known that TRPV1 is mainly expressed in small diameter neurons (22-38%) of adult rodent DRG neurons (Kobayashi et al., 2005; Orozco et al., 2001; Zwick et al., 2002). To compare *TrpV1* expression in *TrkA*-positive peptidergic nociceptors of native human and mouse DRG tissue, dual color *in situ* hybridizations were performed. While in human DRG 54.2 ± 2.9% of *TrkA*-positive cells co-expressed *TrpV1*, in mouse DRG this fraction was significantly reduced (35,4 ± 0.6%, $p < 0.001$; linear mixed model) (Fig. 38).

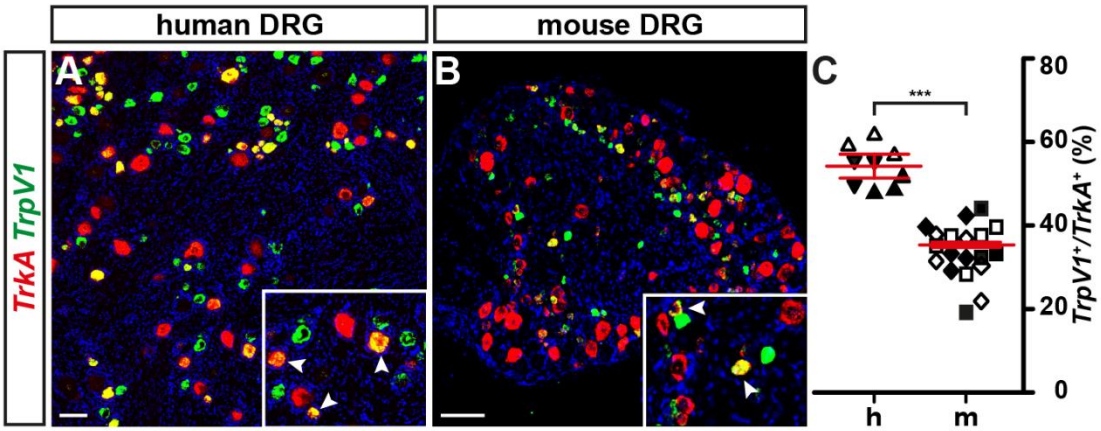

Fig. 38: Dual color in situ hybridizations analysis of human and mouse DRG tissue for *TrkA/TrpV1* expression

Double fluorescent *in situ* hybridization of cryo-section from a native human (A) and mouse (B) DRG, showing the presence of *TrpV1* (green) in combination with *TrkA* (red). In both species *TrpV1* is expressed in a fraction of *TrkA*-positive neurons. Quantifications of three independent individuals revealed that about 54.2 ± 2.9% of human *TRKA* neurons co-express *TRPV1*, compared to the mouse analysis showing about 35,4 ± 0.6% *TrkA/TrpV1*-double positive neurons. Scale bar 100 µm.

TRPA1, another thermosensitive TRP channel family member activated by lower temperatures (around 17 °C, the estimated threshold of noxious cold), and pain-inducing chemicals (such as allyl isothiocyanate, the pungent component of mustard oil), is known to be expressed in a subpopulation of TRPV1-expressing sensory neurons (Jordt et al., 2004; Story et al., 2003). Furthermore, it was also demonstrated that TRPA1 is involved in mediating itch sensation (Kittaka and Tominaga, 2017). In order to test whether human TRPA1-expressing neurons also represent a subpopulation of TRPV1-positive neurons, as already described for mice, double fluorescent *in situ* hybridizations with probes detecting human *TRPV1* and *TRPA1* were performed. Our comparative study confirmed in human what was already described for rodents: all *TRPA1*-positive human DRG neurons were also positive for *TRPV1* (Fig. 39).

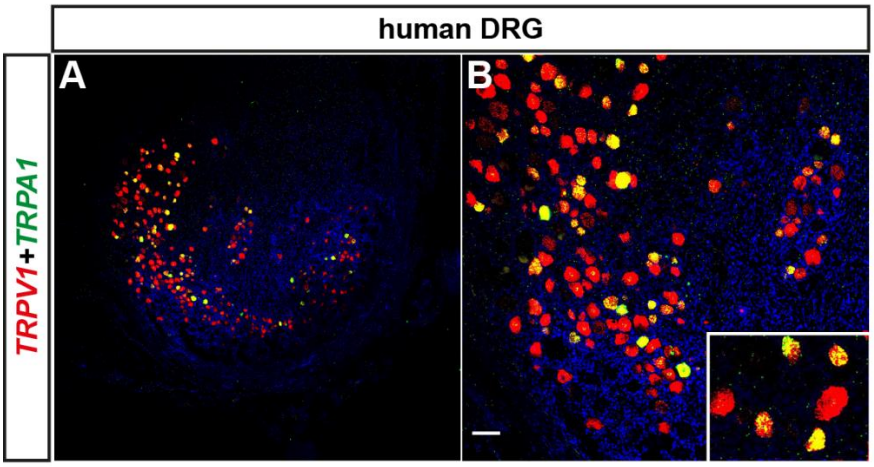

Fig. 39: Dual color *in situ* hybridizations analysis of human DRG tissue for *TRPV1/TRPA1* expression

Double fluorescent *in situ* hybridization of cryosection from a native human DRG (overview image (A), zoom-in picture (B)), showing the presence of *TRPV1* (red) in combination with *TRPA1* (green). Human *TRPA1*-expressing neurons represent a subpopulation of *TRPV1*-positive neurons. Scale bar 100 µm.

To summarize, besides functional Ca^{2+}-imaging recordings or electrophysiological recordings, demonstrating that differentiated, TRKA-positive neurons show characteristic hallmarks of peptidergic nociceptors, our comparative study between hESC-derived nociceptors and native human DRG tissue confirmed that differentiated neurons are physiologically relevant, with an almost similar marker gene expression profile in *post-mortem* DRG neurons (Table. 4).

In addition, our comparative study between human and mouse DRG tissue provides a detailed gene expression profile analysis at cellular resolution and uncovers molecular differences and similarities between the animal mouse model system and the human organism (Table. 4), which may help overcome translational difficulties and improve the prognostic significance of preclinical pain studies.

Table 4: Marker gene analysis (based on *in situ* hybridizations or immunohistochemistry) of differentiated TRKA-positive neurons compared to human and mouse *post-mortem* DRG tissue.

Double positive Marker	Differentiated cells	Human DRG tissue	Mouse DRG tissue
TrkA/TrkB	3.8 %	5.3 %	4.8 %
TrkA/TrkC	19.2 %	16.0 %	10.8 %
TrkA/Ret	77.6 %	45.9 %	23.2 %
TrkA/Piezo2	64.2 %	34.8 %	26.2 %
TrkA/Nav1.7	Not quantified	57.0 %	53.8 %
TrkA/Nav1.8	Not quantified	69.8 %	50.6 %
TrkA/Nav1.9	Not quantified	25.6 %	12.4 %
ISLET1 or TUJ1/NF200	96.7 %	97.3 %	61.7 %

5.4 Role of PIEZO2 in stem cell-derived nociceptors

Mechanotransduction, the transformation of mechanical stimuli into electrical signals, is an elementary physiological process crucial for organ development and homeostasis, and involved in sensing touch, sound waves, proprioception and mechanically-induced pain. These processes, critical for almost all mammalian cells, have been linked to stretch-activated ion channels, from which only few have been described so far. PIEZO1 and PIEZO2 were recently identified as proteins required for mechanically-activated currents in a variety of eukaryotic cell types (Coste et al., 2010; Volkers et al., 2015). While mammalian PIEZO2 is mainly expressed in a subset of DRG and TG somatosensory neurons and Merkel cells, PIEZO1 is mainly expressed in non-sensory tissue (Bron et al., 2014; Cahalan et al., 2015; Coste et al., 2010; Miyamoto et al., 2014; Woo et al., 2014, 2015). We recently demonstrated that PIEZO2 is required for mechanotransduction in stem cell-derived low-threshold mechanoreceptors (LTMRs) (Schrenk-Siemens et al., 2015a). This study and others revealed that PIEZO2 plays a crucial role in mediating innocuous mechanical stimuli. However, only one study indicated that PIEZO2 is also involved in mediating noxious mechanical stimuli (Dubin et al., 2012b). A conditional PIEZO2-KO in DRG and Merkel cells (with a 90% reduction of the overall *Piezo2* transcript) led to specific loss of rapidly-adapting mechanically-activated currents, whereas intermediately-adapting or slowly-adapting currents were not significantly affected (Ranade et al., 2014b).

To assess whether the remaining *Piezo2* transcript level was enough to trigger intermediately and slowly-adapting currents, or if a yet-unknown ion channel is responsible for noxious mechanotransduction, we made use of our established differentiation protocol for the generation of stem cell-derived nociceptors and compared differentiated PIEZO2-WT and PIEZO2-KO cells (an already generated stem cell line in the lab).

As a first proof that differentiated TRKA-positive nociceptors also express PIEZO2, which is a requirement if we want to elucidate the role of PIEZO2 in stem cell-derived nociceptors, we tested *PIEZO2* expression in derived WT nociceptors by dual-color *in situ* hybridization and quantitative RT-PCR. As expected, the *PIEZO2* transcript was detectable by both methods. Quantifications of 4 independent *in situ* hybridization experiments showed that 64.2% of *TRKA*-positive neurons co-expressed *PIEZO2* (Fig. 40A-E). RT-PCR analysis of NGN1-infected PIEZO2-WT and PIEZO2-KO nociceptors (after 7 to 21 days in culture, normalized to the housekeeping gene (*TBP*) and compared to the respective levels in uninfected NCLCs) showed that *PIEZO2* is already expressed after 7 days in culture, and gene expression increases linearly with time in differentiated WT nociceptors (Fig. 40F, green bars). The *PIEZO2* transcript was not detectable in PIEZO2-KO neurons (Fig. 40F, brown bars).

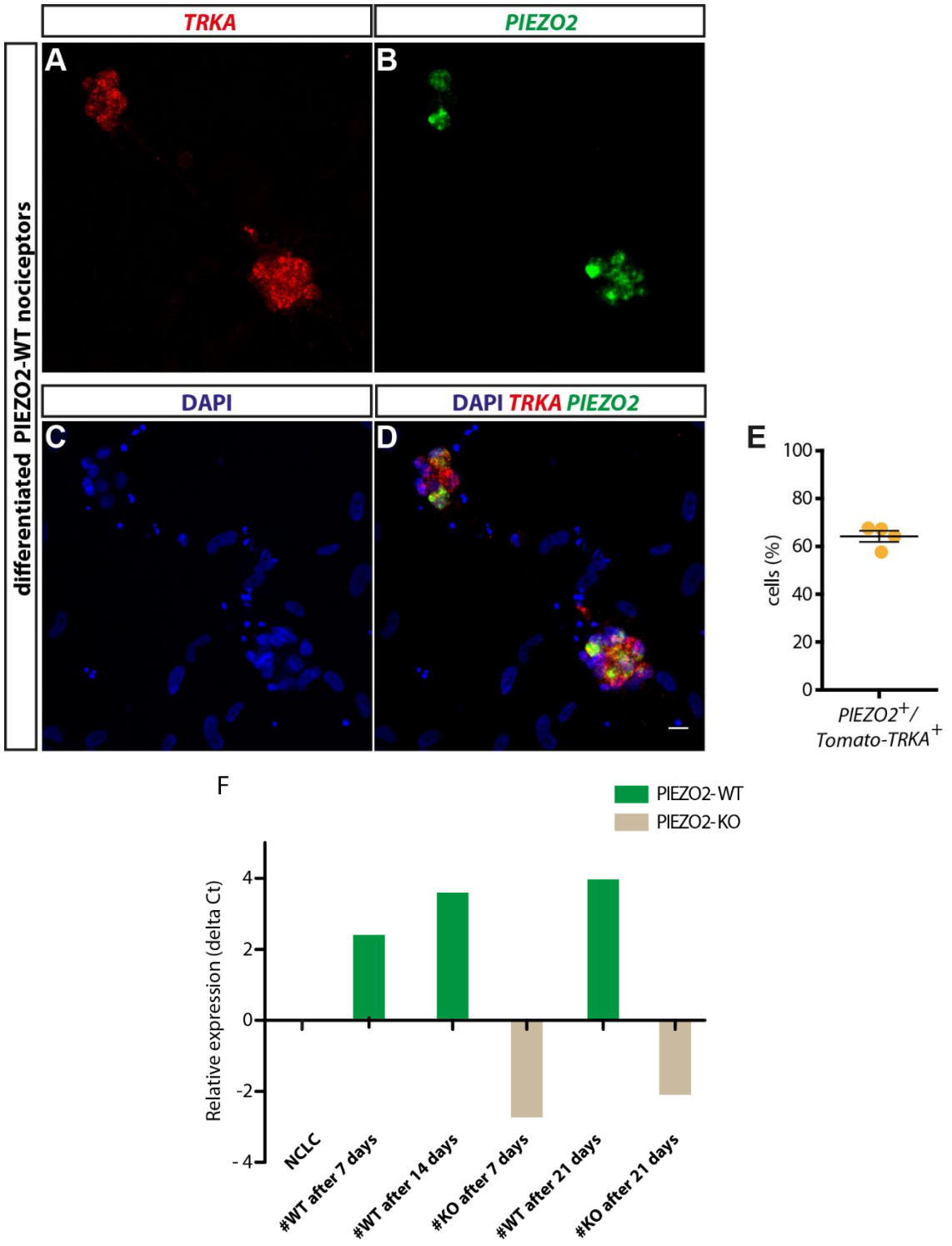

Fig. 40: *PIEZO2* expression in stem cell-derived *TRKA* positive nociceptors

(A-D) Double fluorescent *in situ* hybridizations of differentiated nociceptors showing the presence of *TRKA* (A) in combination with *PIEZO2* (B). DAPI staining showed all cells in the field of view (C). (D) Overlay of all three markers, DAPI in blue, *TRKA* in red and *PIEZO2* in green. Scale bar 20 µm.

(E) Quantification analysis of 4 separate differentiations showing that on average around 64.2% of *TRKA*-positive nociceptors also express *PIEZO2*.

(F) RT-PCR analysis, representing the relative expression level of *PIEZO2* in differentiating PIEZO2-WT (green) or PIEZO2-KO (brown) cells after different time-points of differentiation (after 7, 14 or 21 days) normalized to the housekeeping gene *TBP* and compared to uninfected NCLCs. *PIEZO2* is expressed in PIEZO2-WT cultures and gene expression increases linearly with time. The *PIEZO2* transcript was not detectable in PIEZO2-KO neurons. The mean of the delta Ct values of triplicates of one experiment are shown. Data was pooled before substracting Ct values.

Furthermore, the PIEZO2-KO was verified by *in situ* hybridization with probes detecting human *TRKA* and *PIEZO2*. The *PIEZO2* transcript was completely absent in differentiated *TRKA*-positive PIEZO2-KO nociceptors (Fig. 41).

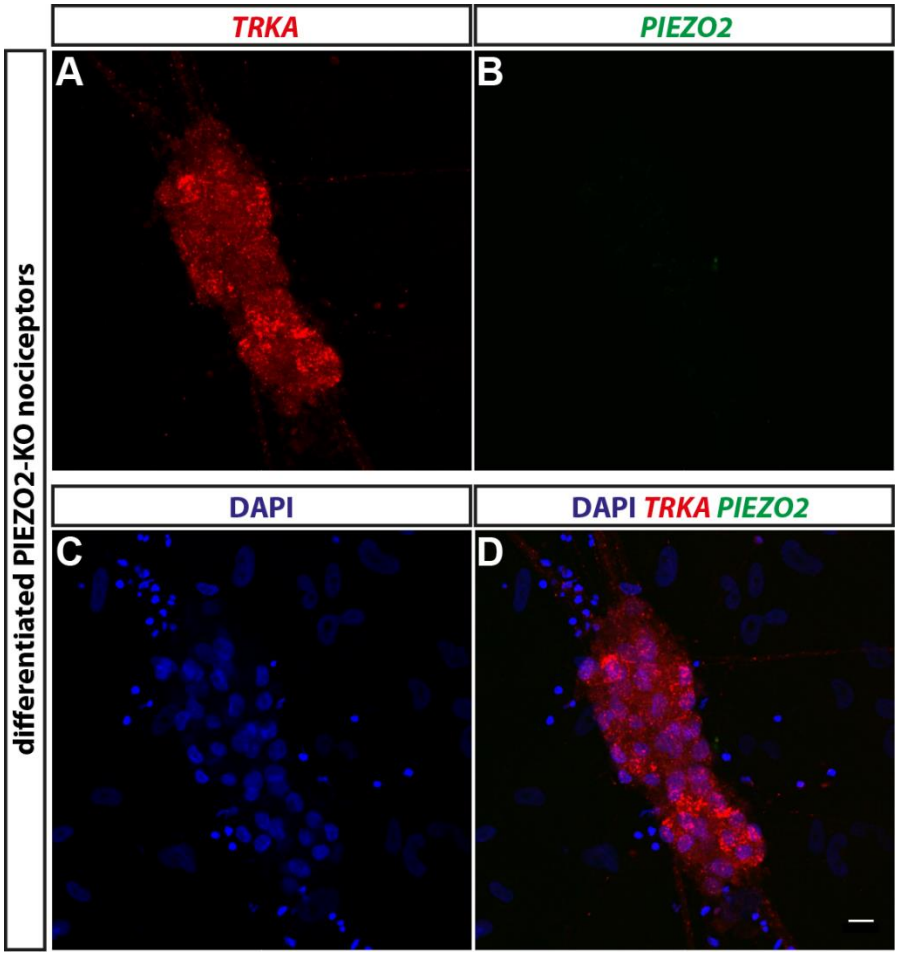

Fig. 41: Verification of the PIEZO2-KO in stem cell-derived nociceptors

Double fluorescent *in situ* hybridizations of differentiated PIEZO2-KO nociceptors showing the presence of *TRKA* (B) and the absence of *PIEZO2* (C) in stem cell-derived nociceptors. DAPI staining showed all cells in the field of view (A). (D) Overlay of all three markers, DAPI in blue, *TRKA* in red and *PIEZO2* in green. Scale bar 20 µm.

To explore whether a subpopulation of TRKA-positive sensory neurons in native DRGs also co-express PIEZO2, *in situ* hybridizations with human (Fig. 42A) and mouse (Fig. 42B) *post-mortem* tissue were performed. In both species, *Piezo2* transcripts (labeled in green) were also expressed in a fraction of native *TrkA*-positive neurons (labeled in red). In human DRG slices, 34.8 ± 3.6% of *TRKA*-positive cells co-expressed *PIEZO2*, whereas in mouse DRG slices, the fraction of *TrkA/Piezo2*-double positive cells was not significantly different (26.2 ± 0.8%, p=0.059; linear mixed model, Fig. 42C). These findings not only indicate that a *TRKA/PIEZO2*-double positive population exists in human stem-cell derived nociceptors and in native DRG tissue, but also that differentiated PIEZO2-WT and PIEZO2-KO neurons can be used for investigating the question

whether PIEZO2 is involved in mediating noxious mechanical stimuli in stem cell-derived peptidergic nociceptors.

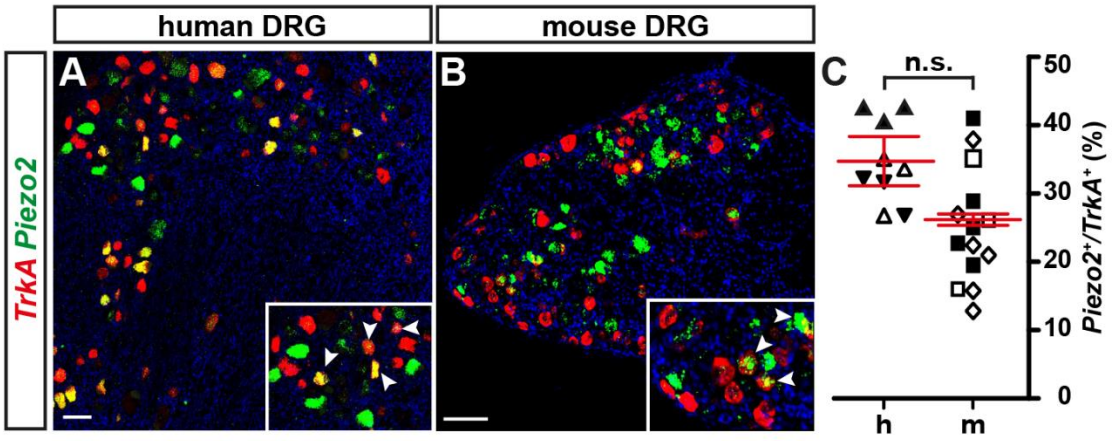

Fig. 42: Dual color *in situ* hybridizations analysis of human and mouse DRG tissue for *TrkA/Piezo2* expression

Double fluorescent *in situ* hybridization of cryo-section from a native human (A) and mouse (B) DRG, showing the presence of *Piezo2* (green) in combination with *TrkA* (red). In both species *Piezo2* is expressed in a fraction of *TrkA*-positive neurons. Quantifications of three independent individuals revealed that about 34.8 ± 3.6% of human *TRKA* neurons co-express *PIEZO2*, compared to the mouse analysis showing about 26.2 ± 0.8% *TrkA/Piezo2* double positive neurons. Scale bar 100 µm.

To explore the role of PIEZO2 in noxious mechanotransduction, electrophysiological recordings of differentiated PIEZO2-WT and PIEZO2-KO nociceptors were performed (by Dr. Jörg Pohle, a researcher in our laboratory). In addition to basic functional examinations, such as action potential properties (to indicate that the PIEZO2-KO did not alter fundamental electrophysiological features), mechanical stimulations were performed. While 61.8% (n=47 out of 76) of TRKA-positive WT nociceptors elicited robust RA, IA or SA mechanically-activated currents in response to membrane indentation of 20 µm (Fig. 43A-B #WT, see also chapter 5.2), in all analyzed PIEZO2-KO nociceptors (n=21) RA mechanically-activated currents were absent (Fig. 43 A-B #KO).

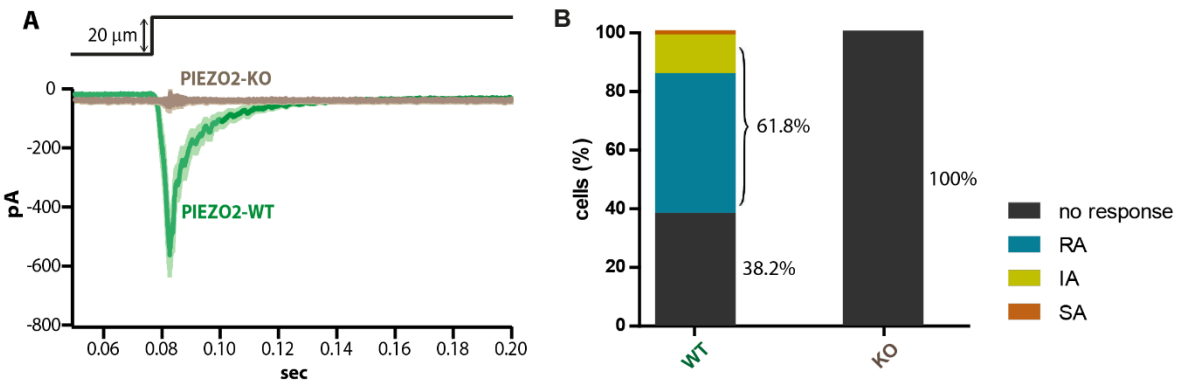

Fig. 43: Mechanical stimulation of stem cell-derived PIEZO2-KO nociceptors. Work done by Dr. Jörg Pohle

(A) Representative traces of mechanically-activated currents of PIEZO2-WT (blue) and PIEZO2-KO nociceptors. While PIEZO2-WT nociceptors elicited robust mechanically activated currents in response to membrane indentation, in PIEZO2-KO neurons mechanically activated currents were absent.
(B) Quantification analysis of mechanically stimulated PIEZO2-WT (WT) and PIEZO2-KO (KO) nociceptors. While approximately 61.8% of TRKA positive WT nociceptors elicited robust (SA/IA/RA) mechanically-activated currents, none of the analyzed PIEZO2-KO nociceptors responded to mechanical stimulation.

To summarize, these data showed that indeed PIEZO2 is not only involved in mediating innocuous mechanical stimuli in derived LTMRs, but is also required for noxious mechanotransduction in stem cell-derived TRKA-positive, peptidergic nociceptors.

5.5 Additional results: Generation and differentiation of a PIEZO2-tagged stem cell line

PIEZO ion channels are huge transmembrane proteins that do not resemble the primary sequences of other ion channels (Coste et al., 2010). Although primary sequence analyses suggested that PIEZO proteins consist of up to 40 transmembrane domains, more recent studies proposed a different possible topology for PIEZO1, indicating that the number of transmembrane domains is markedly lower than previously predicted and only 10-18 α-helices seem to span the cell membrane (Coste et al., 2015). Furthermore, it was demonstrated that isolated mouse PIEZO1 is composed of four single PIEZO1 molecules that assemble into a 1.2 million-dalton homo-tetramer, not being associated with other channel subunits, as it is known for example for voltage gated sodium channels (Coste et al., 2012). Given its remarkable size, and based on what is generally known for other ion channels (with signaling cascades regulated by multiple protein interactions (Dai et al., 2009)), it is likely that other accessory proteins are involved in PIEZO2 functioning. A recent screening for possible interaction partners of PIEZO2, based on antibody purification of native PIEZO2 and mass spectrometry analysis, identified 36 possible binding partners, and suggested pericentrin (PCTN), a protein involved in microtubule network formation, as a modulator of PIEZO2 (Narayanan et al., 2016).

To identify and characterize possible PIEZO2 interaction partners in a more defined subpopulation of primary sensory neurons (instead of whole DRG), and also to work with a human-based model system, we generated a hESC line containing the full-length human PIEZO2 with a triple Flag-His tag fused to its N-terminus. The presence of the attached tag allowed the purification of the protein, for later biochemical analyses and mass spectrometry, in order to identify possible interaction partners of PIEZO2 in differentiated LTMRs (generated based on our already published differentiation protocol). Since almost nothing was known about the PIEZO2 topology, and different signal peptide prediction programs (PrediSi, Phobius or SignalP4.1) provided different

results concerning a putative extracellular or intracellular localization of the N- and C-terminus, we decided to generate a PIEZO2 targeting construct where we directly introduced the 3xFlag-His tag sequence at the 5` end of exon 1 (Fig. 44).

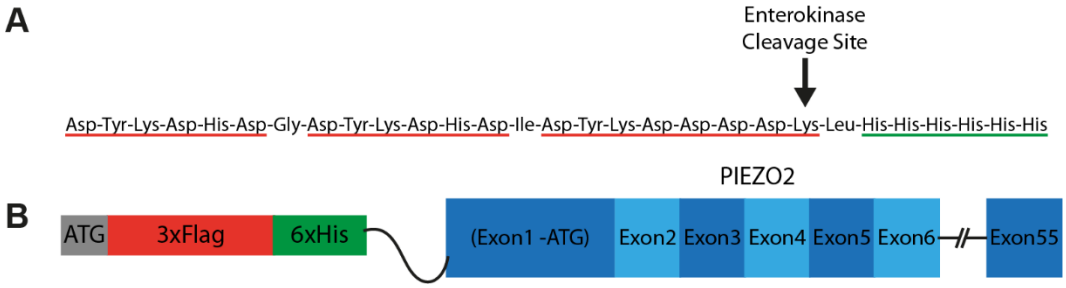

Fig. 44: Amino acid sequence of the 3xFlag-His-tag and schematic illustration of tagged-Piezo2

(A) Amino acid sequence of the 3xFlag-His-tag, a 22-amino acid fusion protein of 3 tandem Flag epitopes and fused to polyhistidine-tag.
(B) Schematic illustration of the tagged-PIEZO2 protein. The 3xFlag-His-tag was fused to the N-terminus of PIEZO2.

To test tagged-PIEZO expression and to optimize the pull-down conditions for isolation of such a huge protein, we also generated a 3xFlag-His-tag PIEZO-GFP expression vector, used for transient transfection experiments in human embryonic kidney (HEK) cells. Due to recurring difficulties with cloning parts or full-length human PIEZO2 and due to the fact that we assumed a similar N-terminal topology for PIEZO1 and PIEZO2, we decided to use a mouse PIEZO1-GFP expression vector backbone, which had been successfully used before for cloning purposes. Specific expression of tagged-PIEZO1 was verified by immunohistochemistry analysis of transfected HEK cells (Fig. 45A), stained with antibodies recognizing the Flag-tag (Fig. 45B) and the PIEZO1-GFP fusion protein (Fig. 45C).

Furthermore, immunoprecipitation (IP) experiments using Flag-antibody coupled magnetic beads were performed, to optimize the pull-down conditions (Fig. 45E). In transiently transfected HEK cells (+), tagged-PIEZO1 was detectable in the supernatant of the total lysate before IP (+B) and absent in non-transfected cells (used as a negative control (-B)). After the IP, PIEZO1 was detectable in the eluate of the total lysate (+E), but barely detectable in the supernatant (+A) (Fig. 45E).

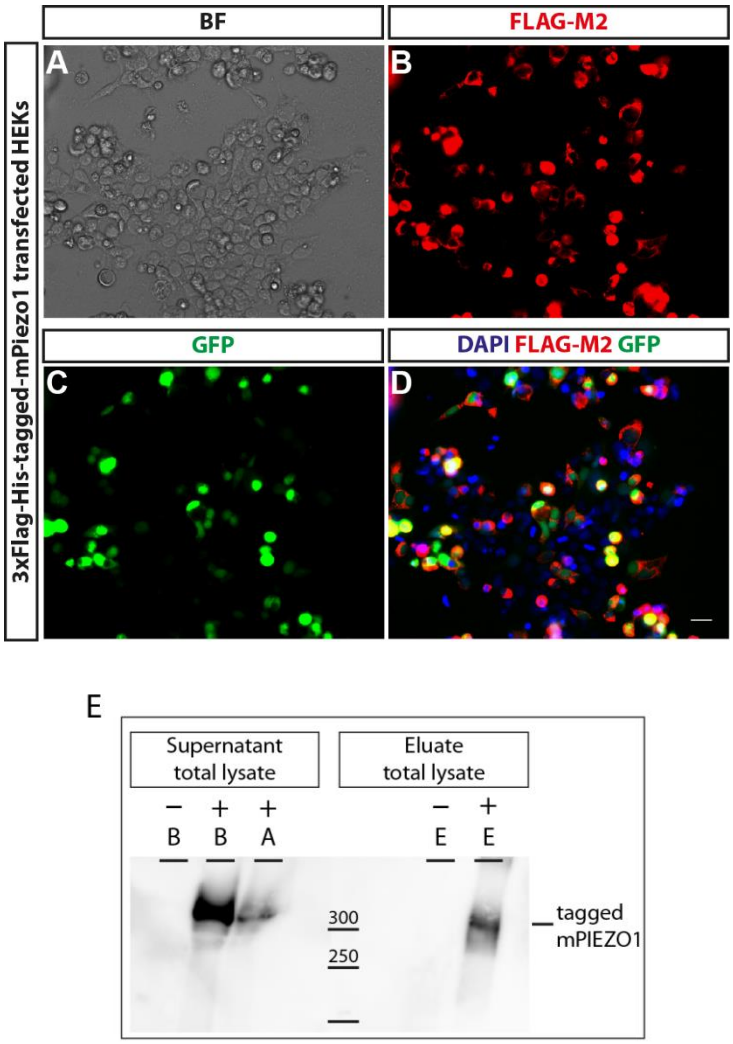

Fig. 45: Tagged-mPIEZO1 expression and immunoprecipitation from transfected HEK293 cells

(A-D) Specific expression of tagged-PIEZO1, verified by immunostainings of 3xFlag-His-tagged mPIEZO1 transfected HEK 293 cells with antibodies recognizing the Flag-tag (B) and the PIEZO1 fusion protein GFP (C). DAPI staining and bright field image showed all cells in the field of view (A). (D) Overlay of all three markers, DAPI in blue, Flag in red and GFP in green. Scale 50 µm.

(E) Immunoprecipitation of 3xFlag-His-tag-PIEZO1 transiently transfected (+) or non-transfected (-) HEK293 cells. Immunoprecipitated PIEZO1, using Flag antibody coupled magnetic beads, was detected in the supernatant of the total lysate before the IP (+B) and in the eluate of the total lysate after the IP (+ E). After the IP, PIEZO1 was depleted in the supernatant of the total lysate. As a negative control, PIEZO1 was not detectable in non-transfected samples.

Based on these preliminary results with the tagged-PIEZO1 construct, we assumed that the human 3xFlag-His-PIEZO2 protein could also be natively expressed and isolated from stem cell-derived mechanoreceptors. Using the heterozygous *PIEZO2*$^{+/-}$-stem cell line as a starting population allowed us to check whether gene targeting resulted in a functional tagged-*PIEZO2* allele, since a *PIEZO2-KO* in only one allele does not suppress mechanically-activated currents (Schrenk-Siemens et al., 2015a).

By making use of CRISPR-Cas9 technology and homologous recombination, we inserted the 3xFlag-His-tag into the endogenous human *PIEZO2*-WT allele (Fig. 46A). In case of correct gene

targeting, we would obtain a targeted stem cell clone in which one allele is N-terminally fused to the 3xFlag-His-tag ("targeted tagged allele") and the other *PIEZO2* allele remains disrupted ("targeted KO allele", Fig. 46B).

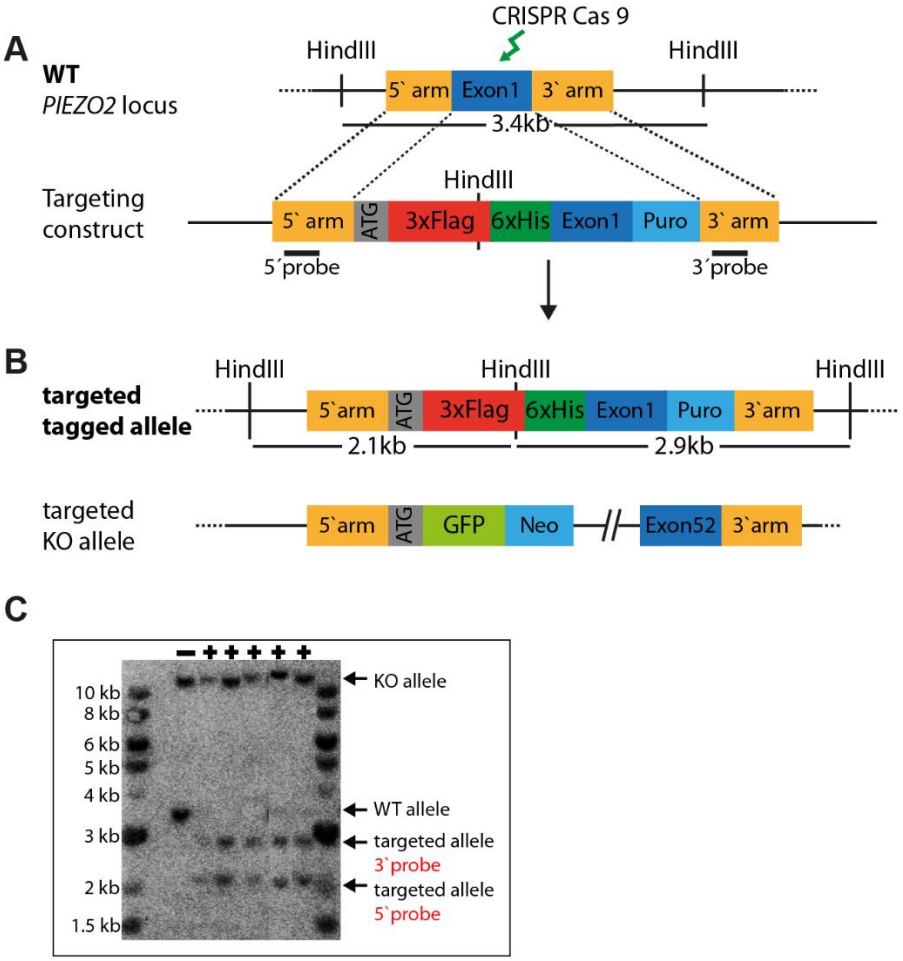

Fig. 46: Piezo2 targeting strategy

(A) Scheme of tag-PIEZO2 targeting construct for the generation of a 3xFlag-His-tagged PIEZO2 stem cell line, where the tag is fused to the endogenous N-terminus of human PIEZO2.

(B) Schematic drawing of the targeted *PIEZO2* alleles. The tag-PIEZO2 targeting was performed with an already targeted stem cell line, having one *PIEZO2-KO* allele. A successful targeting would generate an additional targeted allele where the 3xFlag-His tag is fused to the N-terminal end of PIEZO2.

(C) Verification of positively targeted stem cell clones, carrying a *PIEZO2-KO* allele (KO allele) and an additional 3xFlag-His tagged *PIEZO2* allele (targeted allele 3` probe or targeted allele 5` probe). The upper band shows the *PIEZO2-KO* allele. An additional WT band (unsuccessful targeting) is about 3.4 kb, detectable in the majority of the analyzed clones (data shown for one representative clone (-)). A successful gene targeting shows an additional band of 2.1 kb for the analysis with the 5' probe and a band of about 2.9 kb for the 3' probe (shown for 5 positive clones, (+)).

After screening for more than 100 clones by Southern Blot, we obtained 5 positive clones, with the 3-Flag-His-tag effectively inserted at the N-terminus of endogenous PIEZO2 (Fig 46C). The upper band represents the *PIEZO2-KO* allele that was already modified in a previous gene targeting. If the tag-targeting was not successful, we would expect an additional WT band of about 3.4kb which

was detectable in the majority of the analyzed clones (data shown for one representative clone (-)). If gene targeting was successful, we would expect an additional band of 2.1kb for the analysis with the 5`probe and a band of about 2.9 kb for the 3`probe what is shown for 5 positive clones (Fig. 46C (+)). The remaining negative clones, also resistant to puromycin treatment, had integrated the targeting construct randomly into their genome and therefore did not show the expected targeted bands.

To test whether the generated PIEZO2$^{tag/-}$ hESCs were still able to differentiate into sensory neurons, two clones were expanded and differentiated into LTMRs, that would be used for PIEZO2 pull-down experiments. Compared to mechanoreceptors derived from WT hESCs, immunohistochemistry analysis of PIEZO2$^{tag/-}$ LTMRs indicated that modified hESCs have the continuing ability to differentiate into mechanoreceptors, expressing ISL1, a marker for sensory neurons, as well as MAFA and NF200, two markers more specific for mechanoreceptive neurons (Fig. 47).

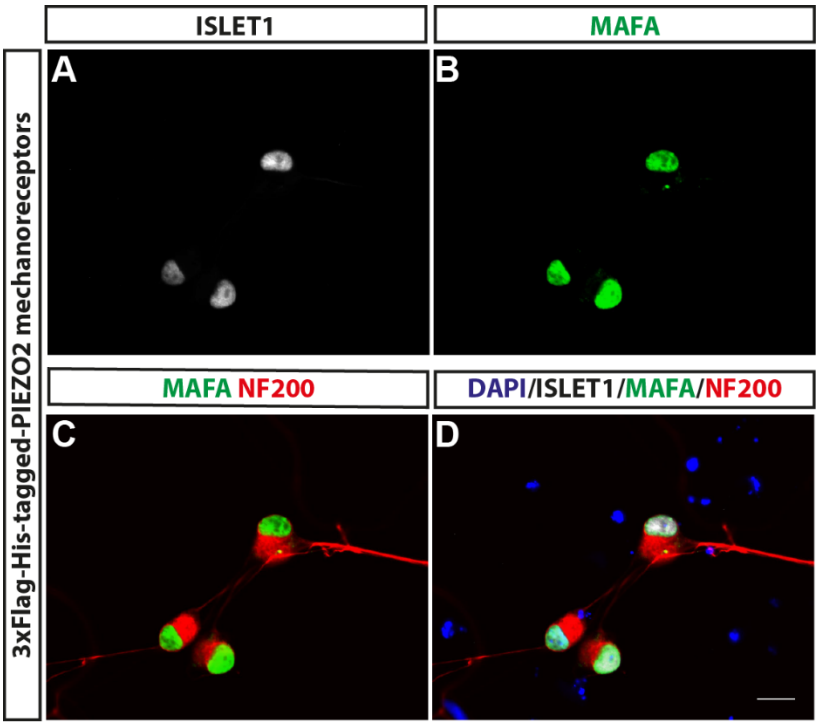

Fig. 47: Immunohistochemistry analysis of differentiated tagged-PIEZO2 mechanoreceptors

Immunohistochemical staining of differentiated PIEZO2-tagged mechanoreceptors for ISL1 (A), a marker for post-mitotic sensory neurons and for MAFA and NF200 (C), two markers expressed in mechanoreceptive neurons. DAPI staining showed all cells in the field of view. (D) Overlay of all three markers, DAPI, ISLET, MAFA and NF200. Scale bar.20 µm.

We next assessed whether differentiated tagged-PIEZO2 mechanoreceptors were still functional and able to trigger mechanosensitive currents in response to mechanical stimulation. To do so, electrophysiological recordings of tagged-PIEZO2 mechanoreceptors in comparison to heterozygous PIEZO2-KO mechanoreceptors as a positive control were performed by Vincenzo Prato and mechanically stimulated with a nanomotor-driven probe.

While heterozygous PIEZO2-KO mechanoreceptors (n=3) elicited robust rapidly-adapting mechanically activated currents in response to membrane indentation (Fig. 48A), PIEZO2$^{tag/-}$ mechanoreceptors (2 separate clones; n=17) did not show mechanically activated currents (Fig. 48B). These results demonstrated that the tagged-PIEZO2 protein was not functionally active any longer and cells were not able to response to mechanical stimuli.

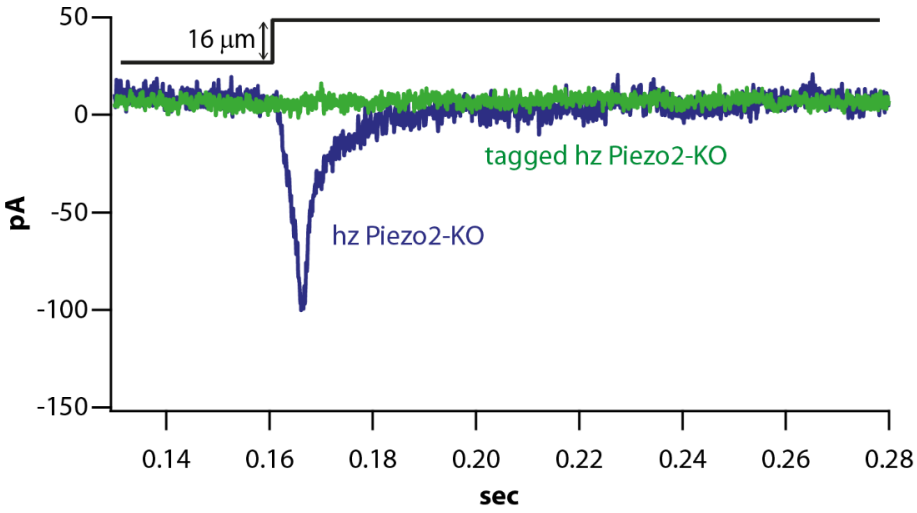

Fig. 48: Mechanical stimulation of tagged-PIEZO2 mechanoreceptors done by Vincenzo Prato

Example voltage-clamp trace of a mechanically-stimulated 3xFlag-His-tag hz PIEZO2-KO mechanoreceptor (green trace) and untagged hz PIEZO2-KO. Mechanically-activated currents were almost completely absent in tagged-PIEZO2 mechanoreceptors.

Genomic DNA sequencing analysis of positively targeted stem cell clones pointed out that the sequences were correct and the CRISPR-Cas9 targeting was successful. Nevertheless, the insertion of the 3xFlag-His tag might have caused conformational changes or disorganization of the PIEZO2 protein, rendering it non-functional, and therefore not suitable for further pull-down experiments. Retrospectively, the assumption that PIEZO1 and PIEZO2 adopt a similar N-terminal topology was perhaps wrong and likely resulted in a misfolded, non-functional tagged PIEZO2 protein.

6. Discussion

6.1 hESC-derived neurons and comparison to human and mouse DRG

Given the fact that human stem cell-based technologies could serve as powerful tools for studying human pain mechanisms, it is of paramount importance to characterize differentiated nociceptors and analyze whether they reflect their *in vivo* correspondents in order to assess if they exist in the human body.

NGN1-infected, developing sensory nociceptors were visualized and identified using a TRKA-tomato reporter line (with the tomato-reporter expressed under the TRKA promotor). After 10-14 days of gene induction, when developing sensory nociceptors start to express TRKA, cells showed a tomato signal. To characterize differentiated TRKA-positive neurons, several functional and biochemical analyses were performed. To elucidate whether differentiated TRKA-positive neurons are physiological relevant, gene expression profiles of *in vitro* differentiated cells were compared to *post-mortem* human DRG tissue. Furthermore, to investigate differences and similarities between the mouse model system and human beings, DRG tissue of both species was analyzed.

TRK receptor expression *in vitro* and *in vivo*

Primary sensory neurons have been extensively studied within the last decades and characterizations based on marker gene expression, functionality or target innervation identified primary sensory neurons as a highly heterogeneous group of neurons (Basbaum et al., 2009; Li et al., 2016b; Marmigère and Ernfors, 2007; Usoskin et al., 2015). Recent single cell-based transcriptome studies of mouse DRG neurons subdivided the three main neuronal populations (nociceptors, mechanoreceptors and proprioceptors) further into at least 11 categories, according to their marker expression (Li et al., 2016b; Usoskin et al., 2015). During sensory neuronal development, TRK receptor expression is highly dynamic and overlapping, and becomes more refined at later developmental stages, where specific TRK expression is linked to distinct neuronal subpopulations and defined peripheral target innervations (Ernsberger, 2009; McMahon et al., 1994). To assess whether TRK receptor expression in differentiated nociceptors is mainly non-overlapping, we performed dual color *in situ* hybridization analysis for *TRKA* in combination with *TRKB* or *TRKC*. Quantifications revealed that, in accordance with the literature, only a minority of the *TRKA*-positive nociceptors co-express either *TRKB* or *TRKC*.

Marker gene expression analysis of *post-mortem* human and mouse DRG tissue, confirmed what we have seen in differentiated cells. Dual color *in situ* hybridization analysis for *TrkA* in

combination with either *TrkB* or *TrkC* revealed that the three main sensory subpopulations can also be found in *post-mortem* human and mouse tissue. In both species, *Trk* receptors are again mainly expressed in a non-overlapping manner and can be used for categorizing different neuronal categories such as mechanoreceptors, proprioceptors and nociceptors.

In addition to neurotrophin receptor expression, it was also demonstrated that rodent sensory neuron soma sizes correlate with different neuronal subpopulations, and can thus be classified in three categories: while small diameter DRG neurons mainly express TRKA, most TRKB-positive cells exhibit an intermediate cell size phenotype and TRKC is mainly found in large diameter neurons (McMahon et al., 1994; Molliver et al., 1997; Silos-Santiago et al., 1995b). Soma cell size distribution analysis of human and mouse DRG, plotting the soma area of *TrkA*, *TrkB* and *TrkC*-positive cells against their relative frequency, revealed a similar relative size distribution in native human DRG tissue. Furthermore, analysis of the overall cell size, comparing the smallest and largest neurons of each *Trk*-receptor subpopulation, showed that on average human DRG neurons (ranging from 400 μm^2 to 3400 μm^2) are larger compared to mouse DRG neurons (ranging from 200 μm^2 to 1600 μm^2), as already described in literature (Davidson et al., 2014; Vega et al., 1994). The soma size of stem cell-derived TRKA-positive neurons increased over the period of differentiation and cells (kept in culture for more than 6 weeks) had cell body sizes up to 400 μm^2, reaching similar soma sizes of human native *TRKA*-expressing DRG neurons (the effect was only quantified once and thus has not been statistically validated).

These findings confirm a similar neurotrophin receptor expression pattern in stem cell-derived nociceptors and human and mouse DRG tissue. Moreover, the relative size distribution of mouse and human DRG neurons is similar and nicely correlated to the expression of the respective member of the neurotrophin receptor family.

RET expression *in vitro* and *in vivo*

The receptor tyrosine kinase RET has also been broadly analyzed and was shown to be important for sensory neuron development and functioning (reviewed by Ernsberger, 2008). RET is expressed in up to 79% of human DRG neurons and about 60% of adult rodent sensory neurons (Bennett et al., 1998; Josephson et al., 2001; Kashiba et al., 1998, 2003; Molliver et al., 1997; Zwick et al., 2002). In addition to the two developmental RET lineages (the early RET population, mainly generating large diameter RET/TRKB expressing LTMRs, and the late RET population, mostly developing into non-peptidergic TRKA-negative nociceptors) (Bourane et al., 2009; Chen et al., 2006; Lallemend and Ernfors, 2012; Luo et al., 2009), two other smaller RET-positive populations were found, a RET/tyrosine-hydroxylase (TH) co-expressing population of unmyelinated C-type fiber LTMRs, and a RET/TRKA double-positive population, representing 5-10% of RET-positive

mouse DRG neurons (Golden et al., 2010; Li et al., 2011; Molliver et al., 1997). Moreover, recent findings revealed a role of these TRKA/RET double-positive cells in itch sensation, triggering the sensory reflex to scratch the affected body surface area (Stantcheva et al., 2016b; Usoskin et al., 2015).

Surprisingly, our results reveal co-expression of *TRKA/RET* in a large fraction of differentiated tomato-positive hESC-derived nociceptors, contrary to what has been found in mouse, where only a small population of TRKA/RET co-expressing cells were found and exclusive RET expression was mainly detectable in non-peptidergic nociceptors.

Co-expression analysis of *TrkA/Ret* double-positive human and mouse DRG neurons confirmed what was seen in differentiated TRKA-positive nociceptors: the amount of *TrkA/Ret* co-expressing neurons was significantly higher in human tissue compared to the double-positive population found in mouse. Quantifications demonstrated that roughly 50% of human adult *TRKA*-positive neurons co-express *RET*, compared to about 20% in mouse DRG neurons, where RET is mainly expressed in non-peptidergic nociceptors that downregulate TRKA. A recent publication proposed a role for a small TRKA/RET double-positive population in mouse DRGs in itch sensation and demonstrated that these "itch-sensing"-neurons also express TRPV1 (Stantcheva et al., 2016b), an additional marker that we found in a larger population of human TRKA positive DRG tissue compared to mouse DRGs. Moreover, in both species, we also detected different *Ret* expression levels, an already described phenotype in mouse (Stantcheva et al., 2016a). Clustering analysis showed again the *TrkA/Ret*-double positive population (high *TrkA*/high *Ret*) in analyzed human DRG, a population almost undetectable in mouse tissue.

Human beings are faced with innumerable environmental stimuli that potentially provoke pruritus, and our skin is not protected by fur as in rodents. If we consider that humans lost their body hair already approximately 1.2 million years ago and clothing is a more modern era development that probably evolved about 170.000 years ago, evolutionary adaptations could explain this higher number of *TRKA/RET*-positive sensory neurons in human DRG neurons (Toups et al., 2011). Nevertheless, there is no clear evidence that this *TRKA/RET* population is actually coupled to itch sensation and further analyses are needed to prove this hypothesis.

NF200 expression *in vivo* and *in vitro*

From rodent studies, it is known that different fiber-types can also be categorized by the presence of different neurofilament subunits and NF200, the heavy neurofilament subunit, was identified as a molecular marker of fast–conducting A-fibers. Interestingly, our data show that almost all (96.7%) human stem cell-derived TRKA-positive neurons were also positive for NF200.

Quantification analysis of immunostainings with two different antibodies, showed that the *in vitro* human phenotype is also found in *post-mortem* human tissue. However, species-specific differences regarding the neurofilament expression exist: almost all TUJ1-positive neurons (97.3%) in the human DRG also expressed NF200, whereas in mouse DRG slices only about 60% of all neurons co-expressed NF200.

These results again demonstrate that differentiated nociceptors seem to be physiologically relevant, as nearly all stem cell-derived neurons and native human DRG express NF200, independent of different neuronal subtypes (as already described by (Vega et al., 1994). Although the universal expression of NF200 in human DRG neurons suggests a correlation between conduction velocity of myelinated fast-conducting A-fibers and the overall increased body size of human beings compared to relatively small rodents, no significant differences regarding conduction velocity were observable (Cain et al., 2001; Hagbarth, 2002; Handwerker et al., 1991). Based on this, we can only assert that, in humans, the heavy neurofilament NF200 cannot be used for classifying different primary sensory subpopulations and furthermore, NF200 does not correlate with myelination as has been assumed to be the case in mice.

Nav channel expression *in vitro* and *in vivo*

Besides TRK receptor or RET expression, VGSCs have been broadly studied and various Nav channels have been associated with mediating pain signals. While Nav1.6-Nav1.9 are known to be expressed in human and mouse DRG neurons, only Nav1.7-Nav1.9 are strongly implicated in human pain disorders such as small fiber neuropathies, episodic pain or congenital insensitivity to pain (Ahmad et al., 2007; Faber et al., 2012; Fertleman et al., 2006; Yang et al., 2004; Zhang et al., 2013a). In our RT-PCR analysis of differentiated neurons, *Nav1.6* was detectable in mechanoreceptors and nociceptors at comparable low levels, whereas *Nav1.7* was expressed at high levels in both neuronal populations. *Nav1.8*, as described in literature, was more restricted to small diameter neurons and only detectable in differentiated TRKA-positive nociceptors (Amaya et al., 2000; Toledo-Aral et al., 1997).

Nav channel expression of stem cell-derived nociceptors and native human and mouse DRG tissue was compared by dual color *in situ* hybridizations for *TrkA* and *Nav1.6-1.9*. Quantification analysis indicated that populations of *TrkA/Nav1.6* and *TrkA/Nav1.7* did not significantly differ between human and mouse tissue and overall the *TrkA/Nav1.6* population was smaller than the population of *TrkA/Nav1.7*, as already seen in differentiated TRKA-positive neurons.

Contrary, gene expression analysis for *TrkA/Nav1.8* and *TrkA/Nav1.9* displayed differences between human and mouse DRG tissue. As already described for differentiated TRKA-expressing neurons, the fraction of *TrkA/Nav1.8*-double positive cells for both species (human and mouse

tissue) was larger than the fraction of *TrkA/Nav1.9*-double positive cells. Furthermore, for both *Nav1.8* and *Nav1.9*, the fraction of double positive cells was significantly larger in human DRG compared to mouse DRG. In conclusion, sodium channel expression in native human and mouse sensory neurons highlights explicit species-specific differences that have to be taken into account and could be useful for the discovery of new therapeutic approaches and analgesic drugs.

TRP channel expression *in vivo* and *in vitro*

In addition to TRK or Nav channel expression, most primary sensory neurons can also be classified by the expression of members of the TRP channel family. One of the best studied family members is TRPV1, a polymodal channel known to be involved in the detection of noxious temperatures and in inflammatory-induced sensitization, and therefore one of the central targets for analgesic drug research (Carnevale and Rohacs, 2016; Caterina et al., 1997). In mice, approximately a third (22-38%) of the DRG neurons express TRPV1; these are mainly non-myelinated peptidergic nociceptors but – to a minor degree – also non-peptidergic neurons (Kobayashi et al., 2005; Orozco et al., 2001; Zwick et al., 2002). Ca^{2+}-imaging experiments, our first readout to characterize differentiated TRKA-positive neurons, also demonstrated that also a certain number of our TRKA-positive neurons (about 10-15%; quantified by me and Katrin Schrenk-Siemens) were activated by capsaicin and therefore express TRPV1. In stem cell-derived neurons the TRKA/TRPV1-double positive population was smaller compared to native human DRG tissue. Although our initial hope was to establish a differentiation protocol for the generation of a homogeneous nociceptor population, it is not surprising that we found slightly different numbers in our *in vitro* culture system when comparing it to *post-mortem* human tissue. Moreover, the comparison of native human and mouse DRG tissue revealed that the amount of *TrkA/TrpV1*-double positive neurons in humans was significantly larger than in native mouse DRG neurons. Due to the fact that TRPV1 is linked to noxious heat detection and thermal hyperalgesia, evolutionary enhancements and benefits could explain this higher number of *TRKA/TRPV1*-positive sensory neurons in human DRG tissue that should prevent further damage of an already injured tissue.

Besides gene expression analysis (performed by immunohistochemistry, *in situ* hybridization or RT-PCR), also functional Ca^{2+}-imaging experiments and electrophysiological analysis supported the evidence that stem cell-derived neurons show characteristic features of nociceptive neurons. In response to step-wise depolarizing currents, differentiated TRKA-positive neurons elicited trains of broad action potentials, a marker for identifying nociceptors compared to non-nociceptive neurons, characterized by only narrow single action potentials (Viatchenko-Karpinski and Gu, 2016; Wainger et al., 2015). Furthermore, mechanical stimulation of differentiated nociceptors by a nanomotor-driven probe elicited robust mechanically-activated currents, increasing in amplitude with increasing membrane indentation. Moreover, elicited currents exhibited all different kinetics

from RA, IA and SA mechanically-activated currents, only detectable in nociceptive neurons (Drew et al., 2002; Hu and Lewin, 2006; Viatchenko-Karpinski and Gu, 2016).

The comparative study between hESC-derived nociceptors and native human DRG tissue confirmed that differentiated TRKA-positive neurons are physiologically relevant, with an almost similar marker gene expression profile in *post-mortem* DRG neurons (Table. 4).

In addition, our comparative study between human and mouse DRG tissue offers a detailed gene expression profile analysis and determines molecular differences and similarities between the animal mouse model system and the human organism already at cellular resolution, which will help to overcome translational difficulties and improve the prognostic significance of preclinical pain studies.

6.2 What can differentiated nociceptors be used for? - A translational approach

For decades, animal models have been broadly used for studying and identifying various aspects of sensory transduction mechanisms such as the perception of pain, and are therefore an invaluable tool for finding pain-relieving medications. But during the last years, there is evidence that human and rodent pain phenotypes differ, resulting in the failure of several preclinical trials reaching routine clinical practice (Burma et al., 2017b; Mogil, 2009b; Percie du Sert and Rice, 2014).

TRP ion channels have characteristic polymodal features and are known to be involved in mediating painful stimuli. Nevertheless, pharmaceutical targeting effects of currently existing TRP-antagonists reported divergent results.

TRPV1 is associated with inflammatory pain and sensitization, leading to pain-mediated hypersensitivity and is therefore a prime target of anti-pain drug research (Caterina et al., 1997; Tominaga et al., 1998). However, treatments with different TRPV1 antagonists for osteoarthritis or synovitis (inflammation of synovial membranes; membranes around bones or joints) in mice, dogs or human patients resulted in complete, moderate or no reduction of pain sensation (Cathcart et al., 2012; Kelly et al., 2015; Miller et al., 2014). In addition to variable pain-relieving efficacies, antagonist-mediated TRPV1 targeting also leads to critical side effects such as accidental burns or hyperthermia, as TRPV1 is also involved in the perception of temperature. Those undesirable adverse effects urge for the development of more selective, modality-dependent antagonists (Carnevale and Rohacs, 2016; Gavva et al., 2007).

To circumvent species-species differences and to prevent additional side effects in a multicellular organism, it is advantageous to combine animal studies with a defined human-based cell culture model for primarily testing analgesic drugs.

Human ESCs as a model system to study signaling of painful stimuli

In contrast to other human tissues such as skin samples or cancer cells, usually straightforward to collect, the peripheral nervous system (and more precisely the DRG, where the cell bodies of the primary sensory neurons are located) is not approachable from living individuals and difficult to receive even *post-mortem*. Therefore, the availability of human embryonic stem cell-based techniques and the development of differentiation protocols for the generation of functional primary sensory neurons came in focus of research (Blanchard et al., 2015b; Chambers et al., 2012b; Schrenk-Siemens et al., 2015a; Wainger et al., 2015).

Our achievement, the development of a differentiation protocol based on viral-induced NGN1 overexpression, resulted in the generation of primary sensory neurons with a characteristic nociceptive phenotype. Differentiated nociceptors were identified by a TRKA-tomato reporter line, generated in our laboratory. Quantification analysis of double fluorescent *in situ* hybridization experiments verified an almost 100% overlap of *tomato* and *TRKA*, demonstrating that the *tomato* signal reflects the endogenous *TRKA* expression. Furthermore, immunohistochemistry analysis revealed that approximately 24.4% of DAPI-positive cells in culture adopted a sensory neuronal phenotype indicated by the ISLET1 immunoreactivity and almost all sensory neurons also co-expressed TRKA. Interestingly, almost all (96.7%) differentiated TRKA-expressing neurons were also positive for NF200, a marker that has been used for identifying fast-conducting myelinated A-fibers in rodents. However, marker gene analysis of differentiated nociceptors and also native human DRG tissue suggested that in humans NF200 is expressed in almost all sensory neurons and cannot be used as a marker for categorizing different primary sensory subpopulations. TRK receptor expression analysis, classically used to categorize sensory neurons into three main subpopulations (with TRKA primarily expressed in small diameter peptidergic nociceptors, TRKB mainly in mechanoreceptors and TRKC mainly in large diameter proprioceptors) (Chen et al., 2006; Ernsberger, 2009; Perez-Pinera et al., 2008; Snider, 1994), confirmed what was already known from rodent studies and showed only a small overlap of *TRKA/TRKB* (3.8%) or *TRKA/TRKC* (19.2%) in differentiated neurons. However, gene expression analysis for *TRKA* and *RET*, a marker known to be expressed in the non-peptidergic nociceptor subpopulation in mice that downregulates TRKA expression during maturation and upregulates RET (Molliver et al., 1997), showed a strong overlap (77.6%) of both populations. Furthermore, RT-PCR analysis of differentiated nociceptor and mechanoreceptor cultures showed that the sodium channel *Nav1.7* was broadly expressed in both neuronal cultures, whereas *Nav1.8*, known to be more restricted to small diameter nociceptive neurons, was only detectable in differentiated TRKA-positive neurons. In comparison to RNA transcriptome sequencing data from Usoskin et al., 2015, where they classify 622 single mouse DRG neurons into 11 neuronal subpopulations, our differentiated TRKA-expressing neurons would (most likely) fit into the peptidergic subgroup 1 (referred to as

PEP1) and peptidergic subgroup 2 (referred to as PEP2), which are defined by either *TrkA/Nf200/Nav1.8/1.9*-expressing slightly myelinated Aδ nociceptive neurons or *TrkA/TrpV1/Nav1.8/1.9*-positive neurons. However, both populations "PEP1 and "PEP2" do not highly express *Piezo2 or Ret* (Usoskin et al., 2015). Although the comparison of our differentiated TRKA-positive nociceptors to transcriptome analysis in mouse DRG suggests a nociceptive phenotype, most closely related to the already described two peptidergic subpopulations, not all analyzed genes match to one another which could be explained by specific species differences, that we also found in native human and mouse DRG tissue. Therefore, it is also conceivable that differentiated human nociceptors express a specific set of marker genes that is unique to humans without having an exact equivalent in mouse DRG neurons

To conclude, not only marker gene expression analysis and functional Ca^{2+}-imaging recordings but also electrophysiological properties (such as trains of broad action potentials or SA, IA as well as RA mechanically-activated currents in response to membrane indentation) demonstrated that differentiated, TRKA-positive neurons show characteristic hallmarks of peptidergic nociceptors.

To assess whether differentiated hESC-derived nociceptors are physiologically relevant and reflect their *in vivo* counterparts, we compared them to human *post-mortem* DRG tissue and found a similar marker gene profile in differentiated cells and human tissue.

Human iPSCs as a model system to study signaling of painful stimuli

In order to develop patient-derived neurons it will be necessary to test whether the differentiation protocol can also be used for the differentiation of iPSCs. Since the discovery of the induction of pluripotency in reprogrammed somatic cells by Yamanaka and colleagues, it is possible to isolate patient tissue and reprogram cells using the viral-induced overexpression of distinct transcription factors into induced pluripotent stem cells (Takahashi et al., 2007b). This approach offers a non-invasive, human-based *in vitro* cell culture model for the generation of patient-derived neurons. It enables the comparison of patient-specific diseases and healthy individuals and therefore a new insight into disease onset, progression and therapy.

Although iPSC-based techniques provide an encouraging course of action, already used for modeling various diseases such as autism, multiple sclerosis, Alzheimer´s disease or amyotrophic lateral sclerosis, stable differentiation protocols are needed for the generation of mature cell types, recapitulating characteristic pathophysiological features (Egawa et al., 2012; Massa et al., 2016; Mohamet et al., 2014; Mokhtari and Lachman, 2016). Differentiated patient-derived neurons or, more precisely in our case, generated human nociceptors can then be used for analgesic drug screening approaches, in a defined individual-specific manner.

Not only analgesic medication screens are conceivable but also cosmetic applications can be performed by testing various potentially irritating or anti-inflammatory ingredients on human stem cell-derived nociceptors. It is generally known that animal models were used for testing cosmetic products, however, the already mentioned differences between rodents and humans called for more translational research, which could be addressed by using human-derived cells instead of animal models (Reisinger et al., 2015).

A cell-based 3D-model system to study signaling of painful stimuli

To eliminate doubts concerning *in vitro* two-dimensional cell culture systems that recapitulate complex and heterogeneous sensory transduction mechanisms, it is also reasonable to transplant Ngn1-infected NCLCs into an *in vitro* three-dimensional skin model. First, this would allow to analyze whether neuronal precursor cells are still able to differentiate into mature nociceptors in a more physiological environment and, second to test how patient-derived nociceptors morphologically or functionally differ from healthy neurons. Three-dimensional skin models consist of a basal collagen matrix populated with isolated human fibroblasts and a layer of keratinocytes, added on top of the collagen-fibroblast matrix. Differentiated keratinocytes, exposed to air on one side and liquid to the other, stratify and form *in vivo*-like epidermal tissue (Carlson et al., 2008; Stark et al., 2004). Human primary sensory neurons, differentiated in an organized *in vivo*-like environment, would represent an impressive tool for studying sensory neuron development, transduction mechanisms and pain-diseases in humans.

6.3 Why initial protocols did not work

Although TRK receptors, and subsequently neurotrophin signaling, are important for assuring survival and differentiation of primary sensory neurons, and their expression is largely overlapping and dynamic during development, in mature neurons TRK receptors are restricted to defined subpopulations of DRG neurons (Averill et al., 1995; Fariñas et al., 1998; Perez-Pinera et al., 2008; Snider, 1994). The overexpression of TRKA to differentiate stem cell-derives NCLCs into nociceptive neurons in the initial lentiviral induction experiments was thought to guide neuronal precursor cells into the nociceptive lineage, since mouse studies demonstrated that almost all developing nociceptors express TRKA and these cells are missing in TRKA or NGF-deficient mice (Crowley et al., 1994; Smeyne et al., 1994). Nevertheless, our results showed that a permanent TRKA overexpression was not sufficient to generate nociceptors with the additional caveat of only very few cells surviving the differentiation procedure. Besides its primary function in promoting cell differentiation, growth and survival of neurons, the artificial TRKA overexpression and

eventually elevated NGF/TRKA signaling seemed to have side or toxic effects on our differentiating neurons, resulting in massive cell death. In this context, it was recently demonstrated that TRKA expression is also linked to macropinocytose-mediated cell death in medulloblastoma cancer cells (Li et al., 2016a). While in pancreatic cancer cells, macropinocytosis is necessary for rapid tumor growth, in brain tumor cells TRKA-induced macropinocytosis is uncontrolled, resulting in cell membrane fragmentation and cancer cell death (Li et al., 2016a). Furthermore, NGF-induced TRKA activation in human glioblastoma cells was associated with autophagy and eventually lead to NFG/TRKA-mediated cell death (Hansen et al., 2007). These findings show that it is quite possible that the TRKA overexpression and the elevated NGF/TRKA signaling result in membrane fragmentation and cell death. However, the exact mechanism (whether cell death is mediated by autophagy, apoptosis or also via micropinocytosis) is not clear and requires further investigation.

RUNX1, also broadly expressed during early mouse development (more than 80% of the TRKA-positive neurons co-express RUNX1) and, at later stages, more defined and restricted to non-peptidergic TRKA-negative neurons (Chen et al., 2006), was also not effective for the differentiation of sensory neurons with a nociceptive phenotype. The constant lentiviral-induced RUNX1 overexpression appeared to be counterproductive and most of infected cells did not tolerate the artificial overexpression treatment. Although there is no evidence that RUNX1 overexpression is linked to neuronal toxicity or apoptosis as it was described for TRKA activation, nevertheless there is no doubt that a permanent overexpression somehow interferes with cell function, which thereupon could lead to cell death.

In addition to non-physiological issues of a permanent overexpression of distinct neurotrophin receptors or transcription factors, it is also possible that neurogenesis induction of main neuronal subpopulations, such as nociceptors, starts upstream of TRKA or RUNX1 expression and is already set at this developmental stage.

To influence neuronal differentiation already at an even earlier developmental time-point and to drive NCLCs towards a nociceptive lineage, we overexpressed NGN1, a basic helix-loop-helix (bHLH) transcription factor known to induce neurogenesis in mice. Whereas NGN2 seems to trigger neuronal diversification of mainly large diameter mechanoreceptive or proprioceptive neurons, NGN1 appears to mediate the differentiation of small diameter, TRKA-positive nociceptive neurons (Ma et al., 1998, 1999a) In our hands, gene induction experiments showed that a transient NGN1 overexpression is sufficient to induces neurogenesis in stem cell-derived NCLCs: the number of ISL1-positive developing sensory neurons was markedly increased when compared to GFP-infected control cells. However, a temporary NGN1-induction of 3 days was not sufficient to differentiate developing human sensory neurons and to allow them to acquire key properties of primary sensory nociceptors. Either the period of three days was not correlated to the

corresponding *in vivo* NGN1 expression (in mice, from around E9-E9.5 to E13), or another essential key molecule was missing (Ma et al., 1999a; Sommer et al., 1996). As already described in earlier chapters (*1.1.2* and *1.3.2*), mammalian development is characterized by a series of defined stages known as morulation, gastrulation and organogenesis. While in mice developmental stages are defined as Theiler stages (TS 1-28), depending on the number of somites, human development is classified according to specific morphological structures in Carnegie Stages (CS 1-23), describing the first 60 days after fertilization (O'Rahilly, 1979; Theiler, 1989). Accordingly, mouse developmental stage E9 to E13, where NGN1 is expressed, represents most likely human Carnegie Stage 11-16, ranging from approximately 23-42 days post conception (dpc) (Xue et al., 2011). Based on these numbers and classifications it may be assumed that a temporary NGN1 induction of 3 days was too short to induce human primary sensory neurons.

Co-overexpression experiments, first inducing NGN1 expression for 3 days and then continuously RUNX1, should trigger the already increased number of developing sensory neurons to differentiate further into nociceptors. The combinatorial gene induction was thought to recapitulate the *in vivo* situation, where initially sensory nociceptor development is mediated by NGN1 and later during differentiation by RUNX1, regulating maturation of a subpopulation of sensory nociceptors (Chen et al., 2006; Ma et al., 1998). The fact that only a small fraction of cells showed a minimal response to capsaicin, a marker for nociceptive properties, indicated that the combinatorial overexpression of NGN1 and RUNX1, according to our defined conditions, was not sufficient for the generation of many nociceptive neurons. Either the time frame was not reflecting the *in vivo* situation or, again, a crucial molecule, important for nociceptor differentiation, was lacking. Moreover, it is also conceivable that the heavy overexpression of two transcription factors (NGN1 and RUNX1) was too much for the cells, preventing them from further differentiation.

In addition to different time-dependent gene expression programs known to be essential for the development of nociceptive neurons, it is also conceivable that some of the ingredients of the differentiation medium might be responsible for the failure or the success of the generation of pain-sensitive neurons. For the initial experiments (TRKA, RUNX1, NGN1 and NGN1/RUNX1 overexpression), infected NCLCs were cultured in a differentiation medium, already proved to be successful for the differentiation of stem cell-derived mechanoreceptors (containing the growth factors BDNF, GDNF, NGF, NT-3 and retinoic acid) (Schrenk-Siemens et al., 2015a). However, the final nociceptor differentiation protocol contained a differentiation cocktail, including only the growth factors BDNF, GDNF and NGF and no retinoic acid or NT-3 (Wainger et al., 2015).

Retinoic acid, the active metabolite of vitamin A, was shown to be important for embryonic organ development and patterning formation, but also for maintenance of fertility, vision or the avoidance of neurodegenerative diseases in adult individuals (reviewed by Niederreither and Dollé, 2008). Although vitamin A and retinoic acid play a crucial role already at very early developmental stages,

and seem to regulate survival and proliferation of neuronal precursors in cultured NCCs, it was also demonstrated that the concentration of retinoic acid, to which teratocarcinoma cells are exposed to, determine the developing cell type (Edwards and McBurney, 1983; Henion and Weston, 1994). Additionally, studies with isolated sympathetic neurons of newborn rats demonstrated that (i) retinoic acid treatment diminishes the *TrkA* mRNA levels and upregulates the expression of *TrkB* mRNA, and (ii) retinoic acid in combination with the bone morphogenetic protein-2 (BMP2) enhanced the expression of *TrkC* and the receptivity to NT-3, mainly activating TRKC receptors (Kobayashi et al., 1994, 1998).

Not only in embryonic development of rodents, but also of lower vertebrates such as *Xenopus laevis*, retinoic acid is involved in neurogenesis and various genes, known to positively regulate neuronal differentiation, are upregulated in embryos treated with retinoic acid. One of these retinoic acid-induced genes is X-ngnr-1, the *Xenopus laevis* homolog of the bHLH transcription factors, most closely related to the mammalian NGN2 (Franco et al., 1999; Nieber et al., 2009), which mediates neuronal diversification of mainly large diameter mechanoreceptive or proprioceptive neurons in mammals.

Based on these findings, it cannot be ruled out that a combinatorial effect of a shortened overexpression of NGN1 (of only 3 days) and the addition of wrong supplementary ingredients hindered NCLCs to adopt a nociceptive phenotype.

6.4 Mechanotransduction of nociceptors and the role of PIEZO2

Besides its physiological role as an internal warning signal, required for survival and avoidance of tissue damage, chronic or pathophysiological pain is one of the most common epiphenomena of many diseases that restrict the quality of life tremendously. Under inflammatory conditions (for example, tissue injury caused by mechanical forces, chemicals or thermal stimuli), inflammatory mediators are released both by non-neuronal cells in close proximity to the injury (such as fibroblasts, endothelial cells, keratinocytes or immune cells) and by nociceptors. Those signaling molecules, known as the “inflammatory soup”, including neurotransmitters, protons, lipids, growths factors cytokines, prostaglandins or neuropeptides such as bradykinin are responsible for the sensitization of neuronal afferents (reviewed by Gangadharan and Kuner, 2013; Gold and Gebhart, 2010; Hucho and Levine, 2007; Julius and Basbaum, 2001). Peripheral sensitization is characterized by enhanced responsiveness of sensory nerve fibers combined with diminished action potential thresholds of sensitized nociceptors, and is known to be mediated by distinct cell membrane transduction proteins that further regulate downstream proteins.

While thermal-induced hyperalgesia (an already noxious thermal stimulus evokes even more intensive pain) was already associated with sensitization of TRPV1, the molecular components involved in mechanical-induced hyperalgesia and peripheral sensitization are still not completely elucidated (Caterina et al., 2000; Davis et al., 2000). TRPV1 thermal sensitization can either be directly mediated by inflammatory molecules or indirectly, for example via G-protein coupled receptors (GPCR) that recruit downstream proteins such as protein kinase A (PKA) or protein kinase C (PKC), phosphorylating TRPV1 residues to sensitize the channel (Rathee et al., 2002; Tominaga et al., 2001).

The neurotrophin NGF is upregulated under inflammatory conditions and released from different cells types, for example Schwann cells or tissue that is innervated by nociceptive fibers. Early studies could demonstrate that NGF administration to the hind paw resulted in prolonged hyperalgesia of newborn and adult rats, and this NGF-induced hypersensitivity was mediated by enhanced levels of TRPV1 channels (Ji et al., 2002; Lewin et al., 1993; Zhang et al., 2005).

In addition to its involvement in regulating TRPV1 thermal-induced hyperalgesia, it was also demonstrated that mechanically-induced currents of sensory neurons can be modulated by NGF (Castro et al., 2006; Lechner et al., 2009). While Castro *et al.* revealed enhanced NGF-mediated current amplitudes in response to mechanical stimulation, Lechner and colleagues showed that NGF-treatment raised the number of sensory neurons, eliciting IA mechanically-activated currents. Nevertheless, the exact molecular components responsible for mechanical hyperalgesia have not yet been clarified.

Recent findings in rodents proposed a role for PIEZO2 as a main transducer of mechanical stimuli in mechanoreceptors as well as proprioceptors (Coste et al., 2010; Ranade et al., 2014b; Schrenk-Siemens et al., 2015a; Woo et al., 2015) and we could demonstrate that PIEZO2 is also required for mechanotransduction in human stem cell-derived mechanoreceptors (Schrenk-Siemens et al., 2015a). However, it was not clear whether PIEZO2 is also involved in mediating noxious mechanical stimuli.

A conditional PIEZO2-KO in mouse DRG and Merkel cells (with a 90% reduction of the overall *Piezo2* transcript) resulted in a specific loss of only rapidly-adapting mechanically-activated currents, whereas intermediately-adapting or slowly-adapting currents were not significantly altered (Ranade et al., 2014b). To assess whether the remaining *Piezo2* transcript was sufficient to mediate intermediately and slowly-adapting currents, or if a yet-unknown ion channel is responsible for mediating noxious mechanical stimuli, we compared human stem cell-derived PIEZO2-WT nociceptors with PIEZO2-KO nociceptors. Mechanical stimulations confirmed that PIEZO2 was also required for mechanotransduction of stem cell-derived nociceptors and rapidly-adapting, mechanically-activated currents (at least those conventionally recorded when using a nanomotor-driven stimulus probe) appeared to be absent in PIEZO2-KO nociceptors. Due to the

fact that differentiated cells were cultured in a differentiation medium containing NGF (known to be involved in inflammation and sensitization), it needs to be clarified whether PIEZO2 is involved in mechanotransduction of nociceptors only in an inflammatory state (when NGF is upregulated), or also under physiological basal conditions.

An indication that PIEZO2 could potentially play a role in mechanical hyperalgesia emerged by a study of Dubin and colleagues, demonstrating enhanced PIEZO2 function in response to bradykinin, an algesiogenic substance known to trigger intensive pain phenotypes. Both transfected HEK cells (as a heterologous expression system) and native sensory neurons showed increased mechanically-activated current amplitudes and prolonged inactivation kinetics after bradykinin administration (Dubin et al., 2012b). The same results were obtained when treating cells with PKC or PKA agonists, reflecting (at least to some extent) inflammation-induced mechanical hyperalgesia mechanisms (Dubin et al., 2012b).

PIEZO2 is not only expressed in LTMRs, but also in about 60% of hESC-derived TRKA-positive nociceptors, and in more than 20% of mouse TRPV1-expressing peptidergic nociceptors (Coste et al., 2010). Capsaicin-induced TRPV1 activation significantly reduced mechanically-activated currents in cultured mouse DRG neurons as well as in TRPV1/PIEZO2 co-transfected HEK cells, clarifying the pain-relieving response of capsaicin treatment (Borbiro et al., 2015). Recent findings proposed a mechanism of mechanical-induced allodynia, in which cyclic AMP-activated EPAC1 protein increased mechanically-activated currents both in DRG neurons and in EPAC1/PIEZO2 transfected HEK cells (Eijkelkamp et al., 2013). Downstream EPAC1-PIEZO2 interaction was shown to be indirectly regulated by RAP1, a GTPase responsible for triggering signaling pathways, including PKC, already described by Dubin and colleagues for its involvement in PIEZO2-mediated mechanical hyperalgesia (Breckler et al., 2011; Dubin et al., 2012b).

In line with these findings, sensory tests performed with patients (bearing inactive *PIEZO2* variants) and control individuals showed significant differences, with reduced sensitivity to innocuous light touch and vibrations in the patients, whereas mechanically-induced pain sensation was not altered between patients and control group (Chesler et al., 2016), indicating that under non-inflammatory, basal conditions, a not-yet discovered transduction channel is involved in mediating noxious mechanical stimuli.

In order to elucidate whether PIEZO2 is involved in mechanotransduction of nociceptors only under inflammatory or also at basal conditions, NGF-deprived differentiated nociceptors need to be analyzed. Due to the fact that, during early neurogenesis, NGF/TRKA signaling is required for proliferation and survival of developing sensory neurons (Crowley et al., 1994; Silos-Santiago et al., 1995b), NGF can only be withdrawn during the last part of differentiation to ensure proper nociceptor development and the analysis of non-sensitized neurons.

6.5 Accessory proteins of PIEZO2 and targeting strategies

The non-selective PIEZO cation-channels have recently been identified as huge, evolutionary conserved, transmembrane proteins and have been described for their involvement in mediating mechanical sensation in various species (Coste et al., 2010; Faucherre et al., 2013; Kamajaya et al., 2014; Kim et al., 2012; Prole and Taylor, 2013).

Although recent publications demonstrated a link between several PIEZO protein mutations and human hereditary diseases as distal arthrogryposis or Marden-Walker or Gordon syndrome (Alisch et al., 2017; Chesler et al., 2016; Coste et al., 2013; McMillin et al., 2014), PIEZO protein topology and functional mechanisms are still not completely uncovered.

Most large transmembrane ion channels are directly or indirectly coupled to interaction partners to assemble as functional, multimeric complexes (as it is known for example from VGSC, where a large α-subunit, composed of sequence repetitive domains, is associated with a least one β-subunit to enable proper functioning). However, initial studies for mouse PIEZO1 revealed the formation of homo-oligomers with no evidence of accessory proteins (Coste et al., 2012).

And although biochemical studies of mouse PIEZO2 identified numerous possible binding partners and activity modulators (as pericentrin), not much is known about human PIEZO2 channel assembly or modulating accessory proteins (Narayanan et al., 2016).

A previous publication by Coste *et al.* already demonstrated a successful targeting of mouse PIEZO1 with either a N-terminal GFP-tag or a C-terminal GST-tag, resulting in mechanically active transiently transfected HEK cells. In this approach, they made use of the tagged mouse fusion protein to verify that PIEZO1 assembles as a homotetramer that forms a 1.2 million Da ion channel complex (Coste et al., 2012).

Furthermore, structural analysis proposed a fundamental role of the C-terminal region of PIEZO1 for channel gating and pore properties. While Coste and colleagues with a PIEZO1 chimera (between mouse PIEZO1 and *Drosophila melanogaster* dPiezo) showed that the C-terminal part of PIEZO1 is required for susceptibility to the pore channel blocker ruthenium red as well as for channel conductance, Ge *et al.* described a C-terminal extracellular domain (CED) that is highly conserved across species and involved in gating properties and most likely associated with the pore (Coste et al., 2015; Ge et al., 2015b).

Given the importance of the C-terminal part of mouse PIEZO1 for channel gating, and given the assumed topological similarity between PIEZO1 and PIEZO2, we generated a hESC line where we directly introduced the 3xFlag-His-tag at the N-terminus of PIEZO2.

Although gene targeting was successful and 3xFlag-His-tagged hESCs had the continuing ability to differentiate into mechanoreceptors (as verified by immunostainings for markers specific for mechanoreceptive neurons), functional analysis with mechanical stimulations revealed that the tagged-PIEZO2 protein was not functional, as cells were not able to respond to membrane indentation. Given that the C-terminal part of mouse PIEZO1 was shown to be important for channel gating properties (and thus not a good site for gene targeting) and that the mouse PIEZO1 N-terminus was already used in previous targeting approaches (resulting in functional tagged-PIEZO1 channels) for our study, using human PIEZO2, the N-terminus was not successful for introducing the 3xFlag-His-tag.

Retrospectively, the initial (and so far, unproven) assumption that PIEZO1 and PIEZO2 adopt a similar N-terminal topology might be wrong and therefore the targeting resulted in a misfolded, non-functional tagged PIEZO2 protein.

Based on more recent findings demonstrating that the insertion of the green fluorescent protein at the C-terminus of mouse PIEZO2 was feasible and did not influence PIEZO2 channel functioning, it would be nonetheless interesting to repeat the hESC targeting by introducing the 3xFlag-His-tag at the C-terminus of human PIEZO2 (Woo et al., 2014).

To test whether PIEZO2 can be successfully modulated at its C-terminus without losing proper function, it would be important to begin with an expression vector containing the human PIEZO2 cDNA with a 3xFlag-His-tag at the C-terminus, that can be used for transfecting a heterologous expression system. With this control system, not only purification conditions but also functionality can be tested and therefore would prevent us from starting laborious targeting experiments with a non-functional protein.

As already mentioned, working with a defined neuronal subtype such as stem cell-derived mechanoreceptors is beneficial compared to a more heterogeneous and complex mouse model system. In the case of mass spectrometry analysis, for example, performed to identify possible interaction partners, a heterogeneous system leads to many hits with probably more background and more false-positive candidates. Therefore, it is of great importance to describe and define features how to interpret candidates, emerged by mass spectrometry.

Cytoskeleton elements have been described as modulators required for proper mechanotransduction, and given the role of PIEZO2 in mechanosensory transduction, there is reason to suspect that cytoskeleton molecules are part of the PIEZO2 interactome (Cho et al., 2002; Drew et al., 2002; Eijkelkamp et al., 2013). Although it has been demonstrated that no other ion channel components are associated with mouse PIEZO1 subunits, this has not been shown for human PIEZO2, and it remains to be seen whether human PIEZO2 is associated with other ion channels, important for regulating PIEZO2-mediated mechanotransduction (Coste et al., 2012).

Possible accessory proteins of PIEZO2, identified by mass spectrometry, need to be verified in a heterologous expression system, testing PIEZO2-mediated mechanosensitivity in presence or absence of the identified interaction partner.

Based on the fact that we successfully established a differentiation protocol for the generation of stem cell-derived nociceptors, it would be interesting to compare human PIEZO2 interaction partners from derived mechanoreceptors and derived nociceptors to elucidate whether accessory proteins and mechanisms of PIEZO2-mediated noxious and innocuous mechanotransduction share similarities or are distinct from each other.

7. Conclusion

In this doctoral thesis, a differentiation protocol for the generation of functional human stem cell-derived nociceptors was established and differentiated neurons were characterized, in order to provide more detailed knowledge on how pain-sensitive neurons develop and evolve their characteristic phenotypes. Functional similarity between hESC-derived nociceptors and their *in vivo* correspondent cell types was confirmed by comparison of marker gene profiles, revealed to be similar in both cases. A comparative study between human tissue and mouse DRG neurons, an animal model broadly used for basic pain research, demonstrated molecular differences already at cellular level that need to be taken into account for the development of new pain-relieving drugs.

Furthermore, functional analysis of PIEZO2, recently identified as a main transducer of innocuous mechanical stimuli in mechanoreceptors and proprioceptors, revealed that PIEZO2 is also required for mechanotransduction in stem cell-derived nociceptors, as mechanically-induced currents were absent in PIEZO2-KO nociceptors.

The main outcome of this project was the creation and adjustment of a differentiation protocol of human nociceptors, enabling us to finally provide a model system to study human pain and pain transduction *in vitro*. This will also allow the identification of differences and similarities between human and mouse nociceptors, joining forces to other ongoing studies to overcome challenges in translational pain research.

8. References

Ahmad, S., Dahllund, L., Eriksson, A.B., Hellgren, D., Karlsson, U., Lund, P.-E., Meijer, I.A., Meury, L., Mills, T., Moody, A., et al. (2007). A stop codon mutation in SCN9A causes lack of pain sensation. Hum. Mol. Genet. *16*, 2114–2121.

Alisch, F., Weichert, A., Kalache, K., Paradiso, V., Longardt, A.C., Dame, C., Hoffmann, K., and Horn, D. (2017). Familial Gordon syndrome associated with a PIEZO2 mutation. Am. J. Med. Genet. A. *173*, 254–259.

Amaya, F., Decosterd, I., Samad, T.A., Plumpton, C., Tate, S., Mannion, R.J., Costigan, M., and Woolf, C.J. (2000). Diversity of Expression of the Sensory Neuron-Specific TTX-Resistant Voltage-Gated Sodium Ion Channels SNS and SNS2. Mol. Cell. Neurosci. *15*, 331–342.

Amit, M., Carpenter, M.K., Inokuma, M.S., Chiu, C.-P., Harris, C.P., Waknitz, M.A., Itskovitz-Eldor, J., and Thomson, J.A. (2000). Clonally Derived Human Embryonic Stem Cell Lines Maintain Pluripotency and Proliferative Potential for Prolonged Periods of Culture. Dev. Biol. *227*, 271–278.

Anderson, D.J. (1999). Lineages and transcription factors in the specification of vertebrate primary sensory neurons. Curr. Opin. Neurobiol. *9*, 517–524.

Anderson, P.A.V., and Greenberg, R.M. (2001). Phylogeny of ion channels: clues to structure and function. Comp. Biochem. Physiol. B Biochem. Mol. Biol. *129*, 17–28.

Árnadóttir, J., and Chalfie, M. (2010). Eukaryotic Mechanosensitive Channels. Annu. Rev. Biophys. *39*, 111–137.

Averill, S., McMahon, S.B., Clary, D.O., Reichardt, L.F., and Priestley, J.V. (1995). Immunocytochemical Localization of trkA Receptors in Chemically Identified Subgroups of Adult Rat Sensory Neurons. Eur. J. Neurosci. *7*, 1484–1494.

Bagal, S.K., Chapman, M.L., Marron, B.E., Prime, R., Storer, R.I., and Swain, N.A. (2014). Recent progress in sodium channel modulators for pain. Bioorg. Med. Chem. Lett. *24*, 3690–3699.

Basbaum, A.I., Bautista, D.M., Scherrer, G., and Julius, D. (2009). Cellular and Molecular Mechanisms of Pain. Cell *139*, 267–284.

Basbaum, A.I. and Jessell, T. (2000). Principles of Neuroscience E.R. Kandel, J. Schwartz, T. Jessel (Appleton and Lange, New York).

Bautista, D.M., Jordt, S.-E., Nikai, T., Tsuruda, P.R., Read, A.J., Poblete, J., Yamoah, E.N., Basbaum, A.I., and Julius, D. (2006). TRPA1 Mediates the Inflammatory Actions of Environmental Irritants and Proalgesic Agents. Cell *124*, 1269–1282.

Bear et al., Neuroscience Exploring the Brain Third Edition (2006) chapter 12.

Becker, A.J., McCULLOCH, E.A., and Till, J.E. (1963). Cytological Demonstration of the Clonal Nature of Spleen Colonies Derived from Transplanted Mouse Marrow Cells. Nature *197*, 452–454.

Bednarz, J., Schrenck, A.R.-V., and Engelmann, K. (1998). Different Characteristics of Endothelial Cells from Central and Peripheral Human Cornea in Primary Culture and after Subculture. In Vitro Cell. Dev. Biol. Anim. *34*, 149–153.

Beltrami, A.P., Barlucchi, L., Torella, D., Baker, M., Limana, F., Chimenti, S., Kasahara, H., Rota, M., Musso, E., Urbanek, K., et al. (2003). Adult Cardiac Stem Cells Are Multipotent and Support Myocardial Regeneration. Cell *114*, 763–776.

Beneski, D.A., and Catterall, W.A. (1980). Covalent labeling of protein components of the sodium channel with a photoactivable derivative of scorpion toxin. Proc. Natl. Acad. Sci. *77*, 639–643.

Bennett, D.L.H., Michael, G.J., Ramachandran, N., Munson, J.B., Averill, S., Yan, Q., McMahon, S.B., and Priestley, J.V. (1998). A Distinct Subgroup of Small DRG Cells Express GDNF Receptor Components and GDNF Is Protective for These Neurons after Nerve Injury. J. Neurosci. *18*, 3059–3072.

Blanchard, J.W., Eade, K.T., Szűcs, A., Sardo, V.L., Tsunemoto, R.K., Williams, D., Sanna, P.P., and and Baldwin, K.K. (2015a). Selective conversion of fibroblasts into peripheral sensory neurons. Nat Neurosci *18*, 25–35.

Borbiro, I., Badheka, D., and Rohacs, T. (2015). Activation of TRPV1 channels inhibits mechanosensitive Piezo channel activity by depleting membrane phosphoinositides. Sci. Signal. *8*, ra15.

Bourane, S., Garces, A., Venteo, S., Pattyn, A., Hubert, T., Fichard, A., Puech, S., Boukhaddaoui, H., Baudet, C., Takahashi, S., et al. (2009). Low-Threshold Mechanoreceptor Subtypes Selectively Express MafA and Are Specified by Ret Signaling. Neuron *64*, 857–870.

Braz, J.M., Nassar, M.A., Wood, J.N., and Basbaum, A.I. (2005). Parallel "Pain" Pathways Arise from Subpopulations of Primary Afferent Nociceptor. Neuron *47*, 787–793.

Breckler, M., Berthouze, M., Laurent, A.-C., Crozatier, B., Morel, E., and Lezoualc'h, F. (2011). Rap-linked cAMP signaling Epac proteins: Compartmentation, functioning and disease implications. Cell. Signal. *23*, 1257–1266.

Bron, R., Wood, R.J., Brock, J.A., and Ivanusic, J.J. (2014). Piezo2 expression in corneal afferent neurons. J. Comp. Neurol. *522*, 2967–2979.

Bronner-Fraser, M., Wolf, J.J., and Murray, B.A. (1992). Effects of antibodies against N-cadherin and N-CAM on the cranial neural crest and neural tube. Dev. Biol. *153*, 291–301.

Burma, N.E., Leduc-Pessah, H., Fan, C.Y., and and Trang, T. (2017). Animal models of chronic pain: Advances and challenges for clinical translation. J Neurosci Res 95 1242–1256.

Burstyn-Cohen, T., Stanleigh, J., Sela-Donenfeld, D., and Kalcheim, C. (2004). Canonical Wnt activity regulates trunk neural crest delamination linking BMP/noggin signaling with G1/S transition. Development *131*, 5327–5339.

Cahalan, S.M., Lukacs, V., Ranade, S.S., Chien, S., Bandell, M., and Patapoutian, A. (2015). Piezo1 links mechanical forces to red blood cell volume. ELife *4*, e07370.

Cain, D.M., Khasabov, S.G., and Simone, D.A. (2001). Response Properties of Mechanoreceptors and Nociceptors in Mouse Glabrous Skin: An In Vivo Study. J. Neurophysiol. *85*, 1561–1574.

Carlson, M.W., Alt-Holland, A., Egles, C., and Garlick, J.A. (2008). Three-Dimensional Tissue Models of Normal and Diseased Skin. In Current Protocols in Cell Biology, J.S. Bonifacino, M. Dasso, J.B. Harford, J. Lippincott-Schwartz, and K.M. Yamada, eds. (Hoboken, NJ, USA: John Wiley & Sons, Inc.), p.

Carnevale, V., and Rohacs, T. (2016). TRPV1: A Target for Rational Drug Design. Pharmaceuticals *9*, 52.

Castro, A.D., Drew, L.J., Wood, J.N., and Cesare, P. (2006). Modulation of sensory neuron mechanotransduction by PKC- and nerve growth factor-dependent pathways. Proc. Natl. Acad. Sci. U. S. A. *103*, 4699–4704.

Caterina, M.J., Schumacher, M.A., Tominaga, M., Rosen, T.A., Levine, J.D., and Julius, D. (1997). The capsaicin receptor: a heat-activated ion channel in the pain pathway. Nature *389*, 816–824.

Caterina, M.J., Rosen, T.A., Tominaga, M., Brake, A.J., and Julius, D. (1999). A capsaicin-receptor homologue with a high threshold for noxious heat. Nature *398*, 436–441.

Caterina, M.J., Leffler, A., Malmberg, A.B., Martin, W.J., Trafton, J., Petersen-Zeitz, K.R., Koltzenburg, M., Basbaum, A.I., and Julius, D. (2000). Impaired Nociception and Pain Sensation in Mice Lacking the Capsaicin Receptor. Science *288*, 306–313.

Cathcart, C.J., Johnston, S.A., Reynolds, L.R., Al-Nadaf, S., and Budsberg, S.C. (2012). Efficacy of ABT-116, an antagonist of transient receptor potential vanilloid type 1, in providing analgesia for dogs with chemically induced synovitis. Am. J. Vet. Res.

Catterall, W.A. (2000). From Ionic Currents to Molecular Mechanisms: The Structure and Function of Voltage-Gated Sodium Channels. Neuron *26*, 13–25.

Cavanaugh, D.J., Lee, H., Lo, L., Shields, S.D., Zylka, M.J., Basbaum, A.I., and Anderson, D.J. (2009). Distinct subsets of unmyelinated primary sensory fibers mediate behavioral responses to noxious thermal and mechanical stimuli. Proc. Natl. Acad. Sci. *106*, 9075–9080.

Chambers, S.M., Qi, Y., Mica, Y., Lee, G., Zhang, X.-J., Niu, L., Bilsland, J., Cao, L., Stevens, E., and Whiting, P. (2012). Combined small-molecule inhibition accelerates developmental timing and converts human pluripotent stem cells into nociceptors. Nat Biotechnol *30*, 715–720.

Chen, C.-L., Broom, D.C., Liu, Y., Nooij, J.C. de, Li, Z., Cen, C., Samad, O.A., Jessell, T.M., Woolf, C.J., and Ma, Q. (2006). Runx1 Determines Nociceptive Sensory Neuron Phenotype and Is Required for Thermal and Neuropathic Pain. Neuron *49*, 365–377.

Chesler, A.T., Szczot, M., Bharucha-Goebel, D., Čeko, M., Donkervoort, S., Laubacher, C., Hayes, L.H., Alter, K., Zampieri, C., Stanley, C., et al. (2016). The Role of PIEZO2 in Human Mechanosensation. N. Engl. J. Med. *375*, 1355–1364.

Cho, H., Shin, J., Shin, C.Y., Lee, S.-Y., and Oh, U. (2002). Mechanosensitive Ion Channels in Cultured Sensory Neurons of Neonatal Rats. J. Neurosci. *22*, 1238–1247.

Corey, D.P., and Hudspeth, A.J. (1979). Response latency of vertebrate hair cells. Biophys. J. *26*, 499–506.

Cosens, D.J., and Manning, A. (1969). Abnormal electroretinogram from a Drosophila mutant. Nature *224*, 285–287.

Coste, B., Mathur, J., Schmidt, M., Earley, T.J., Ranade, S., Petrus, M.J., Dubin, A.E., and Patapoutian, A. (2010). Piezo1 and Piezo2 are essential components of distinct mechanically-activated cation channels. Science *330*, 55–60.

Coste, B., Xiao, B., Santos, J.S., Syeda, R., Grandl, J., Spencer, K.S., Kim, S.E., Schmidt, M., Mathur, J., Dubin, A.E., et al. (2012). Piezo proteins are pore-forming subunits of mechanically activated channels. Nature *483*, 176–181.

Coste, B., Houge, G., Murray, M.F., Stitziel, N., Bandell, M., Giovanni, M.A., Philippakis, A., Hoischen, A., Riemer, G., Steen, U., et al. (2013). Gain-of-function mutations in the mechanically activated ion channel PIEZO2 cause a subtype of Distal Arthrogryposis. Proc. Natl. Acad. Sci. *110*, 4667–4672.

Coste, B., Murthy, S.E., Mathur, J., Schmidt, M., Mechioukhi, Y., Delmas, P., and Patapoutian, A. (2015). Piezo1 ion channel pore properties are dictated by C-terminal region. Nat. Commun. *6*.

Crowley, C., Spencer, S.D., Nishimura, M.C., Chen, K.S., Pitts-Meek, S., Armaninl, M.P., Ling, L.H., McMahon, S.B., Shelton, D.L., Levinson, A.D., et al. (1994). Mice lacking nerve growth factor display perinatal loss of sensory and sympathetic neurons yet develop basal forebrain cholinergic neurons. Cell *76*, 1001–1011.

Cummins, T.R., Dib-Hajj, S.D., and Waxman, S.G. (2004). Electrophysiological Properties of Mutant $Na_v1.7$ Sodium Channels in a Painful Inherited Neuropathy. J. Neurosci. *24*, 8232–8236.

Cummins, T.R., Sheets, P.L., and Waxman, S.G. (2007). The roles of sodium channels in nociception: Implications for mechanisms of pain. PAIN *131*, 243–257.

Dai, S., Hall, D.D., and Hell, J.W. (2009). Supramolecular Assemblies and Localized Regulation of Voltage-Gated Ion Channels. Physiol. Rev. *89*, 411–452.

Davidson, S., Copits, B.A., Zhang, J., Page, G., Ghetti, A., and Gereau IV, R.W. (2014). Human sensory neurons: Membrane properties and sensitization by inflammatory mediators. PAIN® *155*, 1861–1870.

Davis, J.B., Gray, J., Gunthorpe, M.J., Hatcher, J.P., Davey, P.T., Overend, P., Harries, M.H., Latcham, J., Clapham, C., Atkinson, K., et al. (2000). Vanilloid receptor-1 is essential for inflammatory thermal hyperalgesia. Nature *405*, 183–187.

Davis, M.J., Donovitz, J.A., and Hood, J.D. (1992). Stretch-activated single-channel and whole cell currents in vascular smooth muscle cells. Am. J. Physiol. *262*, C1083-1088.

Dhaka, A., Viswanath, V., and Patapoutian, A. (2006). Trp Ion Channels and Temperature Sensation. Annu. Rev. Neurosci. *29*, 135–161.

Dib-Hajj, S., Black, J.A., Cummins, T.R., and Waxman, S.G. (2002). NaN/Nav1.9: a sodium channel with unique properties. Trends Neurosci. *25*, 253–259.

Drew, L.J., Wood, J.N., and Cesare, P. (2002). Distinct mechanosensitive properties of capsaicin-sensitive and-insensitive sensory neurons. J Neurosci *22*.

Dubin, A., Schmidt, M., Mathur, J., Petrus, M., Xiao, B., Coste, B., and and Patapoutian, A. (2012). Inflammatory Signals Enhance Piezo2-Mediated Mechanosensitive Currents. Cell Rep *2*, 511–517.

Dykes, I.M., Lanier, J., Eng, S.R., and Turner, E.E. (2010). Brn3a regulates neuronal subtype specification in the trigeminal ganglion by promoting Runx expression during sensory differentiation. Neural Develop. *5*, 3.

Dykes, I.M., Tempest, L., Lee, S.-I., and Turner, E.E. (2011). Brn3a and Islet1 Act Epistatically to Regulate the Gene Expression Program of Sensory Differentiation. J. Neurosci. *31*, 9789–9799.

Edwards, M.K.S., and McBurney, M.W. (1983). The concentration of retinoic acid determines the differentiated cell types formed by a teratocarcinoma cell line. Dev. Biol. *98*, 187–191.

Egawa, N., Kitaoka, S., Tsukita, K., Naitoh, M., Takahashi, K., Yamamoto, T., Adachi, F., Kondo, T., Okita, K., Asaka, I., et al. (2012). Drug Screening for ALS Using Patient-Specific Induced Pluripotent Stem Cells. Sci. Transl. Med. *4*, 145ra104-145ra104.

Eijkelkamp, N., Linley, J.E., Torres, J.M., Bee, L., Dickenson, A.H., Gringhuis, M., Minett, M.S., Hong, G.S., Lee, E., Oh, U., et al. (2013). A role for Piezo2 in EPAC1-dependent mechanical allodynia. Nat. Commun. *4*, ncomms2673.

Eng, S.R., Gratwick, K., Rhee, J.M., Fedtsova, N., Gan, L., and Turner, E.E. (2001). Defects in Sensory Axon Growth Precede Neuronal Death in Brn3a-Deficient Mice. J. Neurosci. *21*, 541–549.

Eng, S.R., Lanier, J., Fedtsova, N., and Turner, E.E. (2004). Coordinated regulation of gene expression by Brn3a in developing sensory ganglia. Development *131*, 3859–3870.

Eng, S.R., Dykes, I.M., Lanier, J., Fedtsova, N., and Turner, E.E. (2007). POU-domain factor Brn3a regulates both distinct and common programs of gene expression in the spinal and trigeminal sensory ganglia. Neural Develop. *2*, 3.

Ernsberger, U. (2008). The role of GDNF family ligand signalling in the differentiation of sympathetic and dorsal root ganglion neurons. Cell Tissue Res. *333*, 353–371.

Ernsberger, U. (2009). Role of neurotrophin signalling in the differentiation of neurons from dorsal root ganglia and sympathetic ganglia. Cell Tissue Res. *336*, 349–384.

Ernstrom, G.G., and Chalfie, and M. (2002). Genetics of Sensory Mechanotransduction. Annu. Rev. Genet. *36*, 411–453.

Evans, M.J., and Kaufman, M.H. (1981). Establishment in culture of pluripotential cells from mouse embryos. Nature *292*, 154–156.

Faber, C.G., Lauria, G., Merkies, I.S.J., Cheng, X., Han, C., Ahn, H.-S., Persson, A.-K., Hoeijmakers, J.G.J., Gerrits, M.M., Pierro, T., et al. (2012). Gain-of-function Nav1.8 mutations in painful neuropathy. Proc. Natl. Acad. Sci. *109*, 19444–19449.

Fariñas, I., Wilkinson, G.A., Backus, C., Reichardt, L.F., and Patapoutian, A. (1998). Characterization of Neurotrophin and Trk Receptor Functions in Developing Sensory Ganglia: Direct NT-3 Activation of TrkB Neurons In Vivo. Neuron *21*, 325–334.

Faris, R.A., Konkin, T., and Halpert, G. (2001). Liver Stem Cells: A Potential Source of Hepatocytes for the Treatment of Human Liver Disease. Artif. Organs *25*, 513–521.

Faucherre, A., Nargeot, J., Mangoni, M.E., and Jopling, C. (2013). piezo2b Regulates Vertebrate Light Touch Response. J. Neurosci. *33*, 17089–17094.

Fertleman, C.R., Baker, M.D., Parker, K.A., Moffatt, S., Elmslie, F.V., Abrahamsen, B., Ostman, J., Klugbauer, N., Wood, J.N., Gardiner, R.M., et al. (2006). SCN9A Mutations in Paroxysmal Extreme Pain Disorder: Allelic Variants Underlie Distinct Channel Defects and Phenotypes. Neuron *52*, 767–774.

Florez-Paz, D., Bali, K.K., Kuner, R., and Gomis, A. (2016). A critical role for Piezo2 channels in the mechanotransduction of mouse proprioceptive neurons. Sci. Rep. *6*.

Foerster, O. (1933). THE DERMATOMES IN MAN. Brain *56*, 1–39.

Franco, P.G., Paganelli, A.R., Lopez, S.L., and Carrasco, A.E. (1999). Functional association of retinoic acid and hedgehog signaling in Xenopus primary neurogenesis. Development *126*, 4257–4265.

Frank, E., and Sanes, J.R. (1991). Lineage of neurons and glia in chick dorsal root ganglia: analysis in vivo with a recombinant retrovirus. Development *111*, 895–908.

Gangadharan, V., and Kuner, R. (2013). Pain hypersensitivity mechanisms at a glance. Dis. Model. Mech. *6*, 889–895.

García-Castro, M.I., Marcelle, C., and Bronner-Fraser, M. (2002). Ectodermal Wnt Function as a Neural Crest Inducer. Science *297*, 848–851.

Gaudet, R. (2008). TRP channels entering the structural era. J. Physiol. *586*, 3565–3575.

Gavva, N.R., Bannon, A.W., Hovland, D.N., Lehto, S.G., Klionsky, L., Surapaneni, S., Immke, D.C., Henley, C., Arik, L., Bak, A., et al. (2007). Repeated administration of vanilloid receptor TRPV1 antagonists attenuates hyperthermia elicited by TRPV1 blockade. J. Pharmacol. Exp. Ther. *323*, 128–137.

Ge, J., Li, W., Zhao, Q., Li, N., Chen, M., Zhi, P., Li, R., Gao, N., Xiao, B., and and Yang, M. (2015a). Architecture of the mammalian mechanosensitive Piezo1 channel. Nature *527*, 64–69.

Gold, M.S., and Gebhart, G.F. (2010). Nociceptor sensitization in pain pathogenesis. Nat. Med. *16*, 1248.

Golden, J.P., Hoshi, M., Nassar, M.A., Enomoto, H., Wood, J.N., Milbrandt, J., Gereau, R.W., Johnson, E.M., and Jain, S. (2010). RET Signaling Is Required for Survival and Normal Function of Nonpeptidergic Nociceptors. J. Neurosci. *30*, 3983–3994.

Goldin, A.L. (2002). Evolution of voltage-gated Na+ channels. J. Exp. Biol. *205*, 575–584.

Goldin, A.L., Barchi, R.L., Caldwell, J.H., Hofmann, F., Howe, J.R., Hunter, J.C., Kallen, R.G., Mandel, G., Meisler, M.H., Netter, Y.B., et al. (2000). Nomenclature of Voltage-Gated Sodium Channels. Neuron *28*, 365–368.

Güler, A.D., Lee, H., Iida, T., Shimizu, I., Tominaga, M., and Caterina, M. (2002). Heat-Evoked Activation of the Ion Channel, TRPV4. J. Neurosci. *22*, 6408–6414.

Hagbarth, K.-E. (2002). Microelectrode recordings from human peripheral nerves (microneurography). Muscle Nerve *25*, S28–S35.

Han, C., Huang, J., and Waxman, S.G. (2016). Sodium channel Nav1.8: Emerging links to human disease. Neurology *86*, 473–483.

Handwerker, H.O., Kilo, S., and Reeh, P.W. (1991). Unresponsive afferent nerve fibres in the sural nerve of the rat. J. Physiol. *435*, 229–242.

Hansen, K., Wagner, B., Hamel, W., Schweizer, M., Haag, F., Westphal, M., and Lamszus, K. (2007). Autophagic cell death induced by TrkA receptor activation in human glioblastoma cells. J. Neurochem. *103*, 259–275.

Hari, L., Brault, V., Kléber, M., Lee, H.-Y., Ille, F., Leimeroth, R., Paratore, C., Suter, U., Kemler, R., and Sommer, L. (2002). Lineage-specific requirements of β-catenin in neural crest development. J Cell Biol *159*, 867–880.

Hartshorne, R.P., and Catterall, W.A. (1981). Purification of the saxitoxin receptor of the sodium channel from rat brain. Proc. Natl. Acad. Sci. *78*, 4620–4624.

Hartshorne, R.P., Messner, D.J., Coppersmith, J.C., and Catterall, W.A. (1982). The saxitoxin receptor of the sodium channel from rat brain. Evidence for two nonidentical beta subunits. J. Biol. Chem. *257*, 13888–13891.

Henion, P.D., and Weston, J.A. (1994). Retinoic Acid Selectively Promotes the Survival and Proliferation of Neurogenic Precursors in Cultured Neural Crest Cell Populations. Dev. Biol. *161*, 243–250.

Hill, R. (2000). NK1 (substance P) receptor antagonists ? why are they not analgesic in humans? Trends Pharmacol Sci *21*, 244–246.

Hjerling-Leffler, J., Marmigère, F., Heglind, M., Cederberg, A., Koltzenburg, M., Enerbäck, S., and Ernfors, P. (2005). The boundary cap: a source of neural crest stem cells that generate multiple sensory neuron subtypes. Development *132*, 2623–2632.

Hu, J., and Lewin, G.R. (2006). Mechanosensitive currents in the neurites of cultured mouse sensory neurones. J. Physiol. *577*, 815–828.

Huang, E.J., Zang, K., Schmidt, A., Saulys, A., Xiang, M., and Reichardt, L.F. (1999). POU domain factor Brn-3a controls the differentiation and survival of trigeminal neurons by regulating Trk receptor expression. Development *126*, 2869–2882.

Hucho, T., and Levine, J.D. (2007). Signaling Pathways in Sensitization: Toward a Nociceptor Cell Biology. Neuron *55*, 365–376.

Hunt, S.P., and Mantyh, P.W. (2001). The molecular dynamics of pain control. Nat. Rev. Neurosci. *2*, 83–91.

Indo, Y. (2001). Molecular basis of congenital insensitivity to pain with anhidrosis (CIPA): Mutations and polymorphisms in TRKA (NTRK1) gene encoding the receptor tyrosine kinase for nerve growth factor. Hum. Mutat. *18*, 462–471.

Indo, Y., Mardy, S., Miura, Y., Moosa, A., Ismail, E.A.R., Toscano, E., Andria, G., Pavone, V., Brown, D.L., Brooks, A., et al. (2001). Congenital insensitivity to pain with anhidrosis (CIPA): Novel mutations of the TRKA (NTRK1) gene, a putative uniparental disomy, and a linkage of the mutant TRKA and PKLR genes in a family with CIPA and pyruvate kinase deficiency. Hum. Mutat. *18*, 308–318.

Itskovitz-Eldor, J., Schuldiner, M., Karsenti, D., Eden, A., Yanuka, O., Amit, M., Soreq, H., and Benvenisty, N. (2000). Differentiation of human embryonic stem cells into embryoid bodies compromising the three embryonic germ layers. Mol. Med. *6*, 88.

Ji, R.-R., Samad, T.A., Jin, S.-X., Schmoll, R., and Woolf, C.J. (2002). p38 MAPK Activation by NGF in Primary Sensory Neurons after Inflammation Increases TRPV1 Levels and Maintains Heat Hyperalgesia. Neuron *36*, 57–68.

Jordt, S.-E., Bautista, D.M., Chuang, H., McKemy, D.D., Zygmunt, P.M., Högestätt, E.D., Meng, I.D., and Julius, D. (2004). Mustard oils and cannabinoids excite sensory nerve fibres through the TRP channel ANKTM1. Nature *427*, 260–265.

Josephson, A., Widenfalk, J., Trifunovski, A., Widmer, H.R., Olson, L., and Spenger, C. (2001). GDNF and NGF family members and receptors in human fetal and adult spinal cord and dorsal root ganglia. J. Comp. Neurol. *440*, 204–217.

Julius, D., and Basbaum, A.I. (2001). Molecular mechanisms of nociception. Nature *413*, 203–210.

Kamajaya, A., Kaiser, J.T., Lee, J., Reid, M., and Rees, D.C. (2014). The Structure of a Conserved Piezo Channel Domain Reveals a Topologically Distinct β Sandwich Fold. Structure *22*, 1520–1527.

Kanellopoulos, A.H., and Matsuyama, A. (2016). Voltage-gated sodium channels and pain-related disorders. Clin. Sci. *130*, 2257–2265.

Kashiba, H., Hyon, B., and Senba, E. (1998). Glial cell line-derived neurotrophic factor and nerve growth factor receptor mRNAs are expressed in distinct subgroups of dorsal root ganglion neurons and are differentially regulated by peripheral axotomy in the rat. Neurosci. Lett. *252*, 107–110.

Kashiba, H., Uchida, Y., and Senba, E. (2003). Distribution and colocalization of NGF and GDNF family ligand receptor mRNAs in dorsal root and nodose ganglion neurons of adult rats. Mol. Brain Res. *110*, 52–62.

Kawashima, Y., Géléoc, G.S.G., Kurima, K., Labay, V., Lelli, A., Asai, Y., Makishima, T., Wu, D.K., Della Santina, C.C., Holt, J.R., et al. (2011). Mechanotransduction in mouse inner ear hair cells requires transmembrane channel-like genes. J. Clin. Invest. *121*, 4796–4809.

Kedei, N., Szabo, T., Lile, J.D., Treanor, J.J., Olah, Z., Iadarola, M.J., and Blumberg, P.M. (2001). Analysis of the Native Quaternary Structure of Vanilloid Receptor 1. J. Biol. Chem. *276*, 28613–28619.

Keegan, J.J., and Garrett, F.D. (1948). The segmental distribution of the cutaneous nerves in the limbs of man. Anat. Rec. *102*, 409–437.

Kelly, S., Chapman, R.J., Woodhams, S., Sagar, D.R., Turner, J., Burston, J.J., Bullock, C., Paton, K., Huang, J., Wong, A., et al. (2015). Increased function of pronociceptive TRPV1 at the level of the joint in a rat model of osteoarthritis pain. Ann. Rheum. Dis. *74*, 252–259.

Kim, S.E., Coste, B., Chadha, A., Cook, B., and Patapoutian, A. (2012). The role of Drosophila Piezo in mechanical nociception. Nature *483*, 209–212.

Kittaka, H., and Tominaga, M. (2017). The molecular and cellular mechanisms of itch and the involvement of TRP channels in the peripheral sensory nervous system and skin. Allergol. Int. *66*, 22–30.

Kleinsmith, L.J., and Pierce, G.B. (1964). Multipotentiality of Single Embryonal Carcinoma Cells. Cancer Res. *24*, 1544–1551.

Kobayashi, K., Fukuoka, T., Obata, K., Yamanaka, H., Dai, Y., Tokunaga, A., and Noguchi, K. (2005). Distinct expression of TRPM8, TRPA1, and TRPV1 mRNAs in rat primary afferent neurons with aδ/c-fibers and colocalization with trk receptors. J. Comp. Neurol. *493*, 596–606.

Kobayashi, M., Kurihara, K., and Matsuoka, I. (1994). Retinoic acid induces BDNF responsiveness of sympathetic neurons by alteration of Trk neurotrophin receptor expression. FEBS Lett. *356*, 60–65.

Kobayashi, M., Fujii, M., Kurihara, K., and Matsuoka, I. (1998). Bone morphogenetic protein-2 and retinoic acid induce neurotrophin-3 responsiveness in developing rat sympathetic neurons. Mol. Brain Res. *53*, 206–217.

Kramer, I., Sigrist, M., de Nooij, J.C., Taniuchi, I., Jessell, T.M., and Arber, S. (2006). A Role for Runx Transcription Factor Signaling in Dorsal Root Ganglion Sensory Neuron Diversification. Neuron *49*, 379–393.

Lallemend, F., and Ernfors, P. (2012). Molecular interactions underlying the specification of sensory neurons. Trends Neurosci. *35*, 373–381.

Lariviere, R.C., and Julien, J.-P. (2004). Functions of intermediate filaments in neuronal development and disease. J. Neurobiol. *58*, 131–148.

Lawson, J.J., McIlwrath, S.L., Woodbury, C.J., Davis, B.M., and Koerber, H.R. (2008). TRPV1 Unlike TRPV2 Is Restricted to a Subset of Mechanically Insensitive Cutaneous Nociceptors Responding to Heat. J. Pain *9*, 298–308.

Lechner, S.G., Frenzel, H., Wang, R., and Lewin, G.R. (2009). Developmental waves of mechanosensitivity acquisition in sensory neuron subtypes during embryonic development. EMBO J. *28*, 1479–1491.

Lei, L., Laub, F., Lush, M., Romero, M., Zhou, J., Luikart, B., Klesse, L., Ramirez, F., and Parada, L.F. (2005). The zinc finger transcription factor Klf7 is required for TrkA gene expression and development of nociceptive sensory neurons. Genes Dev. *19*, 1354–1364.

Lei, L., Zhou, J., Lin, L., and Parada, L.F. (2006). Brn3a and Klf7 cooperate to control TrkA expression in sensory neurons. Dev. Biol. *300*, 758–769.

Lewin, G.R., Ritter, A.M., and Mendell, L.M. (1993). Nerve growth factor-induced hyperalgesia in the neonatal and adult rat. J. Neurosci. *13*, 2136–2148.

Li, C., MacDonald, J.I.S., Talebian, A., Leuenberger, J., Seah, C., Pasternak, S.H., Michnick, S.W., and Meakin, S.O. (2016a). Unravelling the Mechanism of TrkA-Induced Cell Death by Macropinocytosis in Medulloblastoma Daoy Cells. Mol. Cell. Biol. *36*, 2596–2611.

Li, C.-L., Li, K.-C., Wu, D., Chen, Y., Luo, H., Zhao, J.-R., Wang, S.-S., Sun, M.-M., Lu, Y.-J., Zhong, Y.-Q., et al. (2016b). Somatosensory neuron types identified by high-coverage single-cell RNA-sequencing and functional heterogeneity. Cell Res. *26*, 83–102.

Li, L., Rutlin, M., Abraira, V.E., Cassidy, C., Kus, L., Gong, S., Jankowski, M.P., Luo, W., Heintz, N., Koerber, H.R., et al. (2011). The Functional Organization of Cutaneous Low-Threshold Mechanosensory Neurons. Cell *147*, 1615–1627.

Long, S.B., Campbell, E.B., and Mackinnon, R. (2005). Crystal structure of a mammalian voltage-dependent Shaker family K+ channel. Science *309*, 897–903.

Luo, W., Enomoto, H., Rice, F.L., Milbrandt, J., and Ginty, D.D. (2009). Molecular Identification of Rapidly Adapting Mechanoreceptors and their Developmental Dependence on Ret Signaling. Neuron *64*, 841.

Ma, L., Lei, L., Eng, S.R., Turner, E., and Parada, L.F. (2003). Brn3a regulation of TrkA/NGF receptor expression in developing sensory neurons. Development *130*, 3525–3534.

Ma, Q., Chen, Z., Barrantes, I. del B., Luis de la Pompa, J., and Anderson, D.J. (1998). neurogenin1 Is Essential for the Determination of Neuronal Precursors for Proximal Cranial Sensory Ganglia. Neuron *20*, 469–482.

Ma, Q., Fode, C., Guillemot, F., and Anderson, D.J. (1999a). NEUROGENIN1 and NEUROGENIN2 control two distinct waves of neurogenesis in developing dorsal root ganglia. Genes Dev. *13*, 1717–1728.

Mardy, S., Miura, Y., Endo, F., Matsuda, I., and Indo, Y. (2001). Congenital insensitivity to pain with anhidrosis (CIPA): effect of TRKA (NTRK1) missense mutations on autophosphorylation of the receptor tyrosine kinase for nerve growth factor. Hum. Mol. Genet. *10*, 179–188.

Marmigère, F., and Ernfors, P. (2007). Specification and connectivity of neuronal subtypes in the sensory lineage. Nat. Rev. Neurosci. *8*, 114–127.

Maro, G.S., Vermeren, M., Voiculescu, O., Melton, L., Cohen, J., Charnay, P., and Topilko, P. (2004). Neural crest boundary cap cells constitute a source of neuronal and glial cells of the PNS. Nat. Neurosci. *7*, 930–938.

Martin, G.R. (1981). Isolation of a pluripotent cell line from early mouse embryos cultured in medium conditioned by teratocarcinoma stem cells. Proc. Natl. Acad. Sci. U. S. A. *78*, 7634–7638.

Massa, M.G., Gisevius, B., Hirschberg, S., Hinz, L., Schmidt, M., Gold, R., Prochnow, N., and Haghikia, A. (2016). Multiple Sclerosis Patient-Specific Primary Neurons Differentiated from Urinary Renal Epithelial Cells via Induced Pluripotent Stem Cells. PLOS ONE *11*, e0155274.

McKemy, D.D., Neuhausser, W.M., and Julius, D. (2002). Identification of a cold receptor reveals a general role for TRP channels in thermosensation. Nature *416*, 52–58.

McMahon, S.B., Armanini, M.P., Ling, L.H., and Phillips, H.S. (1994). Expression and coexpression of Trk receptors in subpopulations of adult primary sensory neurons projecting to identified peripheral targets. Neuron *12*, 1161–1171.

McMillin, M.J., Beck, A.E., Chong, J.X., Shively, K.M., Buckingham, K.J., Gildersleeve, H.I.S., Aracena, M.I., Aylsworth, A.S., Bitoun, P., Carey, J.C., et al. (2014). Mutations in PIEZO2 Cause Gordon Syndrome, Marden-Walker Syndrome, and Distal Arthrogryposis Type 5. Am. J. Hum. Genet. *94*, 734–744.

Miller, F., Björnsson, M., Svensson, O., and Karlsten, R. (2014). Experiences with an adaptive design for a dose-finding study in patients with osteoarthritis. Contemp. Clin. Trials *37*, 189–199.

Minett, M.S., Nassar, M.A., Clark, A.K., Passmore, G., Dickenson, A.H., Wang, F., Malcangio, M., and Wood, J.N. (2012). Distinct Nav1.7-dependent pain sensations require different sets of sensory and sympathetic neurons. Nat. Commun. *3*, 791.

Minett, M.S., Falk, S., Santana-Varela, S., Bogdanov, Y.D., Nassar, M.A., Heegaard, A.-M., and Wood, J.N. (2014). Pain without Nociceptors? Nav1.7-Independent Pain Mechanisms. Cell Rep. *6*, 301–312.

Minke, B., Wu, C.-F., and Pak, W.L. (1975). Induction of photoreceptor voltage noise in the dark in Drosophila mutant. Nature *258*, 84–87.

Miyamoto, T., Mochizuki, T., Nakagomi, H., Kira, S., Watanabe, M., Takayama, Y., Suzuki, Y., Koizumi, S., Takeda, M., and Tominaga, M. (2014). Functional Role for Piezo1 in Stretch-evoked Ca2+ Influx and ATP Release in Urothelial Cell Cultures. J. Biol. Chem. *289*, 16565–16575.

Mogil, J.S. (2009). Animal models of pain: progress and challenges. Nat Rev Neurosci *10*, 283–294.

Mohamet, L., Miazga, N.J., and Ward, C.M. (2014). Familial Alzheimer's disease modelling using induced pluripotent stem cell technology. World J. Stem Cells *6*, 239–247.

Mokhtari, R., and Lachman, H.M. (2016). Neurons Derived From Patient-Specific Induced Pluripotent Stem Cells: a Promising Strategy Towards Developing Novel Pharmacotherapies for Autism Spectrum Disorders. EBioMedicine *9*, 21–22.

Molliver, D.C., and Snider, W.D. (1997a). Nerve growth factor receptor trkA is down-regulated during postnatal development by a subset of dorsal root ganglion neurons. J. Comp. Neurol. *381*, 428–438.

Molliver, D.C., and Snider, W.D. (1997b). Nerve growth factor receptor trkA is down-regulated during postnatal development by a subset of dorsal root ganglion neurons. J. Comp. Neurol. *381*, 428–438.

Molliver, D.C., Radeke, M.J., Feinstein, S.C., and Snider, W.D. (1995). Presence or absence of TrKA protein distinguishes subsets of small sensory neurons with unique cytochemical characteristics and dorsal horn projections. J. Comp. Neurol. *361*, 404–416.

Molliver, D.C., Wright, D.E., Leitner, M.L., Parsadanian, A.S., Doster, K., Wen, D., Yan, Q., and Snider, W.D. (1997). IB4-Binding DRG Neurons Switch from NGF to GDNF Dependence in Early Postnatal Life. Neuron *19*, 849–861.

Montell, C., and Rubin, G.M. (1989). Molecular characterization of the drosophila trp locus: A putative integral membrane protein required for phototransduction. Neuron *2*, 1313–1323.

Nagy, J.I., and Hunt, S.P. (1982). Fluoride-resistant acid phosphatase-containing neurones in dorsal root ganglia are separate from those containing substance P or somatostatin. Neuroscience *7*, 89–97.

Nakagawa, S., and Takeichi, M. (1998). Neural crest emigration from the neural tube depends on regulated cadherin expression. Development *125*, 2963–2971.

Narayanan, P., Sondermann, J., Rouwette, T., Karaca, S., Urlaub, H., Mitkovski, M., Gomez-Varela, D., and Schmidt, M. (2016). Native Piezo2 Interactomics identifies Pericentrin as a Novel Regulator of Piezo2 in Somatosensory Neurons. J. Proteome Res.

Nassar, M.A., Stirling, L.C., Forlani, G., Baker, M.D., Matthews, E.A., Dickenson, A.H., and Wood, J.N. (2004). Nociceptor-specific gene deletion reveals a major role for Nav1.7 (PN1) in acute and inflammatory pain. Proc. Natl. Acad. Sci. U. S. A. *101*, 12706–12711.

Newgreen, D.F., and Gooday, D. (1985). Control of the onset of migration of neural crest cells in avian embryos. Cell Tissue Res. *239*, 329–336.

Nieber, F., Pieler, T., and Henningfeld, K.A. (2009). Comparative expression analysis of the neurogenins in Xenopus tropicalis and Xenopus laevis. Dev. Dyn. *238*, 451–458.

Niederreither, K., and Dollé, P. (2008). Retinoic acid in development: towards an integrated view. Nat. Rev. Genet. *9*, 541–553.

Nonomura, K., Woo, S.-H., Chang, R.B., Gillich, A., Qiu, Z., Francisco, A.G., Ranade, S.S., Liberles, S.D., and Patapoutian, A. (2017). Piezo2 senses airway stretch and mediates lung inflation-induced apnoea. Nature *541*, 176–181.

Okubo, M., Fujita, A., Saito, Y., Komaki, H., Ishiyama, A., Takeshita, E., Kojima, E., Koichihara, R., Saito, T., Nakagawa, E., et al. (2015). A family of distal arthrogryposis type 5 due to a novel PIEZO2 mutation. Am. J. Med. Genet. A. *167*, 1100–1106.

O'Rahilly, R. (1979). Early human development and the chief sources of information on staged human embryos. Eur. J. Obstet. Gynecol. Reprod. Biol. *9*, 273–280.

Orozco, O.E., Walus, L., Sah, D.W.Y., Pepinsky, R.B., and Sanicola, M. (2001). GFRalpha3 is expressed predominantly in nociceptive sensory neurons. Eur. J. Neurosci. *13*, 2177–2182.

Overturf, K., al-Dhalimy, M., Ou, C.N., Finegold, M., and Grompe, M. (1997). Serial transplantation reveals the stem-cell-like regenerative potential of adult mouse hepatocytes. Am. J. Pathol. *151*, 1273.

Owsianik, G., D'hoedt, D., Voets, T., and Nilius, B. (2006). Structure–function relationship of the TRP channel superfamily. SpringerLink 61–90.

Park, I.-H., Arora, N., Huo, H., Maherali, N., Ahfeldt, T., Shimamura, A., Lensch, M.W., Cowan, C., Hochedlinger, K., and Daley, G.Q. (2008). Disease-Specific Induced Pluripotent Stem Cells. Cell *134*, 877–886.

Patapoutian, A., Peier, A.M., Story, G.M., and Viswanath, V. (2003). ThermoTRP channels and beyond: mechanisms of temperature sensation. Nat. Rev. Neurosci. *4*, 529–539.

Peier, A.M., Moqrich, A., Hergarden, A.C., Reeve, A.J., Andersson, D.A., Story, G.M., Earley, T.J., Dragoni, I., McIntyre, P., Bevan, S., et al. (2002). A TRP Channel that Senses Cold Stimuli and Menthol. Cell *108*, 705–715.

Percie du Sert, N., and Rice, A.S.C. (2014). Improving the translation of analgesic drugs to the clinic: animal models of neuropathic pain. Br. J. Pharmacol. *171*, 2951–2963.

Perez-Pinera, P., García-Suarez, O., Germanà, A., Díaz-Esnal, B., de Carlos, F., Silos-Santiago, I., del Valle, M.E., Cobo, J., and Vega, J.A. (2008). Characterization of sensory deficits in TrkB knockout mice. Neurosci. Lett. *433*, 43–47.

Perl, E.R. (1996). Chapter 2. Cutaneous polymodal receptors: characteristics and plasticity. Prog. Brain Res. *113*, 21–37.

Petersen, C.C., Berridge, M.J., Borgese, M.F., and Bennett, D.L. (1995). Putative capacitative calcium entry channels: expression of Drosophila trp and evidence for the existence of vertebrate homologues. Biochem. J. *311*, 41–44.

Poole, K., Herget, R., Lapatsina, L., Ngo, H.-D., and Lewin, G.R. (2014). Tuning Piezo ion channels to detect molecular-scale movements relevant for fine touch. Nat. Commun. *5*, 3520.

Prockop, D.J. (1997). Marrow Stromal Cells as Stem Cells for Nonhematopoietic Tissues. Science *276*, 71–74.

Prole, D.L., and Taylor, C.W. (2013). Identification and Analysis of Putative Homologues of Mechanosensitive Channels in Pathogenic Protozoa. PLOS ONE *8*, e66068.

Qi, Y., Andolfi, L., Frattini, F., Mayer, F., Lazzarino, M., and Hu, J. (2015). Membrane stiffening by STOML3 facilitates mechanosensation in sensory neurons. Nat. Commun. *6*.

Ran, F.A., Hsu, P.D., Wright, J., Agarwala, V., Scott, D.A., and Zhang, F. (2013). Genome engineering using the CRISPR-Cas9 system. Nat. Protoc. *8*, 2281–2308.

Ranade, S.S., Qiu, Z., Woo, S.-H., Hur, S.S., Murthy, S.E., Cahalan, S.M., Xu, J., Mathur, J., Bandell, M., Coste, B., et al. (2014a). Piezo1, a mechanically activated ion channel, is required for vascular development in mice. Proc. Natl. Acad. Sci. *111*, 10347–10352.

Ranade, S.S., Woo, S.-H., Dubin, A.E., Moshourab, R.A., Wetzel, C., Petrus, M., Mathur, J., Bégay, V., Coste, B., Mainquist, J., et al. (2014b). Piezo2 is the major transducer of mechanical forces for touch sensation in mice. Nature *516*, 121–125.

Rathee, P.K., Distler, C., Obreja, O., Neuhuber, W., Wang, G.K., Wang, S.-Y., Nau, C., and Kress, M. (2002). PKA/AKAP/VR-1 Module: A Common Link of Gs-Mediated Signaling to Thermal Hyperalgesia. J. Neurosci. *22*, 4740–4745.

Reisinger, K., Hoffmann, S., Alépée, N., Ashikaga, T., Barroso, J., Elcombe, C., Gellatly, N., Galbiati, V., Gibbs, S., Groux, H., et al. (2015). Systematic evaluation of non-animal test methods for skin sensitisation safety assessment. Toxicol. In Vitro *29*, 259–270.

Reubinoff, B.E., Pera, M.F., Fong, C.-Y., Trounson, A., and Bongso, A. (2000). Embryonic stem cell lines from human blastocysts: somatic differentiation in vitro. Nat. Biotechnol. *18*, 399–404.

Rifkin, J.T., Todd, V.J., Anderson, L.W., and Lefcort, F. (2000). Dynamic Expression of Neurotrophin Receptors during Sensory Neuron Genesis and Differentiation. Dev. Biol. *227*, 465–480.

Rohl, C.A., Boeckman, F.A., Baker, C., Scheuer, T., Catterall, W.A., and Klevit, R.E. (1999). Solution Structure of the Sodium Channel Inactivation Gate,. Biochemistry (Mosc.) *38*, 855–861.

Rostock, C., Schrenk-Siemens, K., Pohle, J., and Siemens, J. (*in press*) HUMAN VS. MOUSE NOCICEPTORS - SIMILARITIES AND DIFFERENCES. Neuroscience.

Ruocco, V., Sangiuliano, S., Brunetti, G., and Ruocco, E. (2012). Beyond Zoster: Sensory and Immune Changes in Zoster-affected Dermatomes: A Review.

Saiki, R.K., Bugawan, T.L., Horn, G.T., Mullis, K.B., and Erlich, H.A. (1986). Analysis of enzymatically amplified beta-globin and HLA-DQ alpha DNA with allele-specific oligonucleotide probes. Nature *324*, 163–166.

Satin, J., Kyle, J.W., Chen, M., Bell, P., Cribbs, L.L., Fozzard, H.A., and Rogart, R.B. (1992). A Mutant of TTX-Resistant Cardiac Sodium Channels with TTX-Sensitive Properties. Science *256*, 1202–1205.

Schrenk-Siemens, K., Wende, H., Prato, V., Song, K., Rostock, C., Loewer, A., Utikal, J., Lewin, G.R., Lechner, S.G., and Siemens, J. (2015). PIEZO2 is required for mechanotransduction in human stem cell-derived touch receptors. Nat. Neurosci. *18*, 10–16.

Serbedzija, G.N., Fraser, S.E., and Bronner-Fraser, M. (1990). Pathways of trunk neural crest cell migration in the mouse embryo as revealed by vital dye labelling. Development *108*, 605–612.

Shelanski, M.L., Frappier, T., Georgieff, I., Troy, C., and Mellado, W. (1994). Cytoskeletons of central and peripheral neurons. J. Neurol. Sci. *124*, *Supplement*, 33–37.

Sherrington, C.S. (1903). Qualitative difference of spinal reflex corresponding with qualitative difference of cutaneous stimulus. J. Physiol. *30*, 39–46.

Silos-Santiago, I. (1995). Molecular genetics of neuronal survival. Curr. Opin. Neurobiol. *5*, 42–49.

Silos-Santiago, I., Greenlund, L.J., Johnson, E.M., and Snider, W.D. (1995a). Molecular genetics of neuronal survival. Curr. Opin. Neurobiol. *5*, 42–49.

Silos-Santiago, I., Molliver, D.C., Ozaki, S., Smeyne, R.J., Fagan, A.M., Barbacid, M., and Snider, W.D. (1995b). Non-TrkA-expressing small DRG neurons are lost in TrkA deficient mice. J. Neurosci. *15*, 5929–5942.

Silverman, J.D., and Kruger, L. (1990). Selective neuronal glycoconjugate expression in sensory and autonomic ganglia: relation of lectin reactivity to peptide and enzyme markers. J. Neurocytol. *19*, 789–801.

Simmons, P.J., and Torok-Storb, B. (1991). Identification of stromal cell precursors in human bone marrow by a novel monoclonal antibody, STRO-1. Blood *78*, 55–62.

Sivilotti, L., Okuse, K., Akopian, A.N., Moss, S., and Wood, J.N. (1997). A single serine residue confers tetrodotoxin insensitivity on the rat sensory-neuron-specific sodium channel SNS. FEBS Lett. *409*, 49–52.

Smeyne, R.J., Klein, R., Schnapp, A., Long, L.K., Bryant, S., Lewin, A., Lira, S.A., and Barbacid, M. (1994). Severe sensory and sympathetic neuropathies in mice carrying a disrupted Trk/NGF receptor gene. Nature *368*, 246–249.

Smith, G.D., Gunthorpe, M.J., Kelsell, R.E., Hayes, P.D., Reilly, P., Facer, P., Wright, J.E., Jerman, J.C., Walhin, J.-P., Ooi, L., et al. (2002). TRPV3 is a temperature-sensitive vanilloid receptor-like protein. Nature *418*, 186–190.

Snider, W.D. (1994). Functions of the neurotrophins during nervous system development: What the knockouts are teaching us. Cell *77*, 627–638.

Snider, W.D., and McMahon, S.B. (1998). Tackling Pain at the Source: New Ideas about Nociceptors. Neuron *20*, 629–632.

Soattin, L., Fiore, M., Gavazzo, P., Viti, F., Facci, P., Raiteri, R., Difato, F., Pusch, M., and Vassalli, M. (2016). The biophysics of piezo1 and piezo2 mechanosensitive channels. Biophys. Chem. *208*, 26–33.

Sommer, L., Ma, Q., and Anderson, D.J. (1996). neurogenins,a Novel Family ofatonal-Related bHLH Transcription Factors, Are Putative Mammalian Neuronal Determination Genes That Reveal Progenitor Cell Heterogeneity in the Developing CNS and PNS. Mol. Cell. Neurosci. *8*, 221–241.

Stantcheva, K.K., Iovino, L., Dhandapani, R., Martinez, C., Castaldi, L., Nocchi, L., Perlas, E., Portulano, C., Pesaresi, M., Shirlekar, K.S., et al. (2016). A subpopulation of itch-sensing neurons marked by Ret and somatostatin expression. EMBO Rep. *17*, 585–600.

Stark, H.-J., Szabowski, A., Fusenig, N.E., and Maas-Szabowski, N. (2004). Organotypic cocultures as skin equivalents: A complex and sophisticated in vitro system. Biol. Proced. Online *6*, 55–60.

Story, G.M., Peier, A.M., Reeve, A.J., Eid, S.R., Mosbacher, J., Hricik, T.R., Earley, T.J., Hergarden, A.C., Andersson, D.A., Hwang, S.W., et al. (2003). ANKTM1, a TRP-like Channel Expressed in Nociceptive Neurons, Is Activated by Cold Temperatures. Cell *112*, 819–829.

Stucky, C.L., and Lewin, G.R. (1999). Isolectin B4-Positive and -Negative Nociceptors Are Functionally Distinct. J. Neurosci. *19*, 6497–6505.

Sun, Y., Dykes, I.M., Liang, X., Eng, S.R., Evans, S.M., and Turner, E.E. (2008). A central role for Islet1 in sensory neuron development linking sensory and spinal gene regulatory programs. Nat. Neurosci. *11*, 1283–1293.

Takahashi, K., and Yamanaka, S. (2006). Induction of Pluripotent Stem Cells from Mouse Embryonic and Adult Fibroblast Cultures by Defined Factors. Cell *126*, 663–676.

Takahashi, K., Tanabe, K., Ohnuki, M., Narita, M., Ichisaka, T., Tomoda, K., and and Yamanaka, S. (2007a). Induction of Pluripotent Stem Cells from Adult Human Fibroblasts by Defined Factors. Cell *131*, 861–872.

Teillet, M.-A., Kalcheim, C., and Le Douarin, N.M. (1987). Formation of the dorsal root ganglia in the avian embryo: Segmental origin and migratory behavior of neural crest progenitor cells. Dev. Biol. *120*, 329–347.

Temple, S. (1989). Division and differentiation of isolated CNS blast cells in microculture. Nature *340*, 471–473.

Theiler, K. (1989). The House Mouse: Atlas of Embryonic Development (Springer Science).

Thomson, J.A., Itskovitz-Eldor, J., Shapiro, S.S., Waknitz, M.A., Swiergiel, J.J., Marshall, V.S., and Jones, J.M. (1998). Embryonic Stem Cell Lines Derived from Human Blastocysts. Science *282*, 1145–1147.

Toledo-Aral, J.J., Moss, B.L., He, Z.-J., Koszowski, A.G., Whisenand, T., Levinson, S.R., Wolf, J.J., Silos-Santiago, I., Halegoua, S., and Mandel, G. (1997). Identification of PN1, a predominant voltage-dependent sodium channel expressed principally in peripheral neurons. Proc. Natl. Acad. Sci. *94*, 1527–1532.

Tominaga, M. (2007). The Role of TRP Channels in Thermosensation (CRC Press/Taylor & Francis).

Tominaga, M., Caterina, M.J., Malmberg, A.B., Rosen, T.A., Gilbert, H., Skinner, K., Raumann, B.E., Basbaum, A.I., and Julius, D. (1998). The Cloned Capsaicin Receptor Integrates Multiple Pain-Producing Stimuli. Neuron *21*, 531–543.

Tominaga, M., Wada, M., and Masu, M. (2001). Potentiation of capsaicin receptor activity by metabotropic ATP receptors as a possible mechanism for ATP-evoked pain and hyperalgesia. Proc. Natl. Acad. Sci. U. S. A. *98*, 6951–6956.

Toups, M.A., Kitchen, A., Light, J.E., and Reed, D.L. (2011). Origin of Clothing Lice Indicates Early Clothing Use by Anatomically Modern Humans in Africa. Mol. Biol. Evol. *28*, 29–32.

Tseng, S.C.G. (1996). Regulation and clinical implications of corneal epithelial stem cells. Mol. Biol. Rep. *23*, 47–58.

Usoskin, D., Furlan, A., Islam, S., Abdo, H., Lönnerberg, P., Lou, D., Hjerling-Leffler, J., Haeggström, J., Kharchenko, O., Kharchenko, P.V., et al. (2015). Unbiased classification of sensory neuron types by large-scale single-cell RNA sequencing. Nat. Neurosci. *18*, 145–153.

Vega, J.A., Humara, J.M., Naves, F.J., Esteban, I., and Valle, M.E.D. (1994). Immunoreactivity for phosphorylated 200-kDa neurofilament subunit is heterogeneously expressed in human sympathetic and primary sensory neurons. Anat. Embryol. (Berl.) *190*, 453–459.

Verpoorten, N., Claeys, K.G., Deprez, L., Jacobs, A., Gerwen, V.V., Lagae, L., Arts, W.F., Meirleir, L.D., Keymolen, K., Groote, C.C., et al. (2006). Novel frameshift and splice site mutations in the neurotrophic tyrosine kinase receptor type 1 gene (NTRK1) associated with hereditary sensory neuropathy type IV. Neuromuscul. Disord. *16*, 19–25.

Vescovi, A.L., Galli, R., and Gritti, A. (2001). The neural stem cells and their transdifferentiation capacity. Biomed. Pharmacother. *55*, 201–205.

Viatchenko-Karpinski, V., and Gu, J.G. (2016). Mechanical sensitivity and electrophysiological properties of acutely dissociated dorsal root ganglion neurons of rats. Neurosci. Lett. *634*, 70–75.

Vierbuchen, T., Ostermeier, A., Pang, Z.P., Kokubu, Y., Südhof, T.C., and Wernig, M. (2010). Direct conversion of fibroblasts to functional neurons by defined factors. Nature *463*, 1035–1041.

Voets, T., Talavera, K., Owsianik, G., and Nilius, B. (2005). Sensing with TRP channels. Nat. Chem. Biol. *1*, 85–92.

Volkers, L., Mechioukhi, Y., and Coste, B. (2015). Piezo channels: from structure to function. Pflüg. Arch. Eur. J. Physiol. *467*, 95–99.

Vriens, J., Owsianik, G., Voets, T., Droogmans, G., and Nilius, B. (2004). Invertebrate TRP proteins as functional models for mammalian channels. Pflüg. Arch. *449*, 213–226.

Wainger, B.J., Buttermore, E.D., Oliveira, J.T., Mellin, C., Lee, S., Saber, W.A., Wang, A.J., Ichida, J.K., Chiu, I.M., and Barrett, L. (2015). Modeling pain in vitro using nociceptor neurons reprogrammed from fibroblasts. Nat Neurosci *18*, 17–24.

Wang, F., Knutson, K., Alcaino, C., Linden, D.R., Gibbons, S.J., Kashyap, P., Grover, M., Oeckler, R., Gottlieb, P.A., Li, H.J., et al. (2017). Mechanosensitive ion channel Piezo2 is important for enterochromaffin cell response to mechanical forces. J. Physiol. *595*, 79–91.

Weiss, J., Pyrski, M., Jacobi, E., Bufe, B., Willnecker, V., Schick, B., Zizzari, P., Gossage, S.J., Greer, C.A., Leinders-Zufall, T., et al. (2011). Loss-of-function mutations in sodium channel Nav1.7 cause anosmia. Nature *472*, 186–190.

Wende, H., Lechner, S.G., Cheret, C., Bourane, S., Kolanczyk, M.E., Pattyn, A., Reuter, K., Munier, F.L., Carroll, P., Lewin, G.R., et al. (2012). The Transcription Factor c-Maf Controls Touch Receptor Development and Function. Science *335*, 1373–1376.

Wes, P.D., Chevesich, J., Jeromin, A., Rosenberg, C., Stetten, G., and Montell, C. (1995). TRPC1, a human homolog of a Drosophila store-operated channel. Proc. Natl. Acad. Sci. *92*, 9652–9656.

White, F.A., Silos-Santiago, I., Molliver, D.C., Nishimura, M., Phillips, H., Barbacid, M., and Snider, W.D. (1996). Synchronous Onset of NGF and TrkA Survival Dependence in Developing Dorsal Root Ganglia. J. Neurosci. *16*, 4662–4672.

Woo, S.-H., Ranade, S., Weyer, A.D., Dubin, A.E., Baba, Y., Qiu, Z., Petrus, M., Miyamoto, T., Reddy, K., Lumpkin, E.A., et al. (2014). Piezo2 is required for Merkel-cell mechanotransduction. Nature *509*, 622–626.

Woo, S.-H., Lukacs, V., de Nooij, J.C., Zaytseva, D., Criddle, C.R., Francisco, A., Jessell, T.M., Wilkinson, K.A., and Patapoutian, A. (2015). Piezo2 is the principal mechanotransduction channel for proprioception. Nat. Neurosci. *18*, 1756–1762.

Woolf, C.J., and Ma, Q. (2007). Nociceptors—Noxious Stimulus Detectors. Neuron *55*, 353–364.

Xiao-Jie, L., Hui-Ying, X., Zun-Ping, K., Jin-Lian, C., and Li-Juan, J. (2015). CRISPR-Cas9: a new and promising player in gene therapy. J. Med. Genet. *52*, 289–296.

Xu, H., Ramsey, I.S., Kotecha, S.A., Moran, M.M., Chong, J.A., Lawson, D., Ge, P., Lilly, J., Silos-Santiago, I., Xie, Y., et al. (2002). TRPV3 is a calcium-permeable temperature-sensitive cation channel. Nature *418*, 181–186.

Xue, L., Yi, H., Huang, Z., Shi, Y.-B., and Li, W.-X. (2011). Global Gene Expression during the Human Organogenesis: From Transcription Profiles to Function Predictions.

Yang, Y., Wang, Y., Li, S., Xu, Z., Li, H., Ma, L., Fan, J., Bu, D., Liu, B., Fan, Z., et al. (2004). Mutations in *SCN9A*, encoding a sodium channel alpha subunit, in patients with primary erythermalgia. J. Med. Genet. *41*, 171–174.

Yarmolinsky, D.A., Peng, Y., Pogorzala, L.A., Rutlin, M., Hoon, M.A., and Zuker, C.S. (2016). Coding and Plasticity in the Mammalian Thermosensory System. Neuron *92*, 1079–1092.

Yekkirala, A.S., Roberson, D.P., Bean, B.P., and Woolf, C.J. (2017). Breaking barriers to novel analgesic drug development. Nat. Rev. Drug Discov. *16*, 545–564.

Yu, F.H., and Catterall, W.A. (2003). Overview of the voltage-gated sodium channel family. Genome Biol. *4*, 207.

Zhang, X., Huang, J., and McNaughton, P.A. (2005). NGF rapidly increases membrane expression of TRPV1 heat-gated ion channels. EMBO J. *24*, 4211–4223.

Zhang, X.Y., Wen, J., Yang, W., Wang, C., Gao, L., Zheng, L.H., Wang, T., Ran, K., Li, Y., Li, X., et al. (2013a). Gain-of-Function Mutations in SCN11A Cause Familial Episodic Pain. Am. J. Hum. Genet. *93*, 957.

Zhang, Y., Pak, C., Han, Y., Ahlenius, H., Zhang, Z., Chanda, S., Marro, S., Patzke, C., Acuna, C., Covy, J., et al. (2013b). Rapid Single-Step Induction of Functional Neurons from Human Pluripotent Stem Cells. Neuron *78*, 785–798.

Zwick, M., Davis, B.M., Woodbury, C.J., Burkett, J.N., Koerber, H.R., Simpson, J.F., and Albers, K.M. (2002). Glial Cell Line-Derived Neurotrophic Factor is a Survival Factor for Isolectin B4-Positive, but not Vanilloid Receptor 1-Positive, Neurons in the Mouse. J. Neurosci. *22*, 4057–4065.

Zylka, M.J., Rice, F.L., and Anderson, D.J. (2005). Topographically Distinct Epidermal Nociceptive Circuits Revealed by Axonal Tracers Targeted to Mrgprd. Neuron *45*, 17–25.

I. Abbreviations

BDNF	Brain-derived neurotrophic factor
Cap	Capsaicin
cDNA	Complementary DNA
CGRP	Calcitonin gene-related peptide
CNS	Central nervous system
Ctrl	Control
Cy2	Cyanine-2
Cy3	Cyanine-3
DAPI	4',6-diamidino-2-phenylindole
DMEM	Dulbecco's modified Eagle's medium
DNA	Deoxyribonucleic acid
dNTPs	Deoxynucleotidetriphosphate
DRG	Dorsal root ganglion
E8	Essential 8 ™ Medium
E.coli	Escherichia coli
EGFP	Enhanced green fluorescent protein
GDNF	Glial cell-derived neurotrophic factor
GFP	Green fluorescent protein
HEK293TN	Human embryonic kidney cells 293 (+SV40 large T-antigen)
HEPES	4-2hydroxyethyl-1-piperazineethanesulfonic acid
hESC	Human embryonic stem cell
IB4	Isolectin B4
iPSC	Induced pluripotent stem cell
LB	Luria-Bertani
Menth	Menthol
MiliQ	Ultrafiltrated water (from MiliQ-Plus water system, Millipore)
MO	Mustard Oil
mRNA	Messenger ribonucleic acid
NCLC	Neural crest-like cell
NGF	Nerve growth factor

on	Over night
PBS	Phosphate buffered saline
PCR	Polymerase chain reaction
PFA	Paraformaldehyde
pH	potentiumhydrogenii; potential of hydrogen
PNS	Peripheral nervous system
RNA	Ribonucleic acid
RNase	Ribonuclease
RT	Room temperature
SP	Substance P
TE	Tris-EDTA
TG	Trigeminal ganglion
TM	Transmembrane domain
TrkA	Neurotraophic tyrosine kinase receptor type 1
TrkB	Neurotraophic tyrosine kinase receptor type 2
TrkC	Neurotrophic tyrosine kinase receptor type 3
TRP	Transient receptor potential
TRPA1	Transient receptor potential ankyrin 1
TRPM8	Transient receptor potential cation channel subfamily M member 8
TRPV1	Transient receptor potential Vanilloid 1
TTX	Tetrodotoxin
WT	Wild type

II. Units

°C	degrees celsius
bp	base pair
d	day
g	gram
hr	hour
kb	kilobase
l	liter
M	molar
min	minute
mg	miligram
ml	milliliter
mM	millimolar
ng	nanogram
m	nanometer
rpm	Revolutios per minute
s	second
µg	microgram
µl	microliter
µm	micrometer
µM	micromolar

III Nomenclature

Human	Gene: all letters in upper case/ Italic
	Protein: all letters in upper case/ Regular
Mouse	Gene: only first letter in upper case/ Italic
	Protein: all letters in upper case/ Regular
Human and Mouse together	Mouse regulation